SOME ASPECTS OF SOLAR FLARE AND PROMINENCE THEORY

A. M. Milne

A Thesis Submitted for the Degree of PhD
at the
University of St Andrews

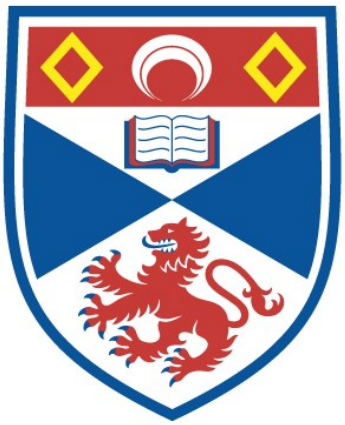

1980

SOME ASPECTS OF SOLAR FLARE AND PROMINENCE THEORY

A. M. MILNE

THESIS SUBMITTED FOR THE DEGREE OF DOCTOR OF PHILOSOPHY

OF THE UNIVERSITY OF ST. ANDREWS

ProQuest LLC.
789 East Eisenhower Parkway
P.O. Box 1346
Ann Arbor, MI 48106 – 1346

SOME ASPECTS OF SOLAR FLARE AND PROMINENCE THEORY

Abstract

Solar flares and solar prominences are amongst the best known features of solar activity. Despite this familiarity, however, there are still significant gaps in our knowledge of these phenomena. In this thesis some theoretical aspects of these events are considered.

We first consider solar prominences. We propose a model for the static equilibrium of quiescent prominences which will simultaneously explain the support mechanism for the dense prominence material and take account roughly of the required energy balance. This model contains two parameters, namely the coronal plasma beta and the horizontal shear angle, Φ, that the magnetic fieldlines make with the prominence normal. We obtain limits on both these parameters which, when exceeded, imply that no equilibrium state is possible. The results obtained provide a possible explanation for several prominence features.

For the remainder of the thesis we consider one aspect of the solar flare problem, namely the possibility of a trigger mechanism for the rapid release of energy in a flare. One candidate for this mechanism is the sudden release of energy stored in excess of potential by a force-free magnetic field which becomes unstable as a result of photospheric motions. For this reason we seek simple analytic solutions to the force-free field equations which may exhibit such an instability.

An alternative trigger mechanism, which requires the presence of a current sheet, is given by the emerging flux model for solar flares. We thus develop a one-dimensional model for current sheets in general, where the conditions within the current sheet are given in terms of several non-dimensional parameters which describe the external conditions. These results are then applied to the emerging flux model.

ACKNOWLEDGEMENTS

I would like to thank Drs. Eric Priest and Bernard Roberts for their supervision during my period as a research student, and also for their highly infectious enthusiasm for their subject. I also wish to thank my fellow students at St. Andrews, Alan Hood and Andrew Webb for many helpful and interesting discussions.

I am grateful to the Science Research Council for financial support.

CERTIFICATE

I certify that Alex. M. Milne has satisfied the conditions of the Ordinance and Regulations and is thus qualified to submit the accompanying application for the degree of Doctor of Philosophy.

POSTGRADUATE CAREER

I was admitted into the University of St. Andrews as a research student under Ordinance General No. 12 in October 1975 to work on aspects of solar flare and prominence theory under the joint supervision of Dr. E. R. Priest and Dr. B. Roberts. I was admitted under the above resolution as a candidate for the degree of Ph.D. in October 1976.

DECLARATION

I declare that the following thesis is a record of research work carried out by me, that the thesis is my own composition, and that it has not been previously presented in application for a higher degree.

(ALEXANDER MITCHELL MILNE)

CONTENTS

Chapter 1: INTRODUCTION

The object of this thesis is to study aspects of two of the best known features of solar activity, namely solar prominences and solar flares. Although both these phenomena have been observed for many years our understanding of them is still far from complete. We begin this introduction (Section 1.1) with a description of the basic equations used throughout this thesis and the assumptions involved in their derivation. In Section 1.2 we describe the observations of solar prominences which acts as a background for the theoretical work described in Chapter 2. In Section 1.3 we similarly describe the observations of solar flares giving the necessary background to the work of Chapters 3 and 4. Finally the aims of this thesis are presented (Section 1.4).

1.1 The basic equations

The equations of magnetohydrodynamics (M.H.D.) are the standard electromagnetic and hydrodynamic equations, modified to take account of the interaction between the motion and the magnetic field, and simplified to filter out rapid electromagnetic oscillations. In M.H.D., plasmas are regarded as continuous fluids, whereas plasma dynamics takes account also of particle effects. Thus, although M.H.D. is more restricted in scope than plasma dynamics, it is, as we shall see, generally adequate for solar applications.

The electromagnetic equations are given by Maxwell's equations (here considered in M.K.S. units). With $\underline{J}$ as the current density and $\underline{B}$ as the magnetic induction, we have (eg Cowling, 1976),

$$\text{curl } \underline{B} = \mu \left(\underline{J} + \frac{1}{c^2} \frac{\partial \underline{E}}{\partial t} \right) \quad . \qquad \ldots (1.1)$$

Also

$$\text{curl } \underline{E} = - \frac{\partial \underline{B}}{\partial t} \quad , \qquad \ldots (1.2)$$

$$\text{div } \underline{B} = 0 \quad , \qquad \ldots (1.3)$$

and

$$\text{div } \underline{E} = \rho_c / \varepsilon \qquad \ldots (1.4)$$

where $\underline{E}$ is the electric field intensity, μ the magnetic permeability, ε the dielectric constant, c the speed of light and ρ_c the charge density.

Material moving with velocity $\underline{v}$ is subject to a total electric field of $\underline{E} + \underline{v} \times \underline{B}$. Thus with σ as the electrical conductivity we have Ohms' Law,

$$\underline{J} = \sigma(\underline{E} + \underline{v} \times \underline{B}) \quad . \qquad \ldots (1.5)$$

The hydrodynamic equation of continuity is

$$\frac{\partial \rho}{\partial t} + \operatorname{div}(\rho \underline{v}) = 0 \quad , \qquad \ldots (1.6)$$

where ρ is the mass density, and the equation of motion, in the absence of viscosity, is

$$\rho \left(\frac{\partial \underline{v}}{\partial t} + (\underline{v}.\nabla)\underline{v} \right) = - \nabla p + \rho \underline{g} + \rho_c \underline{E} + \underline{J} \times \underline{B} \quad , \qquad \ldots (1.7)$$

where $\underline{J} \times \underline{B}$ is the Lorentz force, with gravity as the only other body force, $\rho_c \underline{E}$ the electromagnetic force, and p is the gas pressure.

In the M.H.D. approximation the following assumptions are made

(a) The displacement current $\varepsilon \frac{\partial \underline{E}}{\partial t}$ is negligible compared with the conduction current $\underline{J}$.

(b) The plasma is electrically neutral, so that

$$\rho_c \ll \rho \quad .$$

Assumption (b) is necessary for consistency, given assumption (a). This is due to the fact that displacement currents were originally introduced by Maxwell in order to maintain the convention that electric currents always flow in closed circuits, despite the interruption of flow at places where charges pile up, as in the plates of a capacitor. Thus, when displacement currents are negligible, the interruption of current flow as a consequence of charge build-up must also be neglected.

From these assumptions we may deduce that M.H.D. phenomenon must be non-relativistic. This may be shown by the following order of magnitude calculation.

(1.1) gives

$$J \simeq B/\mu\ell$$

while (1.2) gives

$$E \simeq vB \quad .$$

Thus $$\frac{\partial \underline{D}}{\partial t} / \underline{J} \simeq \frac{\mu\epsilon\, vB\ell}{Bt} \simeq \frac{v^2}{c^2} \quad .$$

Hence if $\frac{\partial \underline{D}}{\partial t}$ is negligible we must have $v^2/c^2 \ll 1$.

In the M.H.D. approximation we therefore take Maxwell's equations in the form

$$\text{curl } \underline{B} = \mu \underline{J} \quad , \qquad \ldots (1.8)$$

$$\text{curl } \underline{E} = -\frac{\partial \underline{B}}{\partial t} \quad , \qquad \ldots (1.9)$$

$$\text{div } \underline{B} = 0 \quad , \qquad \ldots (1.10)$$

$$\text{div } \underline{E} = \rho_c/\epsilon \quad , \qquad \ldots (1.11)$$

and by assumption (a) we neglect the electrostatic force $\rho_c \underline{E}$ in the equation of motion (1.7).

Let us now consider the magnetohydrodynamic case, where, for simplicity we neglect gravity. The equation of motion (1.7) reduces to

$$\nabla p = \frac{1}{\mu} (\nabla \times \underline{B}) \times \underline{B} \quad . \qquad \ldots (1.12)$$

It is useful here to note that the $\underline{J} \times \underline{B}$ force may be considered as comprising two parts, namely

$$\underline{J} \times \underline{B} = (\underline{B} \cdot \nabla)\, \underline{B}/\mu - \nabla(B^2/2\mu) \quad . \qquad \ldots (1.13)$$

The first term represents a tension parallel to $\underline{B}$ of magnitude B^2/μ per unit area, while the second term represents a pressure force of magnitude $B^2/2\mu$. A measure of the relative importance of gas and magnetic effects is thus given by the ratio of the gas pressure to the magnetic pressure, which we define as

$$\beta = 2\mu p/B^2 \quad .$$

Returning to equation (1.12) we note that if magnetic effects dominate (ie if $\beta << 1$) the magnetohydrostatic equilibrium may be described by

$$(\nabla \times \underline{B}) \times \underline{B} = 0 \quad , \qquad \ldots (1.14)$$

coupled with the condition that

$$\nabla \cdot \underline{B} = 0 \quad .$$

This limit is known as the "force-free" limit. With $\underline{J} \times \underline{B} = 0$ we see that electric currents flow along the magnetic field lines and

$$\nabla \times \underline{B} = \mu \underline{J} = \alpha \underline{B}$$

where α is a scalar function of position. The curl-free case ($\alpha = 0$) corresponds to zero current flowing in the region while, if $\alpha \neq 0$, we have

$$(\underline{B} \cdot \nabla)\alpha = 0 \qquad \ldots (1.15)$$

so that α is constant along a field line.

It is useful to consider the induction equation

$$\frac{\partial \underline{B}}{\partial t} = \text{curl}(\underline{v} \times \underline{B}) + \eta \nabla^2 \underline{B} \qquad \ldots (1.16)$$

where

$$\eta = (\mu\sigma)^{-1} \quad , \qquad \ldots (1.17)$$

is the magnetic diffusivity. This is obtained by taking the curl of Ohms' Law and using equations (1.8) and (1.10). Equation (1.16) determines the changes in the magnetic field. If the material is at rest we obtain the usual diffusion equation. This form of the equation also holds if

$$R_m = Lv/\eta \qquad \ldots (1.18)$$

is small compared with unity. By analogy with standard fluid dynamics we call R_m the "magnetic Reynolds number". Here L is a length scale comparable with the dimensions of the fluid, and v is a velocity scale comparable with the velocities present in the fluid. When diffusive processes dominate the magnetic field will decay in the characteristic diffusion time,

$$\tau_r = L^2/\eta \quad .$$

Alternatively we may consider the material to be in motion with negligible electrical resistance (or $R_m \gg 1$). In this case equation (1.12) becomes

$$\frac{\partial \underline{B}}{\partial t} = \text{curl}(\underline{v} \times \underline{B}) \quad . \qquad \ldots (1.19)$$

If we consider the rate of change of magnetic flux through a closed contour moving with the plasma it transpires that this flux remains constant if (1.19) is valid. This implies that the lines of magnetic force move with the plasma, and we say that they are "frozen" into the plasma.

Thus, in summary, the basic equations we shall use are the induction equation (1.16), together with the equation of motion

$$\rho \left(\frac{\partial \underline{v}}{\partial t} + (\underline{v} \cdot \nabla)\underline{v} \right) = -\nabla p + \rho \underline{g} + \frac{1}{\mu} (\nabla \times \underline{B}) \times \underline{B} \quad , \qquad \ldots (1.20)$$

the continuity equation,

$$\frac{\partial \rho}{\partial t} + \nabla \cdot (\rho \underline{v}) = 0 \quad , \qquad \ldots (1.21)$$

and the ideal gas equation of state

$$p = R\rho T \quad , \qquad \ldots (1.22)$$

where R is defined in terms of the gas constant ($\hat{R}$) and the mean molecular weight ($\bar{\mu}$) by

$$R = \hat{R}/\bar{\mu} \quad .$$

Equations (1.16), (1.20), (1.21) and (1.22) determine $\underline{B}$, $\underline{v}$, p and ρ in terms of the temperature T which must be given by an energy equation.

The energy equation is a statement of the first law of thermodynamics in a volume of plasma, equating the heat increase per unit time of a unit volume moving in space to the heat influx due to various sources and sinks in the plasma. The form of the energy equation that we shall use throughout this thesis may be represented, for convenience, as

$$\mathbb{E} = \mathbb{J} + \mathbb{H} + \mathbb{K} - \mathbb{R} \quad , \qquad \ldots (1.23)$$

where $\mathbb{E}$ represents the convective transfer of heat and $\mathbb{J}$, $\mathbb{H}$ and $\mathbb{K}$ represent Joule heating, mechanical heating and thermal conduction respectively, while $\mathbb{R}$ denotes the radiative loss.

The convective term $\mathbb{E}$ may be written

$$\mathbb{E} = \frac{\rho^\gamma}{\gamma - 1} \left(\frac{\partial}{\partial t} + (\underline{v} \cdot \nabla) \right) \left(\frac{p}{\rho^\gamma} \right) \quad , \qquad \ldots (1.24)$$

(Boyd and Sanderson, 1969, p55) where γ is the adiabatic index (= 5/3 for a monatomic gas) and the Joule heating term is given by

$$\mathbb{J} = J^2/\sigma \quad . \qquad \ldots (1.25)$$

The mechanical heating mechanism is at present not fully understood. It was, however, generally accepted (eg Raju 1968) that waves propagate up from the convective zone into the corona and "en route" steepen into shock waves which then dissipate and release their energy. Energy is transferred locally by the wave into kinetic energy of the particles subject to the wave motions, so that when a wave dissipates its energy is thermalised by collisions. As a result, dissipation is greater when more particles are present. On these grounds it is generally assumed that the mechanical heat input by wave dissipation is proportional to the density (Weyman, 1960). We thus take the mechanical heating $\mathbb{H}$ to be

$$\mathbb{H} = H\rho \quad . \qquad \ldots (1.26)$$

For several alternative heating mechanisms see Rosner et al (1978).

Next we consider the form for the thermal conduction term $\mathbb{K}$. This is taken to be

$$\mathbb{K} = \nabla \cdot (\underline{\underline{\kappa}} \nabla T) \qquad \ldots (1.27)$$

where $\underline{\underline{\kappa}}$ is the tensor coefficient of thermal conductivity. For heat conducted parallel to the magnetic field, the coefficient of thermal conductivity is

$$\kappa_{11} = \delta_T \, 2 \times 10^{-10} \frac{T^{5/2}}{\ell n \Lambda} \quad \text{Watt deg}^{-1} \text{ m}^{-1} \qquad \ldots (1.28)$$

(Spitzer (1962)) where $\delta_T = 0.225$ for a hydrogen plasma and $\ell n\Lambda$ is the Coulomb logarithm which is tabulated by Spitzer. For conduction perpendicular to the magnetic field the heat transport is affected by electrons spiralling around the magnetic field lines and we find (Spitzer, 1962)

$$\kappa_\perp = 2 \times 10^{-31}\ n^2\ T^{-3}\ B^{-2}\ \kappa_{11} \quad (\text{Watts deg}^{-1}\ \text{m}^{-1}) \quad . \qquad \ldots (1.29)$$

Both these results are valid only in the limit of

$$\omega\tau >> 1 \quad ,$$

where ω is the ion cyclotron frequency and τ is the ion collision time. The full form for the conductivity when $\omega\tau$ is not large is given by Braginskii (1958). Throughout this thesis we shall follow Orral and Zirker (1961) and take

$$\kappa_{11} = 3 \times 10^{-11}\ T^{5/2} \quad (\text{Watt deg}^{-1}\ \text{m}^{-1}) \quad . \qquad \ldots (1.30)$$

From Equation (1.29) we see that for most solar applications $\kappa_\perp << \kappa_{11}$ and transverse conduction is thus negligible. We must, however, be wary of this since there may be cases where the length scales parallel and perpendicular to the magnetic field are such that the heat conducted in these directions are of the same order. Thus our criterion for neglecting perpendicular conduction will be

$$\kappa_\perp/\ell_\perp^2 << \kappa_{11}/\ell_{11}^2 \qquad \ldots (1.31)$$

or, using (1.24) above,

$$\frac{2 \times 10^{-31}\ n^2}{T^3\ B^2} \left(\frac{\ell_\perp}{\ell_{11}} \right)^2 << 1 \quad , \qquad \ldots (1.32)$$

where ℓ_{11} and $\ell_\perp$ are the length scales parallel and perpendicular to the magnetic field respectively.

Finally we must consider the energy loss due to radiation, $\mathbb{R}$. The amount of energy radiated out of an optically thin plasma has been calculated as a function of temperature by several authors (eg Cox and

Tucker (1969), Raju (1968), Doherty and Menzel (1965), Pottash (1965), Hirayama (1964)). For use in analytic problems these results must be simplified, and to this end we shall employ an average of the above results as given by Hildner (1974). He represents the temperature variation by a piecewise linear function, so that the radiative loss per unit volume and time is of the form

$$\mathbb{R} = \chi \rho^2 T^{\alpha} \qquad \ldots (1.33)$$

in each of five temperature regions. The values of the constants χ and α are given in Table 1.

Table 1

Temperature range (^{o}K)	χ (watt kg^{-2} T$^{-\alpha}$)	α
$T < 1.5 \times 10^4$	1.759×10^{-13}	7.4
$1.5 \times 10^4 \leq T < 8 \times 10^4$	4.290×10^{10}	1.8
$8 \times 10^4 \leq T < 3 \times 10^5$	2.860×10^{19}	0
$3 \times 10^5 \leq T < 8 \times 10^5$	1.409×10^{33}	- 2.5
$T \geq 8 \times 10^5$	1.970×10^{24}	- 1.0

We plot this radiative loss function in Figure 1.1, along with some radiative losses from which Hildner derived his approximate version. At this point we must note a major limitation in this form for the radiative loss function, namely the assumption of an optically thin medium. This is fully acceptable only in regions where the temperature is in excess of 10^5 K. It is made here on grounds of simplicity, since for the most part we will only consider the energy equation under coronal conditions. In regions where this assumption is invalid we note that, by definition (eg Sobolev, 1963), less radiation escapes from an optically thick medium than an optically thin one, and we will reduce the output by some appropriate factor.

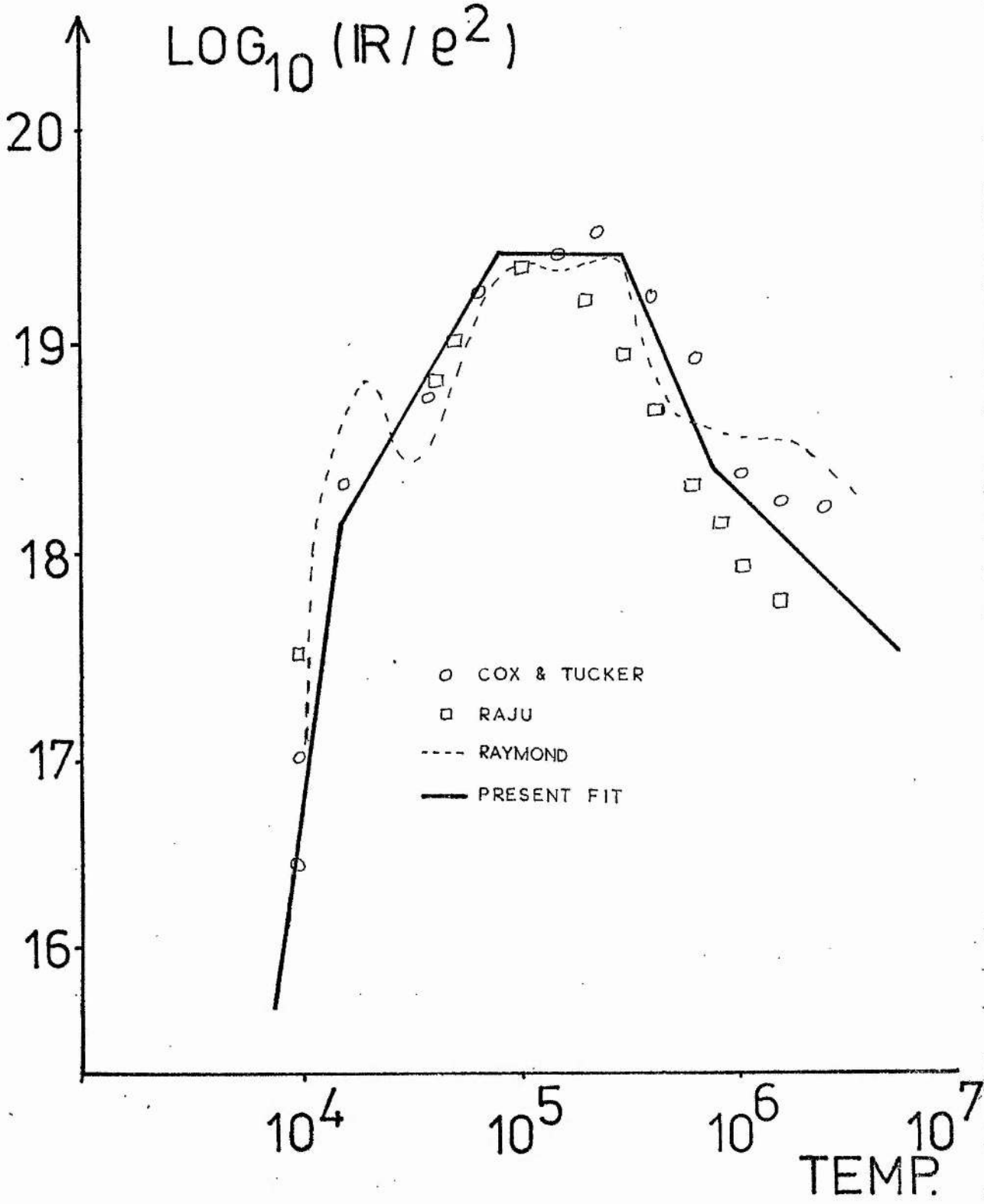

Figure 1.1

Radiative energy loss used throughout this thesis (as defined by Equation (1.33) and Table 1). The present fit is shown by the solid curve with the results as calculated by several authors given for comparison.

1.2 Prominence observations

Prominences are cool, dense objects immersed in the hotter corona. When seen in absorption on the solar disc they are called filaments, but when seen in emission on the solar limb they are generally called prominences. Observational classifications of solar prominences abound, but one of the earliest, due to Secchi (1875), divides them into two classes, namely quiescent and active prominences. The former are long-lived, slowly changing phenomena occurring in quiet regions of the sun, well away from areas of sunspot activity. Active prominences, on the other hand, are short-lived, rapidly changing phenomena seen in and around active regions of the sun. For the purposes of this thesis we shall adopt this classification.

General features

Quiescent prominences are typically 200,000 km long, 50,000 km high and 5000 km thick according to Tandberg-Hanssen (1974) (which acts as a major reference for this Section). Photographs in H_α of quiescent prominences show ragged boundaries and possibly several curves along the length of the sheet. For modelling purposes, however, a sharply bounded vertical sheet is a useful idealisation. These prominences are sometimes connected to the lower regions of the solar atmosphere by so called "feet" (typically two or three along the length of the sheet) in which material streams down from the prominence. The temperature in the centre of these prominences (determined from the optically thin Balmer lines) is of the order of $5{,}000^{\circ}K$, while at the edge and top of the sheet the temperature is about $12{,}000^{\circ}K$ (Bruzek and Kuperus, 1972). The electron number density is in the range 10^{16} to 5×10^{16} m^{-3} (Hirayama, 1971) and is determined from Stark broadening of the high Balmer lines. These values are consistent with gas pressures within prominences of the order of 10^{-3}-10^{-2} Nm^{-2}. Observations along the length of quiescent prominences reveal a

"coronal cavity", where the number density is reduced making the corona more tenuous in the region of a quiescent prominence (Newkirk, 1967; Waldmeir, 1970). This seems suggestive of the prominence forming through condensation out of the ambient corona. Prominence material is generally in approximate horizontal pressure equilibrium with the corona (Hirayama, 1971), thus the vertical pressure gradients are nearly identical. It therefore follows that if the corona is in hydrostatic equilibrium, the dense prominence will require some extra means of support against gravity, probably through an interaction with the magnetic field.

Active region prominences look somewhat similar to quiescent prominences, but are smaller by a factor of three or four. They are only seen inside active regions and have one or both ends attached to a sunspot. The temperature is similar to that in quiescent prominences but the electron number density is larger, with

$$n_e \gtrsim 10^{17}\ m^{-3} \qquad \text{(Hirayama, 1971)} \quad .$$

The lifetimes of prominences vary from one to another but from observations made by d'Azambuja and d'Azambuja (1948) it has been deduced (Martin, 1973) that the average lifetime of active region prominences is 26 days. For quiescent prominences it transpires that the lifetime varies with latitude. Low latitude quiescent prominences last, on average, for 51 days (3 solar rotations) while the corresponding value for high latitudes is 138 days (5 solar rotations). During their lifetime quiescent prominences are subject to a steady poleward drift and due to differential rotation are forced into an East-West orientation. As with sunspots, prominences form at high latitudes in the early stages of the solar cycle, and at progressively lower latitudes as the cycle progresses.

Under sufficiently good seeing conditions, mass motions can be observed in all quiescent prominences. This means that even though the overall shape of such prominences remains essentially unchanged over long

periods of time, the material at any one point in the filament is in motion. On high resolution H_α photographs one sometimes observes that the material is concentrated in thin ropes of diameter less than 300 km (Dunn, 1960), and observations indicate material slowly streaming ($v < 5$ km/sec) down these ropes. The often quoted statement that this filamentation is present in all quiescent prominences is currently being investigated by Zirin (private discussions). He suspects that photographs showing no filamentation are being rejected as evidence on the grounds that the resolution cannot be high enough. Contrary to this viewpoint, he feels that (as one might reasonably expect) photographs showing no filamentation are indicative of no filamentation being present. Superimposed upon this gross downward motion are significantly larger random velocities of the order of 5-10 km/sec (Engvold, 1971). Active region prominences are characterised by motion along the filament. This flow of material is one of the strongest descriptive differences between active and quiescent prominences, since hardly any mass motion is observed along the long axis of a quiescent prominence.

The disappearance of a prominence can occur in one of three ways (Kiepenheuer, 1953): (i) slow dissolution (ii) quasi-eruption and (iii) eruption or "disparition brusque". Method (i) occurs when mass loss due to material flowing into the chromosphere occurs faster than the accumulation of matter into the prominence. Method (ii) is typified by the prominence ascending, breaking into fragments and then flowing into the chromosphere at several places. This is often, but not always associated with a solar flare. Method (iii), which occurs in about half of all low-latitude prominences, involves the prominence material rising and disappearing. Most of the material rises high into the corona, while the rest flows back to the solar disc. For about one third of all cases this disappearance is permanent, while for the rest the prominence reforms

with nearly the same shape as before, usually within a day or two. It is thought that every quiescent prominence suffers at least one sudden disappearance during its life.

Prominence magnetic fields

Limb observations of quiescent prominences give a line-of-sight magnetic field B_{11} that generally ranges from less than 0.5G (1G = 1 gauss = 10^{-4} Tesla), ie no observable field, to 30 or 40G (Tandberg-Hanssen, 1974). From a study involving 135 quiescent prominences Tandberg-Hanssen found the average value of the horizontal field $\langle B_{11} \rangle$ to be 7.3G, with half of the observations in the range $3G \lesssim B_{11} \lesssim 8G$. Rust (1966) measured the line-of-sight magnetic fields in about 80 quiescent prominences and found the following results: (i) Prominences are found where the field lines connecting two photospheric regions are expected to be horizontal and the polarity of magnetic fields within prominences are consistent with these fields threading the prominence. (ii) $\langle B_{11} \rangle \simeq 5G$, with no preferred orientation relative to the long axis of the prominence. (iii) The magnetic field intensity B_{11} increases by a factor of roughly 1.5 over the height of a quiescent prominence. Harvey (1969) echoed these conclusions and found $\langle B_{11} \rangle \simeq 6.6G$.

The question of the magnetic field orientation with respect to the long axis of the prominence was tackled by Tandberg-Hanssen and Anzer (1970). Using 70 quiescent prominences for which a plane-parallel sheet was a good approximation, as the prominence passed across the disk they observed the line-of-sight magnetic field strength variation with the angle between the line-of-sight and the prominence axis. They then assumed a distribution function for the fraction of prominences which have a total magnetic field of strength B_o, say, oriented at an angle α to the prominence axis, and concluded that the average angle between field and axis was $\bar{\alpha} = 15^o$ for the prominences considered. This implies that the

magnetic field in a typical quiescent prominence traverses the prominence at a small angle to the long axis. Implicit in this work, however, was the assumption that the value of the field strength does not affect the angle α. Rust (1972) has suggested that there is some evidence of a relationship between the strength of a magnetic field and its direction in quiescent prominences. He tentatively suggests a possible relationship of the form

$$\alpha = 90^{o} \left(\frac{B_{max} - B}{B_{max}} \right) \quad ,$$

where $$B_{max} \simeq 30G \quad .$$

Similar studies of active region prominences suggest line-of-sight field strengths typically in the range 20G-70G, much larger than quiescent prominence values. At present no results are available for the magnetic field alignment within active region prominences.

1.3 Solar flare observations

As is the case for all astronomical features a wealth of categorisations exist for solar flares. Two basic types are of interest here, namely the simple, compact flare and the two-ribbon flare. The simple, compact flare occurs in a unipolar region or near a simple sunspot and is sometimes accompanied by a surge or stream of plasma (with average number density of 10^{16} m^{-3}) which is ejected for a period of up to 500 seconds. A two-ribbon flare takes place near an active region filament and is characterised by two ribbons of H_{α} emission which move slowly apart during the main phase of the flare. These two-ribbon flares occasionally appear in regions completely devoid of sunspots. Thus the relative simplicity of the field structures for both these events makes it important to try to understand them before considering flares associated with more complex sunspot fields.

In many cases, however, the flare event is inherently complex.

It is therefore necessary in any attempt to describe solar flares to consider the general features which are common to all flares. To this end we split the flare event up into four phases, which are indicated in Figure (1.2). Following Priest (1976) we note that the preflare phase is characterised by soft X-ray (< 10 keV) emission in the upper chromosphere and lower corona lasting for several minutes or so before the flare onset. These emissions are a result of enhanced thermal emission from the coronal plasma. Another type of flare precursor is observed when a quiescent filament is close to the position of the flare. It becomes activated minutes or tens of minutes before the flare occurrence. This gives evidence that in many (and possibly all) cases, changes in the magnetic field start tens of minutes before the flare onset. Note that these preflare changes are of a non-eruptive nature since disruption of the filament only occurs when the flare properly begins.

The actual flare event shows two basic stages. Initially there is a flash phase, which lasts typically 300 seconds, during which the intensity and area of the emission rapidly increase in value. The flash phase is then followed by the main phase, where the intensity slowly decreases over a period of the order of 3000 seconds. An impulsive phase (seen in the high energy part of the spectrum) is sometimes present for between 100 and 1000 seconds at the start of the flare. Flares with this phase present occur predominantly (perhaps exclusively) in magnetically active regions. The impulsive phase is indicated by the appearance of a microwave burst and a hard X-ray burst (> 30 keV). The structure of the hard X-ray emission is somewhat spikey, with the smallest time scales being about 2 seconds in moderate events and 10 seconds in large ones. These emissions give a time scale for electron acceleration during the impulsive phase, and some of the largest events show a distinct second hard X-ray component, which may be a result of a second phase of particle acceleration.

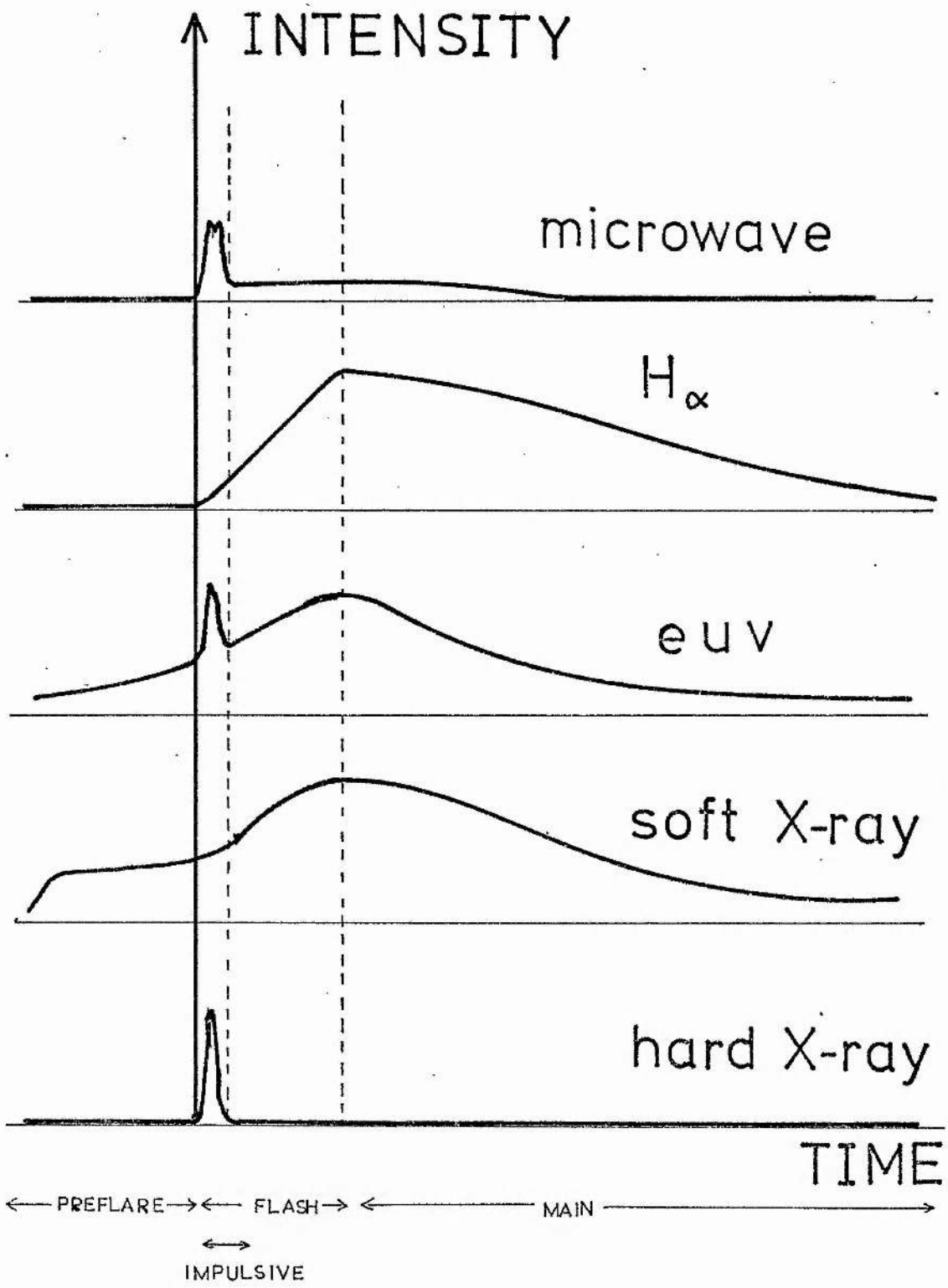

Figure 1.2

A schematic representation of the flare intensity in several wavelengths. Typical time scales for the various phases are preflare - ten minutes: impulsive - one minute: flash - five minutes, and main phase - one hour. (From Priest (1978)).

The electron density in flare elements in the chromosphere is of the order of 10^{19} m^{-3} in the maximum phase of flare development (Kurochka, 1970; Svestka, 1965; de Feiter, 1966; Svestka, 1963) while the density of hydrogen atoms in a major chromospheric flare must be at least 10^{20} m^{-3} (Svestka 1976). The density decreases with height however. It is of the order of 10^{18} m^{-3} just above the chromosphere, and of the order of 10^{16} m^{-3} at a height of about 20,000 km above the chromospheric base. In general we may say that the density in flares is one or two orders of magnitude higher than in the quiet sun throughout the chromosphere, transition layer and low corona.

According to Svestka (1976) the electron temperature in flare elements emitting in hydrogen is less than 10,000K (and in some cases as low as 7000K) in the chromosphere, and slightly higher than 10,000K in the cold flare parts seen in hydrogen above the limb. However, flares are greatly inhomogeneous in temperature in the lower corona since one observes distinct flare parts with temperatures of the order of 10^4K and 10^7K respectively, occuring at the same height.

Some flares are accompanied by spray prominences in which gaseous material is ejected into the corona with speeds in excess of the gravitational escape velocity. In some rare cases a whole portion of the flare is expelled into the corona as a spray. Another common accompaniment to flares in the surge prominence where dense material at first ascends and subsequently descends with velocities of the order of 100 km s^{-1}. Surges differ from sprays, however, in the fact that they do not require a flare to occur and in fact a great number of surges occur without flares. Two-ribbon flares, in particular in sunspot groups, are often accompanied in H_α light by loop prominences which span the two bright ribbons, rise upwards and survive for many hours after the flare decay. The observation of very broad spectral lines in the loop prominences is indicative of non-

thermal particles trapped in flare-associated magnetic loops.

One of the most important features of solar flares is the large amount of energy released. This varies from around 10^{22} Joules in a small subflare to as much as 3×10^{25} Joules in the largest of events. In his recent review of the solar flare phenomenon Priest (1977) gives the following breakdown of types of energy present in the large events:

Electromagnetic radiation up to X-rays	10^{25} J
Interplanetary blast ware	10^{25} J
Fast electrons (Hard X-rays)	5×10^{24} J
Subrelativistic nuclei	2×10^{24} J
Relativistic nuclei	3×10^{24} J
Total energy output	3×10^{25} J

He also points out that a recent estimate (Brown, 1975) suggests the hard X-ray contribution may be as much as 2×10^{25} J.

In general, observations show that complex, rapidly evolving active regions are the most likely flare producers, as opposed to simple bipolar regions, which show little flare activity. One finds that the first brightening in H_α often occurs where the magnetic field gradients are the steepest - that is, where spots of north and south polarity lie closest to one another. Also, there are no large scale changes in the photosphere beneath a flare. Variations in the magnetic flux through sunspots during a flare are due to normal evolutionary changes (Rust, 1976). Flares also have the property of sometimes repeatedly occurring in the same place with very similar characteristics.

Thus, in seeking a model of solar flares we must find some source of instability in large, complex sunspot groups which may be triggered by a smaller event, but which may build up day after day at the same point and in the same configuration. In view of these considerations, and the fact that other sources of energy seem inadequate (eg Zirin, 1966),

it has usually been assumed that it is the magnetic field which supplies the energy for a flare. (The total energy for a large flare would, in fact, be released if the whole of a magnetic field of strength 500 gauss within a cube of 3×10^4 km were annihalated). However, two problems arise from this supposition. Firstly, does the flare energy come into the atmospheric layers from below, during or immediately before the flare process itself, or is it brought there earlier and stored in the solar atmosphere for some time prior to the flare? Secondly, in what form does this energy become available for the actual creation of flares as observed?

In the rest of this Section we will address ourselves to the first problem, with a view to understanding possible "trigger" mechanisms for a major flare event. This emphasis is necessary in order to provide an introduction to the work presented in Chapters 3 and 4. We shall not discuss in detail the observations of, or proposed models for particle acceleration effects in the main phase of a solar flare. The interested reader is referred to either Smith and Smith (1963), or the more recent book by Svestka (1976) for detailed discussion of all aspects of observation and theory, and also a comprehensive bibliography.

Preflare observations and theories

Recently some very high quality H_α photographs of flares have enabled Zirin (1974) to give a detailed description of the development of the H_α flare. He stresses that the majority of flares arise after the emergence of new magnetic flux from below the photosphere. This fact is indicated by the appearance of small satellite sunspots appearing close to large sunspots of the opposite polarity (Rust, 1968; Martres et al, 1968). It appears that flares are especially likely when the satellite is of "following" polarity and emerges just in front of the large spot which has "preceding" polarity. We note here that observations of changes in fibril direction sometimes indicate reconnection of the magnetic field during the

course of a flare. A particular case which strongly indicates this fact is described by Priest (1977). Zirin also finds that large flares may begin at several points and then spread over a large area, giving the impression that the initial flare energy does not simply spread out but stimulates an extra energy release over a large region.

It has long been known (Severny, 1958) that flares tend to occur near the "polarity inversion line", along which the longitudinal (line-of-sight) magnetic field component changes sign and the field is largely horizontal. Rust (1972) has now shown that the location of the impulsive phase H_α kernels lies within 10 arc seconds of that part of the neutral line which skirts a satellite spot. He also showed that flare related photospheric field changes are generally confined to the satellite spots, which show an increase in strength during the preflare phase, followed by a decrease during the flare itself. It appears to be the fact that these satellites are evolving which gives rise to flares, although there is no way of predicting whether the resulting flare will be large or small.

In some cases motions have been observed in the photosphere underlying a flare site. Large scale mass motions were observed by Yoshimura et al (1971) although any relation between these and the flare is doubtful according to Svestka (1976). Upward motions before the flare followed by downward motions during and after the flare were observed by Rust (1973), and these upward motions are considered by Harvey (1974) to be a general preflare property. Harvey also stresses that flares occur when there are shearing motions (see also Zirin and Tanaka, 1973) while Levine and Nakagawa (1974) find flare activity to be located where the rate of strain is a local maximum and the vertical magnetic field or field gradient is zero.

The above observations have stimulated several theoretical approaches to the question of the preflare state. In general the preflare

phase is regarded as one of slow passive evolution of the magnetic configuration, during which the energy is stored in excess of potential. The resulting configuration must be either in force-free or current sheet configuration, since the plasma pressure gradients are several orders of magnitude smaller than the Lorentz forces. The fact that the preflare magnetic state is in many cases highly twisted or sheared led Tanaka and Nakagawa (1973) to consider energy storage in a force-free field. In fact, energy may be stored in a simple magnetic flux loop by twisting the ends and creating a force-free field, which becomes kink unstable when the field line completes more than one revolution about the axis (Raadu, 1972). However, the amount of energy stored in such a loop is too small for a large flare, and Tanaka and Nakagawa showed that sufficient energy can be stored in a more general force-free field. In fact several theories propose the idea that the magnetic configuration evolves passively through a series of equilibrium states until a critical value is reached by some parameter such as twist or shear. At this point the equilibrium becomes unstable and the flare is initiated. These theories, which apply to arcade-like magnetic fields (as an approximation to the observed polarity inversion line where two-ribbon flares occur) are discussed in detail in the introduction to Chapter 3.

Another approach is given by the emerging flux model (Heyvaerts et al, 1977) which suggests that the energy for a two-ribbon flare is stored in a sheared force-free field near a polarity inversion line, but that the release of this energy is triggered by the presence of a relatively small region of emerging flux. When the emerging flux reaches a critical height at which thermal equilibrium is lost, the resistivity in the current sheet formed between the old and new flux increases by several orders of magnitude to a turbulent value. This has the effect of destabilizing the overlying large scale field and causing

fast reconnection. An alternative means of obtaining an anomalous resistivity, particularly in the case of fast emergence of new flux, is proposed by Heyvaerts and Kuperus (1978). The emerging flux model will be considered again in Chapter 4.

An alternative to the above models is proposed by Piddington (1973, 1974). He supposes that the energy is stored below the photosphere in the form of helical twists in the magnetic fields of sunspots, and it is brought into the corona by hydromagnetic disturbances (Alfvén waves) during the flare. The helically twisted magnetic field unwinds into the atmosphere thereby releasing kinetic energy by the upward propagation of the disturbances. The Alfvén waves are assumed to be generated by interactions between the magnetic flux strands or by kinks in the strands. Svestka (1976, p523) quotes a criticism of this model due to Altschuler who points out that helical twists do not produce waves in any simple way. Piddington's model is largely qualitative and much work must be done to put the model on a firm footing.

Alfvén and Carlquist (1967) proposed a model in which a magnetic flux tube undergoes an M.H.D. instability, resulting in a local increase in the current density. The effect of the instability is to cause a local density rarefaction, so that the electrical conductivity tends to zero and the current flow is interrupted. Particles are accelerated to high energies while the flux tube untwists and all its excess energy is dumped at the site of the instability in a time of the order of 100 seconds. A serious criticism of the model is due to Smith and Priest (1972), who point out that Alfvén and Carlquist argued by analogy with a laboratory experiment and suggest that the instability relevant to the solar atmosphere is the ion-acoustic instability. This has the effect of producing plasma turbulence which gives rise to a turbulent resistivity, which in turn may possibly prevent any efficient acceleration of particles

to suprathermal energies. Thus heating as opposed to acceleration would be expected from the amended model. The question has not yet been settled since Spicer (1975) claims that particle simulation experiments confirm the validity of Alfvén and Carlquist's model.

Several authors (Sturrock, 1973; Hudson, 1973; Hirayama, 1974; Hirayama and Endler, 1975) have suggested that the coronal flare is hot gas that has "evaporated" from the chromosphere. The scenario for these models is basically as follows. High energy particles are accelerated in the corona down towards the chromosphere. They thus heat the chromosphere and hence the hot chromospheric gas rises to the corona. This becomes the hot condensation which emits soft X-rays, while the H_α emission is due to heat conduction between the evaporated chromospheric gas and the cooler chromosphere. These models unfortunately depend upon an initial particle stream heating to cause the flare. This fact seems unlikely since the preflare phase of flare development appears to be largely thermal and many flares show mainly thermal behaviour throughout their life. Only in some flares do we observe particle beam effects, and then often only for a short time during the flash phase.

In the above we have considered only a few of the many models available for the solar flare event. A more extensive summary of the published theories together with details of observational results, is given by Svestka (1976).

1.4 Aims of this thesis

For the remainder of this thesis we shall be concerned with certain aspects of solar prominence and flare theory. In this opening chapter we have given a brief review of the observations relevant to these phenomena. In each of the following chapters we shall include an introductory section which describes some existing theories in more detail. We present the material in this way in the hope that each chapter will be

largely self contained.

In Chapter 2 we consider the static equilibrium of a quiescent prominence. Our aim is to develop a single model which will simultaneously explain the support mechanism for the dense prominence material and take account roughly of the necessary energy balance. The model contains two parameters, namely the coronal plasma beta and the horizontal shear angle, Φ, that the magnetic field lines make with the prominence normal. We obtain limits on both these parameters which, when exceeded imply that no equilibrium state is possible. The novel feature of this model is the more realistic coupling of the magnetohydrostatics and the energetics, and the results obtained provide a possible explanation for several prominence features.

In Chapter 3 we consider solutions to the force-free field equations (1.14) which may be of relevance to solar flares. As we have seen in Section 1.3 the solar flare is a remarkably complex event and as such we only consider a small part of the flare problem, namely a possible trigger mechanism for the rapid release of energy in the flare. Our main aim is to seek simple analytic solutions which may exhibit the feature of instability when the photospheric shear exceeds a critical value (as discussed in Section 1.3).

In Chapter 4 we consider an alternative candidate for a flare trigger mechanism; this time in the shape of a current sheet, as described in the emerging flux model of Heyvaerts et al. A one-dimensional model for current sheets in general is developed, where the conditions within the sheet are given in terms of non-dimensional parameters which describe the external conditions. These results are then applied to the emerging flux model for solar flares.

Finally, in Chapter 5, we consider a feature common to all the previous work, namely the possibility of non-equilibrium. We shall briefly

discuss this feature and its possible applications, as well as our conclusions and suggestions for future work.

Chapter 2: A MODEL FOR QUIESCENT PROMINENCES

In this chapter a one-dimensional model is computed for a quiescent prominence in both magnetohydrostatic equilibrium (under a balance between gravity, pressure gradients and the $\underline{J} \times \underline{B}$ force) and also thermal equilibrium (under a balance between thermal conduction, radiation and wave heating). The effects of changing the coronal plasma pressure p_1, the horizontal magnetic field B_x, and the inclination Φ of the horizontal magnetic field to the prominence normal arc investigated. It is found that an equilibrium state is impossible when either the coronal plasma beta ($\beta = 2\mu p_1/B_x^2$) or the magnetic field shear Φ is too large. The limit on the plasma beta leads to a minimum possible height for prominence formation, and implies that active region prominences can form lower in the atmosphere than quiescent ones. It also gives a reason for the existence of feet in quiescent prominences. Exceeding the maximum shear may explain the eruption of a prominence.

We begin by discussing the previous work on this subject.

2.1 Previous work

To date the major part of the theoretical work on prominences has fallen into two categories, namely

(a) the consideration of a magnetic field to show that a volume of denser material can be supported against gravity in the solar atmosphere,

(b) the examination of the energy balance of an idealised fully-formed prominence to show that the achieved state is energetically stable.

Problem (b) has been considered by a number of authors (eg de Jager 1959, Ivanov-Kholodny 1959, Orrall and Zirker 1961, Jefferies and Orrall 1963, Hirayama 1963, Doherty and Menzel 1965, and Poland and Anzer 1971). Most of these models, however, ignore the presence of a

magnetic field, apart from invoking its property of inhibition of thermal conduction. We shall turn our attention mainly to the work in category (a).

Since observations suggest that quiescent prominences are approximately in horizontal pressure balance with the ambient corona throughout their height, we may infer that the vertical pressure gradients within prominences are much the same as in the ambient corona. The fact that the density is several orders of magnitude larger within a prominence than in the corona implies that the gas pressure alone cannot provide a support mechanism and we must thus turn to the local magnetic field.

From equation (1.20) we see that a prominence is in magnetostatic equilibrium when

$$\nabla p = \rho \underline{g} + \frac{1}{\mu} (\nabla \times \underline{B}) \times \underline{B} \qquad \ldots (2.1)$$

is satisfied throughout. In addition we require

$$\nabla \cdot \underline{B} = 0 \quad . \qquad \ldots (2.2)$$

Now since the length of a prominence is large compared to the other dimensions it is convenient to consider the two-dimensional problem with the prominence represented by a sheet of infinite length. We thus consider the coordinate system with z vertical, x normal to the prominence sheet and y along the length of the sheet with $\frac{\partial}{\partial y} \equiv 0$. A further simplification (due to Kippenhahn and Schlüter, 1957) arises from the fact that B_x varies slowly with x. If we thus take B_x independent of x and neglect variations with height, z (since prominence widths are much smaller than their heights) we obtain the one-dimensional system

$$\frac{dp}{dx} + \frac{B_z}{\mu} \frac{dB_z}{dx} = 0 \quad , \qquad \ldots (2.3)$$

$$\frac{B_x}{\mu} \frac{dB_z}{dx} = \rho g \quad . \qquad \ldots (2.4)$$

Menzel (Bhatnagar, Krook and Menzel, 1951) was the first to propose a magnetic field configuration which satisfies (2.1) and (2.2), coupled with the ideal gas law

$$p = R\rho T \qquad \ldots (2.3)$$

and the assumption of constant temperature, and will stably support material against gravity. His suggested field configuration is shown schematically in Figure 2.1. In it excess mass is supported by the magnetic tension in the field at $x = 0$.

An alternative field configuration, due to Dungey (1953) is shown schematically in Figure 2.2. Here the electrical current flows only along the prominence axis, and the prominence material is completely enclosed by field lines. Although this model has the useful feature of thermal insulation provided by the closed field lines it unfortunately requires (as pointed out by Cowling; 1957) the unlikely situation of large currents running in opposite directions in close proximity.

The most generally accepted model in the current literature is that proposed by Kippenhahn and Schlüter (1957). For most of their work they assumed the prominence to be infinitely thin and the magnetic field to have a discontinuity in the vertical component at the prominence sheet. When the gas pressure is considered and the infinitely thin assumption relaxed, they obtained solutions, for an isothermal medium, to (2.3) and (2.4), of the form

$$B_z = B_{z\infty} \tanh \left[\frac{B_{z\infty}}{2B_x} \frac{x}{\Lambda} \right] , \qquad \ldots (2.5)$$

and

$$p = \frac{B_{z\infty}^2}{2\mu} \operatorname{sech}^2 \left[\frac{B_{z\infty}}{2B_x} \frac{x}{\Lambda} \right] , \qquad \ldots (2.6)$$

where it is demanded that

$$B_z \to B_{z\infty} \quad \text{and} \quad p \to 0 \quad \text{as} \quad x \to \infty ,$$

and Λ is the scale height ($= RT/g$).

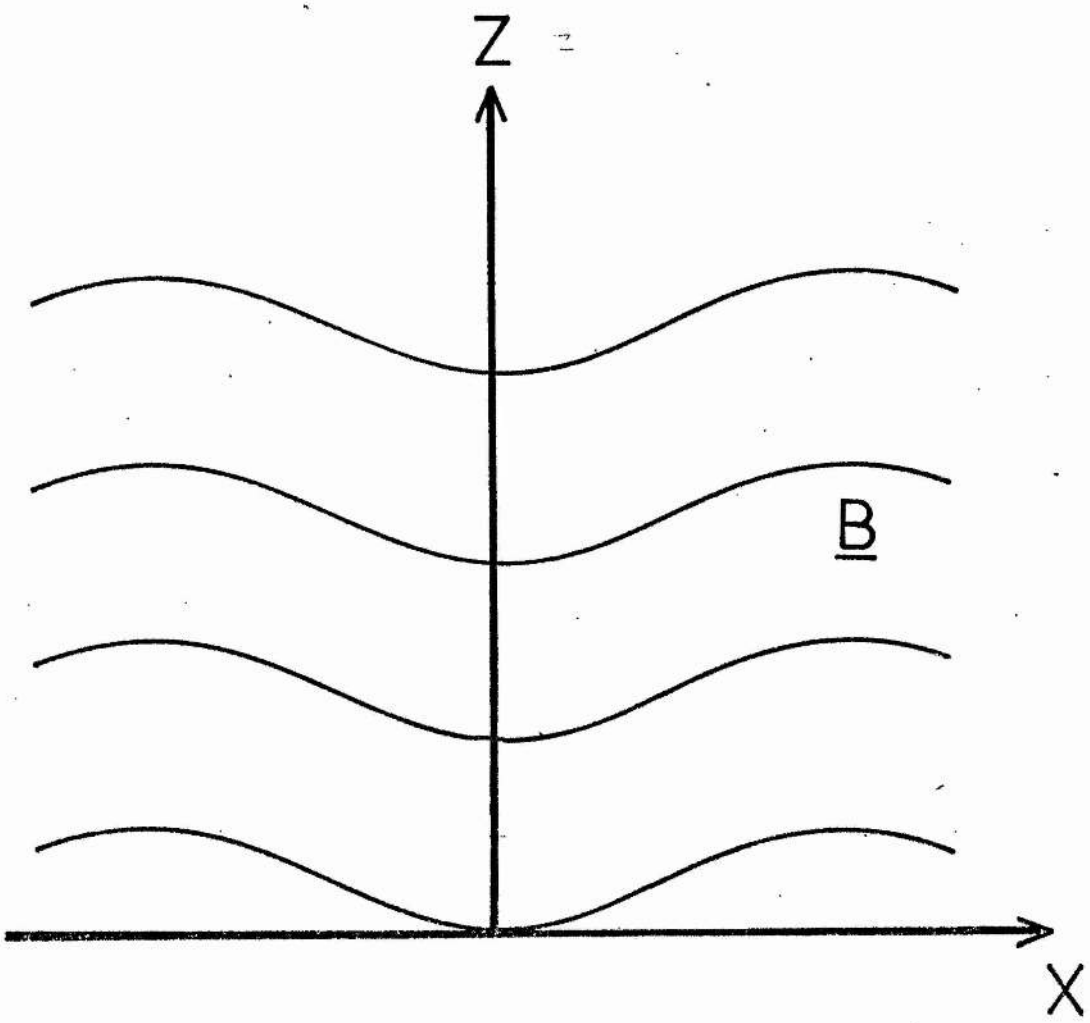

Figure 2.1

Schematic representation of the supporting magnetic field in Menzels' model (see text).

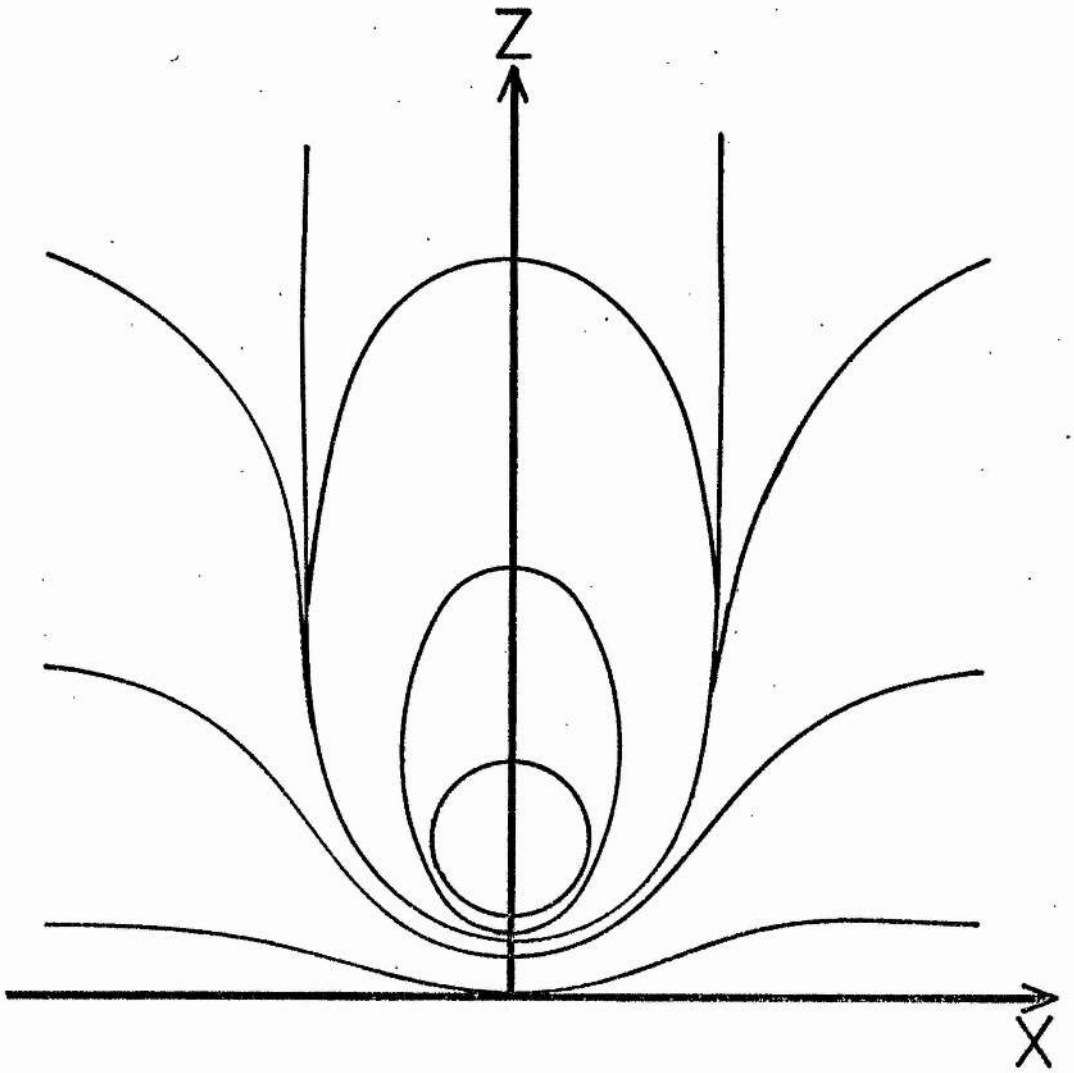

Figure 2.2

Schematic representation of the supporting magnetic field in Dungeys' model (see text).

These solutions are shown schematically in Figure 2.3. Kippenhahn and Schlüters' model allows for number densities of the order of 10^{17} m^{-3} for magnetic fields of only a few gauss threading the prominence.

The three models considered above (Bhatnagar et al, Dungey, Kippenhahn and Schlüter) have all been compared and treated in a uniform way by Brown (1958). Brown showed that for an isothermal medium the pressure, density and field may be regarded as depending only on one scalar function of position, with this function differing in each of the three models. Using a variational technique due to Bernstein et al (1958) he tested the stability of the models against displacement, and found all three models to be stable against vertical displacement. Kippenhahn and Schlüter (1957) considered the stability of their model against both vertical and horizontal displacements and concluded that up to a certain height the model is stable if (i) some of the field lines are sufficiently bowed by the weight of the prominence material that they penetrate the solar surface, and (ii) if the strength of that portion of the total field which is not due to currents within the prominence increases with height in the prominence mid plane.

This stability analysis was extended by Anzer (1969) who derived the stability conditions for an infinitely thin prominence in terms of the total magnetic field in the prominence. These were that, at the mid plane of the prominence, we require

$$[B_z] \frac{dB_x}{dz} \gtrsim 0 \qquad \ldots (2.7)$$

and

$$B_x \frac{d[B_z]}{dz} \lesssim 0 \qquad \ldots (2.8)$$

for stability, where $[B_z]$ denotes the jump in the vertical component of the magnetic field as the thin prominence is traversed in the x direction. He also considered the effect of a uniform field component along the prominence axis and concluded that the stability and equilibrium conditions

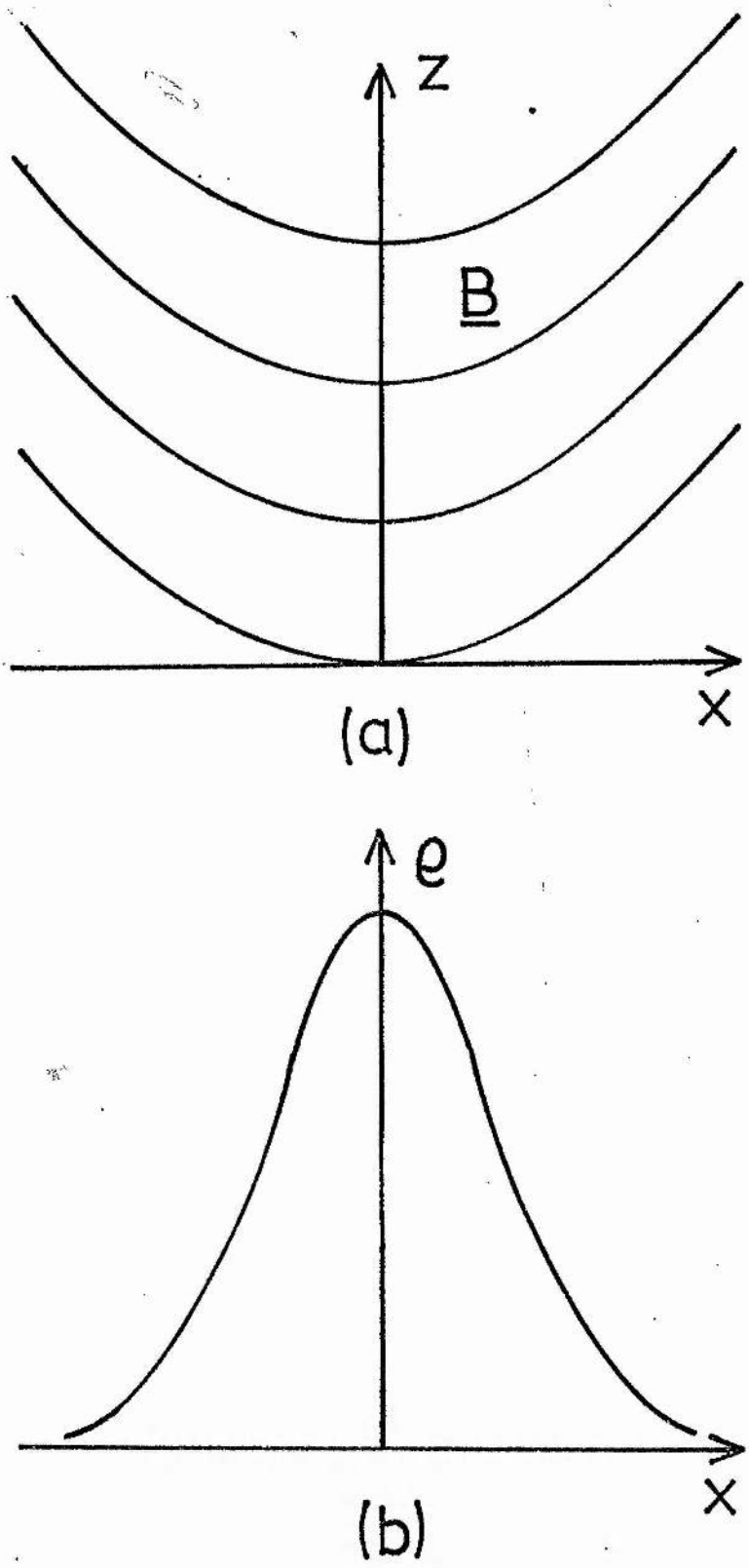

Figure 2.3

Schematic representation of (a) the supporting magnetic field in the vicinity of the prominence for the model of Kippenhahn and Schlüter (see text). (b) the corresponding density profile for the above magnetic field.

are unaffected. We note that although observational evidence indicates that (2.7) is satisfied in quiescent prominences nothing at present may be said about the condition (2.8).

The observations of Rust (1966) and Harvey (1969) that the magnetic fields in prominences apparently have no prefferred orientation with respect to the prominence axis led Nakagawa and Malville (1969) to consider the possibility that the shear between the prominence magnetic field and a field below the prominence might provide support. They considered an upper half-space of plasma permeated by a uniform horizontal magnetic field supported against the vertical pull of gravity by a uniform horizontal magnetic field of arbitrary orientation in the vacuum of the lower half-space. They linearised the M.H.D. equations, neglected radiation and thermal conduction, and investigated the stability of the interface between the upper and lower half-spaces as a function of the angle between the magnetic fields in the two regions. The fastest growing unstable mode is obtained from the resulting dispersion relation, and has a wavelength which predicts the break up of a prominence into regularly spaced regions. Nakagawa and Malville suggest this as an explanation for the often observed arch structure, or feet, of quiescent prominences. The angle of shear between the lower and upper field affects the wavelength at which the instability occurs, and by comparing this wavelength with the observed spacing, they predict this angle to be between 60° and 90°.

A radical alternative to these support mechanisms is suggested by Malville (1976). His main aim is to explain the slow ($v \lesssim 5$ km/sec) downward movement of material that is often observed in quiescent prominences. Higher velocities are observed in many active prominences. Since the observed velocity is much less than the free fall velocity for the solar atmosphere, some process opposing gravity must be present. Malville considers this process to be the Lorentz force acting on a particle

falling along a vertical, twisted flux rope. Thus a terminal velocity v_T for the ions will be reached when

$$m_i\, g = e(\underline{v}_T \times \underline{B})_z \quad .$$

The results, which depend on both the strength and pitch of the vertical magnetic field, suggest terminal velocities of the order of 2-10 km/sec for quiescent prominences while for active prominences terminal velocities of 100-300 km/sec are predicted. Much work is still required to put this model on a firm footing. In particular one must show that the system is stable in order to explain the longevity of quiescent prominences, and also some reason (at present lacking in the model) must be given to explain the fact that prominences occur along polarity inversion lines.

All the above mentioned authors have avoided the question of energy balance by assuming an isothermal plasma. Recently, however, several attempts have been made to combine the magnetostatics and energetics in a single model. Low (1975 a,b) formulated the problem in terms of the scalar potential A(x,z) where

$$A(x,z) = B_o(z + F(x)) \quad ,$$

and $$B_x = -\frac{\partial A}{\partial z} \quad , \quad B_z = \frac{\partial A}{\partial x} \quad , \quad B_y \equiv 0 \quad .$$

Substitution into equations (2.1) and (2.2) gives, on using the ideal gas law, that

$$p(x) + \frac{B_o^2}{2\mu} (F'(x))^2 = \text{constant}$$

and $$p(x) + \frac{R\, B_o^2\, F''(x)\, T(x)}{\mu g} = 0 \quad .$$

Thus we have the equation for F(x)

$$\frac{R}{g} F''(x)\, T(x) + \frac{1}{2} (F'(x))^2 + \text{constant} = 0 \quad ;$$

where T(x) is free to be specified. Taking $T \propto (F(x))^{\gamma}$ Low specifies γ such that the temperature function is consistent with the solution of an

energy equation where thermal conduction is balanced by a heat sink proportional to the density. The major drawbacks with his approach are that the energy equation used is completely unrealistic and despite this assumption the resulting equations are still not amenable to analytic solution. To counteract this second difficulty Lerche and Low (1977), using the same formulation with the same heat loss term, further assume an isotropic thermal conduction coefficient, linear in temperature T. There is no physical basis for this assumption. A further unrealistic feature of these models is that the problem is treated as an initial value problem with all conditions applied at the prominence centre, and no consideration given to coronal boundary conditions.

Another attempt to couple the M.H.D. and energy equation has been made by Heasley and Mihalas (1976). They consider a slab model with a Kippenhahn - Schlüter support mechanism coupled with equations of radiative transfer. The system of equations is solved using techniques developed for the calculation of model atmospheres of early-type stars subject to the constraints of radiative, hydrostatic and statistical equilibrium (Mihalas et al, 1975). They considered only the central, low temperature region of prominences and as such, neglected thermal conduction in the energy balance. Thus the requirement that the prominence plasma match on to the external corona within a reasonable distance from the prominence centre is not considered. Also, since a magnetic field along the prominence axis will tend to insulate the central material, the neglect of thermal conduction removes any effect of shearing the magnetic field from the energy balance. A number of models are considered by Heasley and Mihalas ranging from isothermal and isobaric models to one in which magnetohydrostatic equilibrium is coupled with the radiative transfer equations. For the most part Heasley and Mihalas consider the simpler problems, where the question of support is avoided and conclude that

radiative equilibrium models require diffuse penetration of the radiation field into the prominence slab (cf Hirayama, 1964). In the latter model, however, it was found difficult to obtain prominence widths in excess of a few hundred kilometers, with the greater widths occurring, in general, as the external pressure was reduced, or the transverse magnetic field strength increased.

2.2 Basic equations

In the following we shall consider an extension of the Kippenhahn - Schlüter (1957) model to include thermal effects. To this end we adopt an energy equation which expresses a balance between thermal conduction, radiative loss and wave heating. Following Kippenhahn and Schlüter we shall model the prominence by an infinite vertical sheet, of finite width with variations allowed only in the x-direction across the width of the sheet (see Figure 2.4). Apart from the one-dimensional nature of the model, the main limitation lies in adopting an optically thin form for the radiative loss term. This is fully acceptable only in the outer layers (above 10^5 K) of the plasma sheet. Nonetheless it is made here on grounds of simplicity, since we are primarily concerned with discovering the effect of the magnetic field on the overall structure of the prominence, rather than obtaining an absolute prediction of the temperature within the prominence. The present model should therefore be considered as a necessary preliminary to the coupling of the magnetostatics with the transfer equation in a fully self-consistent manner.

The equations of static equilibrium (in m.k.s units) are repeated here for convenience. The magnetohydrostatic equation, representing a balance between pressure gradients, gravity and the Lorentz force, is

$$\nabla p = \rho \underline{g} + (\nabla \times \underline{B}) \times \underline{B}/\mu \quad . \qquad \ldots (2.1)$$

We also assume the ideal gas law

$$p = R\rho T \quad . \qquad \ldots (2.3)$$

The energy equation, for a balance between thermal conduction, radiation (optically thin), and mechanical heating (assumed proportional to the density), is taken in the form

$$\nabla \cdot (\underline{\underline{\kappa}} \nabla T) = \chi \rho^2 T^{\alpha} - H\rho \qquad \ldots (2.9)$$

where all variables are as defined in Chapter 1. In particular χ and α are known piecewise constants (given by Table 1 in Chapter 1) while the constant H, which is determined by the condition that at the coronal temperature and density the heating balances radiation, is a measure of the importance of heating.

For coronal values, of the two components of $\underline{\underline{\kappa}}$, $\kappa_{\perp}$ is much less than κ_{11} (as defined in Chapter 1). We shall thus consider only conduction parallel to the magnetic field and write

$$\nabla \cdot (\underline{\underline{\kappa}} \nabla T) = \nabla \cdot \left(\kappa_{11} \frac{\partial T}{\partial s} \hat{\underline{s}} \right) \qquad \ldots (2.10)$$

where $\hat{\underline{s}} = \underline{B}/B$ is the unit vector in the direction of the magnetic field. Following Kippenhahn and Schlüter, we assume that all the variables depend on x alone, and take the magnetic components as

$$\underline{B} = (B_o \ , \ B_y \ , \ B_z(x)) \quad ,$$

the horizontal components $B_o \, \hat{\underline{x}}$ and $B_y \, \hat{\underline{y}}$ being constant so as to satisfy div $\underline{B} = 0$ identically. The z-axis is vertical, the x-axis normal to the infinite sheet and y is directed along the prominence. (See Figure 2.4).

We shall, for convenience, introduce dimensionless (barred) variables as follows:

$$p = \overline{p} p_1 \quad , \quad T = \overline{T} T_1 \quad , \quad \rho = (p_1/RT_1)\overline{\rho}$$

$$x = (RT_1/g)\overline{x} \quad , \quad \underline{\underline{B}} = B_o \, \overline{\underline{\underline{B}}} \quad ,$$

where the subscript 1 denotes the coronal value. Values typical of the corona are

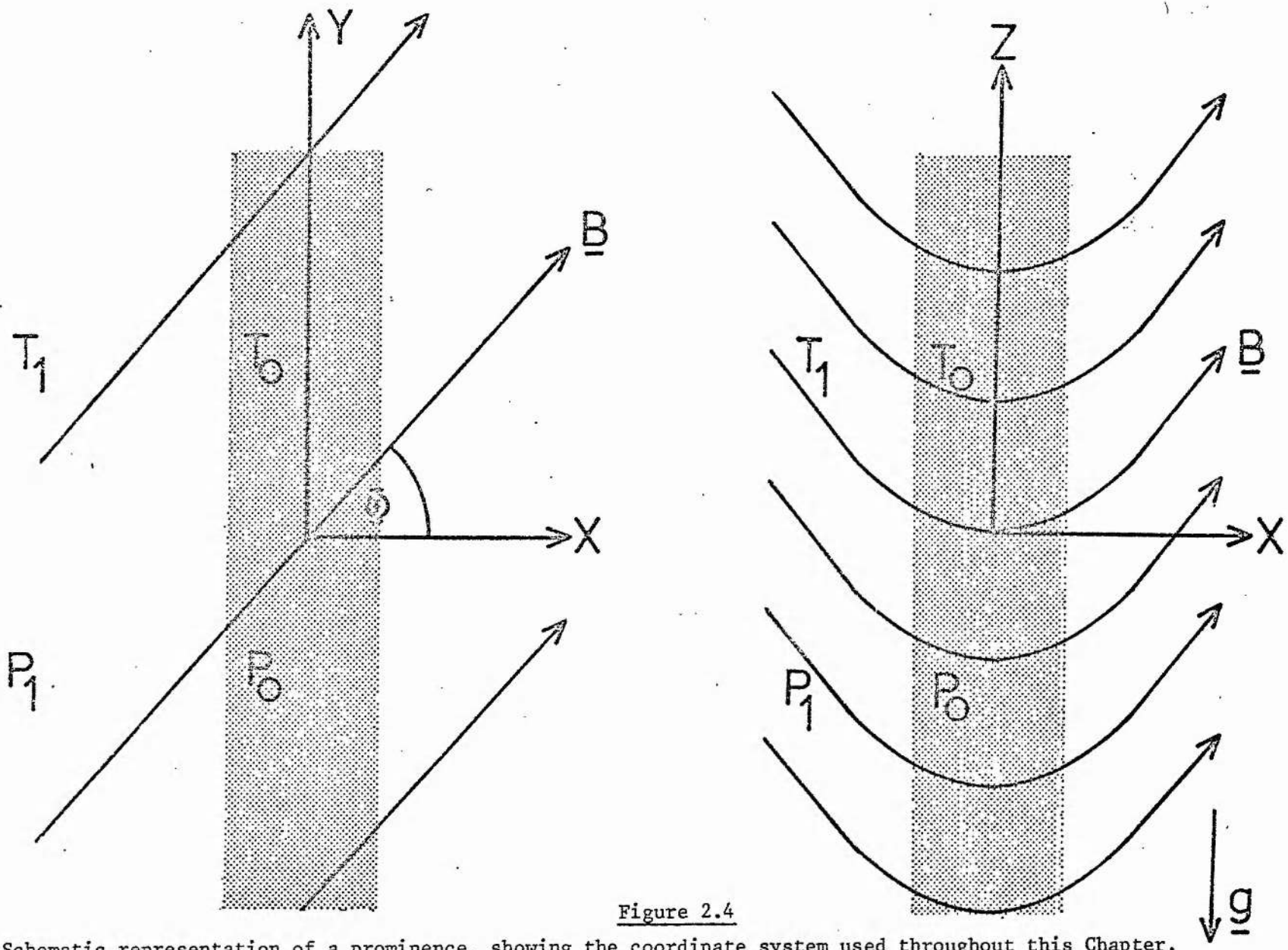

Figure 2.4

Schematic representation of a prominence, showing the coordinate system used throughout this Chapter. The x-axis is normal to the prominence sheet while the y-axis runs along the length of the prominence. The vertical z-axis is in the opposite direction to gravity. Φ is the shear angle between the prominence normal and the horizontal magnetic field. Values at the centre of the sheet are denoted by subscript o, while those in the external corona are denoted by subscript 1.

$T_1 = 2 \times 10^6$ K, $\rho_1 = 1.67 \times 10^{-13}$ kg m^{-3} (ie no. density = 10^{14} m^{-3})

$p_1 = 2.76 \times 10^{-3}$ N m^{-2} , $g = 2.74 \times 10^2$ ms^{-2} ,

and give a coronal scale-height of

$$\Lambda_1 = RT_1/g = 6.02 \times 10^7 \text{ m} \quad .$$

In terms of the above dimensionless variables our basic equations (2.1), (2.3) and (2.9) become

$$\beta \frac{d\bar{p}}{d\bar{x}} = -2\bar{B}_z \frac{d\bar{B}_z}{d\bar{x}} \quad , \qquad \ldots (2.11)$$

$$\frac{d\bar{B}_z}{d\bar{x}} = \frac{1}{2} \beta \bar{\rho} \quad , \qquad \ldots (2.12)$$

$$\bar{p} = \bar{\rho} \bar{T} \quad , \qquad \ldots (2.13)$$

$$\frac{d}{d\bar{x}} \left(\frac{\bar{T}^{5/2}}{\bar{B}^2} \frac{d\bar{T}}{d\bar{x}} \right) = C\bar{\rho}^2 \bar{T}^{\alpha} - C_1 \bar{\rho} \quad , \qquad \ldots (2.14)$$

where $$\bar{B}^2 = (1 + \bar{B}_y^{\,2} + \bar{B}_z^{\,2}) \quad .$$

The (piecewise) constant C is given by

$$C = \frac{\chi p_1^{\,2} T_1^{(\alpha-3.5)}}{g^2 \kappa_o}$$

and is the ratio of radiation to conduction. Note that $\kappa_{11} = \kappa_o T^{5/2}$ where, from equation (1.30), $\kappa_o = 3 \times 10^{-11}$. The constant C_1 is the value of C when $\bar{T} = \bar{\rho} = 1$. The plasma β is defined by

$$\beta = 2\mu \, p_1 / B_o^{\,2} \quad ,$$

and so is the ratio of the coronal plasma pressure to the magnetic pressure of the horizontal field component normal to the sheet.

In order to solve the system (2.11)-(2.14) we need to specify the two parameters β and $\bar{B}_y$, and four boundary conditions. Symmetry demands that both the temperature gradient and the vertical component of

of the magnetic field vanish at the centre ($\bar{x} = 0$) of the prominence sheet, so that

$$B_z = \frac{d\bar{T}}{d\bar{x}} = 0 \text{ at } \bar{x} = 0 \quad . \qquad \ldots (2.15)$$

For the remaining two boundary conditions we take

$$\bar{\rho} = \bar{T} = 1 \text{ at } \bar{x} = 1 \quad , \qquad \ldots (2.16)$$

so that the temperature and density both reach coronal values at a horizontal distance of one scale-height from the centre of the sheet. Other models, in which the coronal values are reached at a distance other than one scale-height may also be considered, and are discussed later.

The problem posed is thus a two-point boundary-value problem, which we shall need to solve numerically. The values of the central ($\bar{x} = 0$) density $\bar{\rho}_o$ and temperature $\bar{T}_o$ are thus determined by the solution. They will be found for a range of values of β and $\bar{B}_y$. The prescription of $\bar{x} = 1$ (ie at $x = \Lambda_1$) as the distance at which coronal values are attained is slightly artificial, but it removes the possibility of the solution reaching coronal temperatures at excessively large distances from the centre. Our model becomes invalid beyond $\bar{x} = 1$, where vertical variations become important.

Note that varying β is equivalent to varying the ambient horizontal magnetic field strength, while keeping the external gas pressure constant. Altering $\bar{B}_y$ is equivalent to varying the shear angle

$$\Phi = \tan^{-1}(\bar{B}_y) = \tan^{-1}(B_y/B_o)$$

that the horizontal magnetic field makes with the x-axis. (See Figure 2.4).

Finally we note that equation (5) has an immediate integral

$$\beta\bar{p} + \bar{B}_z^{\,2} = \beta p_o$$

so that the total pressure (plasma plus magnetic) remains constant through the prominence, the value of the constant being determined by the solution.

However, if we keep the equation in its differential form, the constancy of total pressure may be used as a convenient check on the accuracy of the numerical solution.

2.3 Properties of the solution

Before numerically integrating the full system of equations (2.11)-(2.14) it is of interest to look at some special cases.

2.3.1 Magnetohydrostatics

In the system of equations (2.11)-(2.14), the energy equation may be considered as determining the temperature profile $\overline{T}(\overline{x})$, though it is of course coupled to the other equations through $\overline{B}$ and $\overline{\rho}$. If, instead, $\overline{T}(\overline{x})$ is regarded as being specified, the other equations reduce to two for $\overline{B}_z$ and $\overline{p}$, namely

$$\frac{d\overline{B}_z}{d\overline{x}} = \frac{\beta\overline{p}}{2\overline{T}} \quad , \qquad \ldots (2.17)$$

$$\frac{d}{d\overline{x}}\left(\overline{T}\,\frac{d\overline{B}_z}{d\overline{x}}\right) + \frac{1}{2}\frac{d}{d\overline{x}}\left(\overline{B}_z^{\,2}\right) = 0 \quad ,$$

while

$$\overline{\rho} = \overline{p}/\overline{T} \quad .$$

This system has the solution

$$\overline{B}_z(\overline{x}) = (\beta\overline{p}_o)^{\frac{1}{2}} \tanh\left(\frac{1}{2}(\beta\overline{p}_o)^{\frac{1}{2}}\ell(\overline{x})\right) \quad ,$$

$$\overline{p}(\overline{x}) = \overline{p}_o \operatorname{sech}^2\left(\frac{1}{2}(\beta\overline{p}_o)^{\frac{1}{2}}\ell(\overline{x})\right) \quad , \qquad \ldots (2.18)$$

where

$$\overline{p}_o = \overline{p}(0) \quad ,$$

and

$$\ell(\overline{x}) = \int_0^{\overline{x}} \frac{d\overline{x}'}{\overline{T}(\overline{x}')} \quad .$$

This solution was first derived by Poland and Anzer (1971). With $\overline{T}(\overline{x})$ = constant = 1, say, the solutions (2.18) reduce to those obtained by Kippenhahn and Schlüter (1957) as given in equations (2.5) and (2.6). The solution (2.18) is thus a generalisation of the Kippenhahn - Schlüter model to allow for a non-isothermal temperature profile.

Now the boundary condition, $B_z(0) = 0$, is already satisfied by the above solution (2.18) while the condition that $\overline{p}(1) = 1$ gives

$$\overline{p}_o^{\frac{1}{2}} = \cosh\left(\frac{1}{2}(\beta\overline{p}_o)^{\frac{1}{2}}\ell_1\right)$$

where

$$\ell_1 = \int_o^1 \frac{dx'}{\overline{T}(x')} \quad ,$$

and so determines the constant $\overline{p}_o$. Since the above equation is of the form $z = \cosh \lambda z$, with $z = \overline{p}_o^{\frac{1}{2}}$ and $\lambda = \frac{1}{2}\ell_1\beta^{\frac{1}{2}}$ it admits two solutions (for z) if $\lambda < \lambda_{max}$, one solution if $\lambda = \lambda_{max}$, and no solution if $\lambda > \lambda_{max}$. The critical value λ_{max} is determined by the simultaneous solution of

$$\cosh \lambda z = z \quad \text{and} \quad \frac{d}{dz}(\cosh \lambda z) = 1 \quad .$$

Thus λ_{max} is the root of

$$\cosh(\lambda^2 + 1)^{\frac{1}{2}} = (1 + \lambda^{-2})^{\frac{1}{2}}$$

namely $\lambda_{max} \simeq 0.66$. Thus, for given $\overline{T}(\overline{x})$, there exists a maximum allowable β for the existence of equilibrium solutions. This maximum is given by

$$\beta_{max} = 4\lambda_{max}^2/\ell_1^2 \simeq 1.74/\ell_1^2 \quad .$$

We expect the solution of the complete system of equations to exhibit this same feature of magnetostatic non-equilibrium, namely, that two solutions exist for $\beta < \beta_{max}$, and none for $\beta > \beta_{max}$ for some (as yet undetermined) β_{max}.

To better understand the ordering processes which make this property of the equations possible, consider the isothermal case, $\overline{T} = 1$. In order of magnitude, equations (2.11) and (2.12), with $\overline{\rho} = \overline{p}/\overline{T}$ may be written in the form

$$\beta(\overline{p}(1) - \overline{p}(0)) = -(\overline{B}_z^2(1) - \overline{B}_z^2(0)) \quad ,$$

and

$$\overline{B}_z(1) - \overline{B}_z(0) = \frac{1}{2}\beta\overline{p}(0) \quad .$$

Since $\overline{B}_z(0) = 0$, $\overline{p}(0) = \overline{p}_o$, $\overline{p}(1) = 1$, these become

$$\beta(1 - \bar{p}_o) = - \bar{B}_z(1) \quad , \quad \bar{B}_z(1) = \frac{1}{2} \beta \bar{p}_o \quad .$$

Eliminating $\bar{B}_z(1)$ gives

$$\frac{\beta \bar{p}_o^{\,2}}{4} - \bar{p}_o + 1 = 0 \quad ,$$

which has two solutions

$$\bar{p}_o = \frac{2}{\beta} \left(1 \pm \sqrt{1 - \beta}\right)$$

for the central pressure $\bar{p}_o$.

It is interesting to see that this rough, order of magnitude estimate also predicts that no solutions exist when β exceeds some maximum value (as found earlier), but the value of this maximum is now unity, rather than $1.74\ \ell_1^{-2}$. Moreover, it shows that, for small β, the two possible solutions have the orderings:

either $\quad \bar{p}_o \sim 1 \quad$ and $\quad \bar{B}_z(1) \sim \frac{1}{2} \beta$

or $\quad \bar{p}_o \sim \frac{4}{\beta} \quad$ and $\quad \bar{B}_z(1) \sim 2 \quad .$

Thus, for a solution, either the plasma pressure is of order unity, with a much smaller magnetic pressure $B_z^{\,2}$ ($\sim \beta^2$); or, the magnetic pressure is of order unity and the plasma pressure is large ($\sim \beta^{-1}$). The first solution gives a small deviation from coronal conditions while the second is partly the root of a prominence type solution when temperature variations are included. (See Figure 2.11).

Note that the magnetic field has a dual role in that it must support the material against gravity as well as compressing it in the horizontal direction. The above analysis shows that only two ordering systems allow the magnetic field to be successful in both these roles. Regarding the horizontal field B_o as fixed, so that β is a measure of coronal pressure, the existence of a β_{max} then implies that if the coronal pressure is too large, the magnetic field cannot support the

enclosed material against gravity. Several pairs of solutions given by (2.18), for different values of β, are shown in Figure 2.5.

2.3.2 The limit of a very large magnetic field ($\beta = 0$) - active region prominences

In the solar atmosphere β is generally small compared with unity, so we shall here consider the special case $\beta = 0$ in which $\bar{p} = 1$. In this isobaric limit the vertical magnetic field $\bar{B}_z$ vanishes and the energy equation (2.14) becomes decoupled from the magnetostatics. It may be written (with $\bar{\rho} = \bar{T}^{-1}$)

$$\frac{d}{d\bar{x}}\left[\frac{\bar{T}^{5/2}}{(1+\bar{B}_y^{\,2})}\frac{d\bar{T}}{d\bar{x}}\right] = C\bar{T}^{\alpha-2} - C_1\bar{T}^{-1} \quad , \qquad \ldots (2.19)$$

and is subject to the boundary conditions

$$\frac{d\bar{T}}{d\bar{x}} = 0 \text{ at } \bar{x} = 0 \quad ,$$
$$\bar{T} = 1 \text{ at } \bar{x} = 1 \quad . \qquad \ldots (2.20)$$

Equation (2.19) is equivalent to the pair of first order equations

$$\frac{d\bar{u}}{d\bar{x}} = C\bar{T}^{\alpha-2} - C_1\bar{T}^{-1} \quad ,$$
$$\frac{d\bar{T}}{d\bar{x}} = (1+\bar{B}_y^{\,2})\bar{T}^{-5/2}\,\bar{u} \quad , \qquad \ldots (2.21)$$

and we are interested in solutions of (2.21) which give prominence-type (ie low central temperature) behaviour. System (2.21) possesses two critical points (see, for example, Boyce and De Prima 1969, Chapter 9), namely

$$\bar{u} = 0 \quad , \quad \bar{T} = 1 \quad (\text{since } C = C_1 \text{ for } \bar{T} = 1) \quad ,$$

and $$\bar{u} = 0 \quad , \quad \bar{T} = (C_1/C)^{1/6.4} \quad ,$$

where for the second critical point, which only occurs in the low temperature range, we must have $\alpha = 7.4$.

Consider first the critical point at $\bar{T} = 1$. Putting $\bar{T} = 1 + \bar{t}$

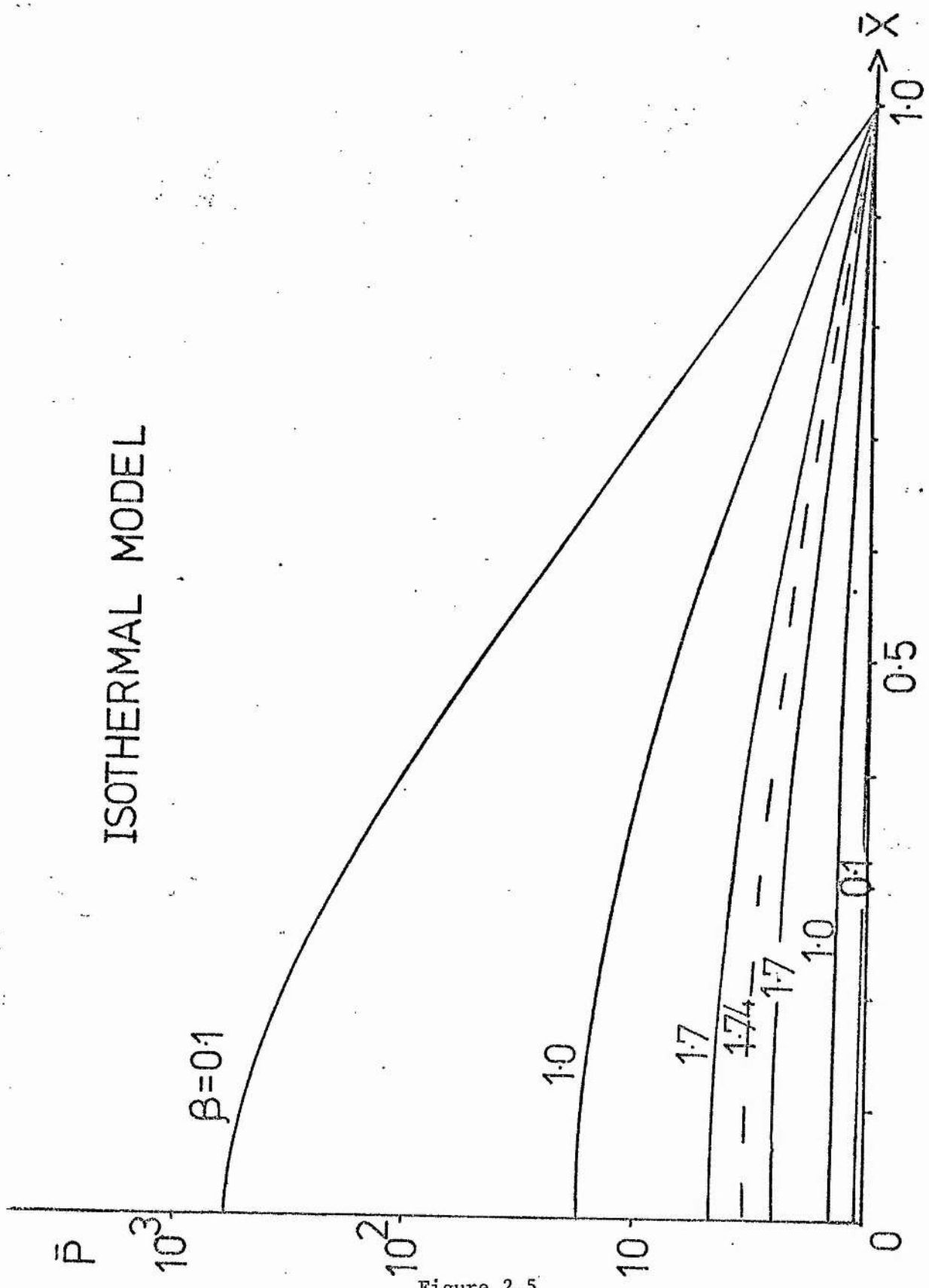

Figure 2.5

Pressure profiles for the isothermal model with $\bar{T} = 1$ for various values of $\beta (= 2\mu p_1/B_o^2$, where p_1 is the coronal pressure and B_o is the magnitude of the component of the magnetic field normal to the prominence sheet). The pressure $\bar{p}$ is units of p_1, while $\bar{x}$ is in units of coronal scale-height (60 Mm for coronal temperature $T_1 = 2 \times 10^6$ K). The dashed curve corresponds to the single solution which occurs when $\beta = \beta_{max}$.

we find, to first order in $\bar{t}$, that

$$\frac{d^2\bar{t}}{d\bar{x}^2} = -4C(1 + \bar{B}_y^2)\bar{t} \quad ,$$

which has <u>oscillatory</u> solutions, implying that the critical point is a <u>centre point</u> where $\bar{T} = T_c$, say.

The second critical point, at $\bar{T} = T_s = (C_1/C)^{1/6.4}$, gives, to first order, on setting $\bar{T} = T_s + \bar{t}$,

$$\frac{d^2\bar{t}}{d\bar{x}^2} = \eta^2\bar{t} \quad ,$$

where $$\eta^2 = (1 + \bar{B}_y^2)(5.4\ CT_s^{1.9} + C_1T_s^{-9/2}) \quad .$$

The solution near this critical point is of the form

$$\bar{t} = Ae^{\eta\bar{x}} + Be^{-\eta\bar{x}} \quad ,$$

and so is a <u>saddle point</u>. The limiting trajectories are given by A or B = 0, the one with positive gradient being

$$\frac{d\bar{t}}{d\bar{x}} = \eta\bar{t}$$

or, in the original variables

$$\frac{d\bar{T}}{d\bar{x}} = \eta(\bar{T} - T_s) \quad . \qquad \ldots (2.22)$$

The phase plane for equations (2.21) is shown schematically in Figure 2.6. The boundary conditions (2.20) mean that we are seeking solutions which start on the horizontal axis $d\bar{T}/d\bar{x} = 0$ and end up on the vertical line (dashed) $\bar{T} = 1$. For a description of a prominence, we are interested only in the trajectories originating just to the right of the lower critical point at T_s and passing through the line $\bar{T} = 1$. Trajectories a, b and c indicate three types of curve. Curve a is of the desired type for a prominence solution, while curve b is the limiting case for this type of solution; but curve b cannot satisfy the boundary conditions (2.20), since the critical point T_s may be reached only when

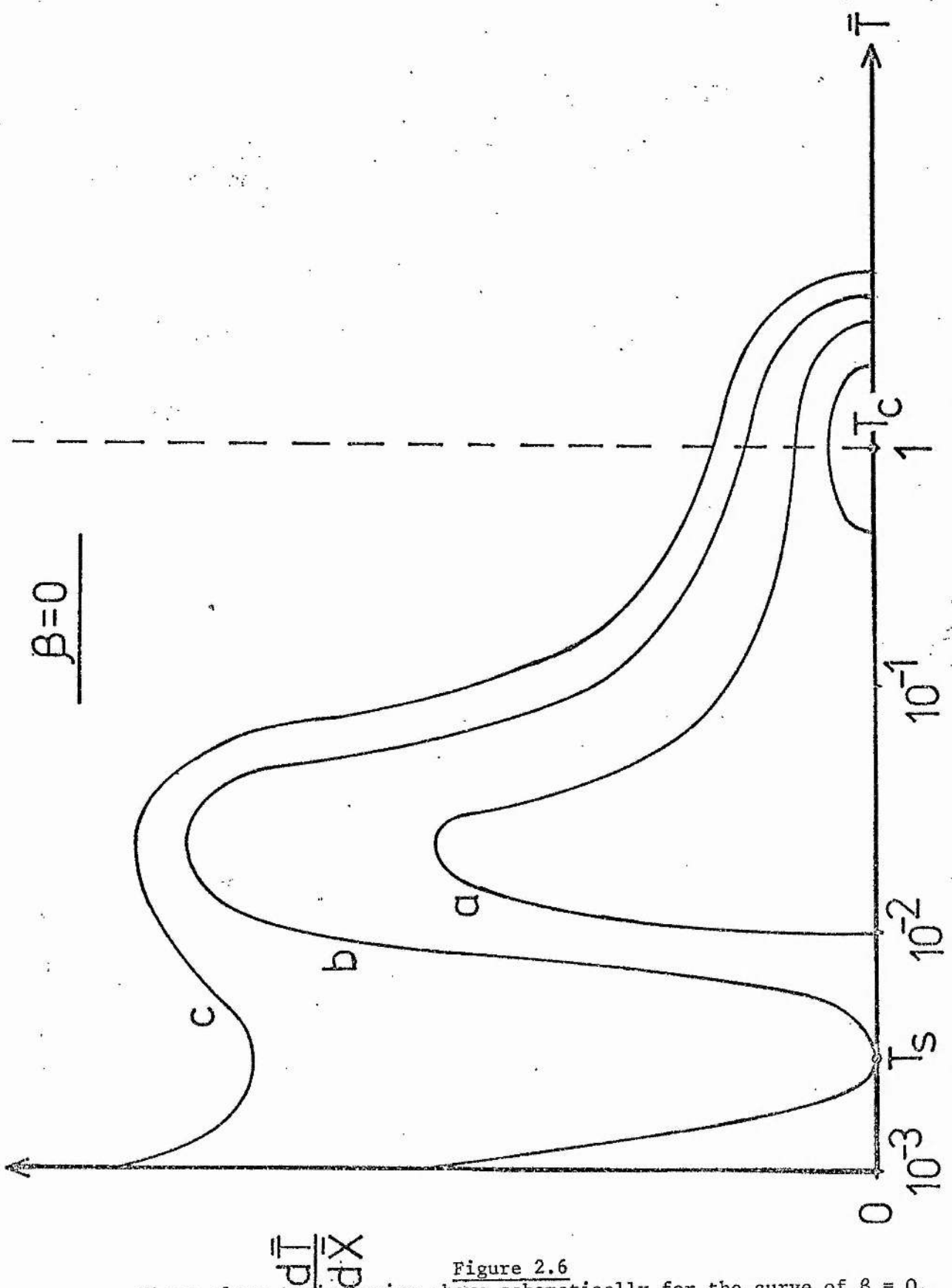

Figure 2.6

Phase plane trajectories shown schematically for the curve of $\beta = 0$, showing the variation of $d\bar{T}/d\bar{x}$ with $\bar{T}$. The two critical points are where $\bar{T} = T_s$ (saddle point) and $\bar{T} = T_c$ (centre point). The three types of trajectory a, b and c are discussed in the text.

$\bar{x} \to \pm \infty$. (Curve c must be discarded, since it does not cross $d\bar{T}/d\bar{x} = 0$ for (prominence) temperatures less than 1). So we see that there is a minimum central temperature for prominence like solutions which is determined mainly by the balance of radiation and heating. This minimum temperature will be found from the full solution of the equations (2.11)-(2.14), and turns out to be somewhat greater than the critical point temperature T_s.

The phase plane does not yield any quantitative information about the $\bar{x}$-dependence of the variables. To obtain this we must solve equation (2.19). We may, however, note that some qualitative information about the "width" of the low temperature region (the prominence) can be obtained. Trajectories close to the saddle point at T_s are flattened out by the presence of the limiting trajectory b. This means that for trajectories near the saddle point, $\bar{T}$ varies appreciably while the temperature gradient $d\bar{T}/d\bar{x}$ remains relatively small. This implies that the length scale, for temperature variations in this region, is larger than in regions near T_c. The closer the trajectory approaches the saddle point T_s, and flattens out, the more the length scale increases. Thus we expect to find in our numerical solutions that, as $\bar{T}_o$ tends to the minimum allowable value, the width of the low temperature region increases. Also, from Figure (2.6), the temperature gradient will increase outwards from $\bar{x} = 0$ to a maximum value, and then decrease towards $\bar{x} = 1$.

We wish to find a solution to (2.19) in addition to the simple isothermal solution ($\bar{T} = 1$). Consider first the case $\bar{B}_y = 0$, and integrate (2.19) numerically, outwards from $\bar{x} = 0$, for a variety of initial temperatures $\bar{T}_o$. The results are rather surprising. For all possible central temperatures $\bar{T}_o$ between T_s and 1 they show that the temperature increases from its central value but is unable to reach the coronal value ($\bar{T} = 1$) at the point $\bar{x} = 1$. Thus, for $\bar{B}_y = 0$, the only possible solution

satisfying the boundary conditions (2.20) is the isothermal one, $\overline{T} = 1$.

To obtain more information about what is happening for $\overline{B}_y = 0$, let us, temporarily, relax the outer boundary condition slightly and pose the following problem instead: for a given central temperature $\overline{T}_s$, and $d\overline{T}/d\overline{x} = 0$ at $\overline{x} = 0$, at what distance from the origin does the temperature $\overline{T}$ attain the values 1.0, 0.9, 0.8, 0.7, 0.6, 0.5 and 0.4?

Figure 2.7 gives the results. For a given $\overline{T}_o$, one can read vertically the values of $\overline{x}$ at which $\overline{T} = 1.0$, 0.9, 0.8 etc are attained. Now, in the original problem we required $\overline{x} = 1$ at $\overline{T} = 1$. However Figure 2.7 demonstrates that, for any central temperature $\overline{T}_o$, the minimum value of $\overline{x}$ to give a non isothermal solution, with $\overline{T} = 1$ attained is $\overline{x} = 7.6$. Thus, for $\beta = 0$ and $\overline{B}_y = 0$ it takes too long to reach coronal temperatures.

The additional effect of varying $\overline{B}_y$ may be seen as follows. From equation (2.19) we note that the constant term $(1 + \overline{B}_y^2)$ appears in the denominator of the conduction term. We may therefore scale $\overline{x}$ against this value by putting

$$\overline{\tilde{x}} = (1 + \overline{B}_y^2)^{\frac{1}{2}} \overline{x} \quad .$$

Thus Figure 2.7 holds for all $\overline{B}_y$ if $\overline{x}$ is replaced by $\overline{\tilde{x}}$. In particular, we see that in order to obtain a non-isothermal solution, with $\overline{T} = 1$ at $\overline{x} = 1$ we need $\overline{\tilde{x}} \gtrsim 7.6$; or, in other words

$$\overline{B}_y \gtrsim 7.54 \quad .$$

Thus prominence type solutions exist in the strong magnetic field limit ($\beta \to 0$) only when the magnetic field is sheared beyond a critical angle $\Phi = \Phi_{crit}$, where

$$\phi_{crit} = \tan^{-1} \overline{B}_y = 82.5^o \quad .$$

This result may be relevant to the formation of steady state filaments inside active regions where β is so much smaller than in the quiet sun.

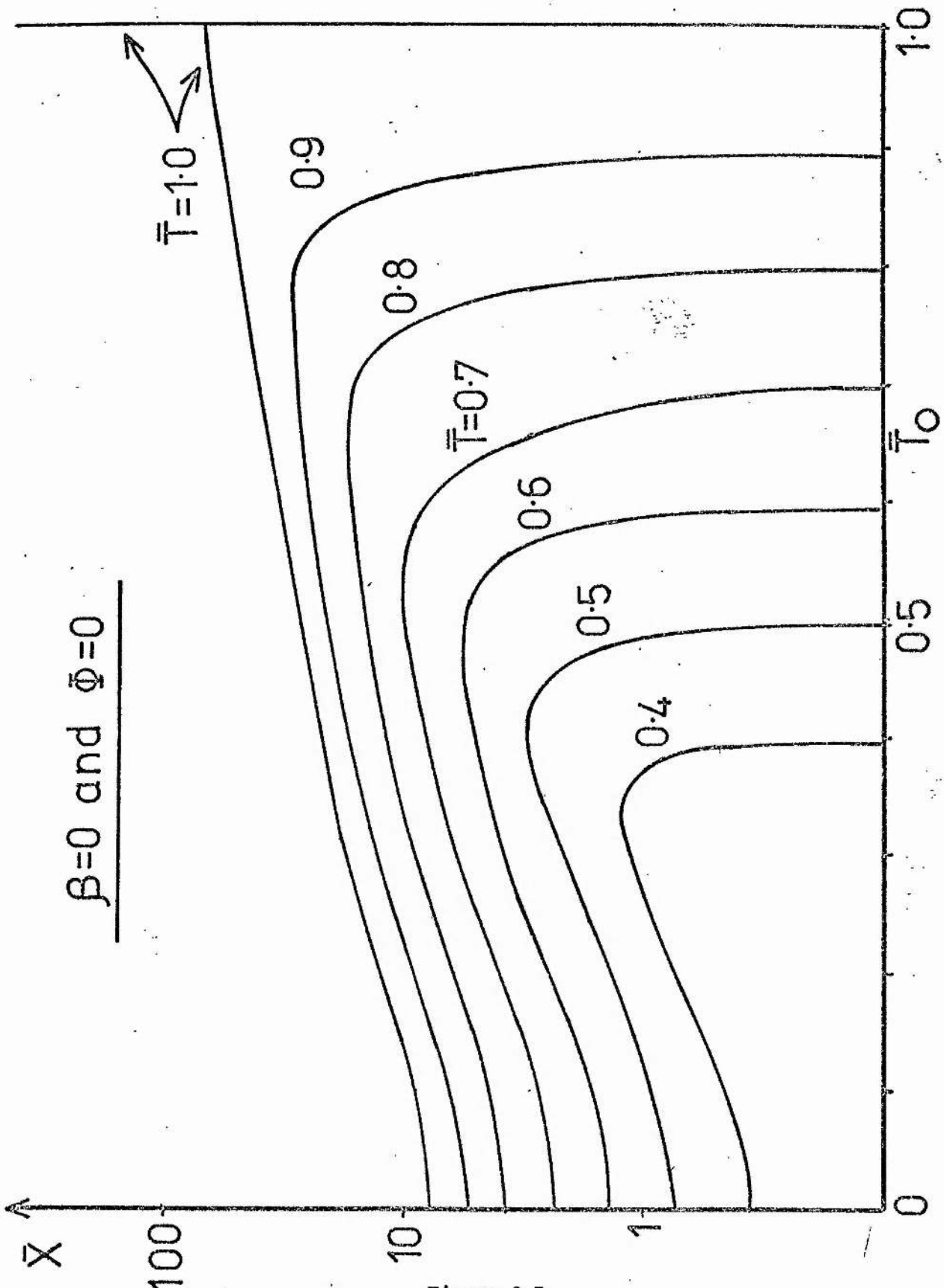

Figure 2.7

The value of $\bar{x}$ at which the temperature reaches $\bar{T}$ = 1.0, 0.9, 0.8... as a function of the central temperature $\bar{T}_o$. $\bar{T}$ is defined to be T/T_1, where $T_1 = 2 \times 10^6$ K is the coronal temperature.

2.3.3 Large magnetic fields ($\beta \ll 1$)

The results discussed above, for the case of $\beta = 0$, suggest that it would be of value to consider next the effect of small perturbations about these solutions. We expand all the variables in power of β about the isothermal solution:

$$\bar{T} = 1 + \beta\bar{T}_1 + O(\beta^2) \quad ,$$

$$\bar{\rho} = 1 + \beta\bar{\rho}_1 + O(\beta^2) \quad ,$$

$$\bar{p} = 1 + \beta\bar{p}_1 + O(\beta^2) \quad ,$$

$$\bar{B}_z = \beta\bar{B}_1 + O(\beta^2) \quad ,$$

where the coefficients $\bar{T}_1$, $\bar{\rho}_1$, $\bar{p}_1$ and $\bar{B}_1$ are to be determined.

We may combine equations (2.11) and (2.12) to give

$$\frac{d\bar{p}}{d\bar{x}} = - \bar{B}_z\bar{\rho} \quad , \qquad \ldots (2.23)$$

and substitute the above expansions into equations (2.12), (2.23), (2.13), (2.14) so that, to order β

$$\frac{d\bar{B}_1}{d\bar{x}} = \frac{1}{2} \quad ,$$

$$\frac{d\bar{p}_1}{d\bar{x}} = - \bar{B}_1 \quad ,$$

$$\bar{p}_1 = \bar{\rho}_1 + \bar{T}_1 \quad ,$$

$$\frac{d\bar{T}_1}{d\bar{x}} = (1 + \bar{B}_y^{\,2})(C\bar{T}_1(\alpha - 2) + 2C\bar{p}_1 - C_1\bar{p}_1 + C_1\bar{T}_1) \quad .$$

Since we are taking perturbations about $\bar{T} = 1$ we put $\alpha = - 1$ and $C = C_1 = 2.9 \times 10^{-4}$.

The solution of the above, subject to the boundary conditions

$$\bar{\rho}_1 = \bar{T}_1 = \bar{p}_1 = \bar{B}_1 = 0 \text{ at } \bar{x} = 1$$

is

$$\bar{T}_1 = \frac{1}{8}\left(1 + \frac{1}{b^2C} - \bar{x}^2 - \frac{\cos b\sqrt{2c}\,\bar{x}}{b^2C\cos b\sqrt{2c}}\right) \quad ,$$

$$\bar{p}_1 = \frac{1}{4}(1 - \bar{x}^2) \quad ,$$

$$\bar{\rho}_1 = \frac{1}{8}\left(\frac{\cos b\sqrt{2c}\,\bar{x}}{b^2C\cos b\sqrt{2c}} - \frac{1}{b^2C} - 1 + \bar{x}^2\right) \quad ,$$

$$\bar{B}_1 = \bar{x}/2 \quad ,$$

where,
$$b^2 = 1 + \bar{B}_y^2 \quad .$$

At the prominence centre this solution gives

$$\bar{T}_1(0) = \frac{1}{8}\left(1 + \frac{1}{b^2C}(1 - \sec b\sqrt{2c})\right) \quad ,$$

which for small $b\sqrt{2c}$ approximates to

$$\bar{T}_1(0) = \frac{1}{8}\left(-\frac{5}{6}b^2C\ldots\right) \quad .$$

Thus to order β for small $b\sqrt{2c}$

$$\bar{T}_o = 1 - \frac{5\beta\, b^2C}{48} \quad ,$$

and the central temperature is less than the coronal value.

Thus, for small β, we have obtained a solution where the temperature remains close to, but slightly less than, $\bar{T} = 1$ over the whole sheet. This expansion procedure supplies a check on the numerical solution with $\bar{T}$ and β in the relevant ranges.

2.3.4 The order of magnitude solution

Another method of obtaining information about the properties of the full system of equations, this time making no assumptions about the size of β, is to consider an order or magnitude approximation, in which the derivatives are approximated by difference equations. (For example, $d\bar{p}/d\bar{x}$ becomes $(\bar{p}(1) - \bar{p}(0))/L$, where L is a characteristic length; in our case $L = 1$, $\bar{p}(1) = 1$ and $\bar{p}(0) = \bar{p}_o$). This procedure is equivalent to considering the truncated Taylor series for $\bar{p}$, $\bar{B}_z$ and $\bar{T}$, namely

$$\bar{p} = \bar{p}_o + \bar{p}_1 \bar{x}^2 \quad ,$$

$$\bar{T} = \bar{T}_o + \bar{T}_1 \bar{x}^2 \quad ,$$

$$\bar{B}_z = \bar{B}_{zo}\bar{x} + \bar{B}_{z1} \bar{x}^3 \quad .$$

If we now apply the boundary condition at $\bar{x} = 1$ we find $\bar{p}_1 = 1 - \bar{p}_o$ and $\bar{T}_1 = 1 - \bar{T}_o$. Substitution of these approximations into equations (2.11), (2.12) and (2.14) with $\bar{\rho} = \bar{p}/\bar{T}$ gives, to zeroth order, the system

$$\bar{p}_o = 2\bar{T}_o^2\left[1 \pm (1 - \beta/\bar{T}_o^2)^{\frac{1}{2}}\right]/\beta \quad , \qquad \ldots (2.25)$$

$$\bar{B}_{zo} = \beta\bar{p}_o/2\bar{T}_o \quad , \qquad \ldots (2.26)$$

$$\bar{T}_o^{5/2}(1 - \bar{T}_o) = 2(1 + \bar{B}_y^2)(C\bar{p}_o^2\bar{T}_o^{\alpha-2} - C_1\bar{p}_o\bar{T}_o^{-1}) \quad , \qquad \ldots (2.27)$$

for the three unknowns $\bar{p}_o$, $\bar{T}_o$ and $\bar{B}_{zo}$. These equations are, of course, only valid when $\bar{p}_1$ and $\bar{T}_1$ are in some sense small. In other words, when $\bar{p}_o$ and $\bar{T}_o$ are "close" to 1.

Equation (2.27) is quadratic in $\bar{p}_o$, with a solution

$$\bar{p}_o = \left[C_1 + (C_1^2 + 2C\bar{T}_o^{\alpha+5/2}(1 - \bar{T}_o)/(1 + \bar{B}_y^2))^{\frac{1}{2}}\right]/2C\bar{T}_o^{\alpha-1} \quad . \qquad \ldots (2.28)$$

Since we require $\bar{p}_o \geq 1$ and are interested in solutions with $\bar{T}_o < 1$ only the positive square root in the solution of the quadratic is relevant. Then, equating (2.28) with (2.25) gives a single equation for $\bar{T}_o$ alone in terms of the parameters β and $\bar{B}_y$. It is simple to show that over the region of validity of the order of magnitude expansion there are two possible solutions for the central temperature for all allowable β and $\bar{B}_y$, suggesting the existence of multiple solutions in the full numerical solution.

If $\bar{T}_o$ becomes less than $\beta^{\frac{1}{2}}$, it can be seen from (2.25) that $\bar{p}_o$ is no longer real and no solution exists. Next we note the existence of a maximum value for $\bar{B}_y$. (2.25) implies that

$$\beta = 4\overline{T}_o^{\,2}(\overline{p}_o - 1)/\overline{p}_o^{\,2} \quad .$$

Now we require $\beta \geq 0$ so we must have $\overline{p}_o > 1$. Since (2.28) is valid only for $\overline{T}_o \sim O(1)$, we take $C = C_1$ and $\alpha = -1$. The condition that $\overline{p}_o > 1$ in (2.28) gives

$$\overline{T}_o^{3/2}(1 - \overline{T}_o) > 2C(\overline{T}_o^{-4} - \overline{T}_o^{-2})(1 + \overline{B}_y^{\,2})$$

ie $$(1 + \overline{B}_y^{\,2}) < \overline{T}_o^{11/2}/(2C(1 + \overline{T}_o)) \quad .$$

Thus since we are interested in $\overline{T}_o \leq 1$ and $\overline{T}_o^{11/2}/(2C(1 + \overline{T}_o))$ is an increasing function of $\overline{T}_o$, there is a maximum value of $\overline{B}_y$ allowed, which occurs at $\overline{T}_o = 1$ and $\beta = 0$, and is given by

$$\overline{B}_{ymax} = (1/2C - 1)^{\frac{1}{2}} \simeq 58 \quad . \qquad \ldots (2.29)$$

This is equivalent to a maximum shear of 89^o.

Note that in this analysis increasing $\overline{B}_y$ is equivalent to increasing both C and C_1. Since there is no lower limit on C or C_1 we may decrease these parameters at will and still find the same multiple valued nature of the solution. (Decreasing C and C_1 may be considered in terms of enhancing the heat conduction).

The information gained from Sections 2.3.1-2.3.4 is invaluable when we come to seek the full numerical solution. In particular, we have the prediction of a maximum β for solutions to exist and its variation with different forms of temperature profile. There is also the prediction of a maximum shear allowable for an equilibrium state. The expansion for small β gives an analytic solution which can be used to check the numerical results, and finally we have the prediction of multi-valued solutions. Without these guidelines the numerical results would have been difficult to obtain and we would have had less confidence in them. They provide the variations with $\overline{x}$ of temperature, pressure and magnetic field, and give the effect of β and $\overline{B}_y$ more accurately than the above analysis.

2.4 Computed solutions for a standard model

We have solved numerically the two-point boundary-value problem given by equations (2.11)-(2.14) together with boundary conditions (2.15) at the prominence centre ($\bar{x} = 0$) and (2.16) at the corona ($\bar{x} = 1$). The method is to consider the associated initial-value problem with initial guesses for the two free boundary conditions. These free boundary conditions are then iterated systematically until results are obtained at the outer boundary which satisfy the correct outer boundary conditions. The numerical integration itself is carried out using a standard Runge-Kutta method. The two effects we wish to investigate in particular are those of varying the parameters β and $\bar{B}_y$. Since $\beta = 2\mu p_1/B_o^2$ and the shear angle (Figure 2.4) is $\Phi = \tan^{-1} \bar{B}_y$, increases in β and Φ correspond to decreasing the horizontal magnetic field strength and shearing the field, respectively.

Consider first the qualitative effect of non-zero values of β on the results of Section 2.3.2 for $\bar{B}_y = 0$. There we found (Figure 2.7) that $\bar{T}$ did not reach unity until well beyond $\bar{x} = 1$. In Figure (2.8) we have shown the effect of varying $\bar{T}_o$ and β on the value of $\bar{x}$ at which $\bar{\rho} = \bar{T} = 1$. It can be seen that for a certain range of $\bar{x}$ there are both low and high temperature solutions, the latter having $\bar{T}_o$ a little less than 1 as predicted in Section 2.3.3. (We are not interested in the possibility of solutions with $\bar{T}_o > 1$). Furthermore, there is a maximum value of $\bar{x}$, beyond which no solution with a cool centre exists. The effect of β increasing from zero is to decrease the values of $\bar{x}$, and decrease the range of $\bar{x}$ allowed for different $\bar{T}$.

However, the problem of interest is to find solutions for $\bar{T}_o$ which give $\bar{x} = 1$ when $\bar{T} = \bar{\rho} = 1$. In other words, the solutions need to lie on the dashed line in Figure 2.8. It is found that for $\beta \lesssim 0.5$ there is only one solution, the almost isothermal one, and that a cool prominence-like solution does not exist, since $\bar{x}$ is greater than unity when $\bar{T}_o$ is small.

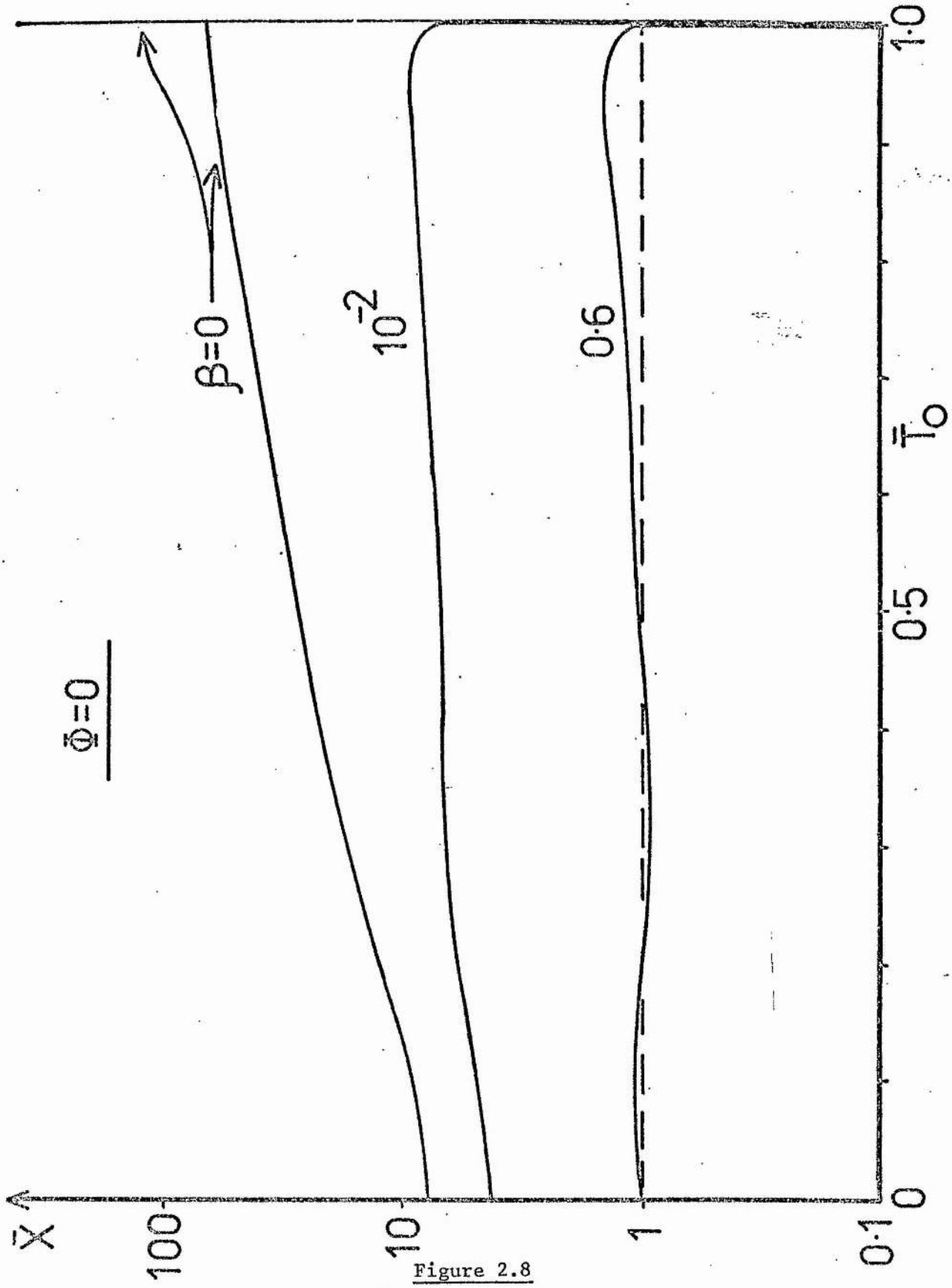

Figure 2.8

The value of $\bar{x}$ at which $\bar{T} = 1$ for various values of β and central temperature $\bar{T}_o$. The dotted line is $\bar{x} = 1$, which the solid curves must intersect to give a solution satisfying the correct boundary conditions. All curves are for zero shear angle ($\Phi = 0$).

In order to obtain a cool solution passing through $\bar{x} = 1$, β needs to be larger than a minimum value so that the left hand ends of the curves in Figure 2.8 are lower than one. Also, there will be a maximum β for solutions to exist. It is the value of β which makes the maximum $\bar{x}$ in Figure (2.8) equal to unity. Beyond β_{max}, the whole of the $(\bar{x},\bar{T}_o)$ curve lies below $\bar{x} = 0$ and so there is neither a cool nor hot solution. Furthermore, since the curves are so flat we may infer that the range of β allowing a cool solution is relatively small.

Let us now describe the results of the numerical integration in detail. We require the effect of the parameters β and $\bar{B}_y$, on the profiles of temperature, density and pressure and also the central values at $\bar{x} = 0$. Another important result is the predicted width of the cool "prominence" region, which we define, for simplicity, to be the distance over which the temperature is less than 10^5 K.

Figure 2.9 shows the variation of central temperature with β for different $\bar{B}_y$ (or shear Φ). Four features are of note.

(a) For values of $\beta > \beta_{max} = 1.70$, no solution exists with central temperatures $\bar{T}_o$ less than unity. This maximum value of β is in good agreement with the results of Section 2.3.1 which predicted $\beta_{max} = 1.74/\ell_1^2$. From the numerical solution for the profile $\bar{T}(\bar{x})$, we may evaluate ℓ_1 for given β and $\bar{B}_y$. For example, with $\bar{B}_y = 0$ and $\beta = 1.7$ the temperature profile gives $\ell_1 = 1.01$.

(b) When $\beta < 1.70$ there is one solution with $\bar{T}_o$ close to 1, in agreement with the expansion of Section 2.3.2.

(c) The curve for $\bar{B}_y = 0$ possesses the following properties. When $\beta < \beta_{min} = 0.60$, only the almost isothermal solution is possible. In the range $0.60 \lesssim \beta \lesssim 0.68$, four possible values of the central

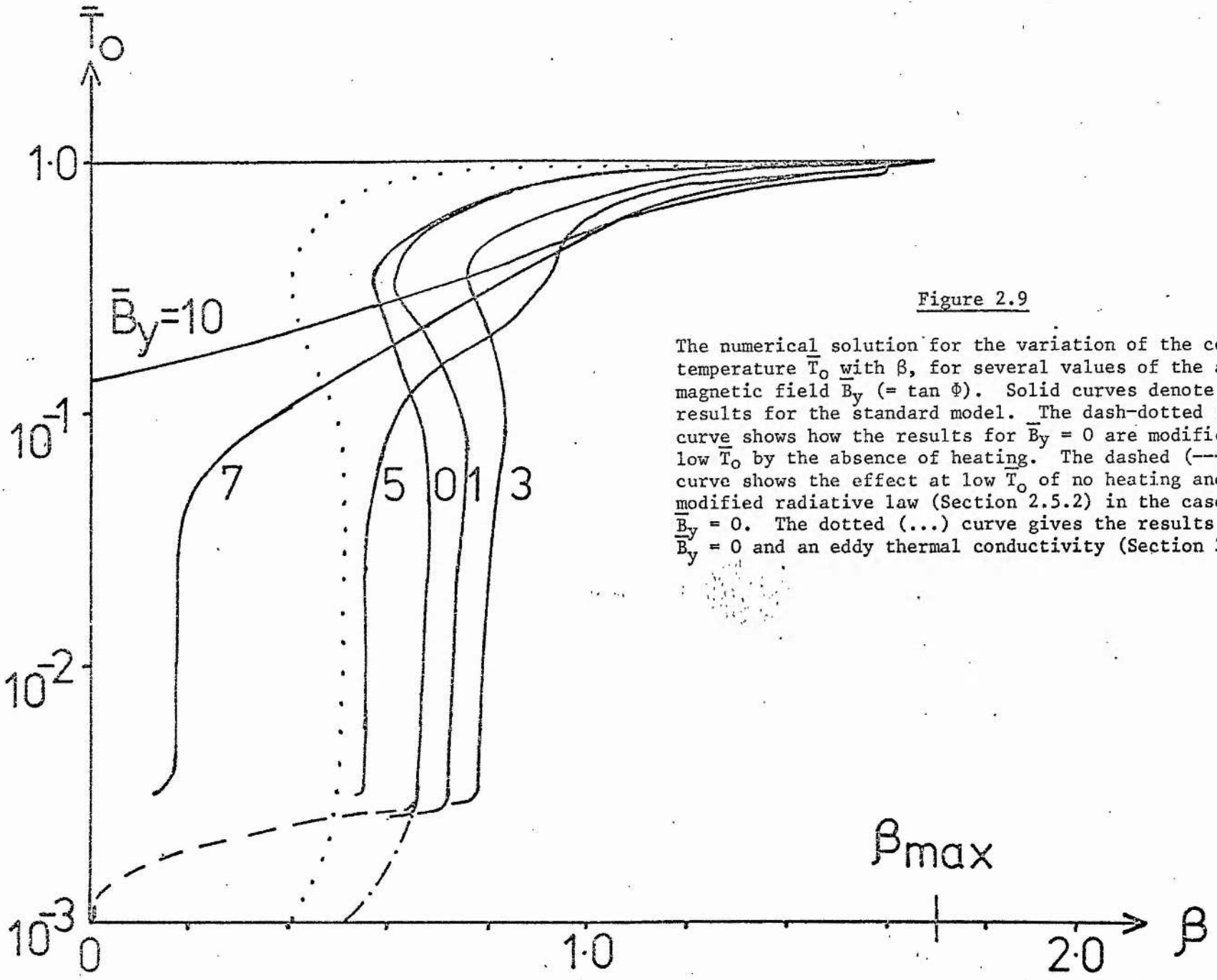

Figure 2.9

The numerical solution for the variation of the central temperature $\bar{T}_o$ with β, for several values of the axial magnetic field $\bar{B}_y$ (= tan Φ). Solid curves denote the results for the standard model. The dash-dotted (-·-·) curve shows how the results for $\bar{B}_y = 0$ are modified at low $\bar{T}_o$ by the absence of heating. The dashed (---) curve shows the effect at low $\bar{T}_o$ of no heating and a modified radiative law (Section 2.5.2) in the case of $\bar{B}_y = 0$. The dotted (...) curve gives the results for $\bar{B}_y = 0$ and an eddy thermal conductivity (Section 2.5.3).

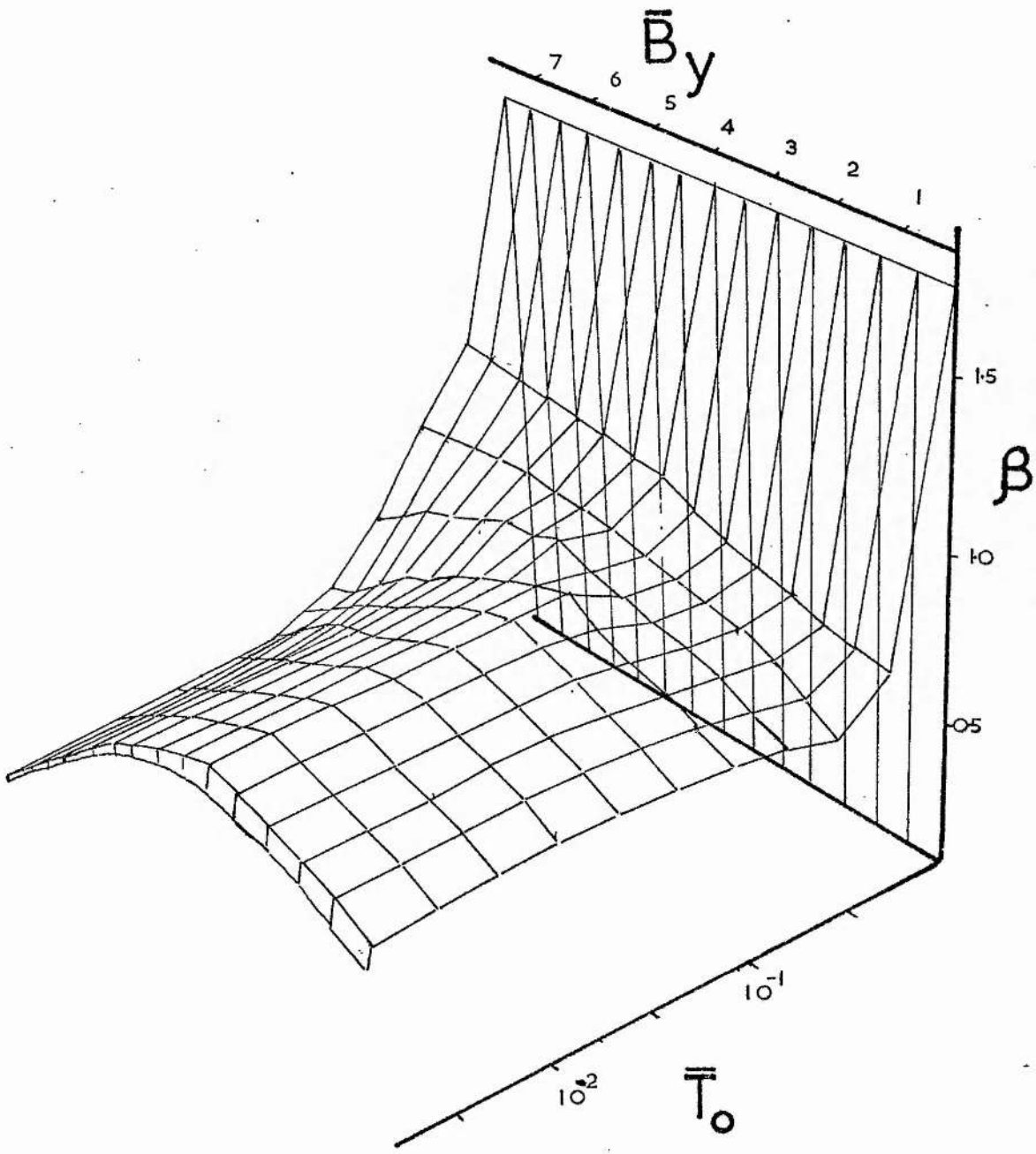

Figure 2.10

Three dimensional representation of the results for the standard model given in Figure 2.9.

temperature $\overline{T}_o$ are obtained, but only the lowest temperature solution is of interest for prominence-like solutions. In the range $0.68 < \beta < 1.7$ there exist two possible solutions, but both give values for $\overline{T}_o$ which are far too high to be of relevance for a prominence model. The existence of quadruple-valued solutions for given β was predicted by the order of magnitude approach in Section 2.3.4, but the sudden cut-off in the low temperature range at β_{min} was not apparent.

(d) As $\overline{B}_y$ is increased in value, so the high temperature bulge to the left in the curves of Figure 2.9 begins to disappear. For $\overline{B}_y = 5$, for example, four values are no longer possible. In this case, for $\beta \gtrsim \beta_{min} \simeq 0.54$ there are two solutions, namely the almost isothermal solution and a low-temperature solution. For $\beta < \beta_{min}$ only the solution with $\overline{T}_o \times 1$ exists. As the shear is increased even further, we find that, for Φ greater than about 83^o ($\overline{B}_y > 7.6$), β_{min} has passed through zero and so no longer exists; two solutions are then present for all values of β less than β_{max}. To show the above results in detail Figure 2.9 is necessarily complex. It is useful, however to show that these curves form a continuous surface in the (β , $\overline{T}_o$, $\overline{B}_y$) space as given in the three-dimensional plot of Figure 2.10.

The results for the central density $\overline{\rho}_o$ and pressure $\overline{p}_o$ show similar features to $\overline{T}_o$. Whenever $\overline{T}_o$ is multiple valued, so too are $\overline{p}_o$ and $\overline{\rho}_o$. At the value β_{min} a maximum value for $\overline{p}_o$ is attained, in contrast to a minimum for $\overline{T}_o$, but it does not give an extremum for $\overline{p}_o$ (Figure 2.11). It is of interest to compare these solutions with the

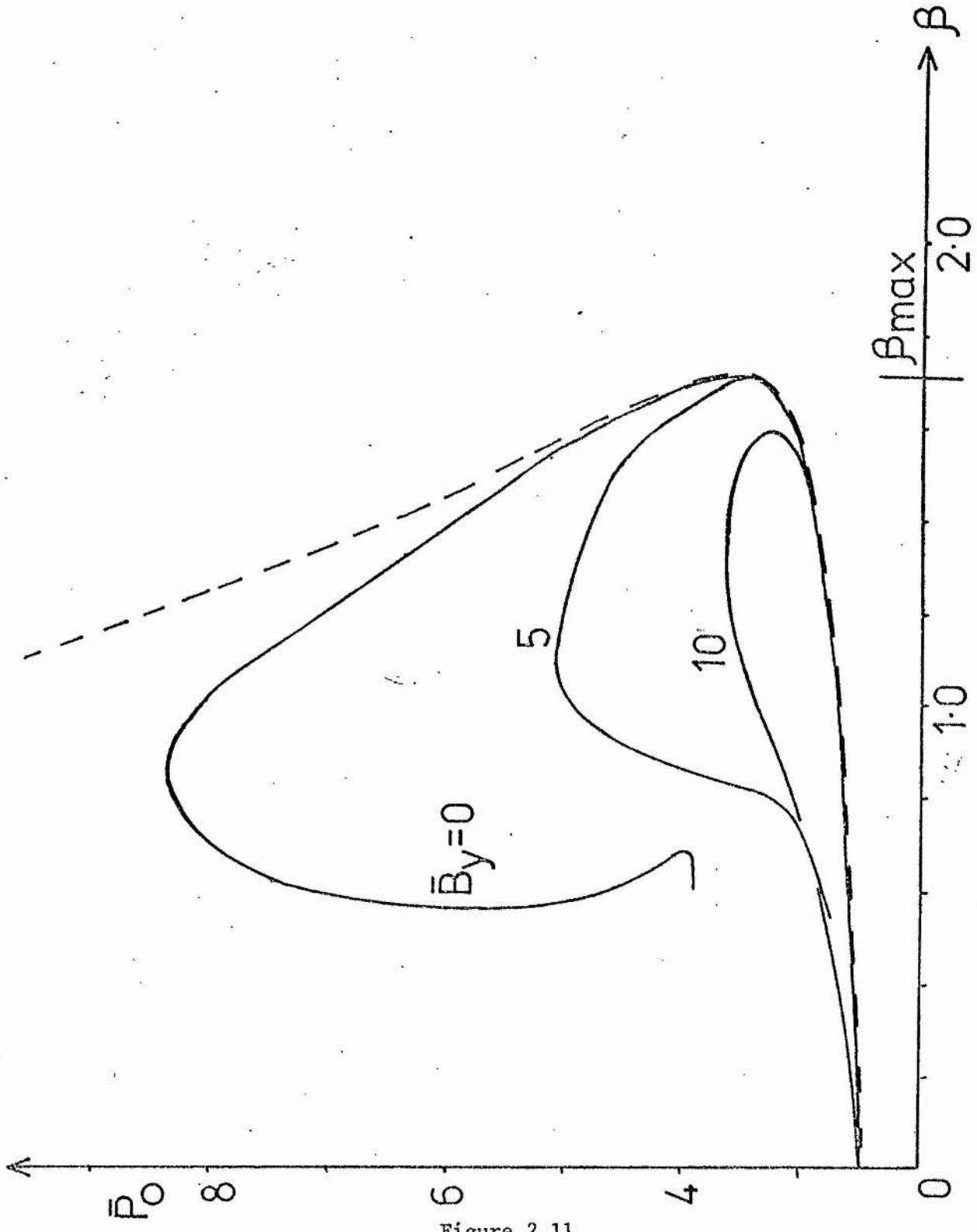

Figure 2.11

The numerical solution for the variation of central pressure $\bar{p}_o$ with β and $\bar{B}_y$ (standard model). The dashed curve arises from the isothermal model (Section 2.3.1).

earlier isothermal solution (shown dashed in Figure 2.11). The low pressure branches of both curves are very similar and the maximum β is present in both. The upper branches are markedly different however, as expected, since they correspond to the lower temperature solutions and so the isothermal approximation is no longer valid.

In order to show the variations with shear Φ more clearly, we plot (in Figure 2.12) the central temperature against Φ for several values of β. The heavy line gives the values at the point where the cut-off at β_{min} occurs. From this Figure we may divide the (β,Φ) plane into regions where different types and numbers of solutions exist, as in Figure 2.13. For convenience we define a "cool" solution to be one having a central temperature $\overline{T}_o < 0.1$, and a "hot" solution as one with $0.1 \leq \overline{T}_o < 1.0$. The extremely narrow range of β that gives us a cool solution is evident. The narrowness is a result of the existence of the cut-off β_{min}, so let us consider the reasons for its occurence.

Recalling the results for $\beta = 0$ (Section 2.3.2), we found a critical point T_s (Figure 2.6) where radiation balances heating at the centre of the sheet. In that case there was a minimum allowable temperature $\overline{T}_o$ for the existence of a solution. It was somewhat greater than the temperature at the critical point T_o. However, it transpires that when β is non-zero, the critical point T_s is absent. This is because a critical point of the full system would require, from equation (2.12) that the density vanish somewhere, which we do not allow on physical grounds. The situation where radiation balances heating at the centre is still of interest, however. If the temperature $\overline{T}_o (< 1)$ is such that heating is greater than radiation at the centre, then the temperature decreases away from the centre and continues to do so for all $\overline{x}$, so that no solution is possible with $\overline{T} = 1$ at $\overline{x} = 1$. This feature was also present in the $\beta = 0$ case. Moreover, for temperatures slightly greater than the above value,

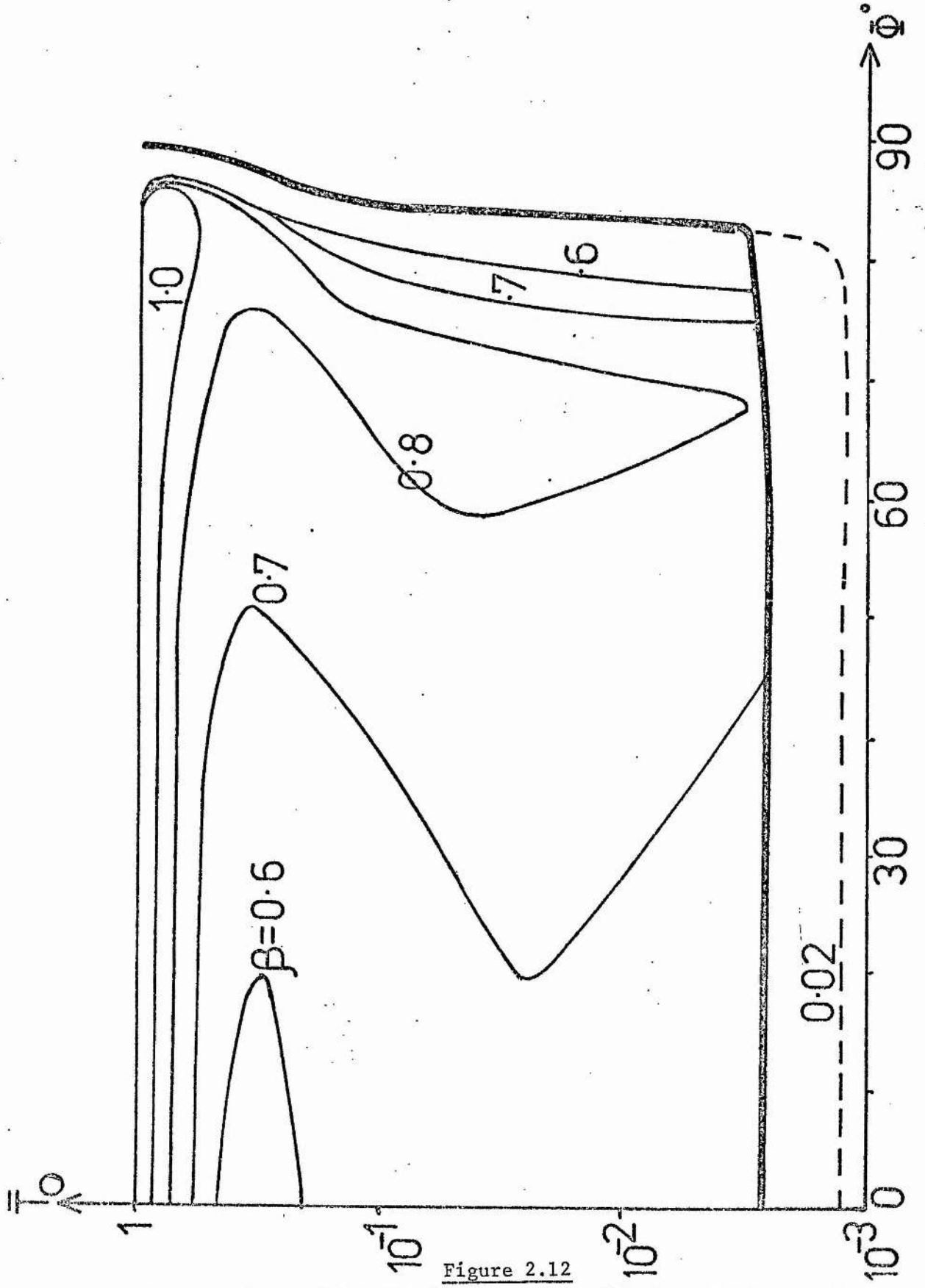

Figure 2.12

The variation of the central temperature $\bar{T}_o$ with shear angle Φ for given values of β, using the standard model. The heavy line denotes the minimum temperature allowed by this model. The dashed line gives $\bar{T}_o$ for $\beta = 0.02$ using the model of Section 2.5.2.

Figure 2.13

Types of solution (for the standard model) allowed in regions of the (Φ,β) plane. Hot solutions have $0.1 \leq T_o \leq 1.0$, while cool solutions have $T_o > 1$. For $\beta > \beta_{max}$, no equilibrium is possible. In the shaded region the modified models give an extra cool solution.

this result remains true.

To show these features, consider the energy equation (2.14) written in terms of temperature, pressure and magnetic field; viz

$$\frac{d}{d\bar{x}}\left(\frac{2}{7\bar{B}^2}\frac{d}{d\bar{x}}(\bar{T}^{7/2})\right) = C\bar{p}^{-2}\bar{T}^{\alpha-2} - C_1\bar{p}\bar{T}^{-1} = \Delta(\bar{x}) \quad , \quad \text{say.} \qquad \ldots (2.30)$$

We note that equation (2.11) implies that the pressure must always decrease away from the centre, and so, $\bar{p}_o$ is the maximum value of the pressure profile. Consider first the case of heating dominating radiation at the centre, ie $\Delta(o) < 0$. Since $\frac{d\bar{T}}{d\bar{x}} = 0$ at $\bar{x} = 0$, $d^2\bar{T}/d\bar{x}^2$ must be negative at the centre, which ensures that $\bar{T}$ decreases initially with $\bar{x}$. With $\bar{p}(\bar{x})$ a decreasing function we note that, for $\alpha \geq 2$, $\Delta(\bar{x})$ will decrease with $\bar{x}$ (ie heating will continue to dominate). Integrating (2.30) gives

$$2\frac{d}{d\bar{x}}(\bar{T}^{7/2})/7\bar{B}^2 = \int_o^{\bar{x}} \Delta(\bar{x})d\bar{x} \quad ,$$

where $\Delta(\bar{x})$ is a negative, decreasing function of $\bar{x}$. Thus since $\bar{B}^2$ is positive definite, the temperature gradient will become more and more negative and $\bar{T}$ will continue to decrease with $\bar{x}$.

Next, suppose that radiation dominates heating at the centre and the temperature increases away from the origin. In this case the heating term $\bar{p}\bar{T}^{-1}$ decreases with $\bar{x}$ while the radiation term has two competing effects, namely the increase with $\bar{x}$ of $\bar{T}^{\alpha-2}$ and the decrease of $\bar{p}^{-2}$. Which term dominates will depend on the initial value of Δ. If $\Delta(o)$ is close to zero then the temperature will not vary very much close to the origin, while pressure decreases. Thus the dominant term will be the pressure variation which will give, since $\bar{p}^{-2}$ varies more rapidly than $\bar{p}$, $\Delta(\bar{x})$ changing sign. Hence the temperature will increase initially and subsequently decrease to zero. Alternatively, if $\Delta(o)$ is large enough, the temperature variation will dominate over the pressure terms and $\Delta(\bar{x})$ will increase with $\bar{x}$, giving an increasing temperature profile. We see

then that a minimum value of $\Delta(o)$ exists for solutions which will satisfy the outer boundary conditions. This, in turn, implies a minimum central temperature allowing solutions to reach coronal values at $\bar{x} = 1$. The value of β for which this temperature occurs is β_{min}, so this cut-off is governed essentially by the balance of radiation and heating in the energy equation.

Having discussed the variation of the central values of the physical variables, let us now consider the full profiles as functions of $\bar{x}$. Some typical ones are shown in Figures (2.14) for the temperature variation, and the corresponding pressure variations in Figure (2.15).

As a check with computing results, we compared with a Taylor series expansion about the origin and found excellent agreement over the range of validity of the expansion. Furthermore, away from the low temperature region, radiation and cooling become unimportant and the energy equation approximates to

$$\frac{d}{d\bar{x}} \left(\frac{2}{7} \frac{d}{d\bar{x}} (\bar{T}^{7/2}) \right) = 0 \quad ,$$

with a solution of the form

$$\bar{T} = (A(\bar{x} - 1) + 1)^{2/7} \quad ,$$

where A is an unknown constant. The computed profiles agree well with this form when $\bar{x}$ is larger than about 0.25. The variation of $\bar{B}_z$ can be deduced from the condition $\beta\bar{p} + \bar{B}_z^2 = \text{constant}$, while the form for $\bar{\rho} = \bar{p}/\bar{T}$ can be estimated from the profiles for $\bar{p}$ and $\bar{T}$.

It is of interest to see the variation with the parameters β and Φ (or $\bar{B}_y$) of the "width" of the low temperature region, defined as the region where the plasma is cooler than 10^5 K. We plot this width against Φ for a range of values of β in Figure 2.16. The presence of a maximum possible width arises from the existence of a minimum allowable temperature, as discussed in Section 2.3.2. Unfortunately the value of the maximum

width is only about 90 km which is an order of magnitude smaller than observed values.

To understand the cause of such small widths it is useful to consider the particular case of $\beta = 0$, where pressure variations do not complicate the picture. In Section 2.3.2, we obtained equation (2.22) for the limiting trajectory of the saddle point in the phase plane (Figure 2.6), namely

$$\frac{d\bar{T}}{d\bar{x}} = \eta(\bar{T} - T_s) \quad , \qquad \ldots (2.22)$$

where

$$\eta^2 = (1 + \bar{B}_y^2)(CT_s^{(\alpha-11/2)}(\alpha - 2) + C_1 T_s^{-9/2}) \quad . \qquad \ldots (2.31)$$

We noted that this limiting trajectory gives approximately the maximum width so that, the smaller the value of η, the wider the cool region becomes. In the present case, η is of the order of 10^4 and so the dimensionless width $\bar{x}$ is about 10^{-4}, corresponding to a dimensional width of only $10^{-4}\ \Delta_1 \sim 6$ km, in agreement with the $\beta = 0$ curve of Figure 2.16. In the following section we will consider modifications to the model which allow much smaller values for η and so give rise to wider structure.

2.5 Modified models

In Section 2.4, we presented the numerical results for the solutions of the equations governing the behaviour of an idealised prominence. As an energy equation we took the balance of thermal conduction, radiation and wave heating. Since the widths of the low temperature region were so small, we consider here modifications to each of these terms which lead to wider structures.

2.5.1 Absence of wave heating near the centre

The heating term models the dissipation of energy in the corona by waves that originate from the photosphere. Since the details of the dissipation are not well understood we have approximated the dissipation

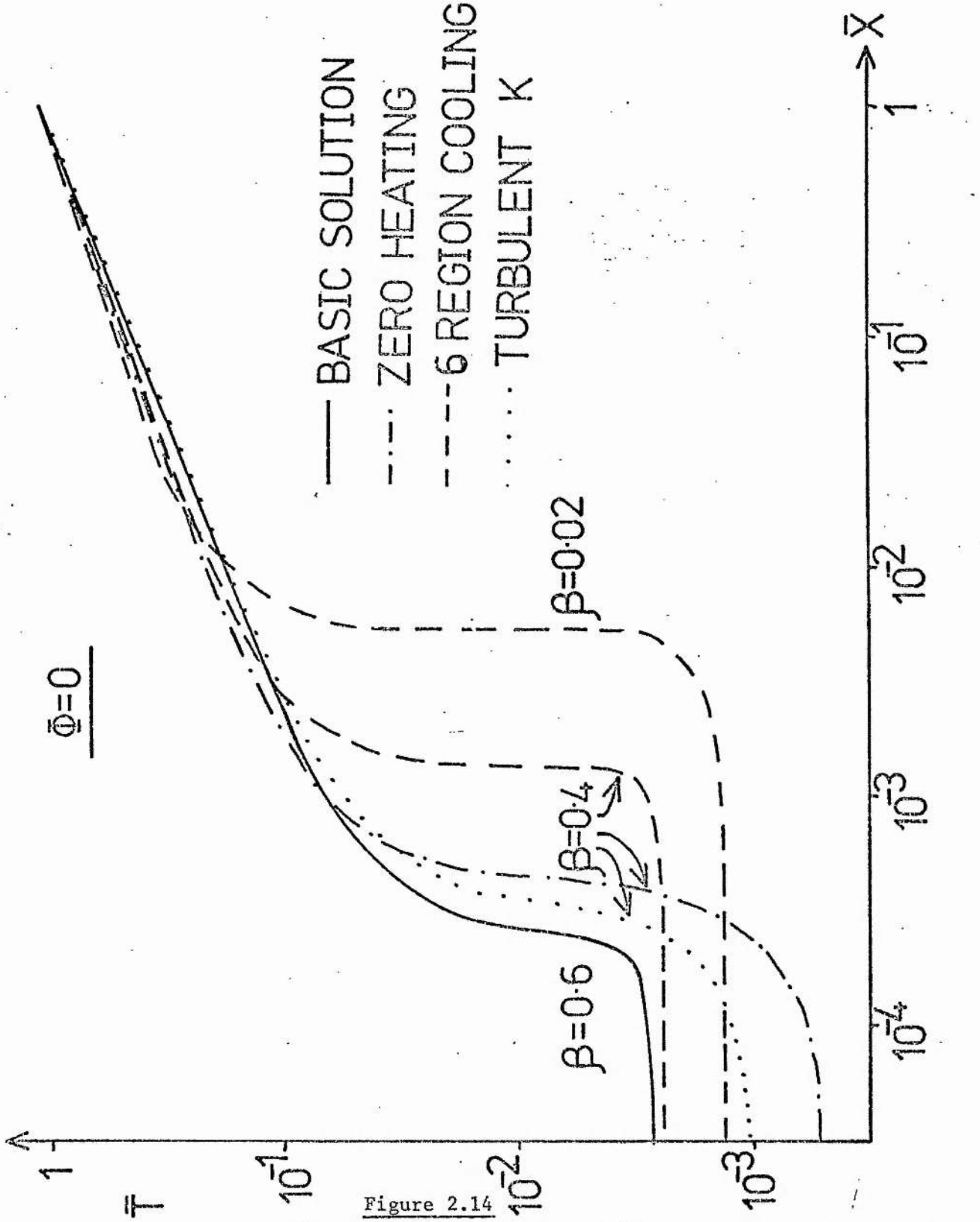

Figure 2.14

The temperature $\bar{T}$ as a function of distance $\bar{x}$ across the prominence from the centre $\bar{x} = 0$. There is no magnetic shear ($\Phi = 0$). The basic solution curve is for $\beta = 0.6$. Three modified solution curves are shown with $\beta = 0.4$ for comparison, and the profile for $\beta = 0.02$ of the six-region cooling model (Section 2.5.2) is also shown.

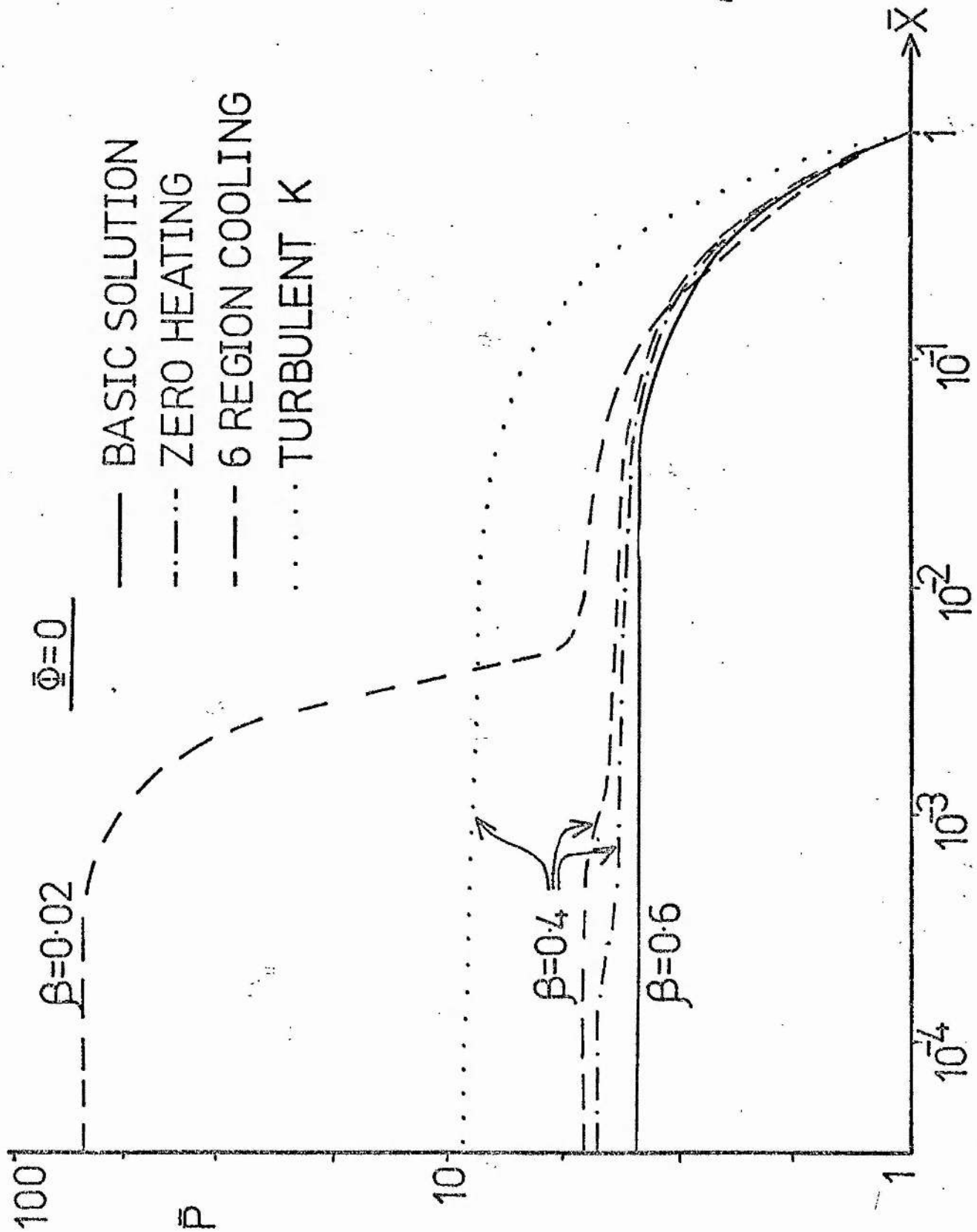

Figure 2.15

The pressure profiles corresponding to Figure 2.14.

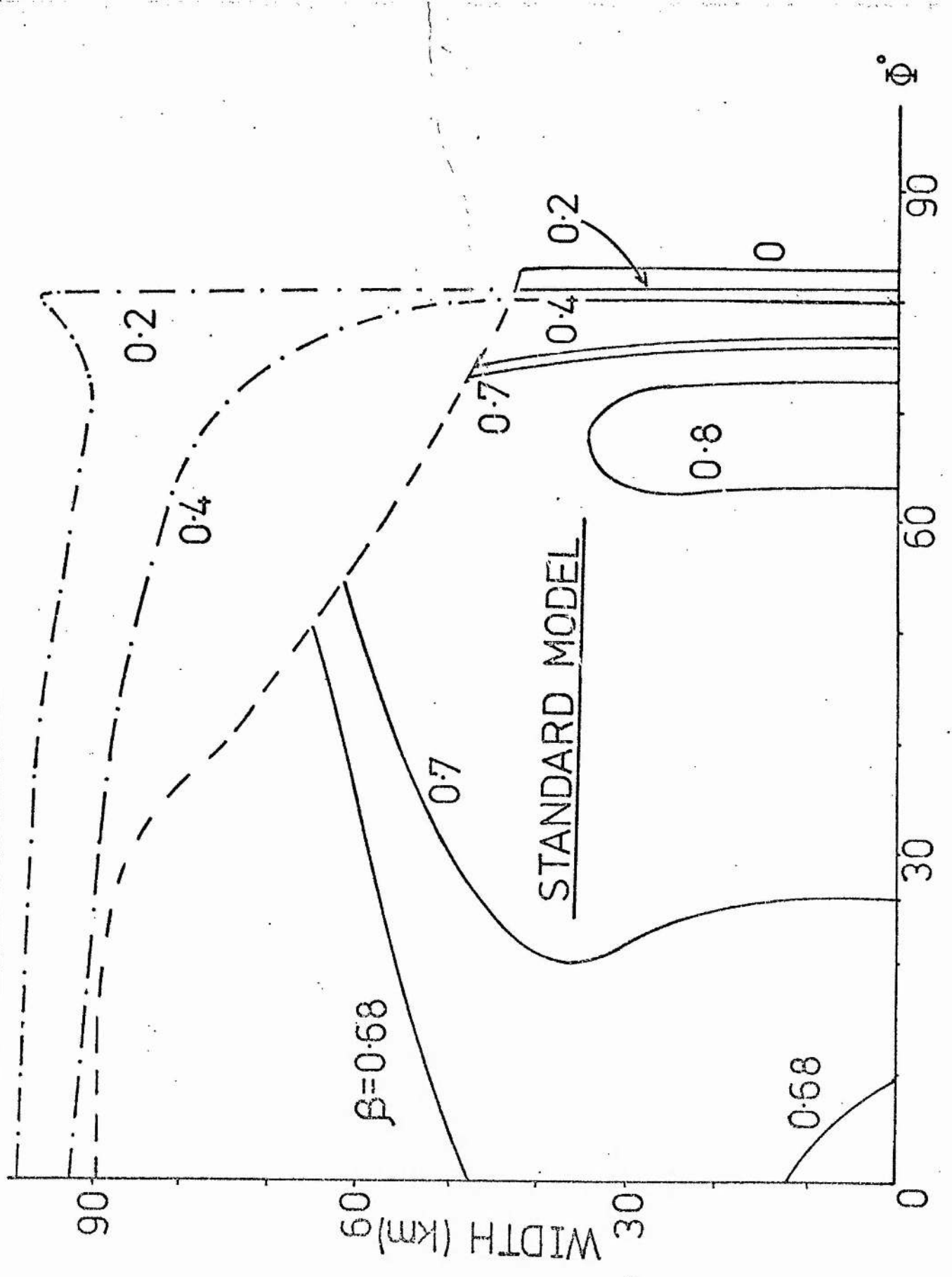

Figure 2.16

The variation of the prominence width with shear angle Φ for given values of β. Solid line curves are for the standard model and the dashed curve denotes the resulting maximum possible width (corresponding to the minimum temperature of Figure 2.12). The dash-dotted curves are obtained from the six-region cooling model (Section 2.5.2).

per unit mass by a constant, H. Some of these waves are incident from below the base of the prominence sheet and probably dissipate most of their energy in the lowest portion of the prominence. Other waves may propagate along magnetic field lines and so enter the prominence from the sides, but again they may dissipate most of their energy before reaching the densest parts of the structure. This would imply the absence of a heating mechanism for much of the prominence.

We shall model this effect by putting H = 0 near the centre of the sheet, for temperatures $\overline{T}$ smaller than 0.1, say. Although we have a discontinuity in the value of H at $\overline{T} = 0.1$ the local effect on the solution curves is negligible since the ratio of heating to radiation there is of the order of 10^{-3}. But near the centre of the structure, the effect of having H = 0 is most important. In particular there is no longer a lower limit on $\overline{T}_o$, as can be seen from Figure 2.9 where the variation of $\overline{T}_o$ with β is indicated by the chained curve. Since the absence of heating modifies the previous solution only at very low temperatures, the multiple-valued nature of the curves is unchanged. Furthermore, the lack of a minimum temperature means that there is now no longer a minimum β. This gives a much wider range of β available for low temperature solutions. In addition, there is no maximum value for the width of the cool structure. For example, the values for $\beta = 0.4$ and 0.2 are indicated by chained curves in Figure 2.16. Taking even smaller values of β produces widths as large as one likes. However, as β decreases, so the central temperature $\overline{T}_o$ becomes unacceptably low, because evidently the form of the radiation term becomes inadequate. For instance, $\beta = 0.2$ gives $\overline{T}_o \simeq 2 \times 10^{-4}$ which corresponds to a central temperature T_o of 400^o K! We therefore proceed to consider an additional modification to the radiative loss term.

2.5.2 Reduced radiation near the centre

The radiative cooling law used in Section 2.4 was an average of

several results, all of which were computed for optically thin plasmas, whereas the prominence plasma is optically thick. This means that the radiative losses used in the model are likely to be far too high for the low temperature regions. The observed central prominence temperatures are of the order of 5000^{o} K, but the optically thin radiative loss curves give values down to only 10^{4} K, and are likely to be in error for temperatures below about 10^{5} K. The tendency of these curves at low temperatures is generally to steepen more than we have allowed for in Table 1 (Chapter 1), where the cooling function power α is only 7.4. For example, the recent results of Raymond (1978), as described in Rosner et al (1978), give α as large as 30 at a temperature of 8×10^{3} K. Increasing α corresponds to lowering the radiative loss at low temperatures, which is in keeping with the suggestion (Bruzek and Kuperus, 1972) that at the centre of a quiescent prominence the H_{α} radiation does not escape, but is balanced by the Lyman continuum absorption.

Let us therefore modify the form of our radiative loss function by adding a sixth region in our cooling curve for temperatures below 10^{4} K, such that the radiative loss at $T = 5000^{o}$ K is lower by a factor of 10^{3}, say, than the previous estimate. This implies a value of $\alpha = 17.4$, with χ chosen to match on continuously at 10^{4} K with the $\alpha = 7.4$ region.

Now at the end of Section 2.4 we pointed out that the resulting width of these models are proportional to η^{-1}. With $C_1 = 0$, so that there is no heating at the centre, we no longer have a critical point at low temperatures for the case of $\beta = 0$. Putting $\overline{T} = \overline{T}_o + t$, where $\overline{T}_o$ is the central temperature, we obtain the results analogous to equation (2.22), namely

$$\frac{d^2t}{d\overline{x}^2} = \nu^2(1 + (\alpha - 2)t/\overline{T}_o) \quad , \qquad \ldots (2.32)$$

where ν (comparable to η in (2.22)) is given by

$$\nu^2 = (1 + \overline{B}_y^2)C\overline{T}^{\alpha-4.5} \quad . \qquad \ldots (2.33)$$

Thus decreasing the radiation by a factor of 10^3 increases the width by a factor of $10^{3/2}$, which is sufficient to give observationally acceptable widths. For this six-region radiative cooling model, with no heating at the centre, the results at high temperatures are unchanged, and only in the low temperature regions do the curves vary. For example, in Figure 2.9, the curves for $\overline{T}_o$ (shown dashed) are much more shallow than before and as such allow reasonable central temperatures for much lower values of β. Typical values for $\overline{B}_y = 0$ are: $\overline{T}_o = 1.7 \times 10^{-2}$, $\overline{p}_o = 15$, width = 500 km for $\beta = 0.1$; $\overline{T}_o = 1.2 \times 10^{-3}$, $\overline{p}_o = 100$, width = 700 km for $\beta = 0.02$. For a greater shear in the magnetic field, $\overline{B}_y = 6$, say, the corresponding values are $\overline{T}_o = 1.3 \times 10^{-3}$, $\overline{p}_o = 3$ and width = 1300 km for $\beta = 0.02$, which are all in good agreement with observations.

The exact values of the central temperature, pressure, etc depend sensitively on the factor by which the radiation at 5×10^3 K is reduced. We took a factor of 10^3 solely to illustrate that realistic values could be obtained. We have considered the effect of varying $\overline{B}_y$ in the case of $\beta = 0.02$. The central temperature is shown dashed in Figure 2.12. As $\overline{B}_y$ increases, so the temperature increases, while the pressure and density decrease. The variation of the width is shown in Figure 2.17. For this value of β, the maximum width is 1500 km, which is of the same order as observed widths. It occurs for a linear shear angle of $\Phi = 80^\circ$, in accord with the results of Tandberg-Hanssen and Anzer (1970) that prominences generally have fields with shear angle of the order of 75°. Finally, note that Figure 2.17 exhibits a maximum shear angle of about 83°, beyond which no cool equilibrium exists.

2.5.3 Turbulent conductivity

The form of the coefficient of thermal conduction which we have

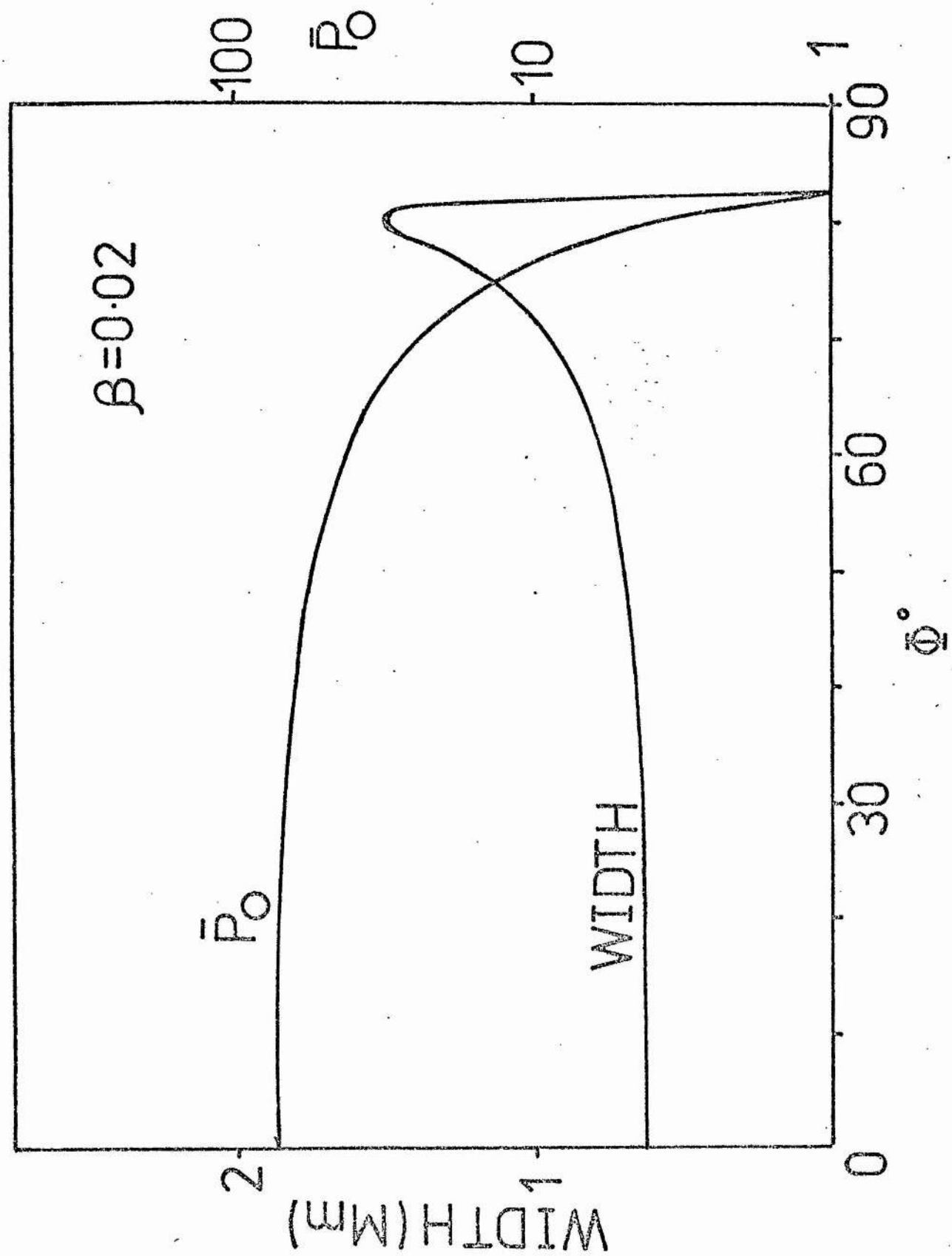

Figure 2.17

The variation of the prominence width (1 Mm = 10^3 km) and central pressure $\bar{p}_o$ with shear angle Φ for $\beta = 0.02$, using the six-region cooling model.

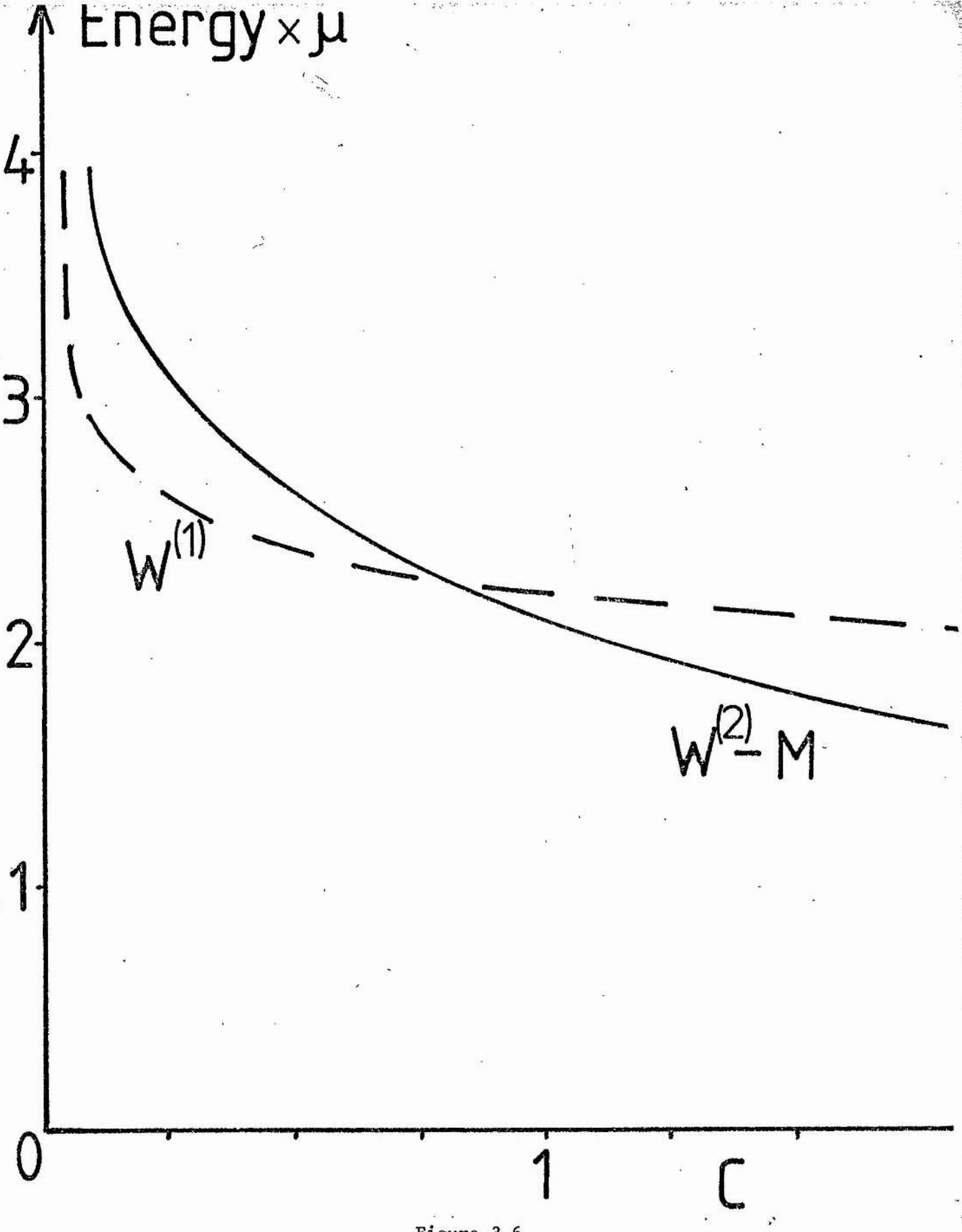

Figure 3.6

The magnetic energies for the two cylindrically symmetric fields with the same shear and normal field. They are calculated out to the radius r_e at which B_ϕ vanishes. As c increases so the shear increases according to Figure 3.4. M is the contribution to the energy of the second field from the magnetic island.

adopted is the standard one for Coulomb collisions. However, there is evidence that the coronal plasma is in a permanently turbulent state (Benz and Gold, 1974). The presence of turbulence means that the conductivity κ will increase above its molecular value (see Knudsen and Katz, 1958). Furthermore, the evidence of a small-scale microstructure in prominences is well-known (Tandberg-Hanssen, 1974, Chapter 2), and is possibly caused by small-scale Rayleigh-Taylor instabilities. Again, the effect on the global equilibrium is to increase κ_{11} to an eddy value.

The effect of increasing κ_{11} has an opposite effect to increasing $\overline{B}_y$ and acts to decrease both C and C_1. From the order of magnitude solutions in Section 2.3.4 we expect to obtain solutions similar to those for small shear angles when κ_{11} is increased. The variation of $\overline{T}_o$ with β, for a conductivity enhancement by a factor of ten, is shown dotted in Figure 2.9 for $\overline{B}_y = \Phi = 0$, and the heating zero at the centre. The curve is of the same general shape as the standard model result for $\overline{B}_y = 0$, showing a four-valued region for certain values of β. The fact that increasing κ_{11} has a similar effect to decreasing $\overline{B}_y$ explains why the curve has moved to the left. We thus conclude that the presence of an eddy conductivity does not change the general features of the model.

2.6 The effect of alternative outer boundary positions

To date, we have concentrated our attention on the case for which coronal conditions are attained at one scale-height from the prominence centre. In this way we were able to present our results without the attendant complexity of an extra parameter. In fact, we show here that our discussion is also applicable to the more general problem, in which coronal values are attained at a distance L from the prominence centre. In place of the boundary condition 2.16 we have now

$$\overline{\rho}(\overline{x}) = 1 \quad \text{and} \quad \overline{T}(\overline{x}) = 1 \quad \text{at} \quad \overline{x} = L/\Lambda_1 \quad , \qquad \ldots (2.34)$$

where the special case of $L = \Lambda_1$ has been considered extensively in the

above. At first sight condition (2.34) appears to add an additional parameter, namely L/Λ_1. In fact, this is not so.

Consider the following transformations,

$$u(\bar{x}) = \bar{B}_z(\bar{x})/(1 + \bar{B}_y^2)^{\frac{1}{2}} \quad , \quad s = (1 + \bar{B}_y^2)^{\frac{1}{2}}\bar{x} \quad ,$$

$$\beta_o = \beta/(1 + \bar{B}_y^2) \quad . \qquad \ldots (2.35)$$

The non-dimensional system of equations (2.11)-(2.14) now become

$$\begin{aligned} \beta_o\bar{p}(s) + u^2(s) &= \beta_o\bar{p}(o) \quad , \\ \frac{du}{ds} &= \frac{1}{2}\beta_o\bar{\rho} \quad , \\ \bar{p} &= \bar{\rho}\,\bar{T} \quad , \\ \frac{d}{ds}\left(\frac{\bar{T}^{5/2}}{(1 + u^2(s))}\right)\frac{d\bar{T}}{ds} &= C\bar{\rho}^2\bar{T}^{\alpha} - C_1\bar{\rho} \quad . \end{aligned} \qquad \ldots (2.36)$$

The system (2.36) is identical to the previous system with $\bar{B}_y = 0$ except that the plasma beta is reduced to β_o. We note also that the length scale s is increased by increasing $\bar{B}_y$, suggesting that increasing shear may increase the prominence "width". (This is, in fact, borne out by the detailed calculations of the previous Sections).

With transformation (2.35) the relevant outer boundary condition for system (2.36) is

$$\bar{\rho}(s) = \bar{T}(s) = 1 \quad \text{at} \quad s = L^*/\Lambda_1 \quad , \qquad \ldots (2.37)$$

where $$L^* = (1 + \bar{B}_y^2)^{\frac{1}{2}}L \quad .$$

Thus, when we originally had three parameters, namely, the coronal plasma beta (β), the distance L of the corona from the prominence centre, and the shear in the magnetic field ($\bar{B}_y$), the above transformed system has only two parameters, namely, the reduced plasma beta (β_o) and an increased coronal distance L^*, with shear effectively zero. The discussion above is therefore immediately applicable (through transformation (2.35)) to the

problem of $L \neq \Lambda_1$ and arbitrary β, provided $L < \Lambda_1$. We simply choose $\overline{B}_y = (\Lambda_1^2 - L^2)^{\frac{1}{2}}/L$.

2.7 Discussion

In the above, we have presented a model calculation for the one-dimensional structure of an equilibrium prominence represented as a vertical sheet of plasma supported by the magnetic tension against gravity. One new feature of this model is that the magnetohydrostatics are coupled to the energetics. This gives a fourth-order two-point boundary value problem, with two symmetry conditions applied at the centre of the structure and the coronal temperature and density specified at a fixed outer edge. The solutions depend on two parameters, namely the coronal plasma beta, $\beta(\equiv 2\mu p_1/B_x^2)$, and the shear angle Φ.

The basic features of the standard model are elicited by means of analytic considerations (Section 2.3) and these are verified in detail by the numerical solutions (Section 2.4). The main fault with the standard model is the narrowness of the prominence width that it predicts (about 100 km). However, relevant modifications to the adopted forms for conduction, radiation and heating in the energy balance lead to much wider structures (greater than 10^3 km), which nevertheless exhibit similar basic features to the standard model. Thus the startling trends which are shown by the standard model would probably exist in more sophisticated treatments.

The most important features of our model are the existence of maximum values for β and Φ for equilibrium states to be possible. The maximum β arises from the magnetohydrostatics. The magnetic field has to fulfil two roles, namely, supporting the plasma vertically against gravity by means of magnetic tension and compressing the plasma from the sides by magnetic pressure. When β_{max} is exceeded both of these roles cannot be undertaken. If B_x is regarded as being constant, the maximum in β means

a maximum in the coronal pressure p_1. Since the coronal pressure decreases with height in the atmosphere the prominence cannot exist below a certain height, h_{min}. The larger the value of B_x, the larger the maximum allowable p_1 becomes and so the prominence may form lower in the atmosphere.

Thus the model predicts that active region prominences can form lower in the solar atmosphere than quiescent prominences (as indeed is commonly observed), since the magnetic field strengths in the former are much stronger. The maximum value of β is about 1.7, which for quiescent prominences with normal magnetic field strength of 1-10 gauss, say, gives values of p_{1max} in the range 6.6×10^{-3}-6.7×10^{-1} Nm^{-2} and h_{min} (according to the atmospheric model of Athay (1976)) in the range 4×10^4-$8 \times 4 \times 10^2$ km respectively. For an active region prominence with a normal magnetic field strength of 100 Gauss (say), the corresponding value is $p_{1max} = 66$ Nm^{-2} which allows formation right down to the middle chromosphere.

If p_1 is held constant, the existence of β_{max} corresponds to a minimum allowable value for B_x. If B_x is smaller than this minimum, then the plasma cannot be supported and so presumably sags down, pulling the magnetic field with it and giving rise to the "feet" that are often observed in quiescent prominences. (In private discussions, Rust confirmed that the magnetic field in the vicinity of these feet appears to be lower than in the rest of the prominence regions, although he felt that more detailed observations were necessary). A minimum β is also present in the models, provided there is some mechanical heating at the centre of the prominence. This gives rise to a maximum height of formation and to a maximum allowable horizontal field B_x. When this maximum field is exceeded, the vertical component of the magnetic tension can no longer be balanced and so the plasma is forced upwards, possibly giving rise to an eruptive prominence.

By contrast, the maximum in the shear (Typically 85^o) is

essentially a result of the energetics. As the shear increases, so the amount of heat conducted into the region falls. To balance this, the total radiation over the region must fall. Since the total radiation over the region is just the area under the cooling curve from $\overline{T}_o$ to 1 we see that $\overline{T}_o$ must increase until ultimately no cool solution is possible. The total radiation is also decreased by decreasing the density. As the maximum shear is approached, so the prominence rapidly heats up, while its' pressure, density and width decrease. Simultaneously, the magnetic field lines spring upwards and possibly produce an erupting prominence.

Altogether, then, our model may be used to explain several major features of prominences, namely the existence of feet, the height of formation and finally a means for the sudden disappearance and eruption of prominences.

Chapter 3: FORCE-FREE MAGNETIC FIELDS WITH RELEVANCE TO SOLAR FLARES

In this chapter simple analytic models for the passive evolution of arcade-like magnetic fields, through a series of force-free equilibria are presented. At the photospheric boundary the normal magnetic field component is prescribed, together with either the longitudinal field component or the photospheric shear. Analytic progress is made by considering the linear force-free field solutions, cylindrically symmetric solutions, or using the technique of separation of variables.

Two distinct cylindrically symmetric force-free fields are obtained that possess the same normal field component and photospheric shear. The second field contains a magnetic bubble (ie a region of space which is not threaded by a magnetic field from the photosphere). As the shear increases beyond a critical value, so the magnetic energy of the first configuration exceeds that of the second. The possibility is therefore simply demonstrated of an eruption of the first field outwards towards the second. Such an eruptive instability is proposed as the origin of a two-ribbon solar flare.

Separation of variables yields a new analytic solution to the force-free field equations, and a general family of solutions may be computed. This technique also yields some solutions already obtained by different analyses.

In Section 3.1 we pose the problems mathematically and discuss much of the previous work on the subject. Section 3.2 deals with the linear force-free field problem while in Section 3.3 we present the cylindrically symmetric solution. In Section 3.4 the application of the separation of variables technique is considered and, finally, in Section 3.5 we present our conclusions.

3.1 Introduction and previous theory

Two explanations have been put forward for the basic instability

of the large-scale force-free field leading to a solar flare. The emerging flux model (Heyvaerts, Priest and Rust (1977); Tur and Priest (1978)) is one of the candidates and will be discussed in detail in Chapter 4 of this thesis. The second suggestion is that there may exist two (or more) solutions to the force-free field equation

$$\underline{j} \times \underline{B} = 0 \quad , \qquad \ldots (3.1)$$

where

$$\underline{j} = \nabla \times \underline{B}/\mu \quad , \qquad \ldots (3.2)$$

and

$$\nabla \cdot \underline{B} = 0 \qquad \ldots (3.3)$$

satisfying the same photospheric boundary conditions, namely a prescription of the normal magnetic field component together with the connections of each fieldline between their points of exit and entrance on the boundary.

The magnetic field evolves passively through one series of force-free equilibrium states and at some point an alternative (second) solution to (3.1) may become possible. If the magnetic energy of the old state exceeds that of the new one, it is then reasonable to suppose that the first state becomes unstable and rapidly evolves into the second, releasing energy in the process.

For the above reasons one of the main aims of recent work on force-free fields has been to seek multiple solutions. Since the two-ribbon flare configuration is much longer than it is either high or wide, it is reasonable to consider two-dimensional solutions, independent of the longitudinal coordinate, z say. The magnetic field components may then be written

$$B_x = B_x(x,y) = \partial A/\partial y \ , \ B_y = B_y(x,y) = - \partial A/\partial x \ , \ B_z = B_z(x,y) \quad , \quad \ldots (3.4)$$

so as to satisfy (3.3) identically, where $A(x,y)\ \hat{\underline{z}}$ is the magnetic vector potential (or flux function) for the transverse components B_x, B_y in the plane perpendicular to the filament axis. Then it can be easily verified that (3.1) and (3.2) imply

$$B_z = B_z(A) \quad , \qquad \ldots (3.5)$$

and $$\nabla^2 A + d/dA \left(\frac{1}{2} B_z^2 \right) = 0 \quad . \qquad \ldots (3.6)$$

Equation (3.5) means that the magnetic component along the axis (z) of the filament (or coronal arcade) is constant along the fieldline in the flux surface

$$A = \text{constant} \quad .$$

Once $B_z(A)$ is specified, equation (3.6) determines A, and hence B_x and B_y. The cases when B_z is a constant and a linear function of A correspond to potential fields and linear (or "constant α") force-free fields, respectively. All other functional forms of B_z make (3.6) a nonlinear differential equation, which is inherently difficult to solve. However, it is the nonlinear nature of (3.6) that allows the possibility of multiple solutions.

Much effort has been expended on trying to solve (3.6) in the semi-infinite region above the plane y = 0, taken to represent the photosphere, subject to two boundary conditions on y = 0. The first is that the normal component be prescribed:

$$(B_y)_{y=o} = B_n(x) \text{ , say} \quad . \qquad \ldots (3.7)$$

For the second condition two distinct types have been considered, giving problems that we shall call (I) and (II). The simpler problem is to specify the form of the axial field

PROBLEM I $$B_z = f(A) \quad . \qquad \ldots (3.8)$$

Since (3.7) implies that A(x,0) is given apart from an arbitrary constant, this is equivalent to prescribing $B_z(x,0)$. The problem that is more relevant to explaining erupting filaments, however, involves specifying the photospheric connections of each field line. In other words the photospheric displacement of the foot-points (see Figure 3.1) is given:

PROBLEM II $$d = d(x) \quad . \qquad \ldots (3.9)$$

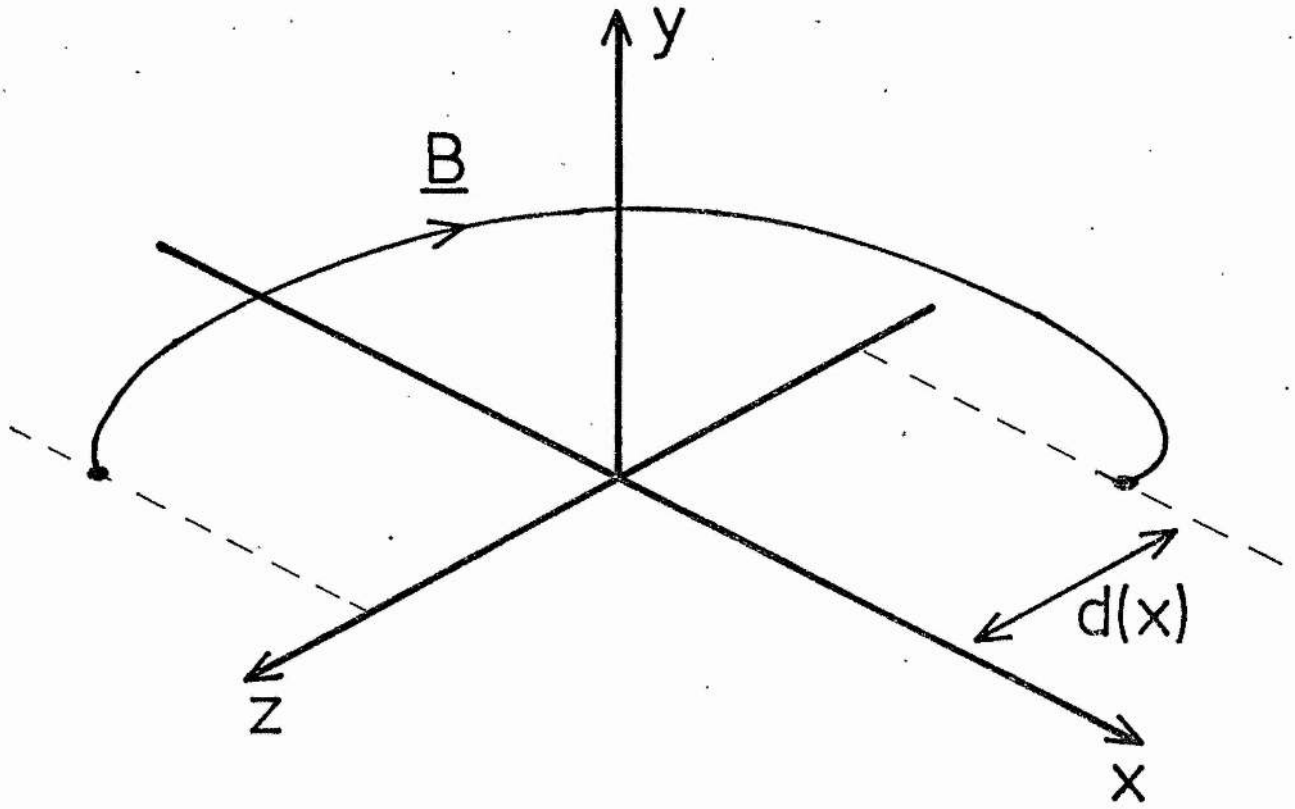

Figure 3.1

Schematic representation of the photospheric displacement d(x) of the footpoints of a force-free magnetic field line. Initially the field is potential and the field line lies in the x-y plane with $d \equiv 0$.

The aim is then to follow the slow evolution of the force-free field through a series of equilibria that are determined by the motion of the photospheric footpoints. In particular, one would like to know whether an equilibrium configuration always exists and whether it is stable. An equilibrium may cease to exist or become unstable when the photospheric shear d(x) reaches a critical value. This would allow the release of magnetic energy as the field relaxes back to a potential field or one of lower energy, and possibly give an explanation for eruptive prominences and two-ribbon flares.

The first attempt at solving problem II was by Sturrock and Woodbury (1967), who considered two lines of monopoles as their sources at points $x = \pm 1$, say, so that

$$d(x) = \begin{cases} +\lambda, & x = 1 \\ -\lambda, & x = -1 \\ 0, & x \neq \pm 1 \end{cases} .$$

As the shear λ increases, so the fieldlines become more distorted and rise higher in the atmosphere, but they found no evidence for multiple solutions or lack of equilibrium. Barnes and Sturrock (1972) made a similar investigation for an axisymmetric structure and again find only one solution. They put forward the hypothesis that the force-free field erupts outwards when its' energy exceeds that of an open configuration containing a current sheet. The resulting open field is then subject to a tearing mode instability. However, their boundary conditions at large distances were not treated adequately and the width of the current sheet would need to be very much less than the original length scale of the overall sheared force-free configuration to provide a solar flare mechanism. This is because the original configuration is itself subject to the tearing-mode on a time scale too long for a flare, namely typically a week.

Low and Nakagawa (1975) solved problem I numerically for

$$B_n(x) = \cos x \quad , \quad |x| < \tfrac{1}{2}\pi$$

and either $$f(A) = -2\varepsilon A(1 + 3A^2)^{-\frac{1}{2}}$$

or $$f(A) = -\varepsilon A^2(1 + A^2)^{-1} \quad .$$

The former case causes the magnetic fieldlines to rise as the parameter ε increases in value and the resulting footpoint displacement $d(x)$ is an increasing function of x. The latter case produces fieldlines that descend as ε increases and a displacement $d(x)$ that possesses a maximum at a certain distance from the axis $x = 0$. In either case only one field, the so-called maximal solution, is computed. Problem I is also investigated numerically by Jockers (1978), who takes

$$B_n(x) = 2x/(1 + x^2)^2$$

and $$f(A) = \lambda A^{(m+1)/2}$$

where m is an integer greater than 3. He treats the semi-infinite region $y \geq 0$ correctly and finds <u>two</u> solutions for each λ less than a maximum value λ_{max}. The one solution B_y^I contains only fieldlines with $0 \leq A \leq 1$ that end on the photospheric boundary $y = 0$, whereas the other solution B_y^{II} sometimes possesses a <u>magnetic island</u> with closed fieldlines ($A > 1$). However, the two solutions correspond to <u>different</u> amounts of shear $d(x)$ (both of which, incidentally, possess a maximum), and they merge in a regular manner as λ_{max} is approached. Thus for a given shear (problem II), Jockers has only one solution and, <u>as the shear increases, first of all λ increases to λ_{max}</u> (with B_y^I being the solution) <u>and then λ decreases</u> (with B_y^{II} the solution). The non-existence of solutions for $\lambda > \lambda_{max}$ is therefore no evidence for the onset of instability, since it is the shear $d(x)$ that must be prescribed rather than $f(A)$. Jockers stresses that one needs to solve problem II and demonstrate <u>the existence of more than one configuration with the same shear</u> (and the

same normal field $B_n(x)$) in order to obtain a flare mechanism with a release of magnetic energy as one configuration evolves suddenly to another.

Problem I has been tackled analytically by Low (1977) and Birn et al (1978). Low considers

$$B_n(x) = -2x/(1 + x^2)$$

and $$f(A) = \lambda e^{-A} \quad .$$

He obtains two solutions, namely

$$A = \log(1 + x^2 + y^2 + y(\lambda/\mu - 2)) \quad , \qquad \ldots (3.10)$$

where $$\mu = (2 \pm (4 - \lambda^2)^{\frac{1}{2}})/\lambda \quad ,$$

and they possess similar features to those found by Jockers. One of the solutions has magnetic islands and the maximum allowable value of λ is 2. The fieldlines are all circles or arcs of circles in the x-y plane.

Birn et al establish some general results about the solutions to problem I of the force-free equation (3.6). With B_z^2 being proportional to a parameter λ they find that, subject to certain conditions on the form of $B_z(A)$, there exists a λ_{max} such that when $\lambda < \lambda_{max}$ there is at least one solution but when $\lambda > \lambda_{max}$ there is no solution. They then put forward the hypothesis that, if the system is forced into a state where λ_{max} is exceeded, then the magnetic field will erupt violently. Although their general ideas may hold in other applications (such as increasing the pressure or the length scale), it is clear from the work of Jockers that, for the present problem where the value of λ is changed by shearing motions, λ_{max} may not be exceeded. Birn et al also establish the following two solutions to problem I in cylindrical polar coordinates, with the axis in the photospheric boundary -

$$B_r = (4b/(c\pi r))\tanh(2b\phi/\pi - b) \quad ,$$

$$B_\phi = -2/(cr) \qquad \ldots (3.11)$$

$$B_z = (2\lambda/c)^{\frac{1}{2}} 2a \cosh b/[r\pi \cosh(2b\phi/\pi - b)] \quad ,$$

where b is either of the two solutions of

$$b = \left(\frac{1}{2} a^2 c\lambda \right)^{\frac{1}{2}} \cosh b \quad .$$

(Note that this is the same equation as was obtained for the central pressure of prominences, in Section 2.3.1 of the previous chapter). The resulting shear is linear,

$$d(x) = x \sinh b$$

and the maximum value of λ is approximately (cf Section 2.3.1)

$$\lambda_{max} = 0.87/(a^2 c) \quad .$$

These two solutions possess similar features to those discussed by Jockers. The two solutions merge as λ_{max} is approached. For problem II with b presented, there is just one solution and, as the shear increases through the value of b, λ just increases to λ_{max} and then decreases without any irregular behaviour occurring.

3.2 Linear force-free fields

A special case of equation (3.6) which is of interest occurs when we put

$$B_z(A) = \alpha A \quad , \qquad \ldots (3.12)$$

which simplifies (3.6) to the linear equation

$$\nabla^2 A + \alpha^2 A = 0 \quad , \qquad \ldots (3.13)$$

where A is the z-component of the vector potential defining the magnetic field components through equation (3.4). One approach to the solution of (3.13) is to use Fourier transform techniques (see, for example, Barbosa (1978); Chiu and Hilton (1977)). Let us therefore put

$$A(x,y) = \int_{-\infty}^{\infty} \frac{dk}{2\pi} e^{ikx} \tilde{A}(k,y) \quad , \qquad \ldots (3.14)$$

so that $\tilde{A}(k,y)$ is the Fourier transform in x of the function $A(x,y)$. Substitution of (3.14) into (3.13) yields

$$\frac{\partial^2 \tilde{A}}{\partial y^2} = (k^2 - \alpha^2)\tilde{A} \quad , \qquad \ldots (3.15)$$

implying

$$\tilde{A}(k,y) = ae^{(k^2-\alpha^2)^{\frac{1}{2}}y} + be^{-(k^2-\alpha^2)^{\frac{1}{2}}y} \quad . \qquad \ldots (3.16)$$

This form of analysis is particularly useful when the boundary conditions are, for example, δ-functions and so we shall here consider analytically a problem similar to that of Sturrock and Woodbury (as discussed in Section 3.1). We recall that their problem dealt with the upper half plane with two lines of monopoles as the photospheric field sources. We thus require that B_y vanish as $y \to \infty$, reducing (3.16) to

$$\tilde{A}(k,y) = be^{-(k^2-\alpha^2)^{\frac{1}{2}}y} \quad .$$

Our photospheric conditions are taken to give monopole sources at $x = \pm x_o$, and so we require

$$B_y(y = 0) = \left(- \frac{\partial A}{\partial x} \right)_{y=o} = \delta(x - x_o) - \delta(x + x_o) \quad . \qquad \ldots (3.17)$$

Thus $$A(y = 0) = H(x + x_o) - H(x - x_o) \qquad \ldots (3.18)$$

where $H(x)$ is the unit step function.

We now insert the transform (3.14) at $y = 0$ to obtain

$$\tilde{A}(k,0) = \int_{-\infty}^{\infty} dx\, e^{-ikx} A(y = 0)$$

$$= \int_{-\infty}^{\infty} dx\, e^{-ikx}(H(x + x_o) - H(x - x_o))$$

$$= \frac{i}{k}(e^{-ikx_o} - e^{ikx_o}) \quad .$$

Thus, with $b = \tilde{A}(k,0)$ we obtain

$$A(x,y) = \int_{-\infty}^{\infty} \frac{dk}{2\pi} \frac{e^{ikx}}{ik}(e^{ikx_o} - e^{-ikx_o})e^{-(k^2-\alpha^2)^{\frac{1}{2}}y} \quad . \qquad \ldots (3.19)$$

Here we have two integrals of the form

$$I = \int_{-\infty}^{\infty} \frac{dk}{2\pi} \frac{e^{ik\xi}}{ik} e^{-(k^2-\alpha^2)^{\frac{1}{2}}y} \quad , \qquad \ldots (3.20)$$

where $\xi = x - x_o$ or $x + x_o$.

Equation (3.20) may be re-written as

$$I = \int_{-\infty}^{\infty} \frac{dk}{2\pi} \int_{o}^{\xi} da\, e^{ika} e^{-(k^2-\alpha^2)^{\frac{1}{2}}y} + \int_{-\infty}^{\infty} \frac{dk}{2\pi} \frac{e^{-(k^2-\alpha^2)^{\frac{1}{2}}y}}{ik} \quad .$$

Noting that the second integral is identically zero, we may change the order of integration to obtain

$$I = \int_{o}^{\xi} da \int_{-\infty}^{\infty} \frac{dk}{2\pi} e^{ika} e^{-(k^2-\alpha^2)^{\frac{1}{2}}y} \quad , \qquad \ldots (3.21)$$

where the k integral is just the Fourier transform of $e^{-(k^2-\alpha^2)^{\frac{1}{2}}y}$ (= F, say), which is (Campbell and Foster, 1948)

$$F = - \frac{\alpha y\, Y_1(\alpha(a^2 + y^2)^{\frac{1}{2}})}{2(a^2 + y^2)^{\frac{1}{2}}} \quad .$$

$Y_1(z)$ is the Bessel function of the second kind as defined by Campbell and Foster, 1948: for more details see, for example, Tranter, 1968. We thus obtain

$$A(x,y) = \int_{o}^{x+x_o} da \frac{\alpha y\, Y_1(\alpha(a^2 + y^2)^{\frac{1}{2}})}{2(a^2 + y^2)^{\frac{1}{2}}} - \int_{o}^{x-x_o} da \frac{\alpha y\, Y_1(\alpha(a^2 + y^2)^{\frac{1}{2}})}{2(a^2 + y^2)^{\frac{1}{2}}} \quad , \qquad \ldots (3.22)$$

as the solution.

We note that the singularity at the origin of $Y_1(x)$ means that (3.22) is not valid for the potential case, $\alpha = 0$. For the potential case, the transform of interest is

$$F = \int_{-\infty}^{\infty} \frac{dk}{2\pi} e^{ika} e^{-ky} \qquad \ldots (3.23)$$

$$= y/\pi(a^2 + y^2) \quad ,$$

giving the solution

$$A(x,y) = \left[\tan^{-1} \frac{x - x_o}{y} - \tan^{-1} \frac{x + x_o}{y} \right] / \pi \quad . \qquad \ldots (3.24)$$

The fieldlines are given by A = constant and with tan A = D, say, we find

$$x^2 + \left(y + \frac{x_o}{D} \right)^2 = x_o^2 (1 + 1/D^2) \quad . \qquad \ldots (3.25)$$

Thus, in the potential case, the fieldlines are circles centred on x = 0, $y = - x_o/D$ with radius $x_o(1 + 1/D^2)^{\frac{1}{2}}$. We see that the distance from the centre to y = 0 is always less than the radius, ie

$$x_o^2/D^2 < x_o^2 (1 + 1/D^2) \quad ,$$

and so, in the potential case, there are no bubbles above the photosphere.

Let us now return to the non-potential case, with vector potential given by (3.22). Evaluation of the component integrals is not possible analytically, but, since $B_y = \frac{\partial A}{\partial x}$, we find

$$B_y = \frac{\alpha y}{2} \left[\frac{Y_1(\alpha[(x + x_o)^2 + y^2]^{\frac{1}{2}})}{((x + x_o)^2 + y^2)^{\frac{1}{2}}} - \frac{Y_1(\alpha[(x - x_o)^2 + y^2]^{\frac{1}{2}})}{((x - x_o)^2 + y^2)^{\frac{1}{2}}} \right] \quad .$$

From the properties of Bessel functions we see that B_y is oscillatory in y (and x).

Because of the difficulty in evaluating (3.22) it is useful to write

$$A(x,y) = \frac{\alpha y}{2} \int_{x-x_o}^{x+x_o} da \, \frac{Y_1(\alpha(a^2 + y^2)^{\frac{1}{2}})}{(a^2 + y^2)^{\frac{1}{2}}} \quad . \qquad \ldots (3.26)$$

In the limit of small x_o we may write this as

$$A(x,y) \simeq 2x_o \frac{\alpha y}{2} \frac{Y_1(\alpha(x^2 + y^2)^{\frac{1}{2}})}{(x^2 + y^2)^{\frac{1}{2}}} \quad .$$

With $x_o \to 0$ we may model the sources of the field as a doublet at x = 0.

This is given by the boundary condition that $A(x,0) = \delta(x)$. A similar analysis to the above yields

$$A(x,y) = \frac{\alpha y}{2} \frac{Y_1(\alpha(x^2 + y^2)^{\frac{1}{2}})}{(x^2 + y^2)^{\frac{1}{2}}} \quad . \qquad \ldots (3.27)$$

Since fieldlines are given by A = constant, we see that the oscillatory nature of the Bessel function $Y_1(z)$ implies the existence of magnetic islands beyond the first zero of $Y_1(z)$. It is obvious from (3.27) that as α increases these islands drift towards the origin, and the region with fieldlines connected to the photospheric sources (defined by $\alpha(x^2 + y^2)^{\frac{1}{2}} < z_o$, where z_o is the value giving the first zero of the Bessel function, $Y_1(z_o) = 0$). The concept of shear is obviously only valid in the region with connected fieldlines and thus we are only interested in that portion of the Bessel function before the first zero.

To study the shear we first note that (3.27) is best transformed to polar coordinates, giving

$$A(r,\phi) = \frac{\alpha \sin \phi \; Y_1(\alpha r)}{2} \quad . \qquad \ldots (3.28)$$

Thus

$$B_r = -\frac{1}{r}\frac{\partial A}{\partial \phi} \quad , \quad B_\phi = \frac{\partial A}{\partial r}$$

and using the fieldline equations

$$\frac{dz}{B_z} = \frac{dr}{B_r} = \frac{r d\phi}{B_\phi}$$

we have

$$z = -\int_o^{r_1} r \tan \phi \; dr \quad .$$

The z displacement of a fieldline is therefore given by

$$z = -\int_o^{r_1} \left[r \tan \left(\sin^{-1} \frac{A}{\alpha Y_1(\alpha r)} \right) \right]_{A=\text{const}} dr \quad . \qquad \ldots (3.29)$$

When considering problem II we wish to know if two (or more) values of α will allow solutions with the same z displacement. This would be equivalent to two solutions with the same shear. It is apparent that (when we are interested in some point defined by z and r_1) the only possibility of multiple solutions is that $\alpha Y_1(\alpha r)$ be multiple valued for r in the range $(0,r_1)$. Coupling this with the fact that only the region of Bessel function before the first zero is of interest and we see that $\alpha Y_1(\alpha r)$ = constant has a unique solution for α in this region.

Thus, specifying α defines a unique shear and the possibility of multiple solutions must be ruled out.

3.3 Cylindrically symmetric solution

In general the solutions to the force-free equations , with B_y given on y = 0 (as $B_n(x)$) and either $B_z = f(A)$ (problem I) or d(x) prescribed, (problem II) are fully two-dimensional depending on x and y. But, in one particular case, they are only one-dimensional, depending on the distance r from some axis parallel to the z-axis. Suppose this symmetry axis is located a distance h below the photospheric boundary, as indicated in Figure 3.2a. (Since we are seeking force-free solutions, only the region above the photosphere may be considered). The magnetic field possesses the components

$$(0 \ , \ B_\phi(r) \ , \ B_z^{(1)}(r))$$

in cylindrical polars with respect to the symmetry axis. Then B_ϕ and $B_z^{(1)}$ are related (according to (1) and (2)) for a force-free field by

$$\frac{d}{dr}\left(\frac{B_\phi^2 + B_z^{(1)2}}{2}\right) + \frac{B_\phi^2}{r} = 0 \quad . \qquad \ldots (3.30)$$

The inclination $\Phi(r_o)$ of the radius vector to a fieldline foot-point is given by

$$\cos \Phi = h/r_o \quad , \qquad \ldots (3.31)$$

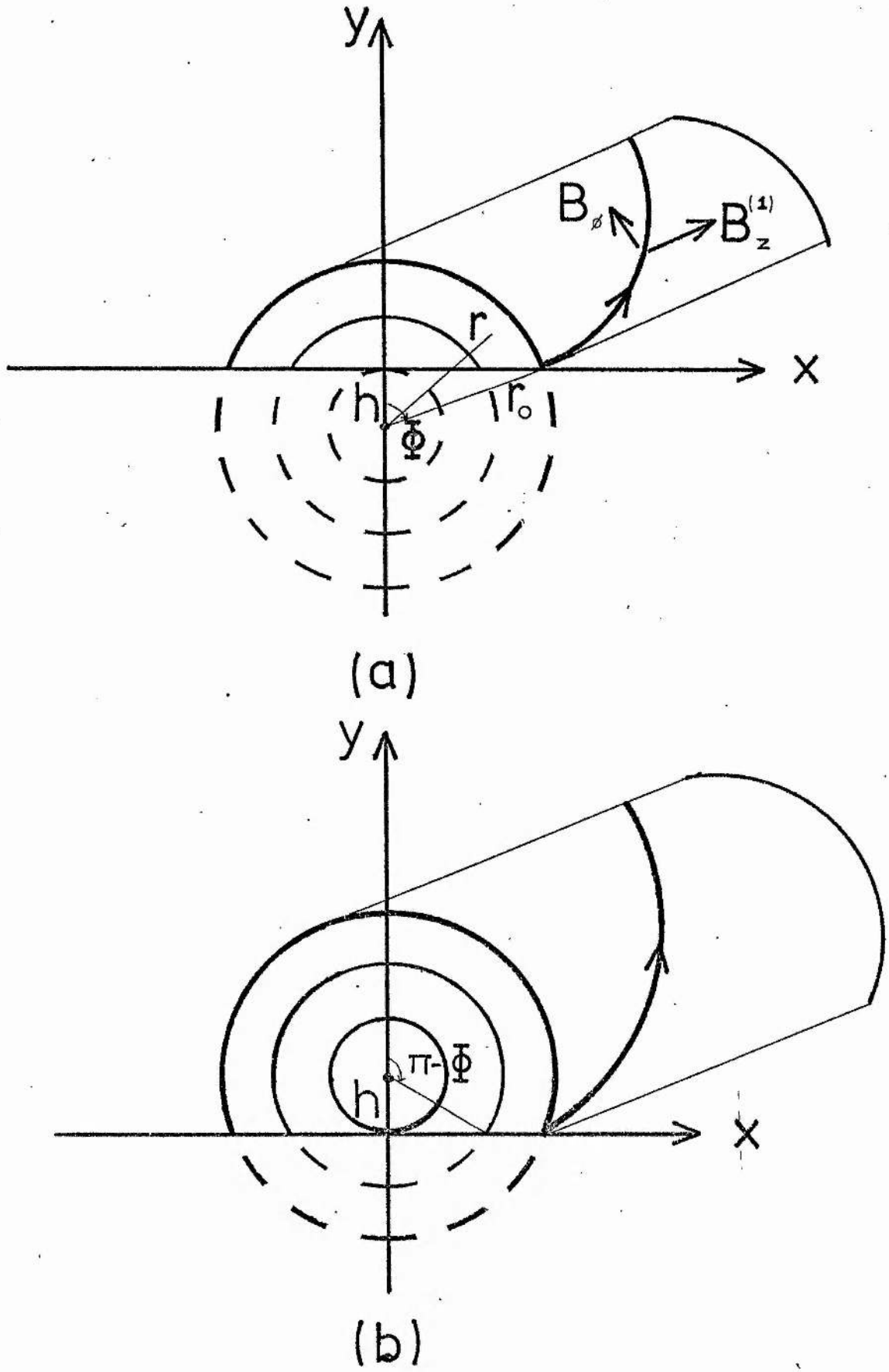

Figure 3.2

Cylindrically symmetric magnetic field arcades whose centre of symmetry is (a) a distance h below the photosphere (y = 0) and (b) a distance h above the photosphere. The projections of field lines on to the x-y plane are arcs of circles.

where $$0 < \Phi < \frac{1}{2}\pi \quad .$$

Also the x-coordinate of the photospheric footpoint (located at y = 0) is

$$x = h \tan \Phi \quad . \qquad \ldots (3.32)$$

In terms of Φ, we may write the normal component of the magnetic field at the photosphere as

$$B_n(x) = B_\phi(r_o) \sin \Phi(r_o) \quad ,$$

or, using (3.3),

$$B_n(x) = B_\phi(r_o)k/r_o \quad , \qquad \ldots (3.33)$$

where $$r_o = (h^2 + x^2)^{\frac{1}{2}} \quad .$$

Furthermore, the photospheric shear, which we define as the difference in the z coordinates of the two footpoints on one fieldline, may be written

$$d^{(1)}(x) = 2\Phi \, r_o B_z^{(1)}(r_o)/B_\phi(r_o) \quad . \qquad \ldots (3.34)$$

Thus, for a given h and $B_n(x)$, we may calculate $B_\phi(r)$ from (3.33) and $B_z^{(1)}(r)$ from (3.30), subject only to the provision that $B_z^{(1)^2}$ be positive. The resulting shear then follows from (3.34).

A second magnetic field

$$(0 \ , \ B_\phi(r) \ , \ B_z^{(2)}(r)) \quad ,$$

with the same normal photospheric component $B_n(x)$ given by (3.33) has a configuration shown in Figure (3.2b), with the symmetry axis now situated a distance h above the photosphere. It possesses some closed fieldlines in a magnetic island and Φ is again given by (3.31), with

$$\frac{1}{2}\pi < \pi - \Phi < \pi \quad .$$

The force-free condition becomes

$$\frac{d}{dr}\left(\frac{B_\phi^2 + B_z^{(2)^2}}{2}\right) + \frac{B_\phi^2}{r} = 0 \qquad \ldots (3.35)$$

and the shear is this time

$$d^{(2)}(x) = 2(\pi - \Phi) r_o B_z^{(2)}(r_o)/B_\phi(r_o) \quad . \qquad \ldots (3.36)$$

Again, given the same h and $B_n(x)$ and so $B_\phi(r)$ as before, one may deduce $B_z^{(2)}(r)$ and $d^{(2)}(x)$ from (3.35) and (3.36), but in general these differ from $B_z^{(1)}$ and $d^{(1)}$.

3.3.1 Problem I

In this case we wish to prescribe $B_n(x)$ and B_z, and determine B_ϕ and the shear d. Once B_n is given (and h too), B_ϕ can be found from (3.33), but B_z cannot be prescribed as we like, this degree of freedom being lost through our assumption of cylindrical symmetry. $B_z^{(1)^2}$ instead must possess the form determined by (3.30) to within a constant. If the same constant of integration is chosen for $B_z^{(2)}$, so that

$$B_z^{(2)} \equiv B_z^{(1)} \quad ,$$

then our two configurations (Figure 3.2a and 3.2b) are both solutions to problem I and their shears are

$$d^{(1)}(x) = 2\Phi\, r_o B_z/B_\phi$$

and

$$d^{(2)}(x) = 2(\pi - \Phi) r_o B_z/B_\phi \quad .$$

As an example, suppose

$$B_n(x) = -2x/(1 + x_o^2) \quad .$$

Then (3.33) gives

$$B_\phi(r) = -2r/(1 - h^2 + r^2)$$

and (3.30) implies that, for $h \lesssim 1$,

$$B_z(r) = 2(1 - h^2)^{\frac{1}{2}}/(1 - h^2 + r^2) \quad .$$

(No force-free cylindrically symmetric field exists with the above normal photospheric field when $h > 1$). Note that the constant of integration has been chosen to make B_z vanish at infinity. The shears that result for the two distinct solutions are

$$d^{(1)}(x) = -2\Phi(1 - h^2)^{\frac{1}{2}}$$

and $$d^{(2)}(x) = -2(\pi - \Phi)(1 - h^2)^{\frac{1}{2}} \quad ,$$

where $$\sin \Phi = x/(h^2 + x^2)^{\frac{1}{2}} \quad .$$

They are sketched in Figure 3.3. The second solution has a non-vanishing shear $d^{(2)}(o)$ at $x = 0$ because the circular fieldline in Figure 3.2b with a radius h has its two ends at points that are a distance $\pi\lambda$ apart on $x = 0$, where

$$\lambda = 2(1 - h^2)^{\frac{1}{2}} \quad .$$

It should be noted that the value of h needs to be the same for the two solutions so as to ensure that B_z is the same. Furthermore, the magnetic potential (such that $B_\phi = -dA/dr$) is just

$$A(r) = \log(1 - h^2 + r^2)$$

and the axial field has the form

$$B_z = \lambda e^{-A} \quad .$$

This example is therefore just the one which Low derived (Equation 3.10) by means of a rather more abstruse analysis. It can be seen that when $h^2 = 1$ we have the potential field $B_\phi = -2/r$.

As h^2 decreases from 1 to a minimum value of 0, so λ increases from 0 to a maximum value of 2 at which the two solutions coincide with the symmetry axis lying on the photospheric boundary, the fieldline projections on the x-y plane being just semicircles and the shears being $-\pi$. It is clear that as the shear changes so λ can increase from 0 to 2 and then decrease to 0 again, there being no violent behaviour at λ_{max}. Furthermore, if the shear at large distances exceeds π there are no solutions of this form but there may well exist force-free fields without cylindrical symmetry.

There is a whole family of analytic solutions with similar

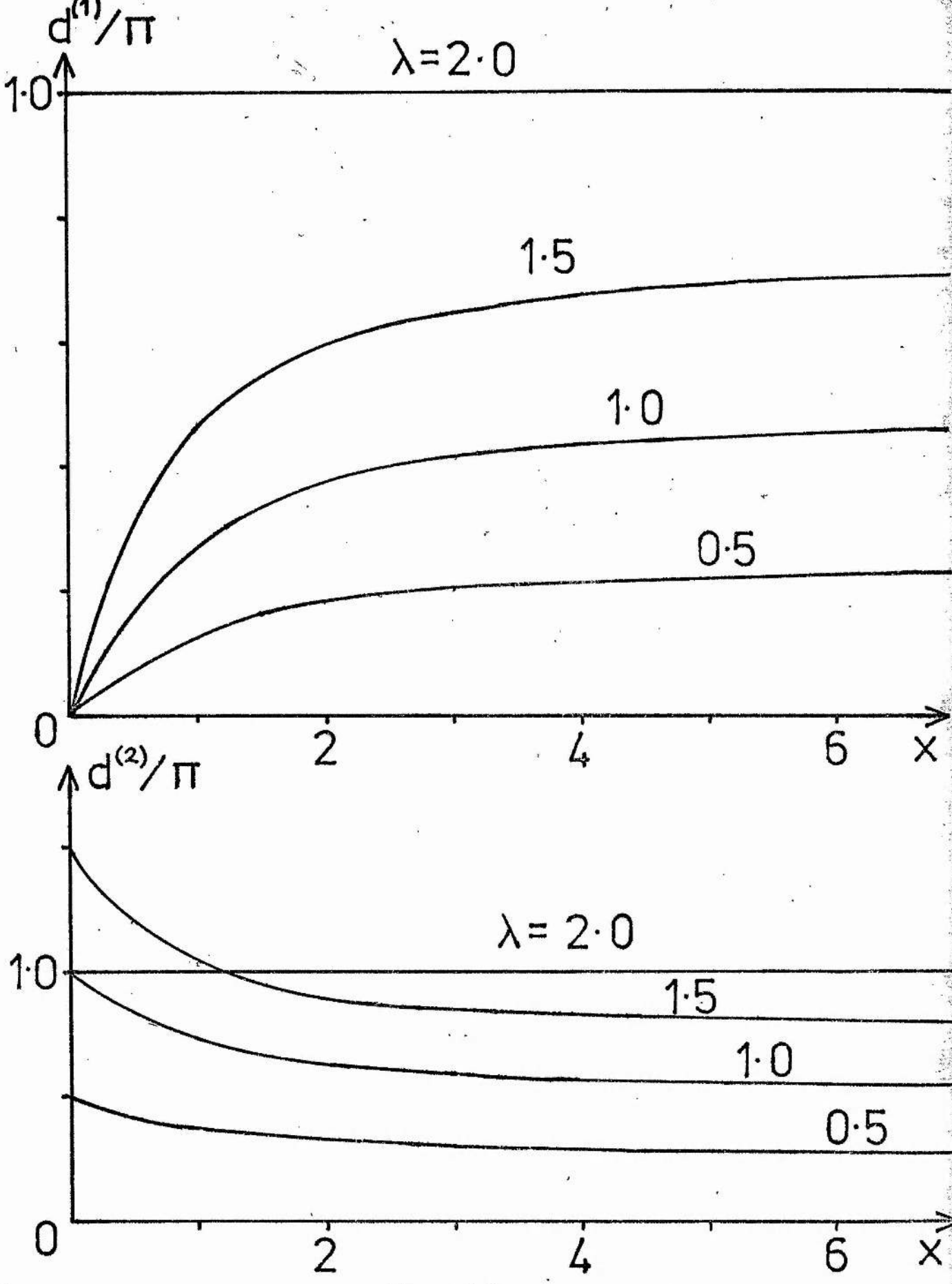

Figure 3.3

The shears $d^{(1)}(x)$ and $d^{(2)}(x)$ that produce cylindrically symmetric force-free fields with a normal photospheric magnetic field of $B_n(x) = -2x/(1 + x^2)$, where $\frac{1}{2}\lambda = (1 - h^2)^{\frac{1}{2}}$ and h is the distance of the centre of symmetry from the photosphere.

properties to the above. They can be derived by imposing different forms for $B_n(x)$. For example, let

$$B_n(x) = x/(1 + x^2)^n \quad .$$

Then

$$B_\phi = r/(1 - h^2 + r^2)^n$$

and

$$B_z^2 = (1 - h^2 + 2(1 - n)r^2)/((2n - 1)(1 - h^2 + r^2)^{2n}) \quad .$$

If we wish B_z to tend to zero as r approaches infinity, n must lie between $\frac{1}{2}$ and 1. The solutions behave in a similar manner to those described above with again a maximum permissible B_z. However, they do not evolve from a potential configuration, since for $n \neq 1$ we cannot have B_z zero everywhere.

3.3.2 Problem II

Now let us examine whether there are forms for the shear $d(x)$ and normal field $B_n(x)$ which allow two distinct cylindrically symmetric force-free fields. They would presumably possess the same $B_\phi(r)$ so as to give the same $B_n(x)$. Their axial components $B_z^{(1)}(r)$, $B_z^{(2)}(r)$ would differ, with $B_z^{(1)}$ exceeding $B_z^{(2)}$ in such a way that the two configurations in Figure 3.2 gave the same shear. Furthermore, the fact that $d^{(1)}(x)$ vanishes at $x = 0$ ($\Phi = 0$ and $r_o = h$) would imply that $B_z^{(2)}$ vanishes there too, assuming that B_ϕ were finite.

The condition that the shears be identical

$$d^{(1)}(x) \equiv d^{(2)}(x)$$

implies from (3.34) and (3.36) that

$$\Phi\, B_z^{(1)} = (\pi - \Phi) B_z^{(2)} \quad . \qquad \ldots (3.37)$$

Also, since we are assuming B_ϕ to be the same, the only way for $B_z^{(1)^2}$ and $B_z^{(2)^2}$ to satisfy both (3.30) and (3.35) and to be distinct is for them to

differ by a non-zero positive constant c, say,

$$B_z^{(2)^2} = B_z^{(1)^2} - c \quad . \qquad \ldots (3.38)$$

Equations (3.37) and (3.38) then determine the axial fields as

$$B_z^{(2)^2}(r) = \frac{c\Phi^2}{\pi(\pi - 2\Phi)} \qquad \ldots (3.39)$$

and

$$B_z^{(1)^2}(r) = \frac{c(\pi - \Phi)^2}{\pi(\pi - 2\Phi)} \quad , \qquad \ldots (3.40)$$

where from (3.31)

$$\cos \Phi = h/r \quad .$$

They are sketched in Figure 3.4 and B_ϕ is given as follows by (3.30), while $d(x_o)$ and $B_n(x_o)$ follow from (3.34) and (3.33) respectively.

Using the results that

$$r = h/\cos \phi$$

and

$$dr/d\Phi = h \sin \Phi/\cos^2\Phi \quad .$$

Equation (3.30) may be expressed in terms of Φ rather than r as

$$\frac{dB_\phi^2}{d\phi} + 2 \tan \Phi \, B_\phi^2 = - \frac{dB_z^{(1)^2}}{d\Phi} \quad ,$$

where from (3.40)

$$\frac{dB_z^{(1)^2}}{d\Phi} = \frac{2c\Phi(\pi - \Phi)}{\pi(\pi - 2\Phi)^2} \quad .$$

The solution of the above equation may be written

$$B_\phi^2 = (B_o^2 - c\, I(\Phi))\cos^2\Phi \quad , \qquad \ldots (3.41)$$

where B_o is the value of B_ϕ at $\Phi = 0$ and

$$I(\Phi) = \int_o^\Phi \frac{2\Phi(\pi - \Phi)}{\pi \cos^2\Phi(\pi - 2\Phi)^2} \, d\Phi \quad .$$

We notice that, if new (dashed) variables are defined by

$$\underline{B} = B_o \underline{B}' \quad , \quad r = hr' \quad , \quad c = B_o^2 c' \quad ,$$

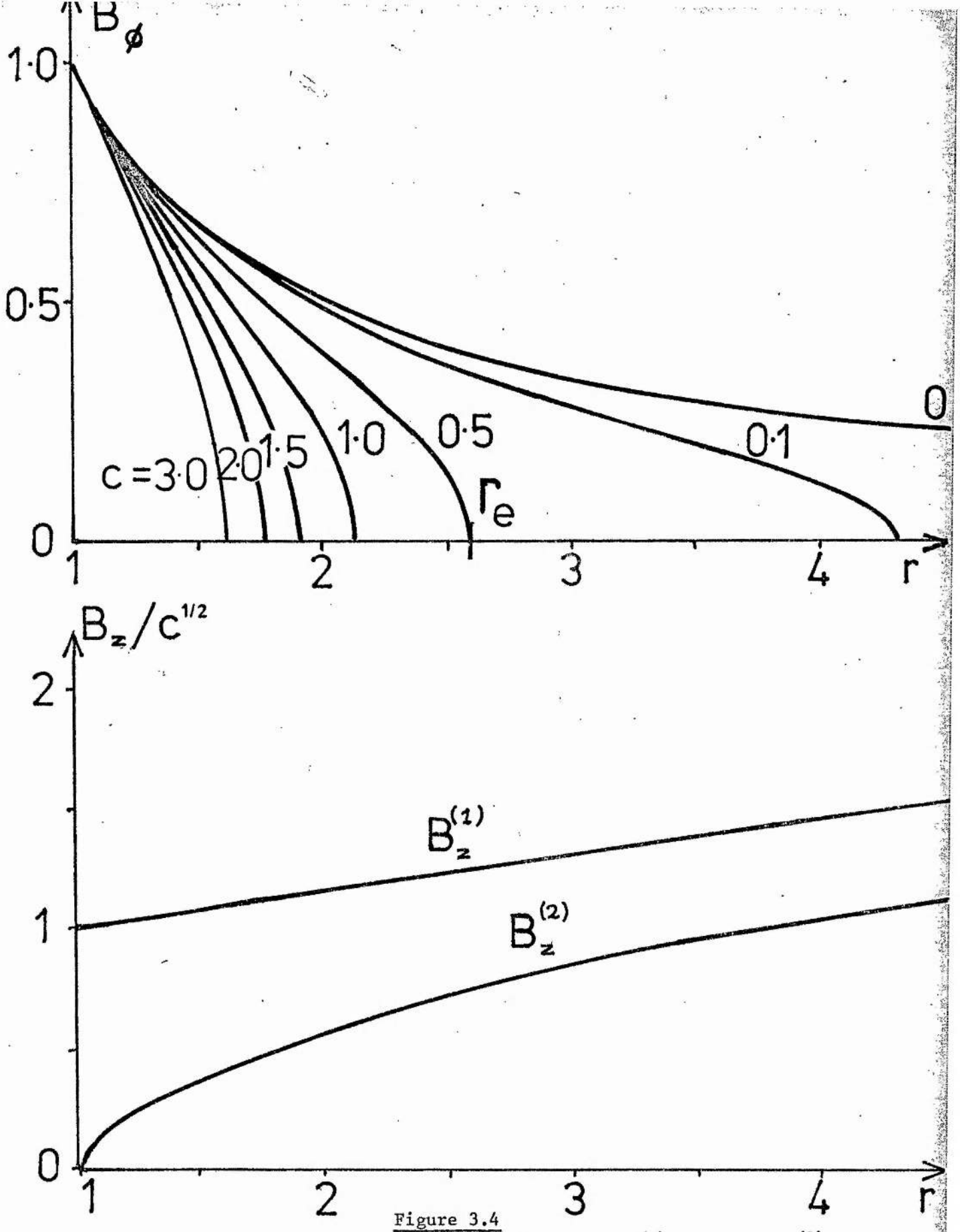

Figure 3.4

The two cylindrically symmetric solutions (B_ϕ, $B_z^{(1)}$) and (B_ϕ, $B_z^{(2)}$) that correspond to the same photospheric shear and normal field. The parameter c gives the difference between $B_z^{(1)2}$ and $B_z^{(2)2}$. r_e is the radius at which B_ϕ vanishes, shown here for the case c = 0.5.

and the dashes then dropped, the effect is simply to put $h = 1$ and $B_o = 1$, and c is now a measure of the strength of B_z. This means that the solutions become

$$B_\phi^2 = (1 - c\, I(\Phi))\cos^2\Phi \quad ,$$

$$B_z^{(2)^2} = B_z^{(1)^2} - c \quad ,$$

$$B_z^{(1)^2} = c(\pi - \Phi)^2\pi^{-1}(\pi - 2\Phi)^{-1} \quad ,$$

$$\cos\Phi = r^{-1}$$

with only one parameter, namely c.

Now, for Φ between 0 and $\pi/2$, I is a monotonically increasing function of Φ and for small values of Φ ($<< 1$)

$$B_\phi^2 \simeq 1 - \left(\frac{1}{2} + c\pi^{-2}\right)\Phi^2 \quad ,$$

$$B_z^{(1)^2} \simeq c(1 + 5\Phi^2/\pi^2) \quad , \qquad \ldots (3.42)$$

$$B_z^{(2)^2} \simeq 5c\,\Phi^2/\pi^2 \quad .$$

Furthermore, the solutions are valid only out to the value of Φ (say Φ_e, with the corresponding value of r being r_e) given by

$$I(\Phi) = c^{-1}$$

at which B_ϕ vanishes. Beyond Φ_e, B_ϕ becomes imaginary. The solutions are sketched in Figure 3.4 together with the corresponding shear d(x) and normal field $B_n(x)$ in Figure 3.5.

In view of the question of stability, it is important to estimate the energies of the two magnetic fields out as far as the radius r_e where B_ϕ vanishes. For the first solution

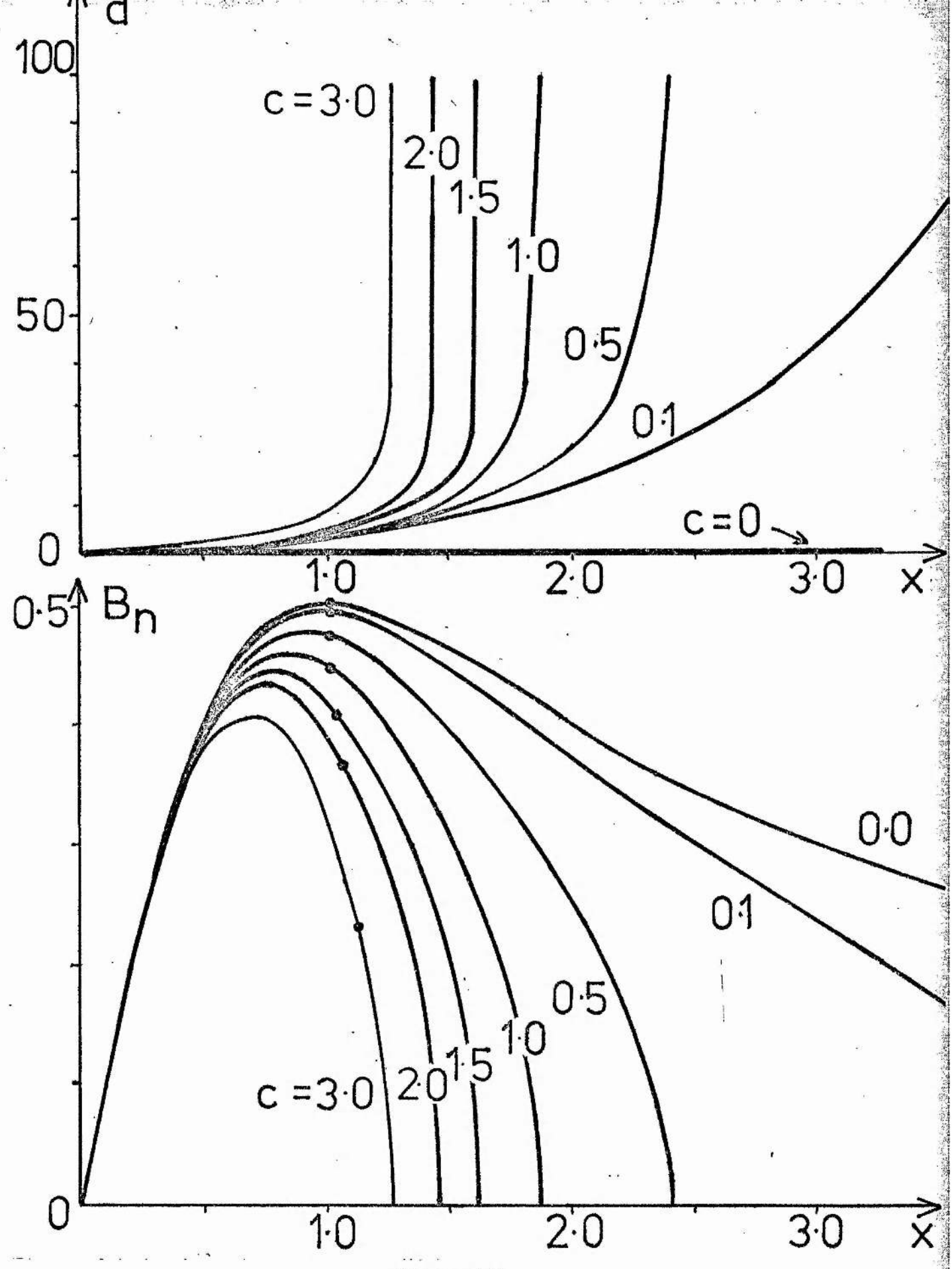

Figure 3.5

The photospheric shear d(x) and normal field $B_n(x)$ which allow the two distinct cylindrically symmetric force-free fields. (The dots indicate the location of the $x^*(c)$ which begins at x = 1 when c = 0).

$$W^{(1)} = \int_{r=1}^{r_e} \int_{\phi=-\Phi}^{\Phi} B^2/2\mu \; r dr d\phi$$

$$= \mu^{-1} \int_{1}^{r_e} B^2 \Phi \; r dr$$

or, after changing the variable from r to Φ,

$$W^{(1)} = \mu^{-1} \int_{0}^{\Phi_e} B^2 \Phi \sin \Phi / \cos^3 \Phi \; d\Phi \quad .$$

The corresponding energy for the second solution is

$$W^{(2)} = \mu^{-1} \int_{0}^{\Phi_e} B^2 (\pi - \Phi) \sin \Phi / \cos^3 \Phi \; d\Phi + M$$

where M is the contribution from the magnetic island.

When c = 0 we have the potential case where

$$B_\phi = \cos \Phi \quad , \quad B_z^{(1)} = B_z^{(2)} = 0$$

and we find $W^{(2)} + M > W^{(1)}$.

If c is large, we see from (24) that the value of Φ which makes B_ϕ vanish is

$$\Phi_e \simeq \pi / c^{\frac{1}{2}}$$

so that

$$W^{(1)} \simeq \pi^3 / (3\mu c^{\frac{1}{2}})$$

and

$$W^{(2)} \simeq 3\pi^2 / (2\mu c) + M \quad .$$

In particular, if M is less than order $c^{-\frac{1}{2}}$, we find

$$W^{(2)} < W^{(1)} \quad .$$

The energies, $W^{(1)}$ and $W^{(2)}$ are calculated numerically and the results shown in Figure 3.6. We see that, when c is large enough, $W^{(2)} - M < W^{(1)}$. This suggests that, provided M is not too large, the field with z component

$B_z^{(1)}$ may be unstable, since there exists another field (namely $B_z^{(2)}$) satisfying the same photospheric boundary conditions and possessing a lower energy.

The contribution to the energy of the magnetic island term depends on the magnetic structure within the island. The minimum possible magnetic energy is that of the potential field which has

$$B_\phi = B_z = 0$$

within the island. I.e. we have a magnetic "bubble". This gives rise to a sheet current on $r = 1$, which does not contribute to the energy of the total field and so we find that the field with energy $W^{(1)}$ becomes unstable beyond the point where the energies cross.

There are three limitations with the above analysis, firstly that the flux through the photosphere changes with the parameter c, secondly that no account has been taken of the field beyond the radius $r = r_e$, and thirdly that there must be some contribution to the energy from the gas within the magnetic bubble (necessary to give pressure balance) due to its potential energy.

The first two inadequacies can be remedied by considering, for example, the model sketched in Figure 3.8. We first demand that the magnetic flux F_o through the photosphere out to the distance $x^*(c)$ remains constant as c increases, so that a fixed group of field lines are considered. It can be seen from Figure 3.5b that, in order to satisfy this, the photospheric field must extend over a larger area as c increases. Thus the photospheric footpoints in this particular example slowly increase their distance from the axis as they are sheared. Also as c increases the situations eventually arises where x^* exceeds $\tan \Phi_e$, so that the constraint of constant flux can no longer be satisfied. Thus the model possesses a maximum allowable shear (i.e. value of c).

In Figure 3.7 we plot the two energies $W^{(1)}$ and $W^{(2)}$ subject to

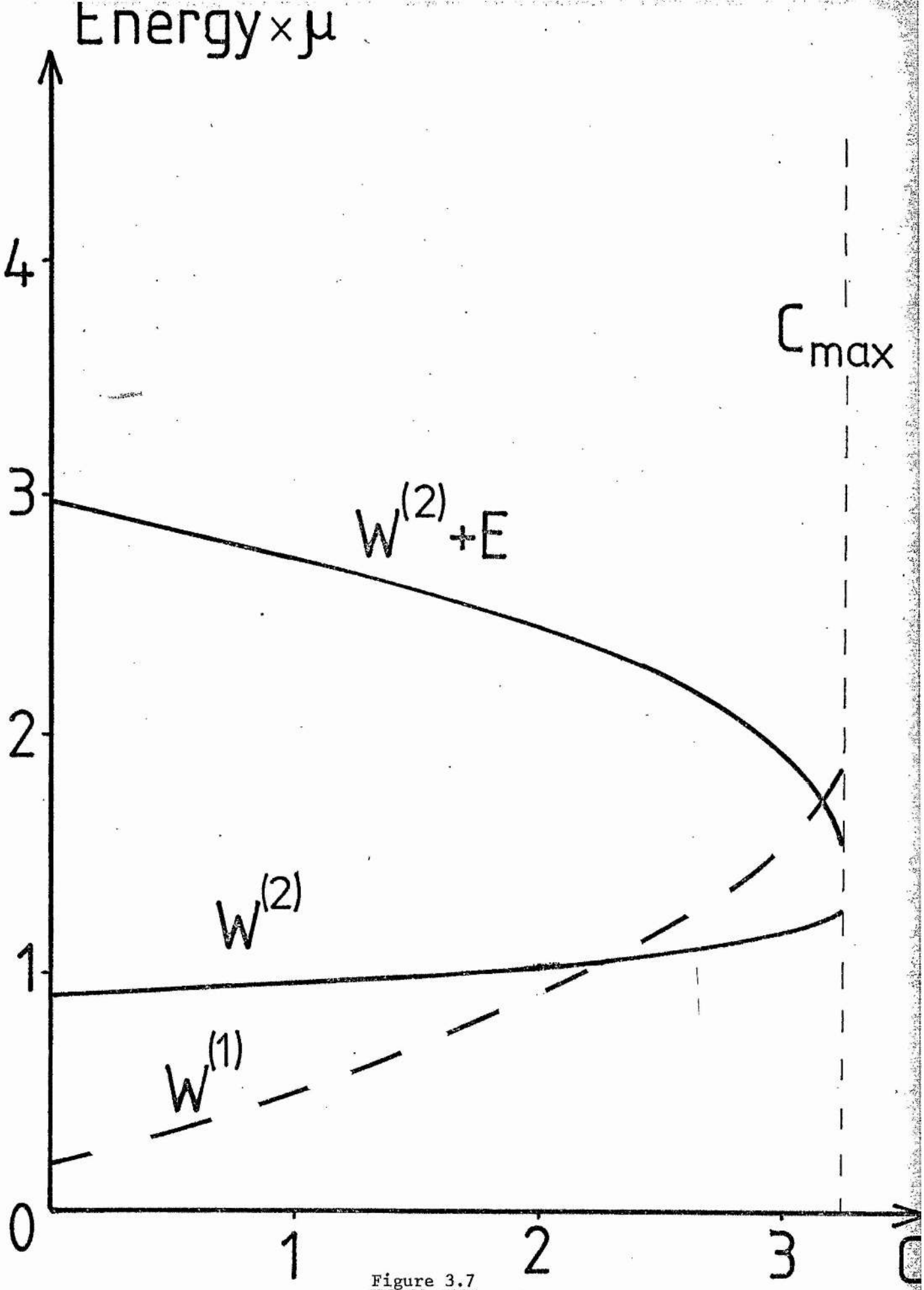

Figure 3.7

The magnetic energies of the two fields in Figure 3.2 where E is defined in the text and M is neglected.

the constraint that the flux F_o remain equal to, for example, 0.35. This is just the flux between $x = 0$ and $x = 1.2$. As c increases from 0 to a maximum value of about 3.2, so the distance x^* out to which the field extends increases from 1 to about 1.2. Figure 3.8b shows that again $W^{(1)} < W^{(2)}$ for small values of c but $W^{(1)} > W^{(2)}$ for large values suggesting the possibility of instability. Smaller values of F_o produce the same conclusion, but, if F_o exceeds the potential flux between $x = 0$ and $x = 1.7$, the curves for $W^{(1)}$ and $W^{(2)}$ no longer cross.

The second modification is to add a contribution to the energy from the external field. Here we suppose the external field is, for simplicity, potential with

$$B_\phi = B^*/r \ , \ B_z = 0 \quad ,$$

where B^* is the ϕ component of the force-free field at its outer boundary $r = r^*$. The azimuthal field B_ϕ is thus continuous at the boundary while the axial field B_z jumps to zero and gives rise to a current sheet. Since B^* is the same for both the internal fields of Figure 3.8, the external fields are identical. Thus we have constructed two fields with the same normal field components and shear along the whole photospheric boundary. Suppose these fields extend to a large finite distance (not infinity since this gives unbounded energies). Then the difference in their external energies is given by the energy of the shaded region in Figure 3.8, which we will denote by E. Comparing $W^{(1)}$ with $W^{(2)} + E$ as shown in Figure 3.7, we see that the curves still cross, and so the field with energy $W^{(1)}$ becomes unstable when the shear parameter c is in excess of a critical value, here about 3.1. This corresponds to a shear angle at $x = x_e/2$ of about 65^o. The importance of the result lies not in the particular shear angle predicted but in giving a simple example of what may be a general property of more complex fields.

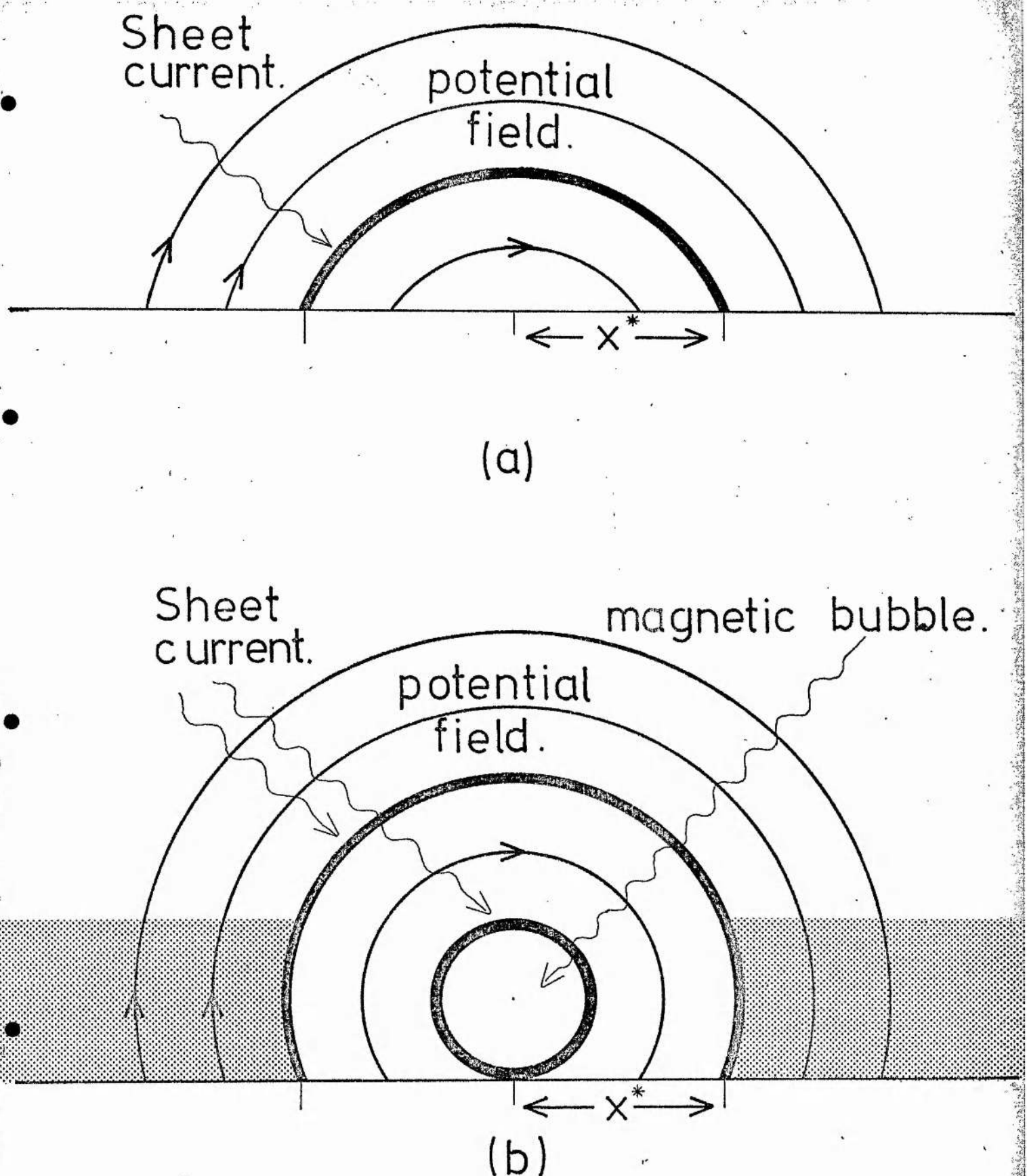

Figure 3.8

The field configurations for two cylindrically symmetric solutions possessing the same shear and normal photospheric field. The heavy lines show the location of the sheet currents which separate the force-free field from the ambient potential field and the magnetic bubble. (a) denotes the field with energy $W^{(1)}$ while (b) denotes the field with energy $W^{(2)}$. When the shear is too large the former field may erupt outwards towards the latter.

The third point to clarify is the possible contribution of the potential energy of the gas within the bubble, in which case we allow for departures from a force-free field. (Of course, we need not only the gas but instead a magnetic field in the z direction as balancing the external magnetic pressure. However, in doing this we find that the energy curves never cross). For the case of gas inside the bubble we assume it to have a pressure equal to the magnetic pressure at the edge. We approximate the potential energy per unit volume of the gas as

$$E_{pot} = \rho g h$$

where ρ is the density of the gas and h is the height of the top of the bubble above the photosphere (as in Figure 3.2b). Since we assume magnetic fields B_o (the field strength at the edge of the bubble) of constant length against h we find the energy of the gas bubble to be

$$E_{pot} = \pi/2\mu\overline{\Lambda}$$

where $\overline{\Lambda} = \Lambda/h$ and $\Lambda(= RT/g)$ is the scale height of the gas.

From Figure 3.7 we require

$$E_{pot} < 0.2/\mu$$

for the energy curves to cross. Hence the condition for instability, $W^{(1)}$ is

$$\overline{\Lambda} > 7.9 \quad .$$

For a coronal scale height this allows a maximum bubble height of 8×10^5 km beyond which there is no instability. (The importance of this result is a mathematical one, namely that it is possible to find two magnetic configurations from the same boundary conditions for which the energy of the first eventually exceeds that of the second if the shear is large enough. We are not suggesting that the solar bubble corresponds precisely to these configurations. Indeed the plasma pressure in the bubble would need to be rather large; for a magnetic field of 0.1 T we find nT to be 3×10^{22} deg. m^{-3}, so that, for example, a

10^6 K means a density of 3×10^{16} m^{-3}).

3.4 Separable solutions

Analytic progress towards finding force-free fields may be made by seeking separable solutions. In particular we consider cylindrical polar coordinates (r,ϕ,z) with the origin located on the photospheric boundary, (rather than at $\pm$ h (Figure 3.2) as in the previous Section). Also we suppose that there is no dependence on z, so that,

$$\underline{B} = \underline{B}(r,\phi) \quad .$$

The r and z components of our basic equation (3.1), together with (3.3) then become

$$B_z \frac{\partial B_z}{\partial r} + \frac{B_\phi}{r}\left(\frac{\partial}{\partial r}(rB_\phi) - \frac{\partial B_r}{\partial \phi}\right) = 0 \quad , \qquad \ldots (3.43)$$

$$\frac{B_\phi}{r}\frac{\partial B_z}{\partial \phi} + B_r \frac{\partial B_z}{\partial r} = 0 \quad , \qquad \ldots (3.44)$$

$$\frac{\partial}{\partial r}(rB_r) + \frac{\partial B_\phi}{\partial \phi} = 0 \quad . \qquad \ldots (3.45)$$

As in the previous Sections, we shall consider more than one form for the boundary conditions to the above equations. These conditions will be described, as and when required, later in this Section.

The assumption that the magnetic field components are of separable form, namely,

$$B_r = R_r(r)F_r(\phi) \ , \ B_\phi = R_\phi(r)F_\phi(\phi) \ , \ B_z = R_z(r)F_z(\phi) \quad ,$$

means that the equations (3.43)-(3.45) reduce to

$$\frac{rR_z}{R_r R_\phi}\frac{dR_z}{dr} + \frac{F_\phi^2}{F_z^2}\frac{1}{R_r}\frac{d}{dr}(rR_\phi) = \ell = \frac{F_\phi}{F_z^2}\frac{dF_r}{d\phi} \quad , \qquad \ldots (3.46)$$

$$\frac{rR_r}{R_\phi R_z}\frac{dR_z}{dr} = m = -\frac{F_\phi}{F_r F_z}\frac{dF_z}{d\phi} \quad , \qquad \ldots (3.47)$$

$$\frac{1}{R_\phi}\frac{d}{dr}(rR_r) = n = -\frac{1}{F_r}\frac{dF_\phi}{d\phi} \quad . \qquad \ldots (3.48)$$

In writing this set of equations, the functions of r and of ϕ have been separated on to different sides, which need to equal constants denoted by ℓ, m and n.

In order to make (3.46) of separable form, we need any of the conditions

$$\frac{F_\phi}{F_z} = \text{constant} \quad , \qquad \ldots (3.49)$$

$$\frac{1}{R_r}\frac{d}{dr}(rR_\phi) = \text{constant} \quad , \qquad \ldots (3.50)$$

or

$$\frac{dR_z}{dr} = 0 \quad .$$

to be satisfied.

The first possibility leads to linear force-free fields, while the second must be further subdivided into the cases of the constant being zero or non-zero, and gives some new solutions. The third produces purely current-free solutions. They are considered in turn below.

3.4.1 Solution with F_ϕ/F_z = constant

We consider here the family of solutions with

$$F_\phi/F_z = 1 \quad ,$$

where the constant in (3.49) has been put equal to unity without loss of generality. The ϕ-dependent parts of equations (3.46)-(3.48) then imply that

$$m = n \quad ,$$

$$\frac{dF_z}{d\phi} = -mF_r \quad ,$$

and

$$\frac{dF_r}{d\phi} = \ell F_z \quad .$$

The solutions that correspond to magnetic arcades with F_r behaving as $\ell\phi$ and vanishing at the summit ($\phi = 0$) while F_z is equal to unity there, have

$$\ell = m$$

and are $$F_r = \sin \ell\phi \quad ,$$

$$F_\phi = F_z = \cos \ell\phi \quad .$$

The r-dependent parts of (3.46)-(3.48) become

$$\frac{d}{dr}(rR_r) = \ell R_\phi \quad , \qquad \ldots (3.51)$$

$$\frac{rR_r}{R_z}\frac{dR_z}{dr} = \ell R_\phi \quad , \qquad \ldots (3.52)$$

$$rR_z\frac{dR_z}{dr} + R_\phi\frac{d}{dr}(rR_\phi) = \ell R_r R_\phi \quad . \qquad \ldots (3.53)$$

Writing the solution in terms of R_r, we have from (3.51)

$$R_\phi = \frac{1}{\ell}\frac{d}{dr}(rR_r)$$

and then, after integrating (3.52) and putting $R_z = R_r$ at $r = 1$, we find

$$R_z = rR_r$$

R_r is given by (3.53), which may be written

$$r^2\frac{d^2R_r}{dr^2} + 3r\frac{dR_r}{dr} + R_r(\ell^2r^2 + 1 - \ell^2) = 0 \quad .$$

Alternatively, in terms of R_z we find

$$r^2\frac{d^2R_z}{dr^2} + r\frac{dR_z}{dr} + R_z(\ell^2r^2 - \ell^2) = 0 \quad ,$$

which is just Bessel's equation, so that

$$R_z = J_\ell(\ell r) \quad ,$$

$$R_r = \frac{1}{r}J_\ell(\ell r) \quad ,$$

$$R_\phi = \frac{1}{\ell}\frac{d}{dr}(J_\ell(\ell r)) \quad .$$

The vector potential for this field is

$$A = -\frac{1}{\ell}J_\ell(\ell r)\cos \ell\phi \quad ,$$

and so $$B_z \alpha A \quad .$$

In other words we have the well-known linear force-free field solution.

3.4.2 Birn's solution

Since the functions R_r, R_ϕ and R_z may be multiplied by constants and F_r, F_ϕ, F_z divided by the same ones without changing the magnetic field components, we shall suppose R_r, R_ϕ, R_z each take the value 1 at $r = 1$. Furthermore, the magnetic field itself may be multiplied by a constant and still satisfy the force-free condition, so we shall, without loss of generality suppose that $B_\phi = -1$ at $r = 1$.

Now consider the special case of (3.50) where

$$\frac{d}{dr}(rR_\phi) = 0 \quad . \qquad \ldots (3.54)$$

Integration of (3.54) and (3.48) then give

$$R_\phi = \frac{1}{r} \quad ,$$

$$R_r = (n \log r + 1)/r \quad ,$$

and

$$\frac{dF_\phi}{d\phi} = -nF_r \quad .$$

Since R_z must satisfy (3.48) and (3.47), we have both

$$\frac{r^3 R_z}{(n \log r + 1)} \frac{dR_z}{dr} = \ell \quad ,$$

and

$$\frac{r(n \log r + 1)}{R_z} \frac{dR_z}{dr} = m \quad .$$

Thus for consistency, it is necessary that

$$\frac{1}{m}(n - (n \log r + 1)) = 1 \quad ,$$

so that, $n = 0$ and $m = -1$.

The condition that $R_z = 1$ at $r = 1$ implies $\ell = -1$ and so

$$R_r = 1/r \quad ,$$

$$F_\phi = -1 \quad ,$$

and

$$R_z = 1/r \quad .$$

The remaining two equations arise from the right hand sides of (3.46) and (3.47), namely,

$$\frac{dF_r}{d\phi} = F_z^2$$

and

$$\frac{dF_z}{d\phi} = - F_r F_z \quad . \qquad \ldots (3.55)$$

F_r may be eliminated to give

$$\frac{d}{d\phi}\left(\frac{1}{F_z}\frac{dF_z}{d\phi}\right) = - F_z^2 \quad ,$$

whose solution is,

$$F_z = p/\cosh(p\phi + q) \quad ,$$

with p and q being the constants of integration. Equation (3.55) then determines F_r as

$$F_r = p \tanh(p\phi + q) \quad .$$

In particular, the symmetric solution, for which B_r vanishes on the vertical axis has q = 0 so that

$$B_r = \frac{p}{r} \tanh p\phi \quad , \qquad \ldots (3.56)$$

$$B_\phi = - \frac{1}{r} \qquad \ldots (3.57)$$

$$B_z = \frac{p}{r \cosh p\phi} \quad . \qquad \ldots (3.58)$$

(If p is put equal to $2b/\pi$ and each magnetic field component is multiplied by 2/c, this solution reduces to the one that Birn et al (1978) discovered by a much more involved method).

Consider the above solution in the light of problems I and II. For problem I, the normal component at the photosphere is prescribed to be

$$B_n(r) = (B_\phi)_{\phi=\frac{\pi}{2}} = - r^{-1} \quad ,$$

while the axial field at the photosphere is prescribed to be k/r say. By

comparing with (3.58) we see that p is determined in terms of the prescribed constant k by

$$\frac{p}{\cosh(p\pi/2)} = k \quad .$$

Provided k is not too large this gives two solutions for p. (In the notation of Birn et al, k is replaced by $2a\pi^{-1}(2\lambda/c)^{\frac{1}{2}}$). For problem II it is the photospheric shear that is prescribed and in this case the shear is

$$d(x) = x \sinh \tfrac{1}{2} p\pi \quad .$$

Imposing the shear in this linear form therefore fixes a unique value for p and hence a unique solution (3.56)-(3.58). The fact that $\sinh \frac{1}{2} p\pi$ is a monotonic function of p means that it is not possible to have two solutions with the same shear and in the form (3.56)-(3.58).

3.4.3 Generalisation of Birn's solutions

We here consider the case when

$$\frac{d}{dr}(rR_\phi) = kR_r \quad , \qquad \ldots (3.50)$$

where k is constant and for the special case k = 0 the solutions reduce to those of the previous Section.

Combining (3.48) and (3.50) gives

$$r^2 \frac{d^2R_r}{dr^2} + 3r \frac{dR_r}{dr} + (1 - nk)R_r = 0 \quad .$$

and

$$R_\phi = \frac{1}{n} \frac{d}{dr}(rR_r) \quad ,$$

the solutions being

$$R_r = C r^{-1 - (nk)^{\frac{1}{2}}} + D r^{-1 + (nk)^{\frac{1}{2}}}$$

$$R_\phi = (k/n)^{\frac{1}{2}} \left(-C r^{-1 - (nk)^{\frac{1}{2}}} + D r^{-1 + (nk)^{\frac{1}{2}}}\right)$$

Equations (3.46), (3.47) then determine R_z as

$$R_z^2 = (\ell/m) R_r^2$$

with the consistency conditions that

$$C = 0 \quad \text{and} \quad \ell((nk)^{\frac{1}{2}} + 1) = m(nk)^{\frac{1}{2}} \quad . \qquad \ldots (3.59)$$

As before, we require that, without loss of generality, $R_r = R_\phi = R_z = 1$ at $r = 1$, and hence find

$$\ell = m \ , \ n = k \ , \ B = 1 \quad .$$

Thus the r -dependent solutions become

$$R_r = r^{-1-k} \quad , \qquad \ldots (3.60)$$

$$R_\phi = r^{-1-k} \quad , \qquad \ldots (3.61)$$

and

$$R_z = \pm \, r^{-1-k} \quad , \qquad \ldots (3.62)$$

while the consistency condition (3.59) reduces to

$$m = k + 1 \quad .$$

The ϕ-dependent equations give

$$F_r = - \frac{1}{k} \frac{dF_\phi}{d\phi} \quad , \qquad \ldots (3.63)$$

$$|F_z| = \lambda |F_\phi|^{\frac{k+1}{k}} \qquad \ldots (3.64)$$

where F_ϕ satisfies

$$\frac{d^2F_\phi}{d\phi^2} + k^2 F_\phi + \lambda^2 k(k+1) F_\phi |F_\phi|^{2/k} = 0 \quad , \qquad \ldots (3.65)$$

and λ is a constant of integration arising from (3.47).

For symmetric solutions we require that $F_r(0) = 0$ and also the normal component of the field $(B_\phi)_{\phi=0}$ must be specified. The problem therefore reduces to solving (3.65) for given k, and a range of values of λ, subject to the boundary condition that

$$\frac{dF_\phi}{d\phi} = 0 \quad \text{at} \quad \phi = 0$$

and

$$F_\phi \left(\frac{\pi}{2} \right) = \rho \ , \ \text{say} \quad .$$

Scaling F_ϕ against ρ has the effect of changing λ to $\lambda\rho^{-1/k}$, so we need consider only the case $F_\phi\left(\frac{\pi}{2}\right) = 1$.

We note that $\lambda = 0$ gives $B_z = 0$ and thus the potential field, while $k = -1$ gives the current free solution with B_z = constant. Before attempting to solve (3.65) more generally it is of interest to consider the phase-plane behaviour for various ranges of k and λ. To do this we rewrite (3.65) as a pair of first order equations, namely

$$\frac{dF_\phi}{d\phi} = u \quad ,$$

$$\frac{du}{d\phi} = -k^2 F_\phi - \lambda^2 k(k+1) F_\phi |F_\phi|^{2/k} \quad . \qquad \ldots (3.66)$$

Now we are particularly interested in arcade-like solutions of the equations which develop from the potential field ($\lambda = 0$) as the footpoints are sheared. Thus we require that the solutions with $\lambda = 0$ be arcade-like. This means that at no point in the range $\left[-\frac{\pi}{2}, \frac{\pi}{2}\right]$ is the field purely radial, which restricts us to values of k satisfying $|k| < 1$. (Other values of k produce solutions with field lines which originate at infinity but do not cross the photosphere).

Critical points of the system occur when the right hand sides of (3.66) are identically zero, and it transpires that they are always centre points.

For $\lambda = 0$ or $k > 0$ the point $u = 0$, $F_\phi = 0$ is a critical point, while for $-1 < k < 0$ a critical point occurs at $u = 0$,
$F_\phi = \pm \left|k/(\lambda^2(k+1))\right|^{2/k}$.

One interesting feature of the solution is the form of the resulting shear d(x). To evaluate this we note that the vector potential for the field is

$$A = -r^{-k} F_\phi / k \quad , \qquad \ldots (3.67)$$

and $$B_r = - r^{-1-k} \frac{dF_\phi}{d\phi}/k \quad , \qquad \ldots (3.68)$$

$$B_\phi = - r^{-1-k} F_\phi \quad , \qquad \ldots (3.69)$$

$$B_z = \lambda r^{-1-k} |F_\phi|^{(k+1)/k} \quad . \qquad \ldots (3.70)$$

The equations for the fieldlines are given by

$$\frac{dz}{B_z} = \frac{dr}{B_r} = \frac{r d\phi}{B_\phi} \quad ,$$

and, in particular, we have

$$\frac{dz}{d\phi} = \frac{rB_z}{B_\phi}$$

$$= \pm \lambda r F_\phi^{\frac{1}{k}} \qquad \ldots (3.71)$$

The shear is just the displacement of the footpoint of a fieldline initially at z = 0, so we may use (3.67) to eliminate r in (3.68) and integrate along a fieldline from $\phi = 0$ to $\phi = \frac{\pi}{2}$, giving

$$d(x) = \pm \int_0^{\pi/2} \lambda \left(- \frac{F_\phi^2}{Ak} \right)^{\frac{1}{k}}_{A=\text{constant}} d\phi$$

$$= \pm \lambda |A|^{-1/k} \int_0^{\pi/2} \left| \frac{F_\phi^2}{k} \right|^{\frac{1}{k}} d\phi \quad .$$

Now substituting for A gives solution of the form

$$d(x) = mx$$

where $$m = \pm \lambda \left[\left| \frac{F_\phi}{k} \right|^{-\frac{1}{k}} \right]_{\pi/2} \int_0^{\pi/2} \left| \frac{F_\phi^2}{k} \right|^{\frac{1}{k}} d\phi \quad ,$$

and the square brackets $\left[\right]_{\pi/2}$ denote evaluation at $\pi/2$. So we see that, for all k, the shear implied by the solution is linear in x.

An analytic solution of (3.65) may be obtained for the particular case of $k = -\frac{1}{2}$. Note that F_ϕ may be positive or negative, so for simplicity we consider only the case $F_\phi > 0$, satisfying

$$F_\phi'' + \frac{1}{4} F_\phi - \frac{\lambda^2}{4} F_\phi^{-3} = 0 \quad ,$$

where dashes denote differentiation with respect to ϕ. This equation admits two solutions with $F_\phi'(0) = 0$ and $F_\phi\left(\frac{\pi}{2}\right) = 1$, namely

$$F_\phi = (\pm (1 - \lambda^2)^{\frac{1}{2}} \cos \phi + 1)^{\frac{1}{2}} \quad , \qquad \ldots (3.72)$$

and we need

$$\lambda^2 \leq 1$$

in order that they be real. The components of $\underline{B}$ are thus

$$B_r = 2r^{-\frac{1}{2}} F_\phi' \quad ,$$

$$B_\phi = - r^{-\frac{1}{2}} F_\phi \quad ,$$

$$B_z = \lambda r^{-\frac{1}{2}} F_\phi^{-1} \quad ,$$

with vector potential

$$A = 2r^{\frac{1}{2}} F_\phi \quad .$$

The field lines for various λ are sketched in Figure 3.9 and the corresponding photospheric shear (Figure 3.10) is given by

$$d(x) = \frac{x}{\lambda} \left[\pm (1 - \lambda^2)^{\frac{1}{2}} - \frac{2}{\lambda} \tan^{-1} \left| \frac{\lambda}{1 \pm (1 - \lambda^2)^{\frac{1}{2}}} \right| \right] \quad .$$

If $\lambda^2 < 1$ there are two shears for one value of λ, but when $\lambda^2 = 1$, the two shears merge into one, namely

$$d(x) = \frac{1}{2} \pi x$$

and the field becomes cylindrically symmetric with $F_\phi = 1$.

For other values of k in the range of interest equation (3.65) must be solved numerically. The solutions for $-1 < k < 0$ are typefied by the results shown in Figure 3.11, where we have plotted the fieldline gradient m against λ for several values of k. Birn's solution is given by $k = 0$. All the curves exhibit a maximum allowable λ for a solution to

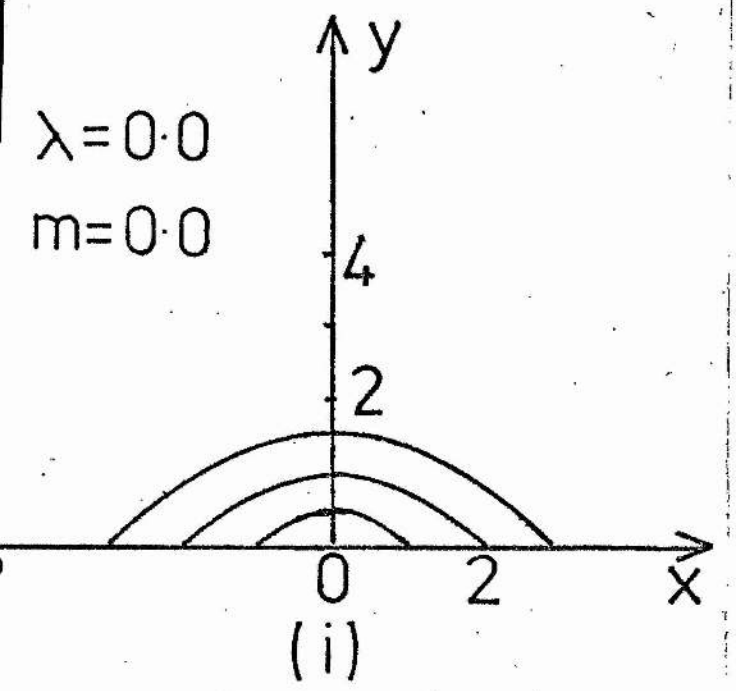

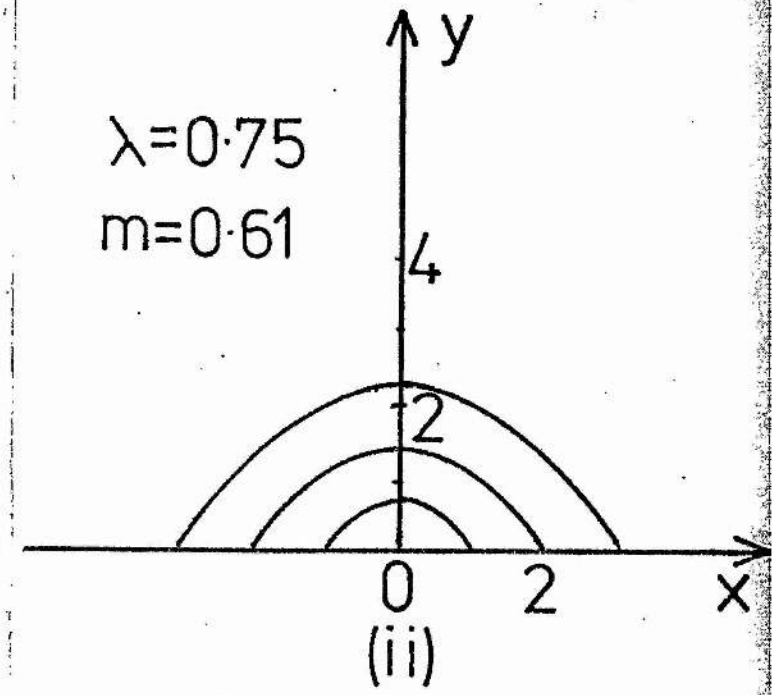

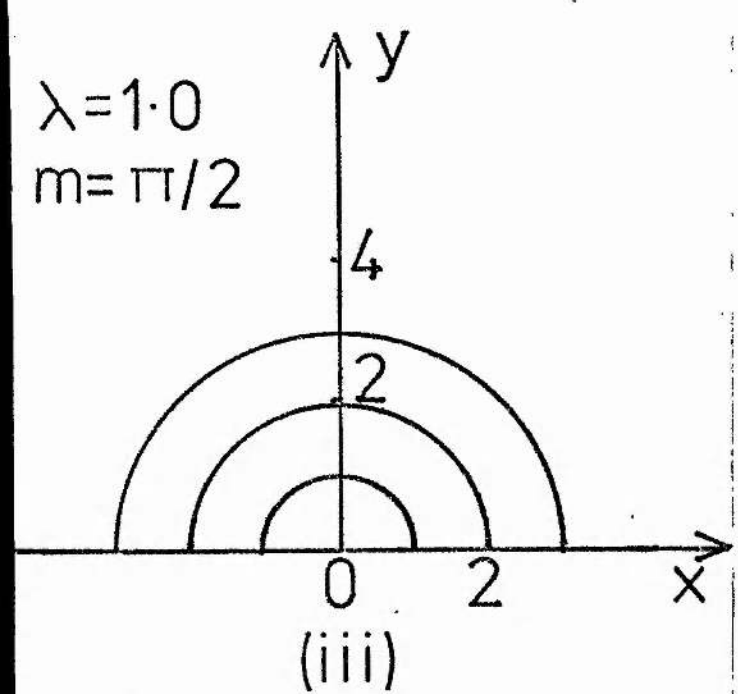

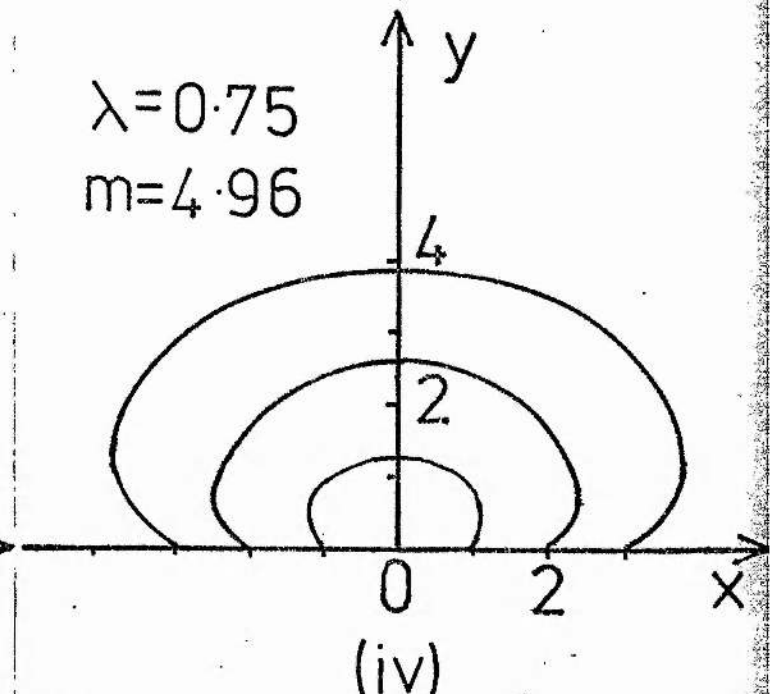

Figure 3.9

(a) The projections on to the vertical (x,y) plane of the fieldlines resulting from the solution in Section 3.3.3 for $k = -\frac{1}{2}$, and several values of λ. The corresponding shear gradient m is also indicated. It increases monotonically as λ reaches its maximum value of 1 and decreases again.

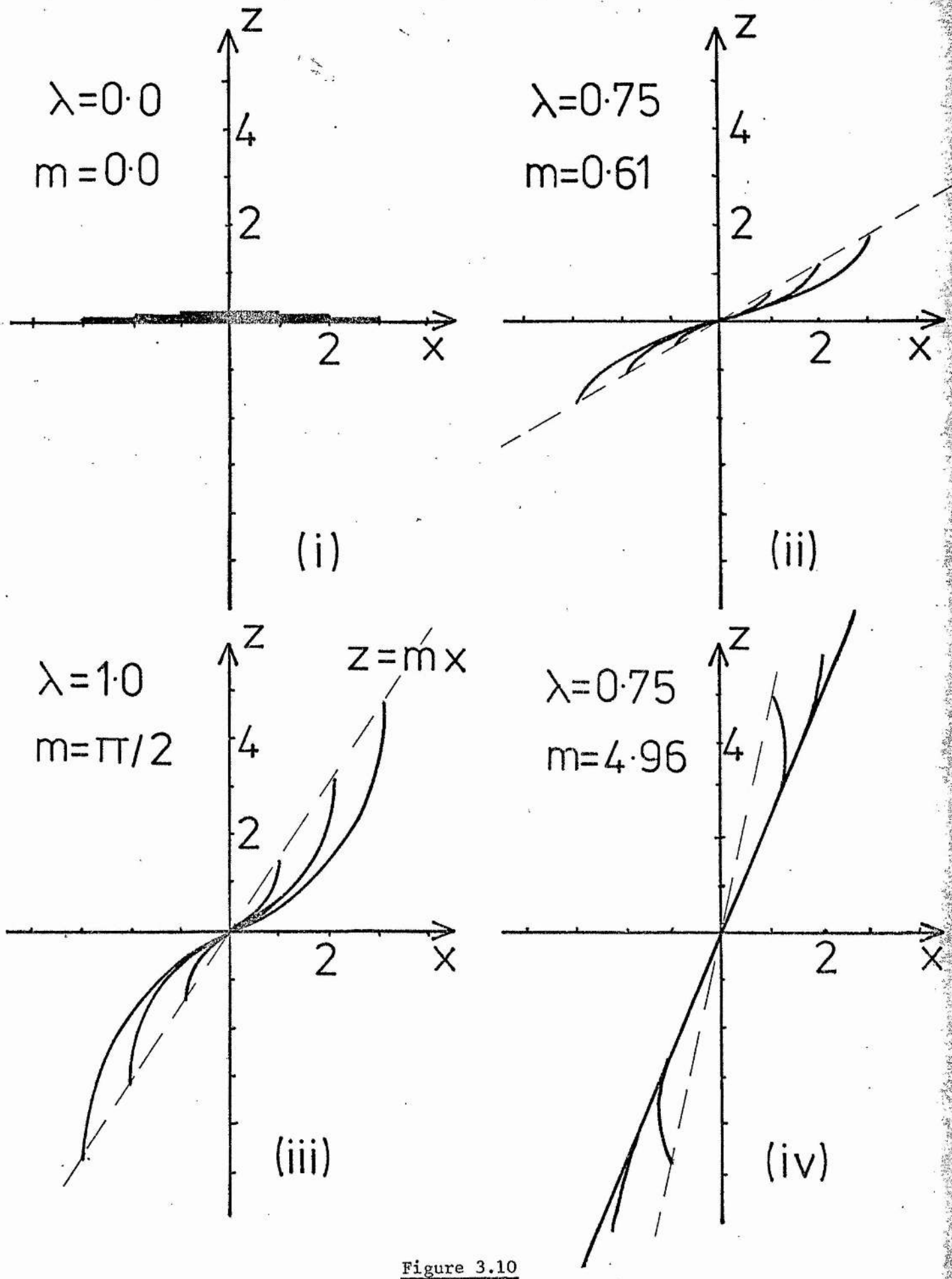

Figure 3.10

The corresponding projection of fieldlines on to the horizontal (x,z) plane. The dashed line, z = mx gives the location of the footpoints initially lying on the x-axis.

exist (namely λ_{max}, say) and two possible solutions for $\lambda < \lambda_{max}$. For each value of the shear gradient m, however, only one solution arises. As m increases from zero, so λ increases to its maximum value and then decreases again.

With k in the range $0 < k < 1$ we find again that there is a maximum allowable λ and for each shear gradient m there exists only one possible solution. This behaviour, the same as for the range $-1 < k < 0$, occurs for a different reason mathematically, best illustrated by considering the phase plane. In Figure 3.12 we show schematically the phase planes for the cases of $-1 < k < 0$ and $0 < k < 1$. In the former case there is one solution with positive gradient and another with negative gradient, starting from $F_\phi' = 0$ and reaching the required value of $F_\phi = 1$ in a "distance" $\phi = \frac{\pi}{2}$. In the latter case no solution with positive gradient is possible but there are two negative gradient solutions reaching the specified $F_\phi = 1$ in a distance of $\phi = \frac{\pi}{2}$.

The above solution may be considered in terms of problem I and II, with similar conclusions to those obtained by Birn et al. For problem I, specifying the normal component as $B_n(x) = p|x|^{-1-k}$, say, and the longitudinal component as $B_z = q(\lambda)\ |x|^{-1-k}$, say, allows two solutions for each value of λ, provided $\lambda < \lambda_{max}$, which depends on the values of k and p chosen. In terms of problem II, we see that specification of $B_n(x)$ and the shear $d(x) = mx$, say, gives a unique solution for all m. Thus again it is not possible to have two solutions with the same shear and in the form (3.68)-(3.70).

3.4.4 Current free solutions

The condition

$$\frac{dR_z}{dr} = 0$$

leads to separable current-free solutions as follows. Equation (3.47) gives

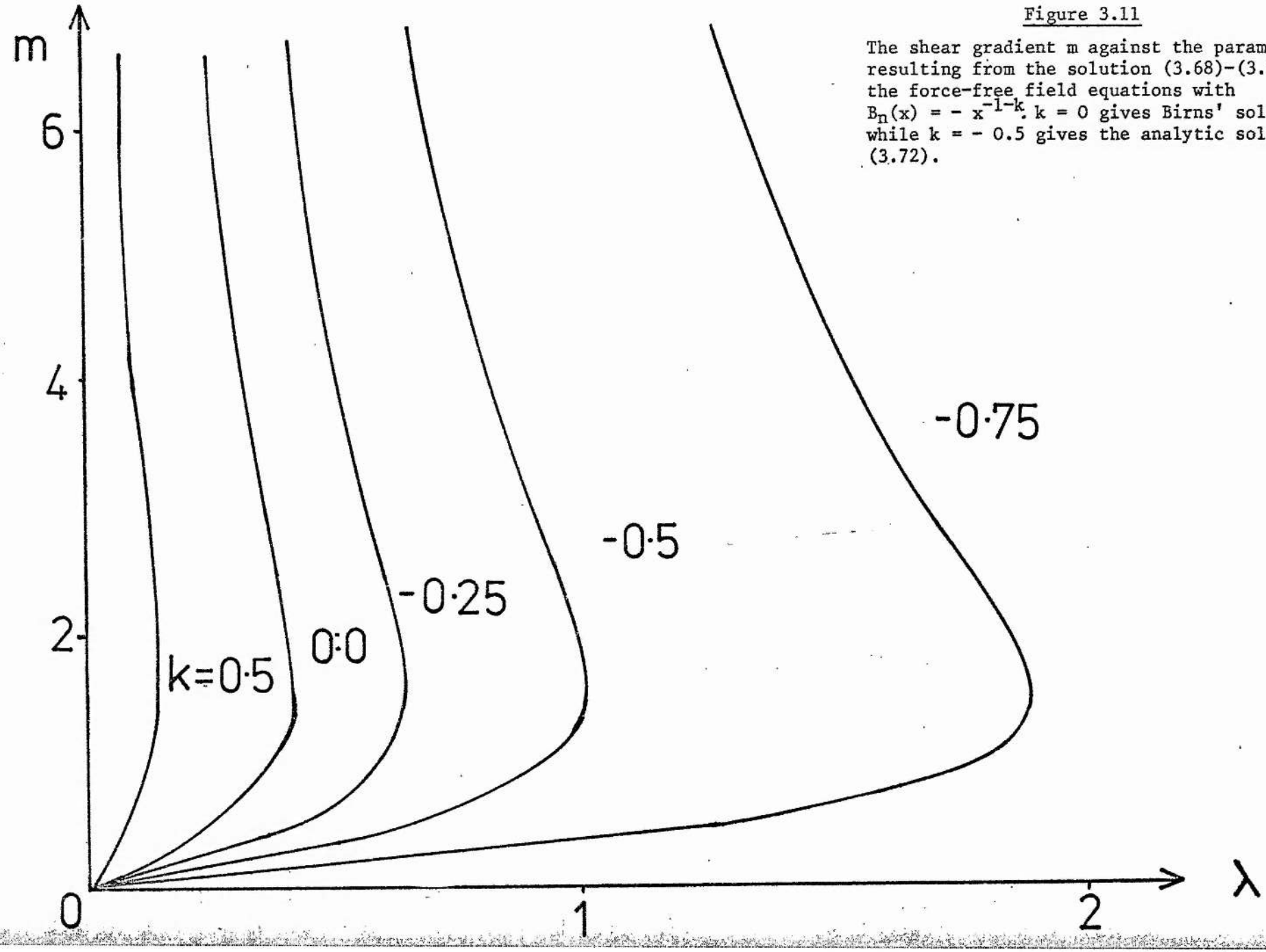

Figure 3.11

The shear gradient m against the parameter λ resulting from the solution (3.68)-(3.70) of the force-free field equations with $B_n(x) = - x^{-1-k}$. k = 0 gives Birns' solution, while k = - 0.5 gives the analytic solution (3.72).

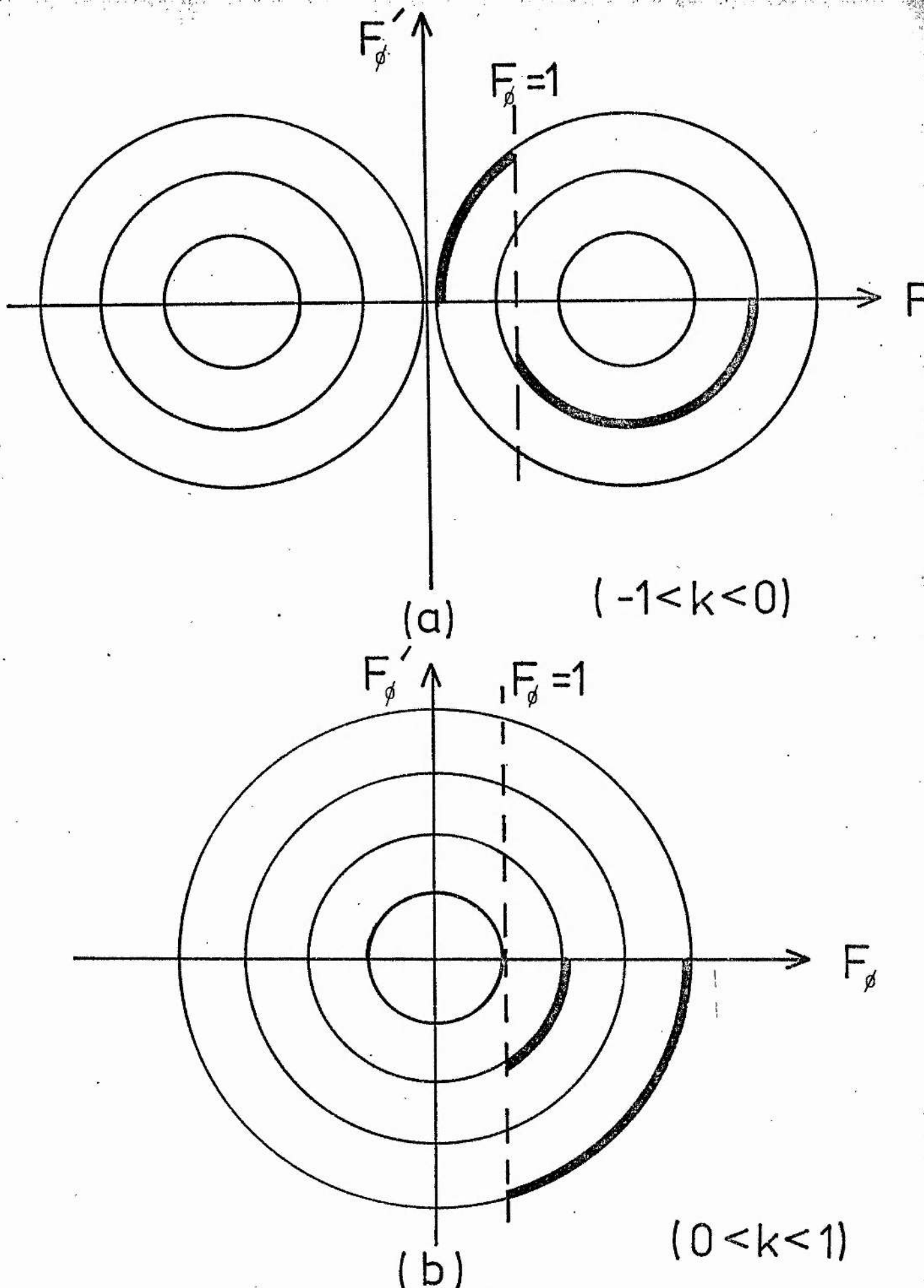

Figure 3.12

Phase plane for equation (3.65) showing the different behaviour when $k > 0$ and $k < 0$. The heavy curves show the possible solutions subject to $F_\phi'(0) = 0$ and $F_\phi(\pi/2) = 1$.

$$R_z = \text{constant}$$

and $$F_z = \text{constant}$$

so that $$B_z = b, \text{ say} \quad .$$

Then we may write (3.46) as

$$\frac{1}{R_r}\frac{d}{dr}(rR_\phi) = \ell = \frac{1}{F_\phi}\frac{dF_r}{d\phi} \quad ,$$

which, when coupled with (3.48) gives

$$R_r = \frac{1}{2}\left(\left(1 - \sqrt{\frac{n}{\ell}}\right) r^{-1-\sqrt{n\ell}} + \left(1 + \sqrt{\frac{n}{\ell}}\right) r^{-1+\sqrt{n\ell}} \right) \qquad \ldots (3.73)$$

and $$R_\phi = \frac{1}{2}\left(-\left(1 - \sqrt{\frac{\ell}{n}}\right) r^{-1-\sqrt{n\ell}} + \left(1 + \sqrt{\frac{\ell}{n}}\right) r^{-1+\sqrt{n\ell}} \right) \quad , \qquad \ldots (3.74)$$

where the condition that $R_r = R_\phi = 1$ at $r = 1$ has been applied. The ϕ-dependent equations, subject to $F_r = 0$ at $\phi = 0$, yield

$$F_r = a \sin \sqrt{n\ell}\,\phi \quad ,$$

$$F_\phi = a\sqrt{\frac{n}{\ell}} \cos \sqrt{n\ell}\,\phi \quad ,$$

where a is an arbitrary constant. We note that for $n = \ell = 1$ (3.73)-(3.74) reduce to the case of $k = -1$ in Section 3.4.3.

The special case of $n = \ell = 0$ yields the solutions

$$F_\phi = \text{constant} \quad , \quad F_z = \text{constant} \quad ,$$

while the r-dependent equations allow

$$R_r = 0 \quad \text{or} \quad \frac{1}{r} \quad ,$$

$$R_\phi = 0 \quad \text{or} \quad \frac{1}{r} \quad .$$

In particular consider the two solutions

$$\underline{B}_1 = \left(0 \, , \, \frac{1}{r} \, , \, b_1\right) \quad ,$$

which is cylindrically symmetric, and

$$\underline{B}_2 = \left(\frac{a}{r} \, , \, \frac{1}{r} \, , \, b_2\right)$$

where $a \neq 0$ and the projections of the fieldlines on to the (r,ϕ) plane trace out curves

$$r = \text{const. } e^{a\phi} \quad .$$

Both $\underline{B}_1$ and $\underline{B}_2$ give a normal component $B_n(x) = x^{-1}$ at the photosphere. For $\underline{B}_1$ the photospheric footpoints lie on the curves

$$z = \pi b_1 x^2 + \text{constant}$$

in the horizontal (x,z) plane. For $\underline{B}_2$ the footpoints lie on the curves

$$z = b_2 x^2 (1 - e^{-2a\pi})/2a + \text{const.} \quad .$$

Thus if b_1, b_2, a are chosen to make

$$b_2 = 2a\pi b_1/(1 - e^{-2a\pi}) \quad ,$$

$\underline{B}_1$ and $\underline{B}_2$ have the same normal components and footpoints lying on the same curve in the photosphere. However, $\underline{B}_1$ and $\underline{B}_2$ do not have the same photospheric connections, since $\underline{B}_2$ is asymmetric while $\underline{B}_1$ is symmetric, and so they do not represent a satisfactory solution to problem II.

From the general solutions to the current-free equations we note that the existence of shear does not preclude potential fields as is sometimes assumed in interpreting H_α and X-ray structures. We may impose a photospheric shear which allows the field to remain potential. In other words an observed shear or twist in a solar magnetic configuration does not immediately rule out the possibility that the field may be potential.

3.5 Discussion

We have considered the problem of passively evolving, two dimensional force-free magnetic fields and in Section 3.1 discussed some of the previous work on this topic. In particular we have discussed problem I, where the photospheric normal and longitudinal components of the field are prescribed, and problem II, where the photospheric shear and normal magnetic field component are given. Problem II is the more relevant

to the sun, since it is photospheric motions that cause the field to evolve.

To make analytic progress, three main approaches have been followed. Firstly, in Section 3.2, linear force-free fields were considered and no possibility of instability was found. Secondly, in Section 3.3, the assumption of cylindrical symmetry was made. For problem I, the solution given by Low (1977) was easily generated, together with other fields possessing similar properties. For problem II we have obtained two fields satisfying the same photospheric boundary conditions of prescribed normal field and shear. The second field contains a magnetic island where the fieldlines do not connect to the phososphere. As the shear increases, the energy of the first field ultimately exceeds that of the second and therefore we suggest that the first field may become unstable and erupt outwards towards the second. The importance of the result lies in giving an example of a feature that may well exist for more general force-free fields, in view of its relevance to two ribbon solar flares. It has proved extremely difficult to obtain numerical solutions to the force-free field equations (Jockers, 1978; Heyvaerts, 1979); the present analytic result may act as a stimulus to seeking the general conditions under which force-free fields become unstable.

In order to make analytic progress we have had to sacrifice generality in considering cylindrically symmetric fields. It would not be essential, in general, to allow photospheric motions that consist of an expansion as well as a shearing, as we have been forced to do. Furthermore, it is clear that the magnetic bubble would not be an essential feature of the second equilibrium solution for more general fields; indeed, in order for the first field to erupt into the second the magnetic island would need to be squeezed across the photospheric boundary (in a manner that is not observed), locally relaxing the condition that B_n remain constant in the process. Once a force-free field becomes magnetohydrodynamically

unstable the details of the subsequent behaviour are unclear, but a likely scenario is that the field is stretched out to a configuration that is tearing-mode unstable; this allows the magnetic field to reconnect and ascend further.

The third analytic approach (in Section (3.4)) is to employ the method of separation of variables. In addition to the well-known linear force-free fields and potential fields this leads to the solution discussed in detail by Birn et al (1978). It also produces a wider class of fields of the form

$$B_r = -\frac{1}{kr^{1+k}} \frac{dF_\phi}{d\phi} \quad ,$$

$$B_\phi = \frac{1}{r^{1+k}} F_\phi \quad ,$$

$$B_z = \frac{\lambda}{r^{1+k}} F_\phi^{1+1/k} \quad ,$$

where F_ϕ satisfies equation (3.65), and the potential satisfies

$$\nabla^2 A + \lambda^2 (k+1)(kA)^{(1+1/k)} = 0 \quad .$$

The particular case $k = -\frac{1}{2}$ gives a useful analytic solution. These solutions have similar properties to those described in Birn et al. In terms of problem I, we find a maximum allowable λ (namely λ_{max}) for a solution to exist, with two solutions occurring when $\lambda < \lambda_{max}$. However, for problem II there is a unique solution for a given photospheric shear, with no untoward behaviour as λ approaches λ_{max}.

Chapter 4: RECONNECTING CURRENT SHEETS AND THE EMERGING FLUX MODEL

In this chapter a steady state model for reconnecting current sheets is considered. Our aim is to understand the relationship between the central value of temperature, density and pressure within the sheet and the prescribed external values of both these parameters and also the magnetic field strength and inflow velocity (reconnection rate). The dimensions of the sheet, and their variation with the prescribed parameters, will be obtained from the model, as will the conditions on the existence of a steady state. For simplicity, the model is taken to be one-dimensional, with only variations across the sheet, at the centre of symmetry, considered. We also consider the application of these results to the emerging flux model (Heyvaerts, Priest and Rust, 1977) for solar flares.

In Section 4.1 we discuss current sheets with particular reference to the order of magnitude treatment used by Tur and Priest (1978), and in Section 4.2 their results are described. In Section 4.3 we present the general theory and results of our model for current sheets and, finally, in Section 4.4 the application to the emerging flux model is described.

4.1 Order of magnitude treatment of current sheets

When two regions of uniform magnetic field, equal in magnitude but opposite in direction, are placed in contact a current sheet is formed at the interface between the two regions. If the magnetic field permeates a stationary plasma of finite electrical conductivity then diffusion acts so as to annihilate the field in the region of the current sheet which thickens so that its' width at time t is given by

$$\ell = (t/\mu\sigma)^{\frac{1}{2}} \quad , \qquad \ldots (4.1)$$

where μ is the magnetic permeability and σ is the electrical conductivity of the fluid. If there is a fluid motion towards the centre of the sheet a situation arises where convection of the magnetic fieldlines balances the

competing effect of lateral diffusion. This phenomenon has been considered by many authors, but we will not discuss these papers here, save to refer the reader to a review article by Vasyliunas (1975) and to the paper by Soward and Priest (1977) which put the generally accepted physical model of Petschek (1964) on a firm mathematical basis. Instead we shall consider the order of magnitude approach to the problem as given by Heyvaerts and Priest (1976), Tur and Priest (1977), and Syrovatskii (1976).

We consider an idealised current sheet as shown in Figure 4.1, where the subscript c denotes central current sheet values and the subscript ∞ denotes external values. The outflow velocity at the ends of the sheet is denoted by v_o. As a first attempt at understanding the physical processes within the system we consider an order of magnitude approach to the energy equation as given by equation (1.23). In the steady state the convective term (1.24) may be written in the form

$$\frac{\gamma}{\gamma - 1} \frac{p}{T} (\underline{v} \cdot \nabla T) - (\underline{v} \cdot \nabla p) \quad , \qquad \ldots (4.2)$$

where the notation is as in Chapter 1. The convective derivative $\underline{v} \cdot \nabla$ may be approximated by

$$\underline{v} \cdot \nabla \simeq \frac{v_\infty}{\ell} + \frac{v_o}{L} \quad ,$$

but by using the continuity equation we find

$$\frac{v_\infty/\ell}{v_o/L} \simeq \frac{\rho_c}{\rho_\infty} \quad .$$

We shall be particularly interested in conditions where $\rho_c >> \rho_\infty$ and thus we take the convective derivative in the form

$$\underline{v} \cdot \nabla \simeq \frac{v_\infty}{\ell} \quad . \qquad \ldots (4.3)$$

If we assume a balance between internal gas pressure and total external pressure (see Section 4.3 for a justification) we have

$$p_c = p_\infty + B_\infty^2/2\mu \quad , \qquad \ldots (4.4)$$

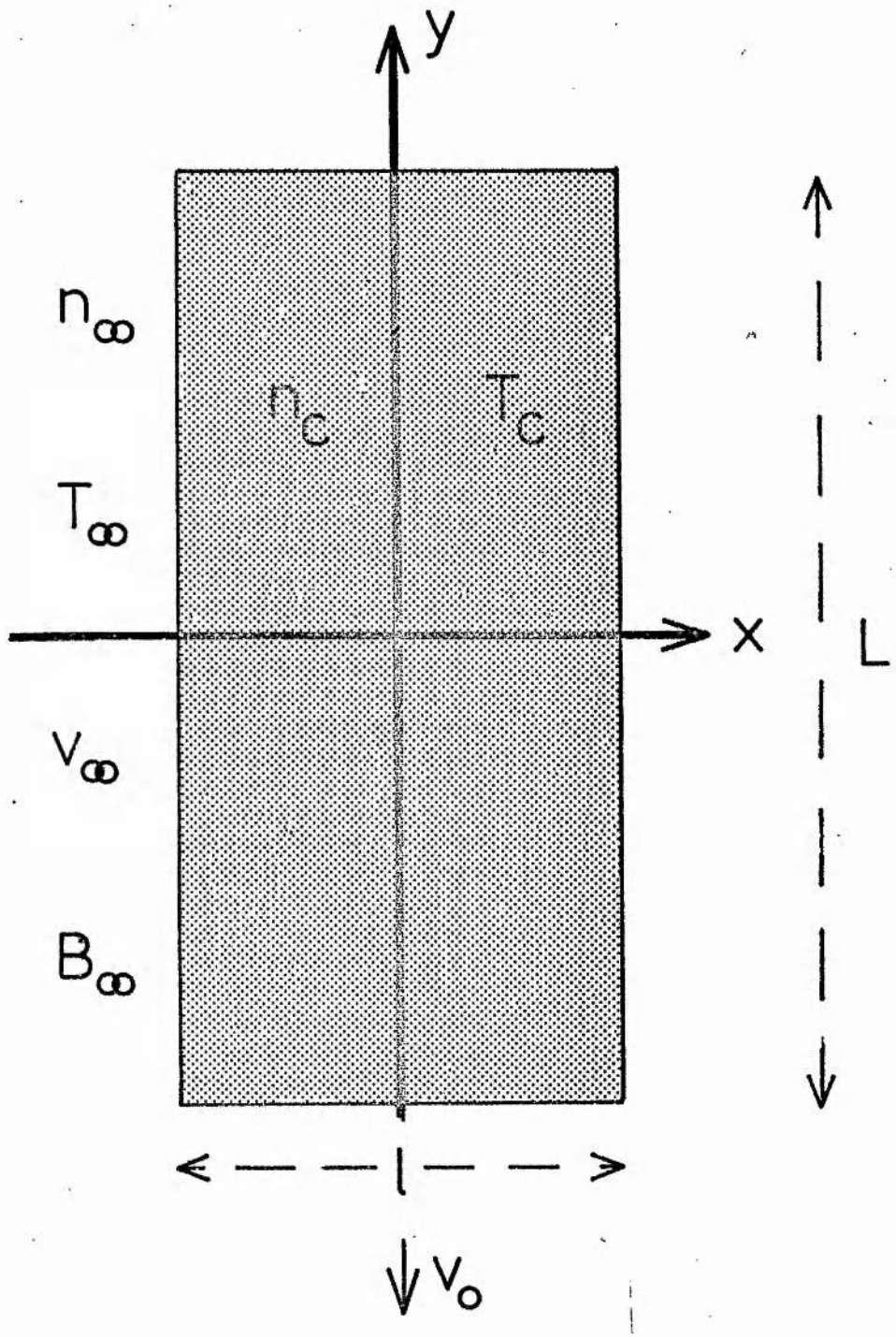

Figure 4.1

Schematic diagram showing the coordinate system used throughout this Chapter. Central values within the current sheet (shaded) are denoted by a subscript c, while external values are denoted by the subscript ∞.

and defining the parameter

$$\beta_\infty = 2\mu p_\infty / B_\infty^2 \quad , \qquad \ldots (4.5)$$

we may write the convective term IE as

$$\frac{v_\infty}{\ell} \frac{B_\infty^2}{2\mu} \left[\frac{\gamma}{\gamma - 1} (1 + \beta_\infty) \left(1 - \frac{T_\infty}{T_c} \right) - 1 \right] \qquad \ldots (4.6)$$

we note here that the width ℓ of the sheet is not easily estimated, but a suitable lower bound may be obtained from the induction equation (1.16), which gives

$$\ell \simeq \eta / v_{max} \quad .$$

We take

$$\eta = 8 \times 10^8 \, T_c^{-3/2} (m^2 s^{-1})$$

and note from the work of Soward and Priest (1976) that a maximum reconnection rate occurs with an approximate value of

$$v_{max} \simeq v_A / 40 \quad ,$$

where v_A is the external Alfvén speed.

When the inflow velocity v_∞ is less than the maximum reconnection speed, steady reconnection may occur at the sheet and we may approximate the width of the current sheet by

$$\ell = \eta / v_\infty \quad . \qquad \ldots (4.7)$$

At this point we note that when using a continuous fluid approach one must always beware that the length scales considered are not below the minimum allowable length scale. Generally this minimum length scale is the mean free path, below which fluid descriptions should be abandoned in favour of individual particle models. Vasyliunas (1975), however, claims that the fluid approach remains valid even when the length scales fall below the mean free path, provided that they exceed the electron inertial length (λ_e, say). He takes the width of the current sheet to be

$$\ell = \frac{\eta}{2v_\infty} + \left(\frac{\eta^2}{4v_\infty^2} + \lambda_e^2 \right)^{\frac{1}{2}} \quad ,$$

which has ℓ tending asymptotically to λ_e as η/v_∞ becomes small compared with λ_e.

We next approximate the joule heating term $\mathbb{J}$ (equation 1.25) by

$$\mathbb{J} = B_\infty^2/(\mu^2\ell^2\sigma) \quad . \quad (\text{watt m}^{-3}) \qquad \ldots (4.8)$$

The radiative cooling term $\mathbb{R}$ (equation 1.33) is taken as

$$\mathbb{R} = \chi\rho_c^2 T_c^\alpha \quad , \quad (\text{watt m}^{-3}) \qquad \ldots (4.9)$$

where χ and α are the values given in Table 1 of Chapter 1. Using equation (4.4) and the perfect gas law, the plasma density within the sheet (ρ_c) is taken as

$$\rho_c = \rho_\infty \left(1 + \frac{1}{\beta_\infty} \right) \frac{T_\infty}{T_c} \quad . \qquad \ldots (4.10)$$

As in Chapter 1 the mechanical heating term $\mathbb{H}$ is assumed proportional to the density ρ,

$$\mathbb{H} = H\rho \quad ,$$

and we determine H through the condition that mechanical heating is balanced by radiative losses outside the sheet ($\mathbb{H} = \mathbb{R}$). This gives

$$H = \rho_\infty \rho_c \chi T_\infty^\alpha \quad , \qquad \ldots (4.11)$$

where χ and α are the values consistent with whatever value of T_∞ is used.

Finally the thermal conduction term $\mathbb{K}$ is split into two parts which describe conduction along and perpendicular to the magnetic fieldlines:

$$\mathbb{K} = K_{11}(T_\infty - T_c)/L^2 + K_\perp(T_\infty - T_c)/\ell^2 \quad , \quad (\text{watt m}^{-3}) \qquad \ldots (4.12)$$

where K_{11} and $K_\perp$ are as given in Chapter 1 (equations 1.29) and (1.30)), but evaluated for central values of the temperature and density and the external magnetic field strength. The length (L) of the current sheet may be obtained from mass continuity as

$$L \simeq \ell \left(\frac{v_o}{v_\infty} \right) \frac{\rho_c}{\rho_\infty} \quad , \qquad \ldots (4.13)$$

where v_o is the outflow speed from the reconnection region, and is given by the Alfvén speed based on the density ρ_c of the plasma being ejected, namely

$$v_o = B_\infty / (\mu \rho_c)^{\frac{1}{2}} \quad .$$

Using all these approximations the energy equation is reduced to the form of an algebraic equation which may be solved for the internal temperature of the sheet T_c in terms of any given set of parameters T_∞, n_∞, B_∞ and v_∞ for the surrounding atmosphere.

4.2 Emerging flux model

The origins of the emerging flux model lie in the observational results quoted in Chapter 1. There we noted that a common precursor to the flare event was new magnetic flux loops rising through the surface of the sun. This fact led Heyvaerts, Priest and Rust (1977) to consider the physical processes involved in such an emergence of new magnetic flux in an attempt to explain many of the solar flare observations. In this model they suggest that small loop flares occur in three stages as the emerging magnetic flux interacts with the overlying field. These phases are illustrated in Figure 4.2. During the preflare phase, steady reconnection occurs in the current sheet (or diffusion region in Petscheks' mechanism) formed between the new and old magnetic flux. Then, at some critical height, the current sheet finds itself in an unstable state and heats up, seeking a new equilibrium. During this process, the current density may exceed the threshold value for the onset of plasma microinstabilities. This leads to the impulsive phase, in which particles are accelerated to high velocities by the resulting large electric fields. The attainment of the critical current density in the sheet is regarded as the trigger for the flare. Finally, in the main phase, a new state of steady magnetic field

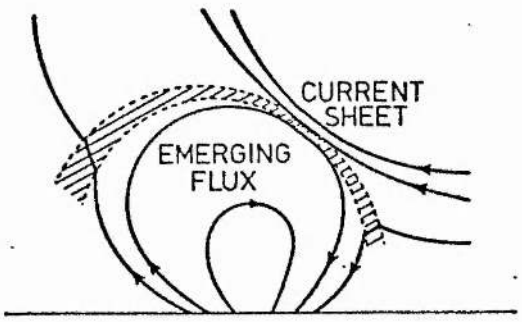

(a) Preflare Heating

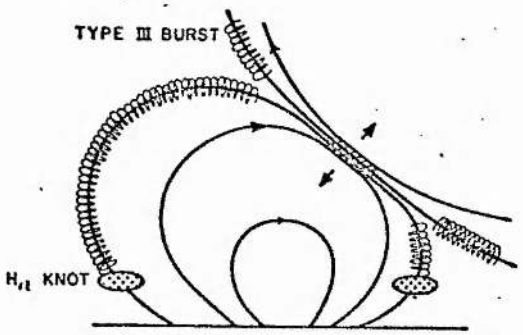

(b) Impulsive Phase

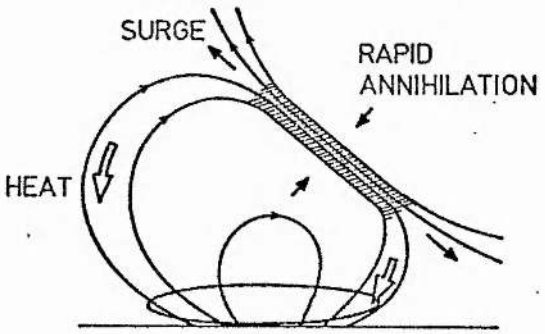

(c) Main Phase

Figure 4.2

Sequence of events in the emerging flux model of solar flares

(a) The emerging flux reconnects with overlying field. Shock waves (shown dashed) emanate from a small current sheet and heat the plasma.

(b) When the sheet reaches a critical height in the atmosphere an impulsive electric field accelerates electrons, which then escape along fieldlines. Those which move downwards produce H_α knots and hard X-rays, while those which escape upwards into an open field configuration produce type III radio bursts.

(c) A new steady state is achieved, with reconnection based on a turbulent resistivity. Magnetic energy is given to particles and heat, which are conducted down to the chromosphere and produce the H_α flare.

(From Heyvaerts et al, 1977)

reconnection is reached, the current sheet being a marginally turbulent one. For a large two-ribbon flare, the production of a small turbulent region by the above processes stimulates the release of stored magnetic energy from the much larger overlying force-free field.

A possible trigger mechanism for this model was considered by Tur and Priest (1977). They used the order of magnitude approach as outlined in Section 4.1 together with the model atmosphere given in Table 2 which relates n_∞ and T_∞ to the height h in the atmosphere. The resulting algebraic energy equation was solved for various values of B_∞ and v_∞ and the resulting value of the central temperature T_c plotted against the height h. Their results are best illustrated by the schematic diagram of Figure (4.3), which shows the possible equilibrium temperatures T_c for each value of h. As the current sheet rises in the atmosphere the temperature moves along the equilibrium curve AB. This behaviour characterises the preflare heating stage of the emerging flux model. The impulsive phase begins when the current sheet reaches a height h_{crit} (point B in the diagram). As the sheet continues to rise, no neighbouring equilibrium is found and, since the heating terms dominate in the energy equation the central temperature rises dramatically along the path BC, seeking a new equilibrium at the point C. In doing so, however, the temperature exceeds the temperature T_{turb} which marks the onset of turbulence. The instability which is considered to cause the turbulence is the Buneman instability (Buneman, 1959). This instability is chosen because it gives an upper limit on the threshold current density for turbulence, namely

$$J_{turb} = n_c e v_{sc} \quad , \qquad \ldots (4.14)$$

where v_{sc} is the electron sound speed at the centre of the sheet and e is the electronic charge. Comparison of equation (4.14) with our standard form for the current density

$$J = B_\infty/\mu_o \ell \qquad \ldots (4.15)$$

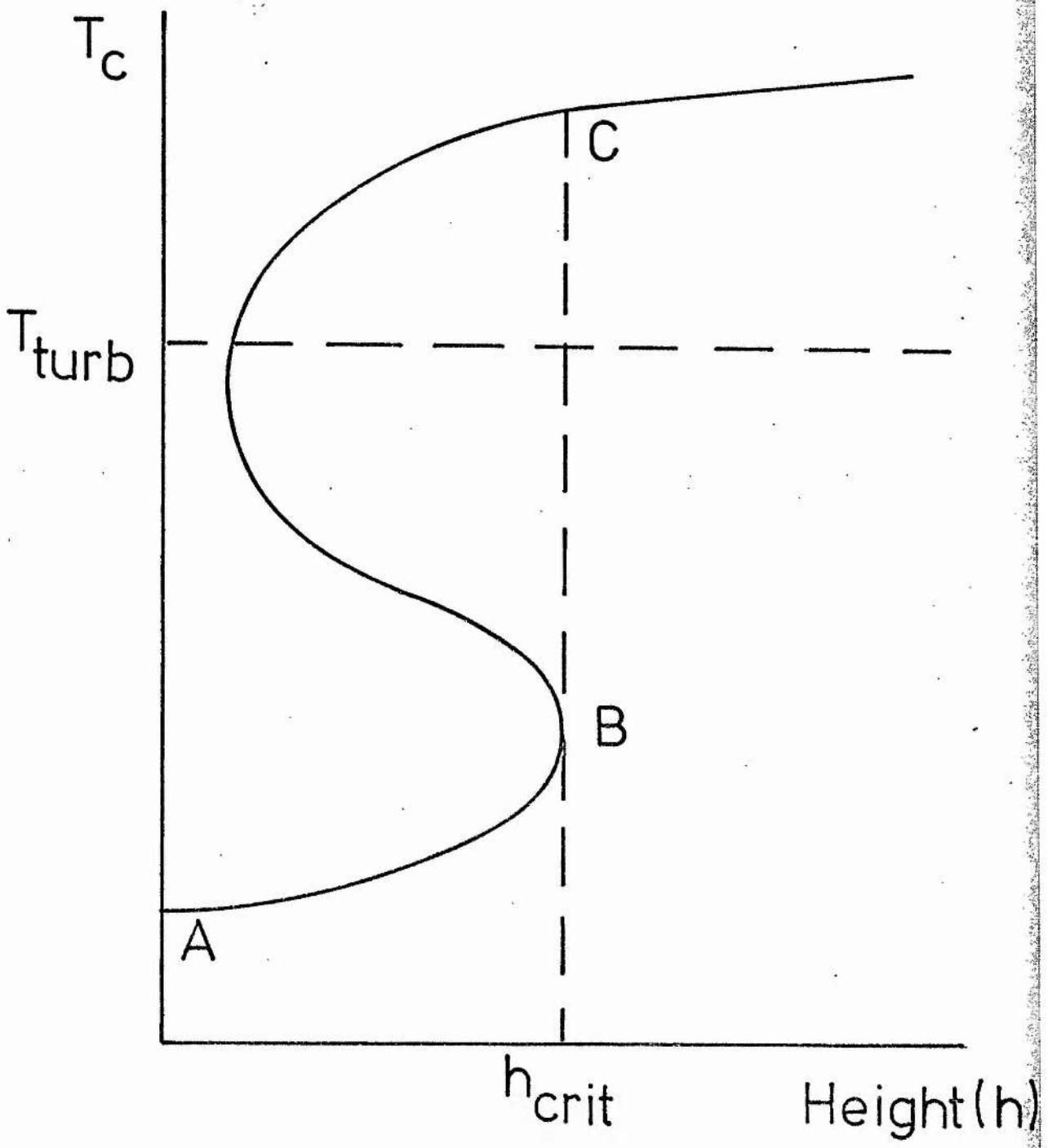

Figure 4.3

Schematic representation of the order of magnitude results of Tur and Priest. The central equilibrium temperature T_c is shown as a function of height h in the solar atmosphere. As the sheet rises, the equilibrium solution moves along AB. When the critical height, h_{crit}, is attained, there are no neighbouring equilibria and the sheet heats up dynamically along the path BC. As the temperature T_{turb} is exceeded, the critical current density for the onset of turbulence is surpassed.

Table 2

Temperature (T_∞) and density (ρ_∞) for a model solar atmosphere (from Heyvaerts and Priest, 1976).

Height h (mm)	T_∞ (^oK)	ρ_∞ (kg m^{-3})
0	4.4×10^3	1.33×10^{-5}
0.5	4.9×10^3	5.28×10^{-7}
1	5.2×10^3	6.65×10^{-8}
2	5.8×10^3	6.65×10^{-9}
3	6.3×10^3	6.65×10^{-10}
4	7.4×10^3	3.34×10^{-10}
5	1.3×10^4	8.36×10^{-11}
6	3.0×10^4	2.64×10^{-11}
7	5.5×10^4	1.06×10^{-11}
8	1.6×10^5	4.20×10^{-12}
9	3.0×10^5	2.36×10^{-12}
10	4.0×10^5	1.33×10^{-12}
11	4.9×10^5	1.05×10^{-12}
12	5.7×10^5	8.36×10^{-13}
13	6.9×10^5	6.69×10^{-13}
14	8.5×10^5	5.29×10^{-13}
15	1.0×10^6	5.29×10^{-13}
16	1.2×10^6	5.29×10^{-13}

yields the threshold temperature for the onset of turbulence T_{turb}. One effect of the onset of turbulence is to increase the magnetic diffusivity thereby allowing reconnection to proceed at a greater rate and so release more magnetic energy.

Tur and Priest also found that two types of solution are possible. Firstly, there is the form of solution as shown in Figure 4.3 where the turbulent threshold is crossed rapidly. Alternatively, for small values of B_∞ or large values of v_∞ the $T_c(h)$ curve may be monotonic and as such the threshold for turbulence is slowly exceeded. We expect the former type of trigger mechanism to be more violent and thus more likely to produce an impulsive, rather than a thermal flare.

Some other important conclusions from this work are as follows:

(a) If the ratio B_∞/v_∞ is held constant, the curves for T_c as a function of height do not vary to any great extent.

(b) The critical height at which the sheet becomes unstable varies considerably. As either v_∞ decreases or B_∞ increases, h_{crit} increases in value, often giving a site for the flare onset well into the corona. The variation of h_{crit} with v_∞ and B_∞ is given in Figure 4.4.

(c) The internal temperature of the current sheet at the critical point of the triple valued curves does not vary significantly with either v_∞ or B_∞ and is typically between 15,000 and 20,000 K.

(d) For large field strength and low velocities the sheet length L exceeds the upper realistic value of 10^7 to 10^8 m, thus rendering the theory invalid in this regime.

4.3 Reconnecting current sheets: general theory

In this Section we propose a model for reconnecting current sheets which, although it does not represent the complete solution to the

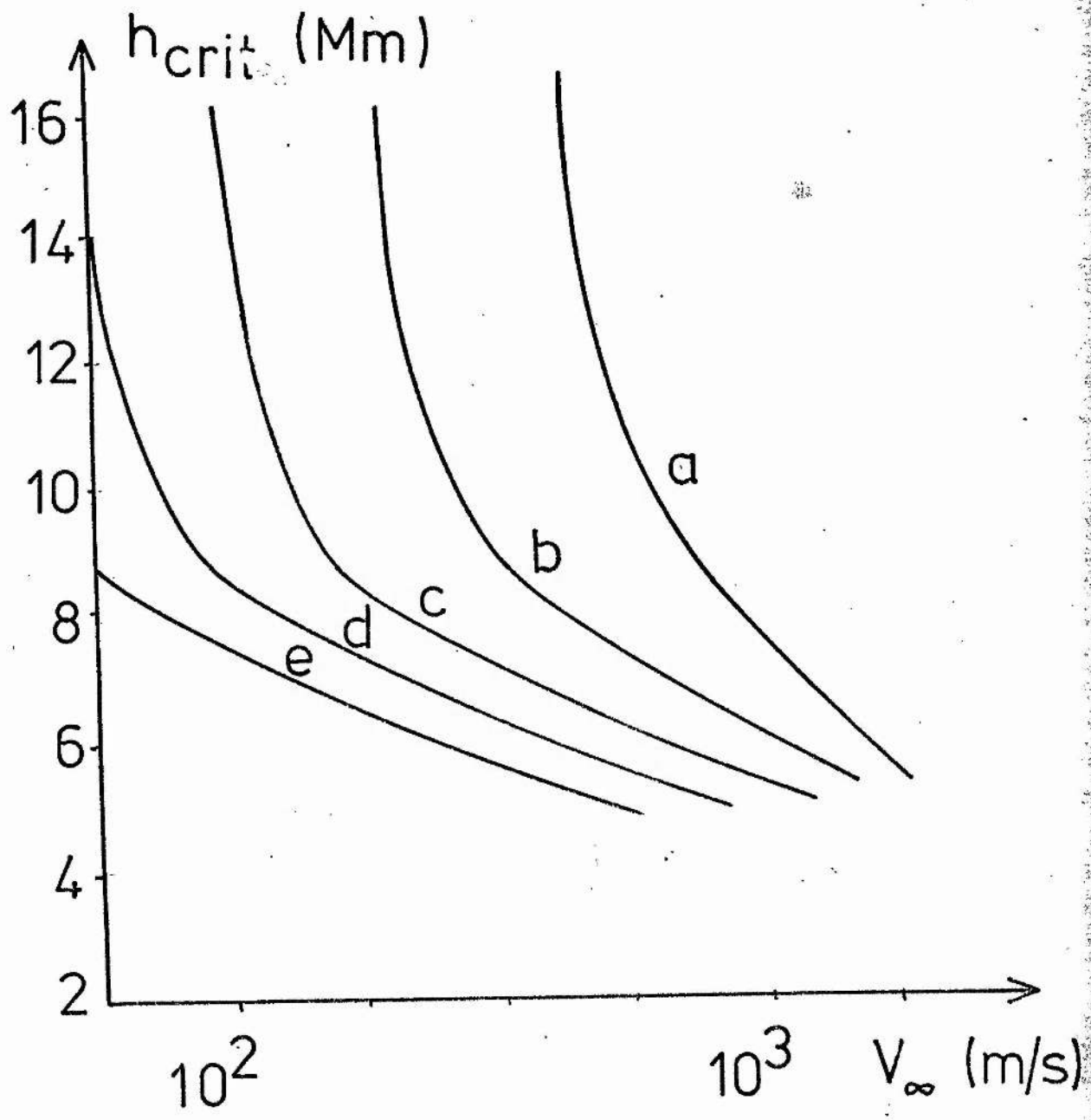

Figure 4.4

The results of Tur and Priest for the variation of the critical height with v_∞ for several values of B_∞: (a) $B_\infty = 10^{-1.5}$, (b) $B_\infty = 10^{-1.75}$, (c) $B_\infty = 10^{-2.0}$, (d) $B_\infty = 10^{-2.25}$, (e) $B_\infty = 10^{-2.5}$.

problem, is a significant improvement on the order of magnitude approach described above. The use of the full M.H.D. equations demand the solution of a set of non-linear partial differential equations. Our aim here is to simplify this system into a set of ordinary differential equations. Thus we must consider a steady one-dimensional model. The full system of equations reduces to a one-dimensional problem if we consider only the values of the variables along the axis of symmetry of the sheet, taken here to be the x-axis (see Figure 4.1), and neglect variations in the y direction (assuming the length scale in this direction to be very much greater than ℓ).

Along the line y = 0, we have

$$\underline{B} = (0 \ , \ B_y^*(x) \ , \ 0) \quad , \quad \underline{v} = (v_x^*(x) \ , \ 0 \ , \ 0) \quad , \qquad \ldots (4.16)$$

where * is used to denote the value along y = 0. Also, Ohms Law reduces to

$$E_z^* + v_x^* B_y^* = \eta \frac{dB_y^*}{dx} \quad . \qquad \ldots (4.17)$$

While along y = 0 the y-component of the equation of motion gives

$$\frac{\partial p^*}{\partial y} = 0 \quad \text{ie} \quad p^* = p^*(x) \quad , \qquad \ldots (4.18)$$

The x-component of the equation of motion is now

$$\rho^* v_x^* \frac{\partial v_x^*}{\partial x} = - \frac{dp^*}{dx} - \frac{1}{\mu_o} B_y^* \frac{dB_y^*}{dx} \quad . \qquad \ldots (4.19)$$

The ratio of the inertial term to the magnetic pressure term in (4.19) is

$$\frac{v_x^{*2}}{B_y^{*2}/\mu_o \rho^*} = v_x^{*2}/V_A^{\,2} \quad ,$$

so, assuming $v_x^{*2} \ll V_A^{\,2}$ we obtain

$$p^* + \frac{B_y^{*2}}{2\mu_o} = \text{constant} \quad . \qquad \ldots (4.20)$$

Finally, for the continuity equation,

$$\frac{d}{dx}(\rho v_x) + \frac{\partial}{\partial y}(\rho v_y) = 0 \qquad \ldots (4.21)$$

our simplifying assumption of one dimensionality cannot be applied in a straightforward manner. The neglect of y variations in (4.21) would give

$$\rho v_x = \text{constant} \quad .$$

However, symmetry conditions require v_x to be zero at the centre of the sheet, and so this model would imply an infinite density at the centre. Instead we need to evaluate the second term in (4.21). In order to retain the overall simplicity of our one-dimensional approach it is necessary to approximate the gradient. We shall here consider v_y as the result of pressure variations in the y direction,

$$\rho \frac{d}{dy}\left(\frac{1}{2} v_y^{\,2}\right) = \frac{dp}{dy} \quad . \qquad \ldots (4.22)$$

Since we require only an x dependence in the variables, we shall approximate the y variations by order of magnitude, reducing (4.22) to

$$v_y^* = (2(p^* - p_\infty)/\rho^*)^{\frac{1}{2}} \quad . \qquad \ldots (4.23)$$

Using (4.23) we thus write (4.21) as

$$\frac{d}{dx}(\rho^* v_x^*) = -(8\rho^*(p^* - p_\infty))^{\frac{1}{2}}/L \quad . \qquad \ldots (4.24)$$

We thus see that the approximation of the y variation in the system of equations introduces the length of the current sheet L as a parameter.

These equations must be supplemented by an energy equation, which we shall take here to be a balance between convection, radiative losses, Joule heating and a mechanical heating function. Some explanation is required for the neglect of thermal conduction. Because of our assumption of one-dimensionality the relevant form for thermal conduction is that of conduction <u>across</u> field lines. In order of magnitude we find perpendicular conduction to be

$$6 \times 10^{-42}\, n_c^{\,2} T_c^{\,\frac{1}{2}} B_\infty^{-2}/\ell^2 \quad .$$

Correspondingly we take radiative cooling to be

$$IR = \chi \rho_c^{\,2} T_c^{\,\alpha} \quad .$$

Thus if we take typical values for the current sheet of $T_c \simeq 2 \times 10^4$ K, $n_c \simeq 10^{20}$ m^{-3}, $B_\infty \simeq 100$ G we obtain

$$IK_\perp / IR \simeq 1.6 \times 10^{-5}$$

for a width of 100 m. The thermal conduction along fieldlines is given by

$$IK_{11} = 3 \times 10^{-11} T_c^{\,7/2} / L^2$$

and so, using the same values as above we find

$$IK_{11} / IR \simeq 0.5 \times 10^{-10}$$

for a length of 100 km. We shall thus neglect thermal conduction in our energy equation. One limitation of this assumption is that our solutions will not be valid for high temperatures ($\simeq 10^6$ K) where thermal conduction effects become dominant. In fact one may use the order of magnitude treatment of Section 4.1 to determine the dominant terms in the energy equation for each region of the atmosphere. This has been done by Tur and Priest (1977) and their results may also be used to justify the neglect of thermal conduction in regions with temperatures $< 10^6$. Our energy equation is thus taken to be

$$\frac{\rho^* \gamma v_x^*}{(\gamma - 1)} \frac{d}{dx} \left(\frac{p^*}{\rho^{*\gamma}} \right) = \frac{\eta}{\mu} \left(\frac{dB_y^*}{dx} \right)^2 - \chi \rho^{*2} T^{*\alpha} + H\rho^* \quad , \qquad \ldots (4.25)$$

which, despite the above simplification, is by no means straightforward to solve.

We note here that the formulation of the problem in the above manner allows for the effects of compressibility in the system, and thus provides an alternative to the simplifying assumption of incompressibility which has to date been the norm in the literature.

4.3.1 Non-dimensionalisation and parameters

We shall now non-dimensionalise the above equations against external values of the variables. For ease of notation we shall now omit the superscript * with the understanding that all the variables that follow denote the values taken along the line y = 0. Thus we put

$$T = T_\infty \bar{T} \ , \ \rho = \rho_\infty \bar{\rho} \ , \ p = p_\infty \bar{p} \ , \ B_y = B_\infty \bar{B} \quad ,$$

$$v_x = v_\infty \bar{v} \ , \ x = \frac{\ell}{2} \bar{x} \quad .$$

The boundary conditions at $x = \frac{\ell}{2}$ were

$$\rho = \rho_\infty \ , \ p = p_\infty \ , \ B_y = B_\infty \ , \ T = T_\infty \ , \ \frac{dB_y}{dx} = 0 \ , \ v_x = - v_\infty$$

which, in dimensionless form, become

$$\bar{\rho} = \bar{B} = \bar{T} = \bar{p} = 1 \ , \ \bar{v} = - 1 \quad \text{and} \quad \frac{d\bar{B}}{d\bar{x}} = 0 \quad \text{at} \quad \bar{x} = 1 \quad .$$

The condition that the magnetic field gradient must vanish at the edge implies

$$E_z = v_\infty B_\infty \ ,$$

and so Ohms Law becomes

$$1 + \bar{v}\bar{B} = \frac{2\eta}{v_\infty \ell} \frac{d\bar{B}}{d\bar{x}} \quad . \qquad \ldots (4.26)$$

The x component of the momentum equation is now

$$\beta p + \bar{B}^2 = (\beta + 1) \quad , \qquad \ldots (4.27)$$

where $\beta (= 2\mu \ p_\infty / B_\infty^{\ 2})$ is the external plasma beta. The non-dimensional continuity equation is written

$$\frac{d}{d\bar{x}} (\bar{\rho}\bar{v}) = - \frac{\ell}{L} \left(\frac{2p_\infty}{\rho_\infty v_\infty^{\ 2}} \right)^{\frac{1}{2}} (\bar{\rho}(\bar{p} - 1))^{\frac{1}{2}} \quad , \qquad \ldots (4.28)$$

and the energy equation is now

$$\bar{\rho}^{\gamma}\bar{v}\frac{d}{d\bar{x}}\left(\frac{\bar{p}}{\bar{\rho}^{\gamma}}\right) = \frac{2\eta B_\infty{}^2(\gamma-1)}{\mu\, v_\infty p_\infty \ell}\left(\frac{d\bar{B}}{d\bar{x}}\right)^2 - \frac{\rho_\infty{}^2 T_\infty{}^{\alpha}\chi(\gamma-1)\ell}{2v_\infty p_\infty}(\bar{\rho}^2\bar{T}^{\alpha}) \qquad \ldots (4.29)$$

$$+ \frac{H\rho_\infty(\gamma-1)\ell}{2v_\infty p_\infty}\,\bar{\rho} \quad .$$

We note that

$$\eta = \eta_o T^{-3/2} \qquad (m^2\ s^{-1})$$

and thus write

$$\eta = \eta_o T_\infty{}^{-3/2}\,\bar{T}^{-3/2} \qquad \ldots (4.30)$$

where $\eta_o = 8 \times 10^8$ for fully ionised hydrogen. We shall now define the following non-dimensional parameters;

$$R_m = \frac{2\eta_o T_\infty{}^{-3/2}}{v_\infty \ell} = \frac{\ell_o}{\ell}\ , \text{ say}\ , \qquad \ldots (4.31)$$

where
$$\ell_o = 2\eta_o/(v_\infty T_\infty{}^{3/2}) \qquad \ldots (4.32)$$

is a characteristic width of the current sheet. (Note that R_m, which appears in Ohms' Law, is in fact the magnetic Reynolds number). We also have

$$D = \frac{\ell}{Lv_\infty}\left(\frac{2p_\infty}{\rho_\infty}\right)^{\frac{1}{2}} = \frac{\ell}{\ell_o}\frac{L_o}{L}\ , \text{ say}\ , \qquad \ldots (4.33)$$

where,
$$L_o = \frac{2\eta_o}{v_\infty{}^2}\left(\frac{2p_\infty}{\rho_\infty T_\infty{}^3}\right)^{\frac{1}{2}}\ , \qquad \ldots (4.34)$$

and L_o is the characteristic length of the current sheet;

$$r = \frac{\eta_o \rho_\infty{}^2 T_\infty{}^{\alpha-3/2}\chi(\gamma-1)}{v_\infty{}^2 p_\infty} \quad : \qquad \ldots (4.35)$$

$$r_\infty = \frac{H\eta_o \rho_\infty T_\infty{}^{-3/2}(\gamma-1)}{v_\infty{}^2 p_\infty}\ , \qquad \ldots (4.36)$$

where $H = \chi_\infty \rho_\infty T_\infty^{\alpha_\infty}$ is chosen in order that the radiative loss term is balanced by the heating term at the outer boundary. We shall be interested in variations in the width of the sheet and have thus considered the magnetic Reynolds number, R_m, in terms of the ratio of a length scale ℓ_o, which varies with the external conditions, to the dimensional width ℓ of the sheet. The parameter D arises from our continuity equation and as above we use this to define a length scale L_o which varies with the external parameters and will be used to yield the dimensional length L of the sheet. The parameter r is simply the ratio of the radiative loss term to the convective term, while r_∞ is the value of this ratio at the edge. Thus our equations may be written

$$R_m \frac{d\bar{B}}{d\bar{x}} = (1 + \bar{v}\bar{B})\bar{T}^{3/2} \quad , \qquad \ldots (4.37)$$

$$\beta\bar{p} + \bar{B}^2 = \beta + 1 \quad , \qquad \ldots (4.38)$$

$$\frac{d}{dx}(\bar{\rho}\bar{v}) = -D(\bar{\rho}(\bar{p} - 1))^{\frac{1}{2}} \quad , \qquad \ldots (4.39)$$

$$\bar{\rho}^{\gamma}\bar{v}\frac{d}{d\bar{x}}\left(\frac{\bar{p}}{\bar{\rho}^{\gamma}}\right) = \frac{2R_m}{\beta}(\gamma - 1)\bar{T}^{-3/2}\left(\frac{d\bar{B}}{d\bar{x}}\right)^2 - \frac{r}{R_m}\bar{\rho}^2\bar{T}^{\alpha} + \frac{r_\infty}{R_m}\bar{\rho} \quad , \qquad \ldots (4.40)$$

coupled with the ideal gas law,

$$\bar{p} = \bar{\rho}\bar{T} \quad . \qquad \ldots (4.41)$$

Furthermore, (4.38) and (4.41) may be used to eliminate $\bar{p}$ and $\bar{T}$ and so give a system of equations for $\bar{B}$, $\bar{\rho}$ and $\bar{v}$ alone, namely

$$\frac{d\bar{B}}{d\bar{x}} = \frac{1}{R_m}(1 + \bar{v}\bar{B})\left(\frac{1 + (1 - \bar{B}^2)/\beta}{\bar{\rho}}\right)^{3/2} \quad , \qquad \ldots (4.42)$$

$$\frac{d\bar{\rho}}{d\bar{x}} = -\frac{1}{\gamma\bar{v}}\left(\frac{1 + (1 - \bar{B}^2)/\beta}{\bar{\rho}}\right)^{\frac{1}{2}}\left[\frac{2R_m(\gamma - 1)}{\beta}\left(\frac{1}{R_m}(1 + \bar{v}\bar{B})\right)\right.$$

$$- \frac{r}{R_m}\bar{\rho}^2\left[\frac{1 + (1 - \bar{B}^2)/\beta}{\bar{\rho}}\right]^{\alpha-3/2} + \frac{r_\infty}{R_m}\bar{\rho}\left[\frac{1 + (1 - \bar{B}^2)/\beta}{\bar{\rho}}\right]^{-3/2}$$

$$\left. + \frac{2\bar{v}\bar{B}}{\beta R_m}(1 + \bar{v}\bar{B})\right] \quad , \qquad \ldots (4.43)$$

and
$$\frac{d\bar{v}}{d\bar{x}} = -\frac{D}{\beta^{\frac{1}{2}}\bar{\rho}}\left(\bar{\rho}(1-\bar{B}^2)\right)^{\frac{1}{2}} - \frac{\bar{v}}{\bar{\rho}}\frac{d\bar{\rho}}{d\bar{x}} \quad . \qquad \ldots (4.44)$$

These must be solved subject to the boundary conditions that

$$\bar{B} = \bar{\rho} = 1 \ , \quad \text{and} \quad \bar{v} = -1 \quad \text{at} \quad \bar{x} = 1 \qquad \ldots (4.45)$$

and, by symmetry, that

$$\bar{v} = \bar{B} = 0 \quad \text{at} \quad \bar{x} = 0 \quad . \qquad \ldots (4.46)$$

In other words the system of equations and boundary conditions (4.42)-(4.46) form an eigenvalue problem where we must vary the two eigenvalues R_m and D (and so the length scales ℓ and L) in order to obtain a solution.

4.3.2 Properties of the equations

Before attempting to solve the above system numerically we must study the equations to see if there are any difficulties likely to arise and also to find any properties of the system which will simplify the solution. The first point of note is the fact that the critical points of the system are when $\bar{\rho} = 1$, $\bar{B} = \pm 1$ and $\bar{v} = \pm 1$ (i.e. at the outer boundary). A critical point is simply a point at which all the derivatives are zero and so the system admits the critical point values as constant solutions. We require the variables to be non-uniform within the current sheet and as such must look for solutions which match on to these critical points. We must attempt to find the solution close to these points if we are to be able to integrate numerically away from them.

For simplicity we transform the critical point at $\bar{\rho} = 1$, $\bar{B} = 1$, $\bar{v} = -1$, to the origin, i.e.

$$\bar{B} = B' + 1 \ , \ \bar{\rho} = \rho' + 1 \ , \ \bar{v} = v' - 1 \ , \ \bar{x} = x' + 1 \quad .$$

We thus have the system

$$\frac{dB'}{dx'} = \frac{1}{R_m}(v' - B' + v'B')\left(\frac{1 - B'(B'+2)/\beta}{\rho' + 1}\right)^{3/2} \ , \qquad \ldots (4.47)$$

$$\frac{d\rho'}{dx'} = -\left(\frac{1 - B'(B' + 2)/\beta}{\rho' + 1}\right)^{\frac{1}{2}} \frac{1}{\gamma(v' - 1)} \left(\frac{2(\gamma - 1)}{\beta R_m}\left[v' - B' + v'B'\right]^2\right.$$

$$- \frac{r}{R_m}(\rho'^2 + 2\rho' + 1)\left[\frac{1 - B'(B' + 2)/\beta}{\rho' + 1}\right]^{\alpha} + \frac{r_\infty}{R_m}(\rho' + 1)$$

$$\left. + \frac{2(v' - B' + v'B' - 1)}{\beta R_m}(v' - B' + v'B')\right) \quad , \qquad \ldots (4.48)$$

and

$$\frac{dv'}{dx'} = -\frac{D}{\beta^{\frac{1}{2}}(\rho' + 1)}\left[(\rho' + 1)(-B'^2 - 2B')\right]^{\frac{1}{2}} - \frac{(v' - 1)}{(\rho' + 1)}\frac{d\rho'}{dx'} \quad , \ldots (4.49)$$

with a critical point occurring when $(B',\rho',v') = (0,0,0)$.

To obtain the behaviour near the critical point one performs a Taylor expansion of the right hand sides of the equations about the critical point at the origin to obtain the "almost linear" form of the equations. The solution of the resulting linear system will thus be valid close to the critical point and may be used to integrate away from the critical point. Linearisation of (4.47) and (4.48) yields

$$\frac{dB'}{dx'} = \frac{1}{R_m}(v' - B') \quad , \qquad \ldots (4.50)$$

$$\frac{d\rho'}{dx'} = \frac{2(r\alpha + 1)}{R_m\beta\gamma}B' + \frac{r(\alpha - 1)}{\gamma R_m}\rho' - \frac{2}{R_m\beta\gamma}v' \quad , \qquad \ldots (4.51)$$

where we have used the fact that $r_\infty = r$ at the edge.

In equation (4.49) we note that the dominant terms are not linear, but square root in nature. Thus including the square root terms and linear terms (4.49) approximates to

$$\frac{dv'}{dx'} = -\frac{D}{\beta^{\frac{1}{2}}}(-2B')^{\frac{1}{2}} + \frac{2(r\alpha + 1)}{R_m\beta\gamma}B' + \frac{r(\alpha - 1)}{R_m\gamma}\rho' - \frac{2}{R_m\beta\gamma}v' \quad . \quad \ldots (4.52)$$

The system of equations (4.50)-(4.51) does not have the simplifying factor of linearity and so to obtain an approximate solution near to the edge which will enable us to integrate away from the boundary we must seek a self-consistent ordering system which will give a valid solution in the region of interest.

Suppose we consider only terms of order the square root or less in the system. We would obtain

$$\frac{dB'}{dx'} = 0 \ , \ \frac{d\rho'}{dx'} = 0 \ , \ \frac{dv'}{dx'} = - \frac{D}{\beta^{\frac{1}{2}}} (- 2B')^{\frac{1}{2}} \quad .$$

This implies $B' = \rho' =$ constant $= 0$ and so we obtain

$$v' = \text{constant} = 0 \quad .$$

Thus we do not gain any information by considering so simple an ordering system.

Consider next the lowest non-zero order in each equation. We put

$$- B' = b^2 \quad ,$$

and obtain

$$- 2b \frac{db}{dx'} = \frac{1}{R_m} (v' + b^2) \quad , \qquad \ldots (4.53)$$

$$\frac{d\rho'}{dx'} = - Lb^2 + M\rho' - Nv' \quad , \qquad \ldots (4.54)$$

$$\frac{dv'}{dx'} = - Qb - Lb^2 + M\rho' - Nv' \quad , \qquad \ldots (4.55)$$

where $$L = \frac{2(r\alpha + 1)}{R_m \beta\gamma} \quad , \quad M = \frac{r(\alpha - 1)}{R_m \gamma} \quad ,$$

$$N = \frac{2}{R_m \beta\gamma} \quad , \quad Q = D(2/\beta)^{\frac{1}{2}} \quad .$$

Since we are interested in the behaviour of these equations near $b = v' = \rho' = 0$ we expect b to dominate over b^2 but will further assume that close to the origin b also dominates ρ' and v'. This assumption may be checked a posteriori. Thus we retain equations (4.53), (4.54) and consider (4.55) as simply

$$\frac{dv'}{dx'} = - Qb \quad . \qquad \ldots (4.56)$$

Coupling (4.56) with (4.53) gives

$$\frac{d^2}{dx'^2} (b^2) + \frac{1}{R_m} \frac{d}{dx'} (b^2) - \frac{Q}{R_m} b = 0 \quad .$$

If we neglect the first derivative we obtain the solution

$$b = \frac{Q}{12R_m} x'^2 \quad . \qquad \ldots (4.57)$$

Note that

$$\frac{d}{dx'}(b^2) \simeq O(x'^3) \quad \text{while} \quad \frac{d^2}{dx'^2}(b^2) \simeq O(x'^2) \quad ,$$

and so we are justified in our neglect of the first derivative if we are interested only in the vicinity of the origin. (We find also that if we neglected the highest derivative we would obtain $b \simeq O(x')$ and $\frac{d}{dx}(b^2) \simeq O(x')$ while the second derivative would be $O(1)$ thus invalidating this approximation). With b as above, (4.56) implies

$$v' = -\frac{Q^2}{36R_m} x'^3 \quad . \qquad \ldots (4.58)$$

Furthermore, since we neglected $\frac{d\rho'}{dx'}$ compared with x'^2 in equation (4.56), we require $\rho' \simeq O(x'^4)$. Thus (4.54) is approximately

$$\frac{d\rho'}{dx'} = -Nv' = \frac{NQ^2}{36R_m} x'^3$$

implying

$$\rho' = \frac{NQ^2}{144R_m} x'^4 \quad . \qquad \ldots (4.59)$$

In terms of the original (barred) variables we find that (4.57), (4.58) and (4.59) give the self consistent expansion about the critical point to be

$$\bar{B} = 1 - \frac{D^2}{72R_m\beta}(\bar{x} - 1)^4 \quad , \qquad \ldots (4.60)$$

$$\bar{v} = -1 - \frac{D^2}{18R_m\beta}(\bar{x} - 1)^3 \quad , \qquad \ldots (4.61)$$

$$\bar{\rho} = 1 + \frac{D^2}{36R_m^2\beta^2\gamma}(\bar{x} - 1)^4 \quad . \qquad \ldots (4.62)$$

We shall use the above expansion (4.60)-(4.62) to allow us to

allow us to integrate away from the critical point, and thus determine the variation of the temperature, density and magnetic field across the sheet.

One of the main aims of this work is to obtain the relationship between the central values of temperature and density and the corresponding external values. Let us therefore consider the energy equation,

$$\bar{v}\frac{d\bar{\rho}}{d\bar{x}} = -\frac{\bar{T}^{\frac{1}{2}}}{\gamma R_m}\left[\frac{2(\gamma-1)}{\beta}(1+\bar{v}\bar{B})^2 - r\bar{\rho}^2\bar{T}^{\alpha-3/2} + r_\infty\bar{\rho}\bar{T}^{-3/2} + \frac{2\bar{v}\bar{B}}{\beta}(1+\bar{v}\bar{B})\right] .$$

We intend to solve the full system of equations and boundary conditions at the edge as well as the central conditions that $\bar{B} = \bar{v} = 0$ at $\bar{x} = 0$. These conditions will only be satisfied for certain values of the eigenvalues R_m and D are chosen. Now if we put $\bar{v} = \bar{B} = 0$ in the energy equation we obtain the condition that

$$\frac{2(\gamma-1)}{\beta} - r\bar{\rho}^2\bar{T}^{\alpha-3/2} + r_\infty\bar{\rho}\bar{T}^{-3/2} = 0$$

at the centre. Using (4.38) with $\bar{B} = 0$ we find

$$\frac{2(\gamma-1)}{\beta} - r(1+1/\beta)^2\bar{T}_o^{\alpha-3.5} + r_\infty(1+1/\beta)\bar{T}_o^{-2.5} = 0 \qquad \ldots (4.63)$$

as the equation determining the central temperature $\bar{T}_o$. We note immediately that (4.63) is <u>independent of either of the eigenvalues</u> R_m and D. Thus, if the solution exists, equation (4.63) determines the central temperature $\bar{T}_o$ and equation (4.38) the central density $\bar{\rho}_o$ in terms of the external parameters β and r, <u>without knowledge of the full solution</u>. It can be shown that equation (4.63) allows only two real solutions for the central temperature $\bar{T}_o$ (see Figure 4.5), thus our solutions must differ from the triple valued solutions (see Figure 4.3) predicted by the order of magnitude analysis. This result is not too surprising since our energy equation is valid only for central temperatures less than 10^6 K, where conduction is negligible. Equation (4.63) gives only the two lower branches of the curve in Figure (4.3) since the highest branch of that

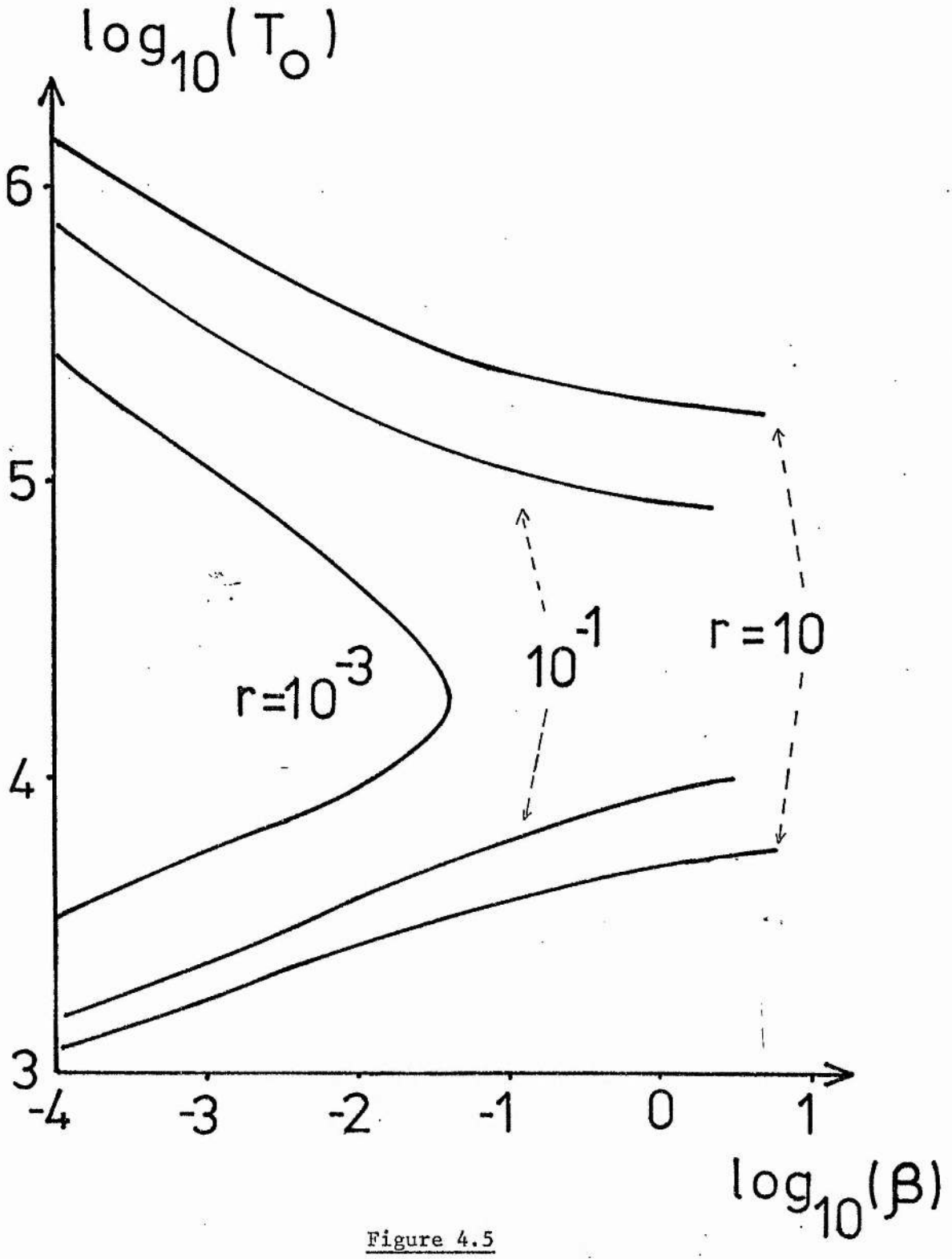

Figure 4.5

The variation of the central temperature T_o with the plasma beta ($\beta = 2\mu p_\infty / B_\infty^2$) and the ratio of radiation to convection

$$(r = \eta_o \rho_\infty^2 T_\infty^{\alpha-3/2} \chi(\gamma - 1)/(v_\infty^2 p_\infty))$$

as given by equation (4.63).

solution has conduction dominant.

Since two branches are predicted it is of interest to consider the stability of these possible solutions. A simple indication as to the stability of the solution may be obtained as follows. The time dependent energy equation, at constant pressure and neglecting the temperature structure may be written

$$C_p \frac{\partial \overline{T}}{\partial t} + \mathbb{E} = \mathbb{J} - \mathbb{H} + \mathbb{R} \quad ,$$

where C_p is the specific heat at constant pressure and the other terms are as defined in Chapter 1. Furthermore, at the centre of the sheet the convective term $\mathbb{E}$ is identically zero and so locally the energy balance must be

$$C_p \frac{\partial \overline{T}}{\partial t} = \mathbb{J} - \mathbb{R} + \mathbb{H} = F(\overline{T}) \text{ , say} \quad . \qquad \ldots (4.64)$$

Consider a perturbation about the equilibrium temperature $\overline{T}_o$ such that

$$\overline{T} = \overline{T}_o + \overline{T}_1 \quad .$$

Taylor expansion of the right hand side of (4.64) yields

$$C_p \frac{\partial T_1}{\partial t} = F(\overline{T}_o) + \left(\frac{\partial F}{\partial \overline{T}} \right)_{\overline{T}_o} \overline{T}_1 \quad \ldots \quad .$$

Now $F(\overline{T}_o) \equiv 0$ and so, if we assume $\overline{T}_1 \propto e^{\sigma t}$ we find the stability conditions:

$$\left(\frac{\partial F}{\partial \overline{T}} \right)_{\overline{T}_o} < 0 \quad \text{for stability} \quad ,$$

and

$$\left(\frac{\partial F}{\partial \overline{T}} \right)_{\overline{T}_o} > 0 \quad \text{for instability} \quad .$$

To apply this result it is useful to consider a schematic representation of the possible equilibrium solutions (Figure 4.6). The two solutions for the central temperature occur at points (1) and (2) in the Figure. We see that as $\overline{T}$ increases across solution (1) then $F(\overline{T}) = \mathbb{J} + \mathbb{H} - \mathbb{R}$ changes from positive to negative. Similarly as

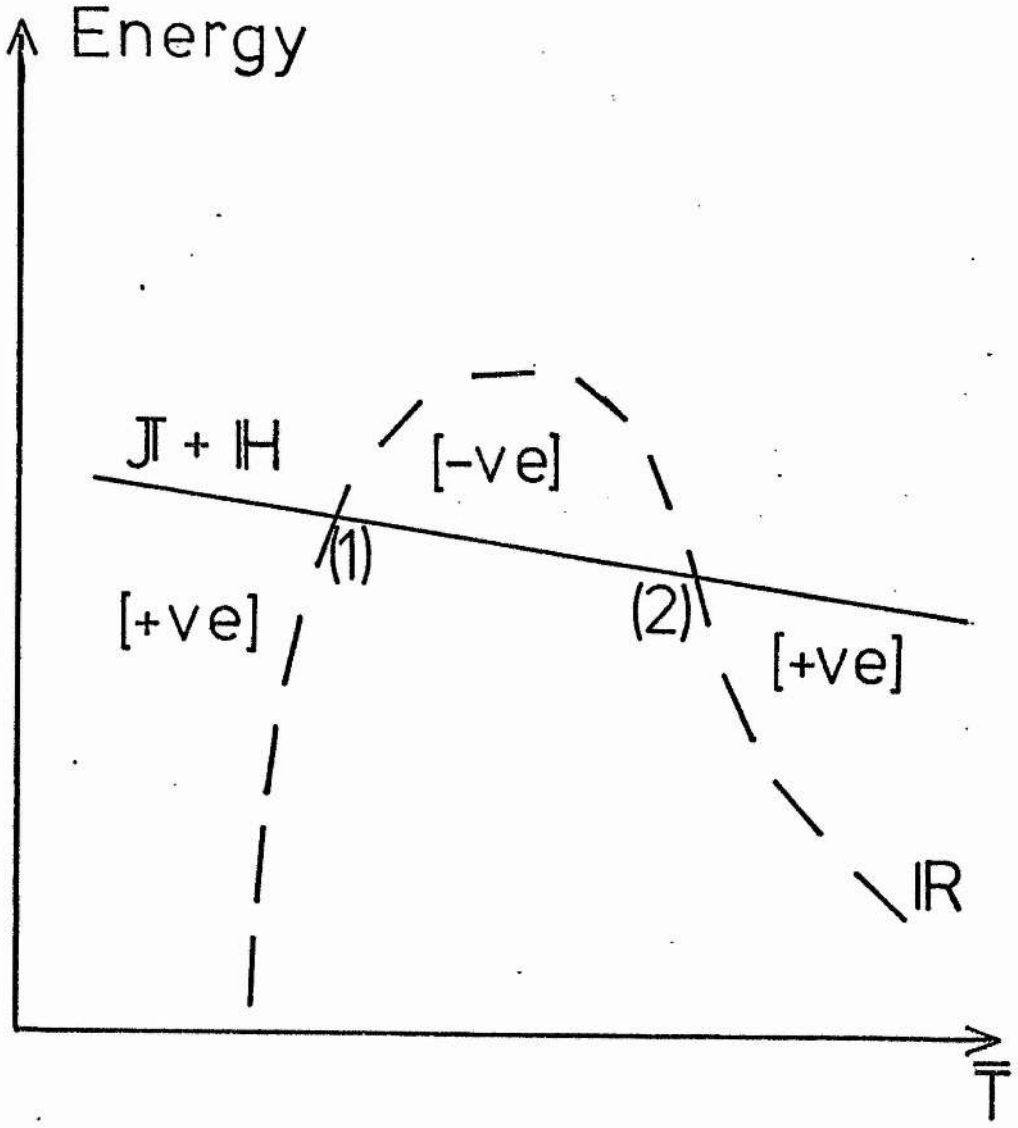

Figure 4.6

Schematic representation of energy balance for the current sheet. The two equilibrium solutions are shown at points (1) and (2) where the radiation curve ($\mathbb{I}R$) intersects the Joule heating and wave heating ($\mathbb{J}+\mathbb{I}H$) curve. As described in the text, only the low temperature equilibrium (1) is stable.

solution (2) is traversed F(T) changes sign from negative to positive. Thus at solution (1)

$$\frac{\partial F}{\partial \bar{T}} < 0$$

and so the lower temperature solution is stable while the upper temperature solution (2) is unstable.

Although we have found a useful method of predicting the central temperature and density we still require to solve the full system of equations. Here we must vary two eigenvalues R_m and D (effectively the width and length of the sheet) to obtain a solution satisfying all the required boundary conditions. It is only from the full solution that we can obtain the dimensions of the sheet and also be sure of the existence of solutions with the predicted central values. The problem of finding a solution by varying <u>two</u> eigenvalues is not simple and we would like to find some way of simplifying the problem. To this end it is useful to consider the reduced system of equations

$$\frac{d\bar{B}}{d\bar{\rho}} = -\gamma\bar{v}(1 + \bar{v}\bar{B})(1 + (1 - \bar{B}^2)/\beta)/F\bar{\rho} \quad , \qquad \ldots (4.65)$$

$$\frac{d\bar{v}}{d\bar{\rho}} = R_m D\gamma\bar{v}(1 + (1 - \bar{B}^2)/\beta)(\bar{\rho}(1 - \bar{B}^2))^{\frac{1}{2}}/L\bar{\rho}^2\beta^{\frac{1}{2}} - \bar{v}/\bar{\rho} \qquad \ldots (4.66)$$

obtained by eliminating the $\bar{x}$ dependence from equations (4.42)-(4.44). In the above we have put

$$F = \frac{2(\gamma - 1)}{\beta}(1 + \bar{v}\bar{B})^2 - r\bar{\rho}^2\left(\frac{1 + (1 - \bar{B}^2)/\beta}{\bar{\rho}}\right)^{\alpha-3/2}$$

$$+ r_\infty\bar{\rho}\left(\frac{1 + (1 - \bar{B}^2)/\beta}{\bar{\rho}}\right)^{-3/2} + \frac{2\bar{v}\bar{B}}{\beta}(1 + \bar{v}\bar{B}) \quad .$$

We note with interest that in the above system the parameters R_m and D appear only in the combination $R_m D$ and so we only have one parameter to vary. This aids our computation considerably. In the reduced system of equations (4.65), (4.66) we have $\bar{\rho}$ as the independent variable, and we know

the necessary central value of $\bar{\rho}$ without solving the equations. Thus we can vary the combination $R_m D$ until the extra conditions of $\bar{B}$ and $\bar{v}$ vanishing at the centre are satisfied.

Finally we note that the full system (4.42)-(4.44) may be scaled to generate a class of solutions from one solution. That is if we define $\bar{x} = \lambda \bar{x}'$ $R_m = \lambda R_m'$ and $D = D'/\lambda$ we obtain the same set of equations for the dashed and undashed variables while the outer conditions are imposed at $\bar{x}' = \lambda^{-1}$ and $\bar{x} = 1$ respectively.

Thus to determine the eigenvalues R_m and D, and thus the full solution, we need only consider the simpler single-eigenvalue problem presented by the reduced equations (4.65), (4.66). The full solution for the profiles $\bar{B}(\bar{x})$, $\bar{\rho}(\bar{x})$, $\bar{v}(\bar{x})$ then follows by solving the system of equations (4.42)-(4.44) for any values of R_m and D which conserve the product $R_m D$ found previously and then deducing the required values of R_m and D by a suitable scaling which makes the outer conditions satisfied at $\bar{x} = 1$.

Another feature readily apparent from the reduced system is that difficulties may arise if F changes sign during the integration. If we consider the phase space $(\bar{B},\bar{\rho},\bar{v})$ this eventuality would imply $\bar{B}$ decreasing towards zero while $\bar{\rho}$ and $\bar{v}$ reach maxima and subsequently decrease. Should this maximum value of $\bar{\rho}$ be less than the necessary central value (as given by the method described previously) we see that no trajectory in the phase space will pass through both the outer and central values required to satisfy the imposed conditions. Since the behaviour of the term F in the phase space is determined by the parameter β and r we expect to find ranges of this parameter for which no solution exists. This phase plane behaviour is illustrated in Figure (4.7). A solution which satisfies all the conditions must pass through both point (1) and point (2). The curves marked (a) represent the skeletal structure for a surface which obviously

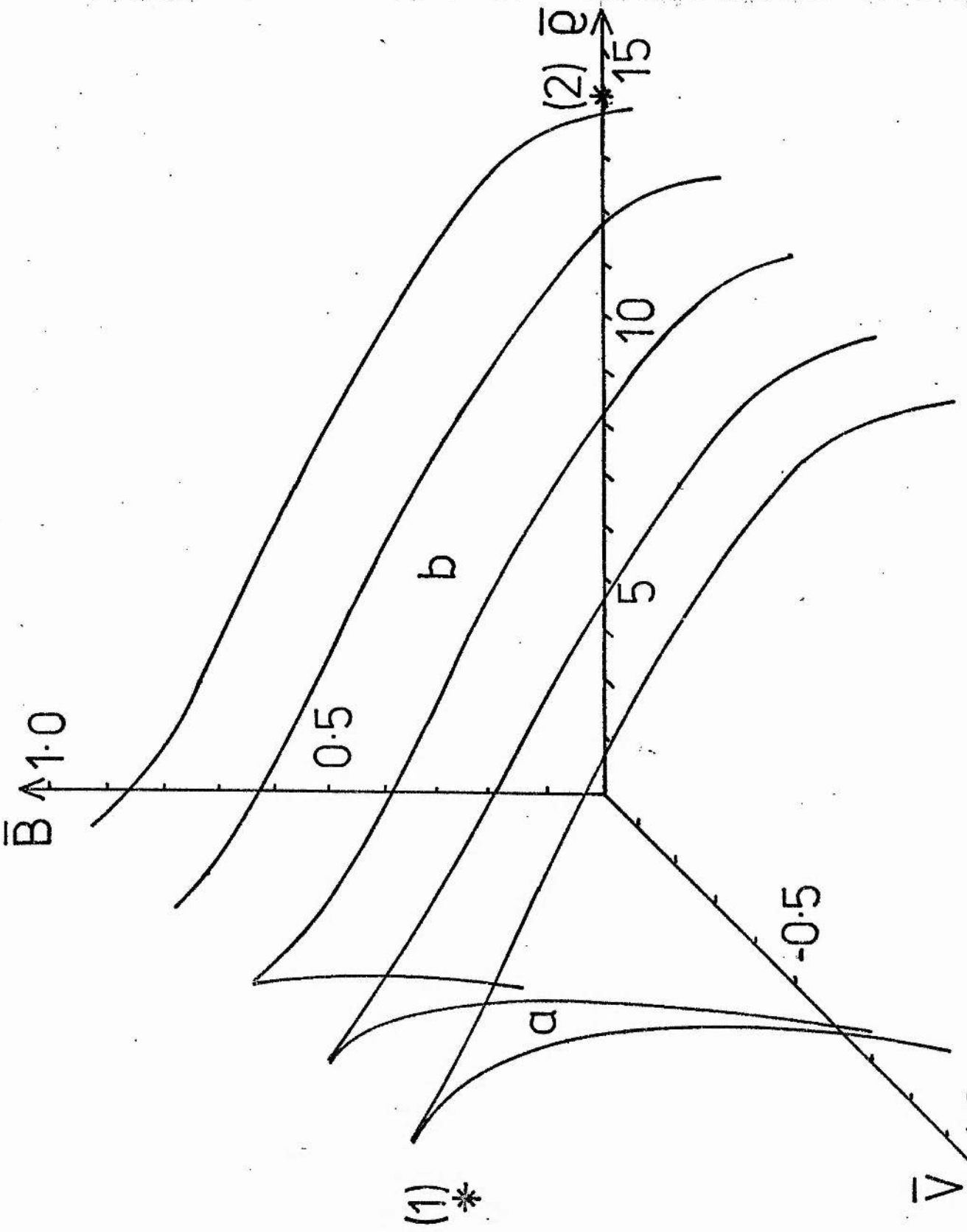

Figure 4.7

Skeletal structures for two possible phase surfaces of the reduced system of equations. A solution satisfying the boundary conditions must pass through both points (1) and (2). A solution lying on the surface (a) cannot satisfy the boundary conditions while one on surface (b) can do so.

will not allow a trajectory passing through the points (1) and (2). Any values of β and r which give such a surface do not permit a solution. Alternatively, the curves marked (b) give the skeletal structure for a surface which obviously can permit a trajectory passing through both points and hence the corresponding values of β and r do permit a solution.

Thus, armed with the above information about the properties of the equations we may proceed to solve the system numerically. We have outlined a simple method for obtaining the central values of the temperature and pressure but the phase plane analysis indicates that there may not always be a solution for which these values are attained.

4.3.3 Results

In the previous Section we noted that solutions do not exist for certain values of the parameters r and β. In Figure 4.8 we show the regions in the parameter space where solutions are possible. We see that if β is too small (corresponding to a low external pressure, or high external magnetic field strength) no solution will exist. Similarly if r is too small (corresponding to convection dominating radiative cooling) no solution exists. A simple-minded justification of the above results may be obtained by considering the full system of equations with the limiting cases of $\beta = 0$ or $r = 0$. Firstly with β identically zero we have that the magnetic field must be constant across the sheet, which obviously cannot satisfy the condition that $\overline{B}$ be zero at the centre, unless $\overline{B} = 0$ everywhere. Secondly, with r identically zero (and thus $r_\infty = 0$ also) our energy equation is a balance between convection and Joule heating. The condition that the velocity vanish at the centre would thus imply from (4.40) that

$$\frac{d\overline{B}}{d\overline{x}} = 0$$

at the centre. Ohms' Law, however, shows that the field gradient cannot vanish when $\overline{v} = 0$ and thus no solution is possible.

Having discovered the region in the parameter space where

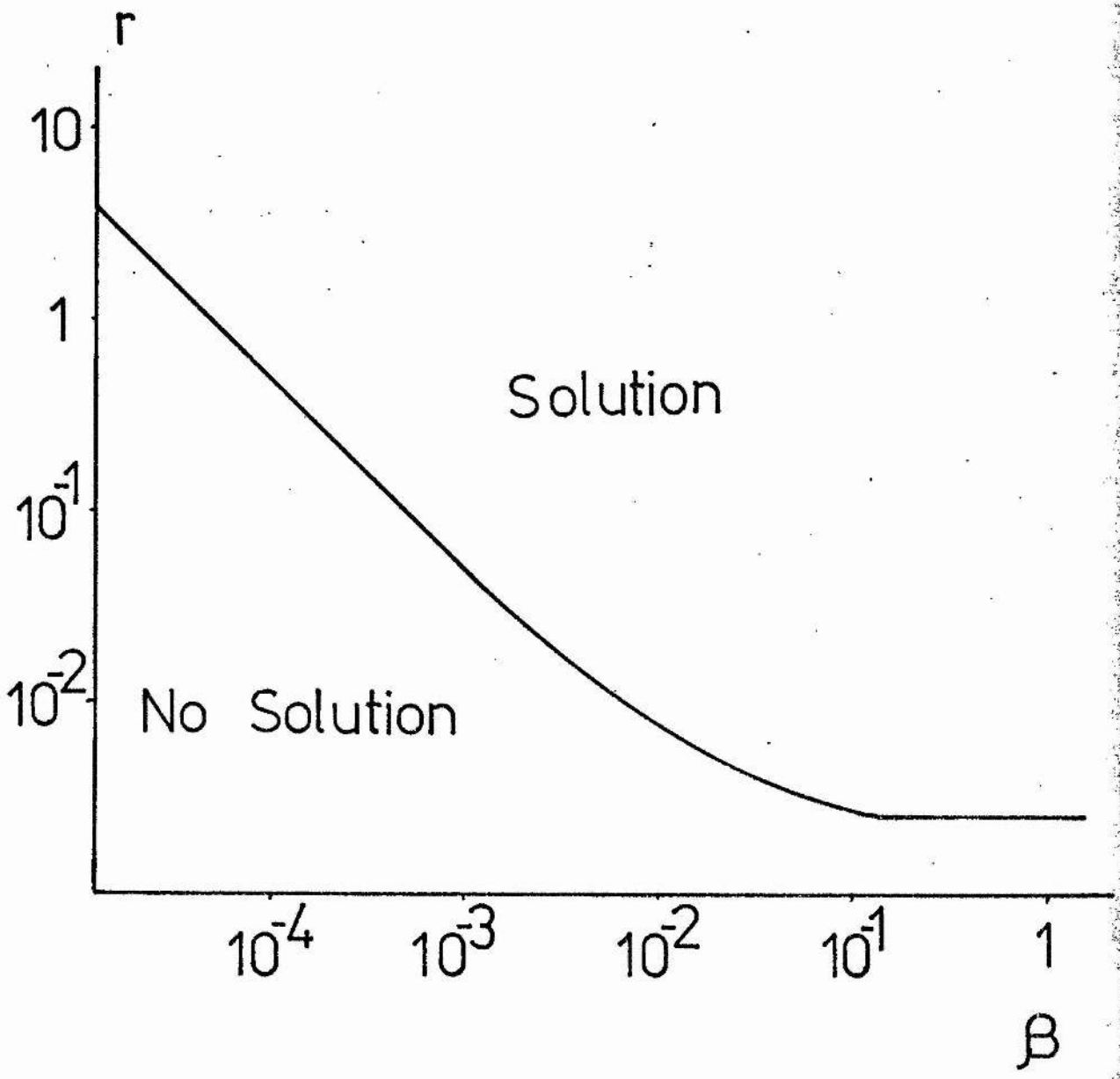

Figure 4.8

Regions of the (β,r) parameter spare for which equilibrium solutions are possible. Here β is the external plasma beta ($= 2\mu p_\infty / B_\infty^2$) while r is the ratio of radiation to convection as given by equation (4.35).

solutions are possible, our next interest is to see how the dimensions ($\ell = \ell_o/R_m$, $L = L_o(R_m D)$) of the sheet vary with the dimensionless parameters β,r describing the external conditions. It is also of interest to see how good an approximation is the order of magnitude approach to the problem, and to this end we plot, in Figure (4.9), ℓ/ℓ_o against β for various values of the parameter r. Note that

$$\ell_o = 2\eta_o/v_\infty T_\infty^{3/2}$$

represents the order of magnitude approximation to the width of the sheet (shown dashed in the Figure). We find that, for values of the parameters far from the dividing line of Figure 4.8 (i.e. large r and β), the width ℓ is larger than the order of magnitude solution by a factor of about 2.8, and is almost independent of β. For smaller values of r and β marked variations are apparent. Note that $r = 8 \times 10^8 \rho_\infty^2 T_\infty^{\alpha-3/2} \chi(\gamma - 1)/(v_\infty^2 p_\infty)$ and is typically $\sim 10\text{-}10^{-2}$ in the chromosphere/lower transition region while in the upper transition region/corona values of 10^{-6}-10^{-8} are more typical. Similarly $\beta = 2\mu p_\infty/B_\infty^2$ ranges from $\sim O(1)$ in the lower atmosphere to $O(10^{-4})$ in the upper atmosphere (for $B_\infty \simeq 100$ Gauss).

Similarly, we plot in Figure (4.10) the length L against β, for various r, with L measured in units of

$$L_o = \frac{2\eta_o}{v_\infty^2} \left(\frac{2p_\infty}{\rho_\infty T_\infty^3} \right)^{\frac{1}{2}} .$$

The scale L_o, which represents the simple order of magnitude approximation to the length which is independent of β and T_c. A more sophisticated approximation to the length of the sheet which does vary with β is obtained from the order of magnitude approach in Section 4.1, where the outflow velocity is related to an Alfvén speed (and hence β). Thus using (4.13) we may write

$$L_{om} = L_o((1+1/\beta)T_\infty/\beta T_c)^{\frac{1}{2}} .$$

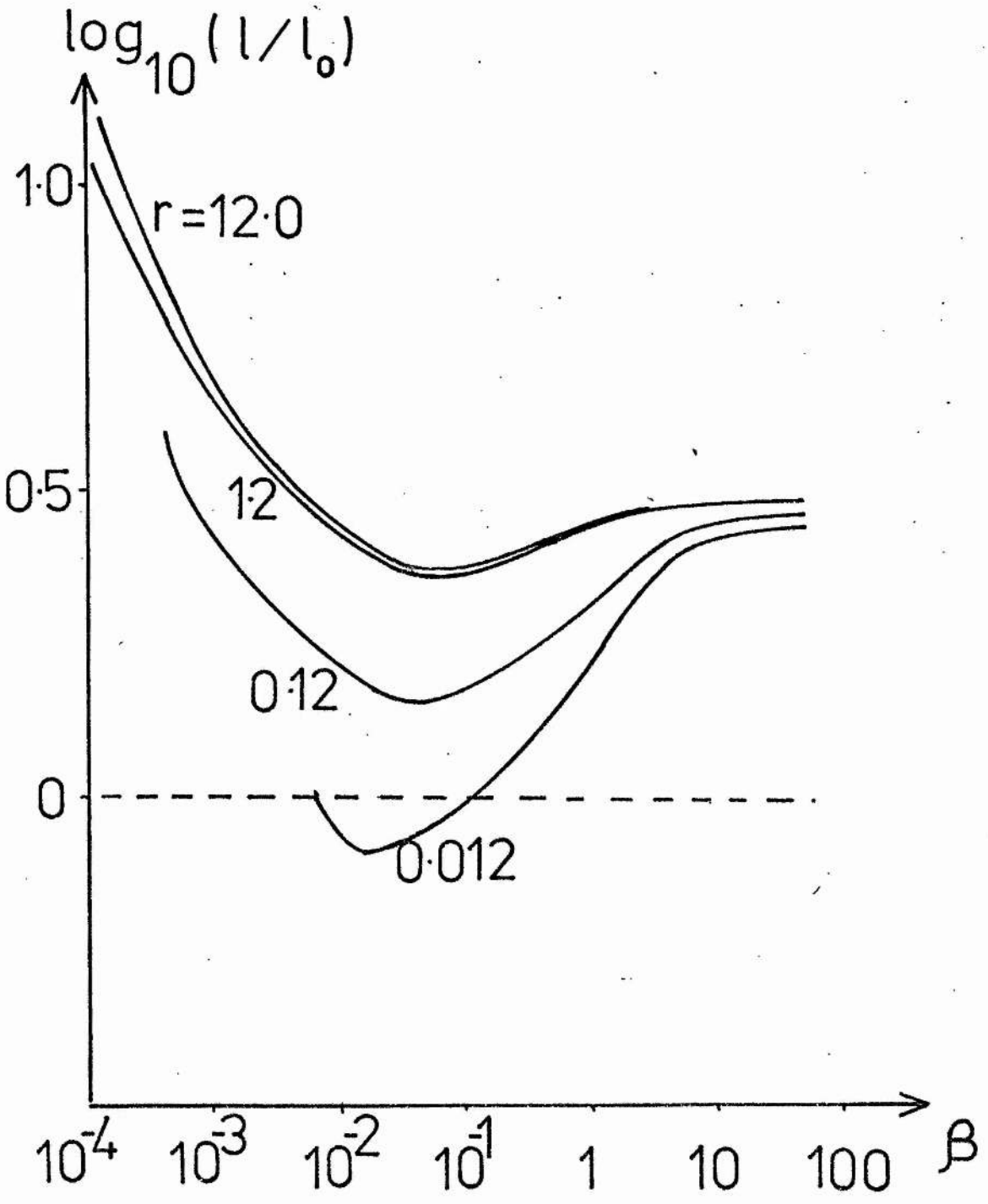

Figure 4.9

Computed results for the width, ℓ, of the current sheet. We have plotted the ratio ℓ/ℓ_0 (where ℓ_0 is the order of magnitude approximates to the width) against $\beta(= 2\mu p_\infty/B_\infty^2)$, for various values of $r(= \eta_0 \rho_\infty^2 T_\infty^{\alpha-3/2} \chi(\gamma - 1)/(v_\infty^2 p_\infty))$. The dashed line shows the order of magnitude result.

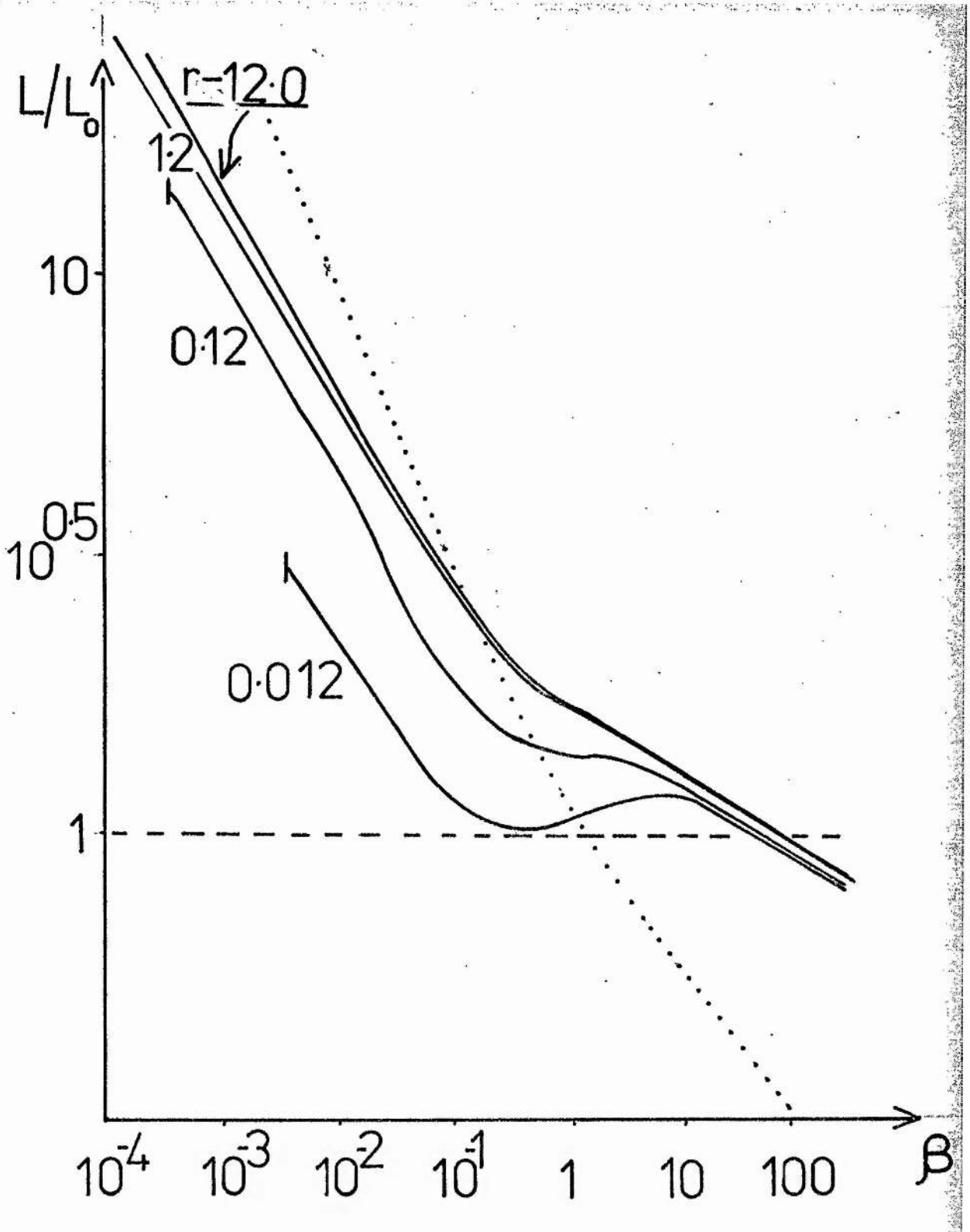

Figure 4.10

Computed results for the length, L, of the current sheet in terms of L_o, the order magnitude approximation to the length, against β for various values of r. The dashed line shows the order of magnitude approximation while the dotted curve gives the "improved" order of magnitude approximation, L_{om}/L_o, described in the text.

For simplicity we take T_∞/T_c to be unity giving the behaviour shown dotted in Figure 4.10. Thus we see that the above approximation describes reasonably well the actual behaviour shown in the Figure. For both the width and the length, however, a major difference from the order of magnitude behaviour is the cut off value occurring when the critical values of β and r are reached.

The full numerical solution to the problem also yields the spatial profiles of $\bar{v}$, $\bar{\rho}$ and $\bar{B}$. For the case of $r = 1.2 \times 10^{-2}$ (corresponding to, for example, $v_\infty = 10^{2.5}$ and height $h = 1$ in the model atmosphere) we plot these variations for various values of β. Figure 4.11 shows the variation of the non-dimensional velocity $\bar{v}$ against the non-dimensional distance $\bar{x}$. We note that for large β the velocity increases smoothly from its edge value of -1 to its central value of 0 as required. As β decreases towards its cut-off value (of 0.6×10^{-2} for this value of r) the profile steepens locally, tending towards a step function. The density profile (Figure 4.12) shows a similar behaviour with the central value of $\bar{\rho}$ increasing as β decreases, thus giving a sharper profile. The behaviour of the magnetic field profile as β varies is shown in Figure (4.13). The pressure may be obtained from the above information using

$$\bar{p} = 1 + (1 - \bar{B}^2)\beta \quad ,$$

and similarly the temperature is given by

$$\bar{T} = (1 + (1 - \bar{B}^2)/\beta)/\bar{\rho} \quad .$$

The usefulness of keeping the above results in a non-dimensional format may be illustrated when we take account of the suggestion that the corona is always in a turbulent state (Benz, private communication). Heavy ions appear in the solar wind in nearly coronal abundances, which seems unlikely unless the Coulomb collision rate is enhanced by turbulence. Benz (Benz and Gold, 1976) consider that the turbulence may be of the Whistler type, caused by evaporating ions. The effect of the turbulence is to enhance the

Figure 4.11

Dimensionless inflow velocity profile in current sheet (with centre at origin) for various values of β and $r = 1.2 \times 10^{-2}$.

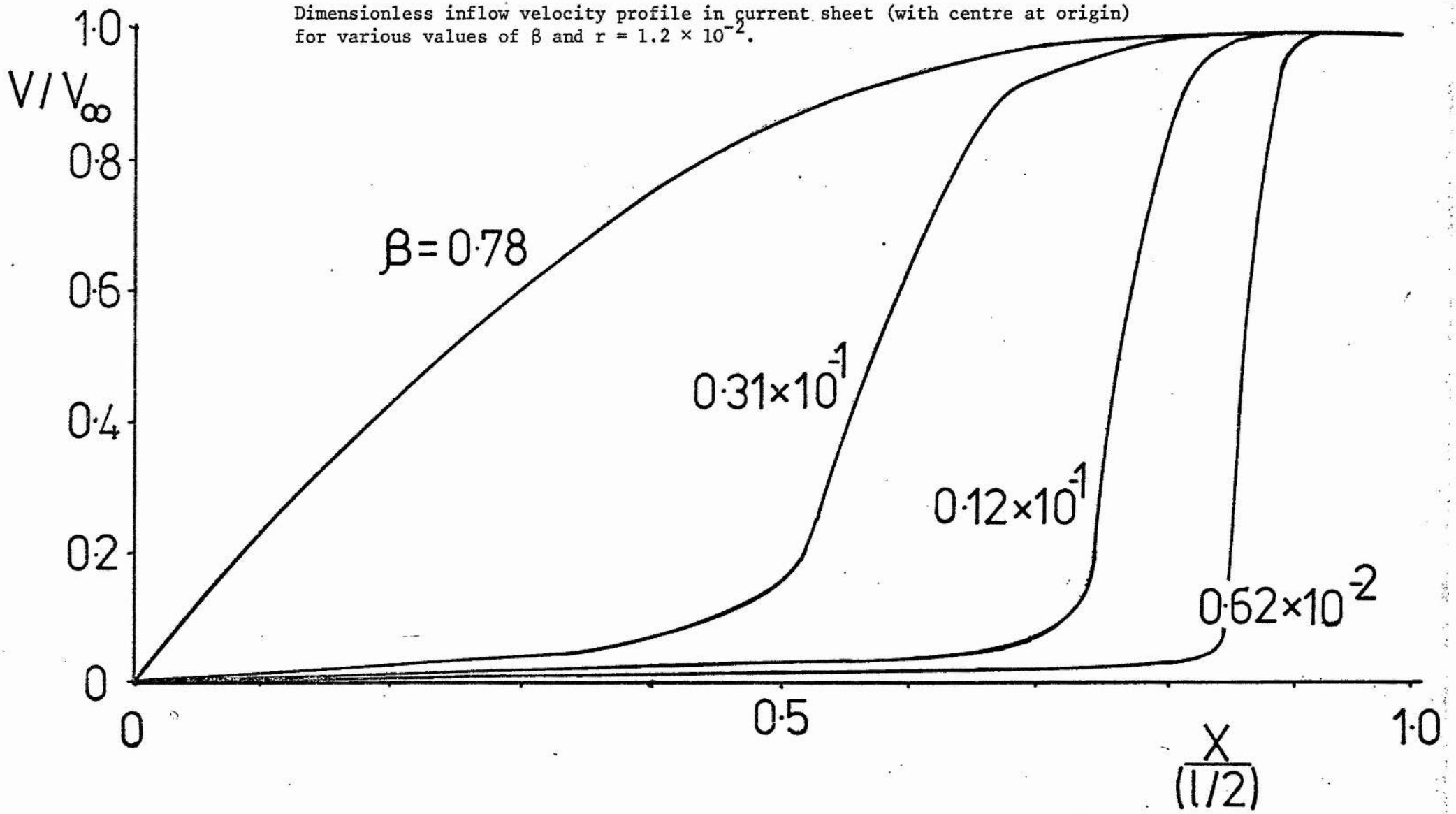

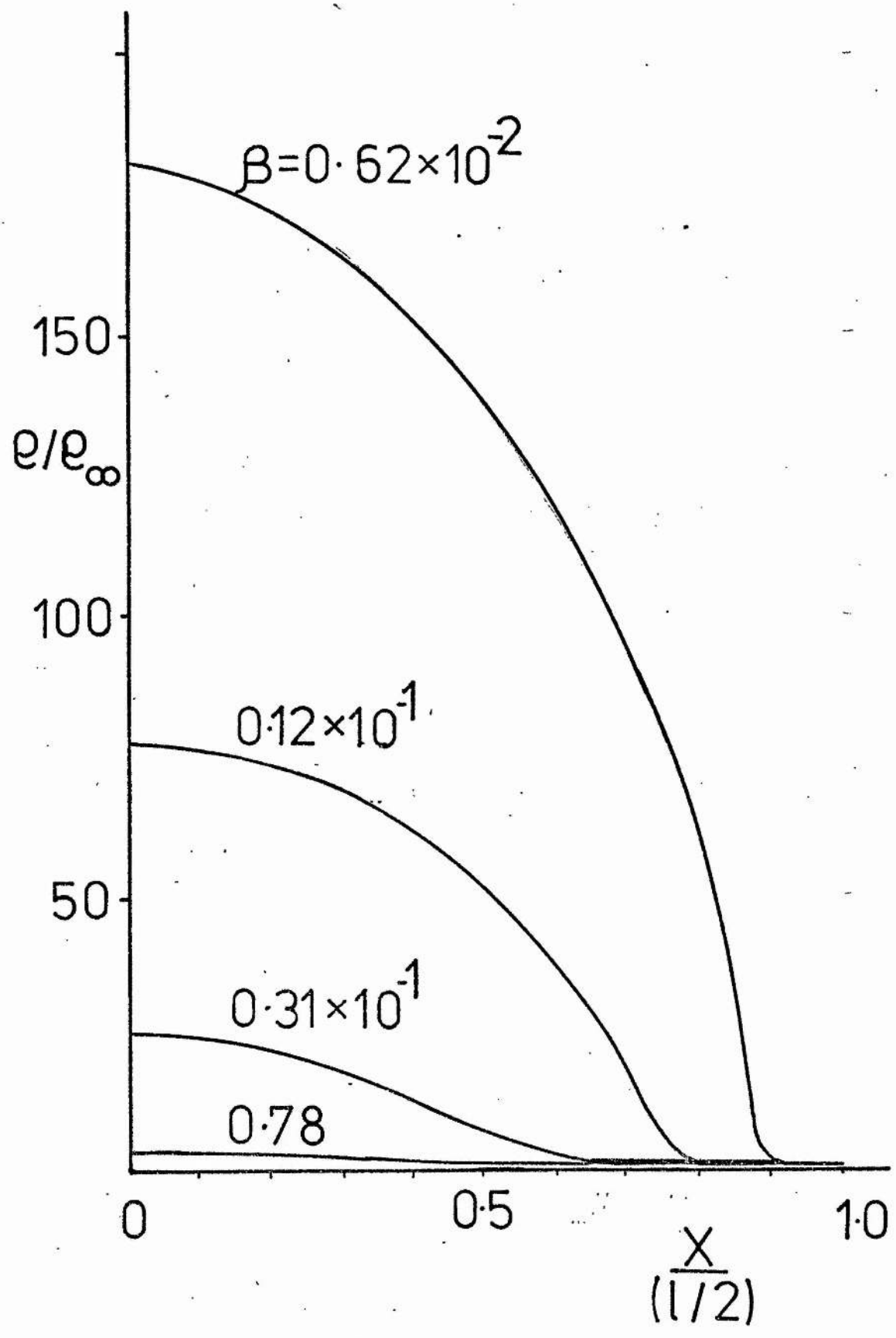

Figure 4.12

Dimensionless density profile for the case of $r = 1.2 \times 10^{-2}$ and various values of β.

Figure 4.13

Dimensionless magnetic field profile for $r = 1.2 \times 10^{-2}$ and various values of β.

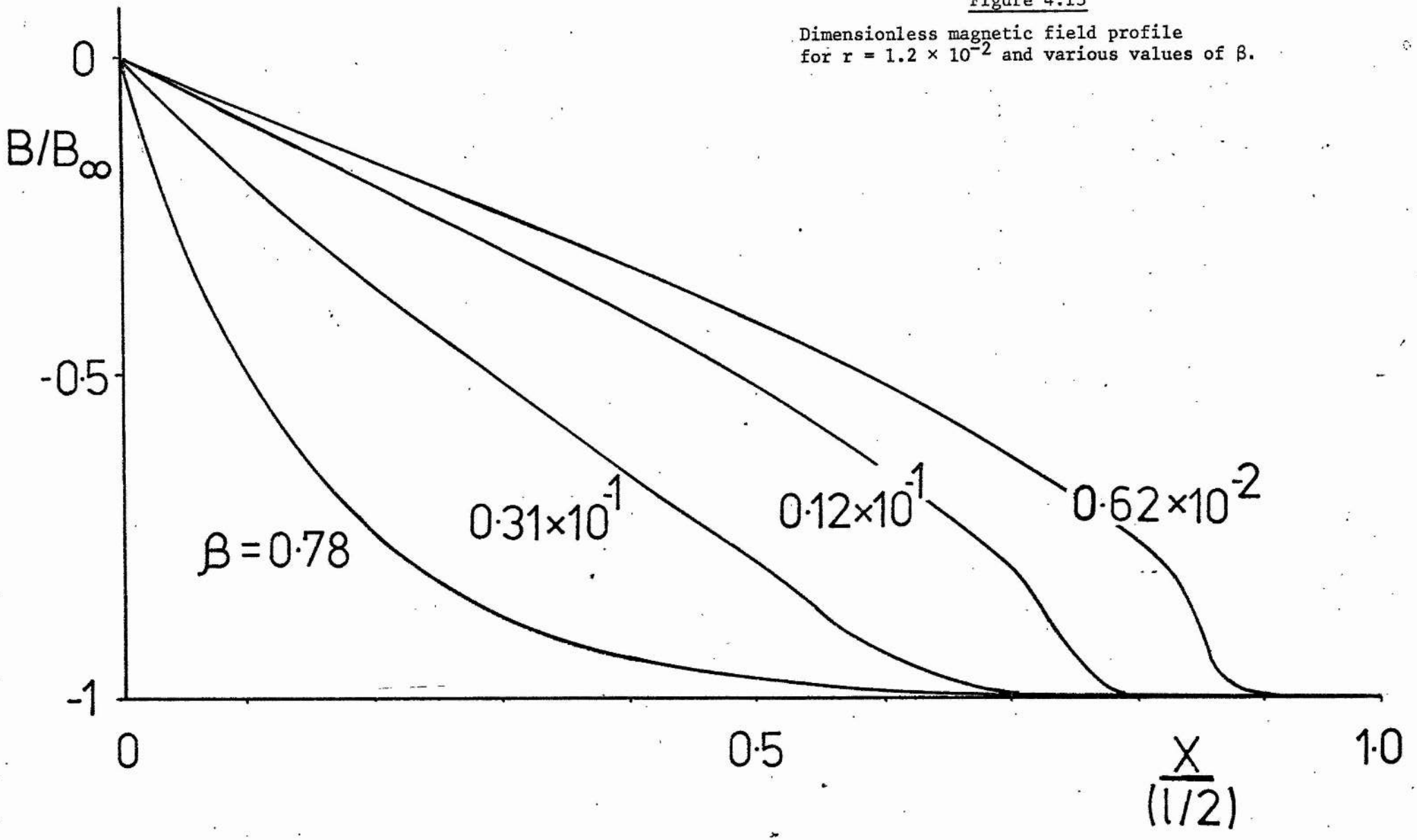

collision rate (and thus also the resistivity) by a factor of about 100. In our problem the resistivity appears only in the parameters

$$R_m = 2\eta_o / v_\infty T_\infty^{3/2} \ell \quad (= \ell_o/\ell) \quad ,$$

and

$$r = \eta_o \rho_\infty^2 T_\infty^{\alpha - 3/2} \chi(\gamma - 1)/v_\infty^2 p_\infty \quad ,$$

so that the effect of turbulence will be to increase both the length scale ℓ_o and the ratio, r, of radiation to convection.

In the next Section we wish to apply these results to the emerging flux model. In so doing we will relate the parameters to a model atmosphere and thus the length scales (ℓ_o,L_o) for different regions of the sun will be estimated.

4.4 Application to the emerging flux model

In Section 4.1 we have described the order of magnitude approach to current sheets which was used by Tur and Priest (1977) to suggest a possible trigger mechanism for the emerging flux model. This approach led to solutions which represent approximate values for the central temperature and density and also the dimensions of the sheet. A model atmosphere was used to relate the external density and temperature to some given height and the variation of the central values and dimensions with the height in the atmosphere, and also with the external magnetic field strength (B_∞) and inflow velocity (v_∞). From this method several conclusions (as outlined in Section 4.2), were obtained. In this Section we wish to see how these conclusions are altered by our more careful modelling of the current sheet.

The model atmosphere for temperature and density variations with height in the solar atmosphere used by Heyvaerts and Priest (1976) and Tur and Priest (1977) is given in Table 2. The size of the transition region as given by this model is rather large but the way ρ_∞ and T_∞ vary is reasonable and, for ease of comparison with previous results we shall retain this model. Furthermore, it is useful to consider the variation of

the non-dimensional parameters used above with the height h. In Figure 4.14 we show the variation of r with h, while in Figures 4.15 and 4.16 we give the height variations of the length scales ℓ_o and L_o respectively.

One of the advantages of the order of magnitude approach to the emerging flux model was the fact that a simple algebraic equation for the central temperature and density of the current sheet results. As we have seen above we may, rather surprisingly, also obtain an algebraic equation for these values using the present theory, namely

$$\frac{2(\gamma - 1)}{\beta} - r(1 + 1/\beta)\bar{T}_o^{2\alpha-3.5} + r_\infty(1 + 1/\beta)\bar{T}_o^{-2.5} = 0 \quad . \qquad \ldots (4.63)$$

Tur and Priest found that the solution curves for the central temperature did not vary greatly if the ratio V_∞/B_∞ was kept constant. For our solutions we note from (4.63) that, for small β, the parameters appear only in the combination r/β and, since r/β is proportional to B_∞^2/V_∞^2 we have the same feature as Tur and Priest.

In applying the above theory to the emerging flux model, we are particularly interested in the possibility of a maximum height in the atmosphere for an equilibrium solution to exist. There are, in the present approximation, two ways that such an event might occur. Firstly, there is the possibility of no solution existing to (4.63). Secondly, as the current sheet rises in the atmosphere, we enter the region of parameter space where no solution is possible (Section 4.3.3), despite the fact that equation (4.63) has a solution. In both these ways a height h_{crit} is attained where no neighbouring equilibrium exists and we associate this height with the site for the onset of flare activity (as discussed in Section 4.2).

We plot h_{crit} for various values of v_∞ and B_∞ in Figure 4.17. We note immediately that the variation of h_{crit} with B_∞ is exactly opposite to the order of magnitude results shown in Figure 4.4. This is due to the fact that in Figure 4.17 h_{crit} arises from the second of the above mentioned

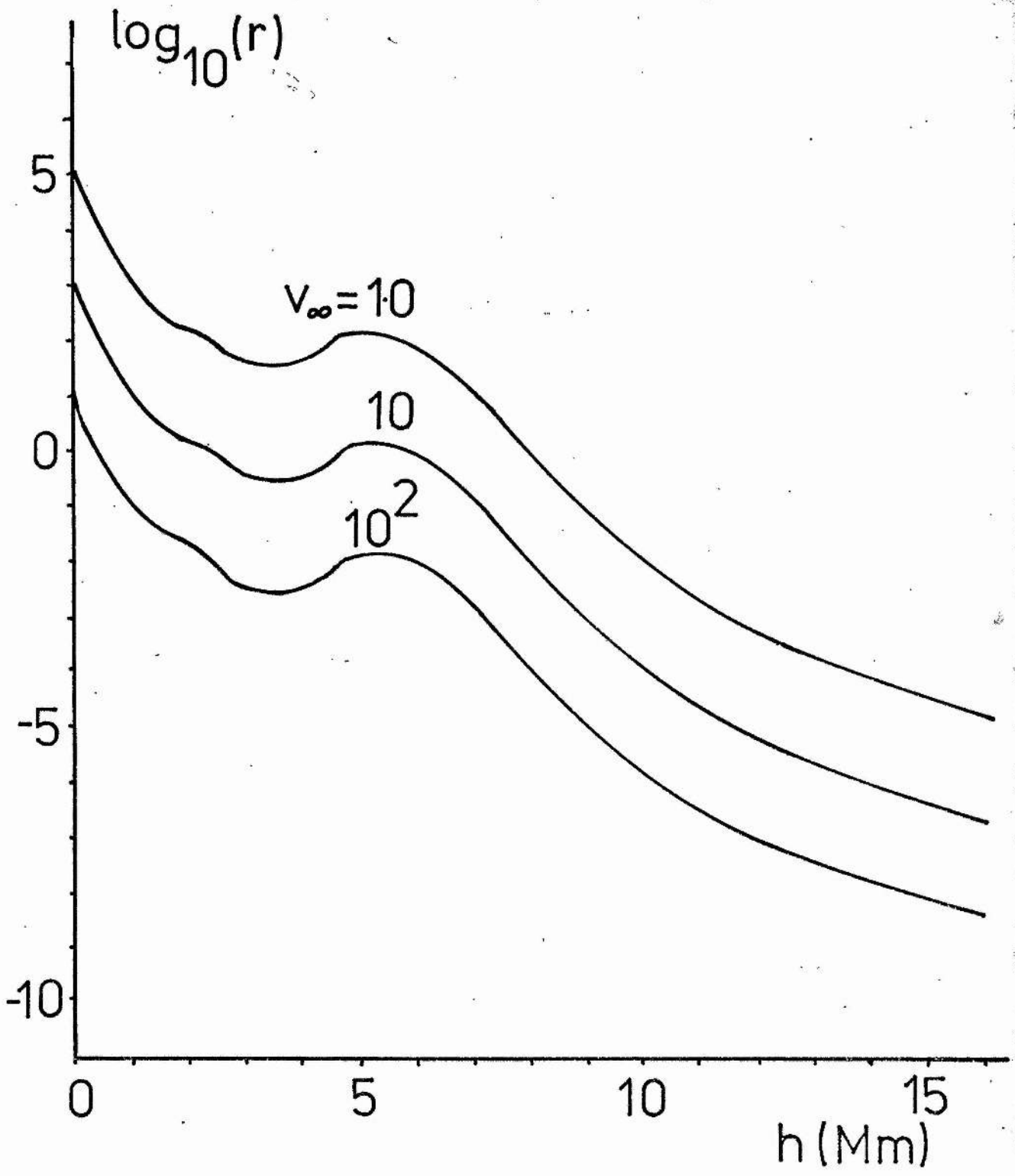

Figure 4.14

The variation of the parameter

$$r = \eta_o \rho_\infty^2 T_\infty^{\alpha-3/2} \chi(\gamma - 1)/(v_\infty^2 p_\infty)$$

(= ratio of radiation to convection) with height h for the model atmosphere of Table 2 for various values of v_∞ (m s^{-1}). We here assume a classical diffusivity. If η is enhanced by a factor of 100, then so is r.

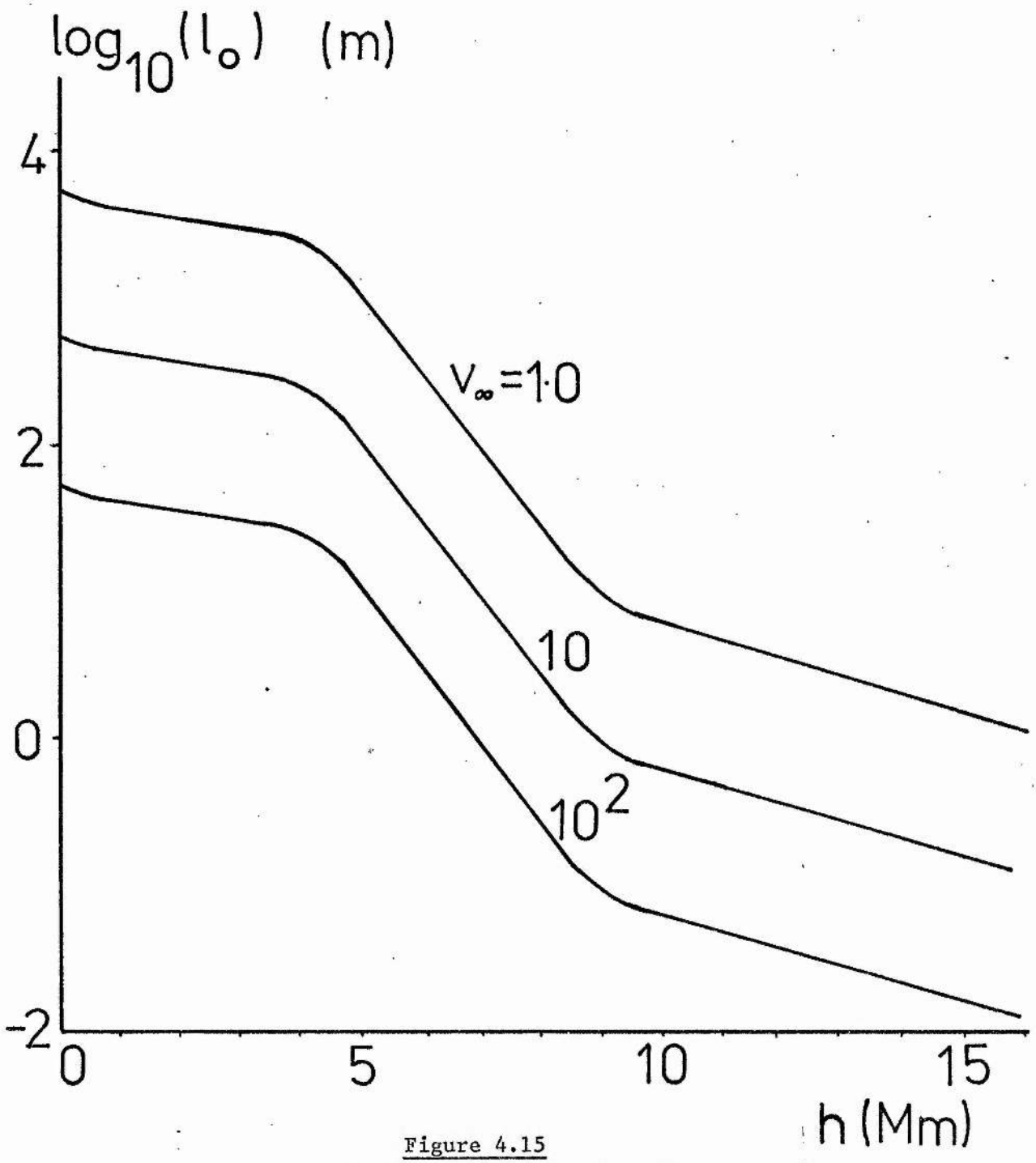

Figure 4.15

Variation of the order of magnitude approximation to the width of the current sheet, $\ell_o (= 2\eta_o T_\infty^{3/2}/v_\infty)$ with height h in the model atmosphere for a classical Coulomb diffusivity. If the diffusivity is enhanced by a factor 100, say, due to weakly turbulent conditions, then ℓ_o is larger by the same factor.

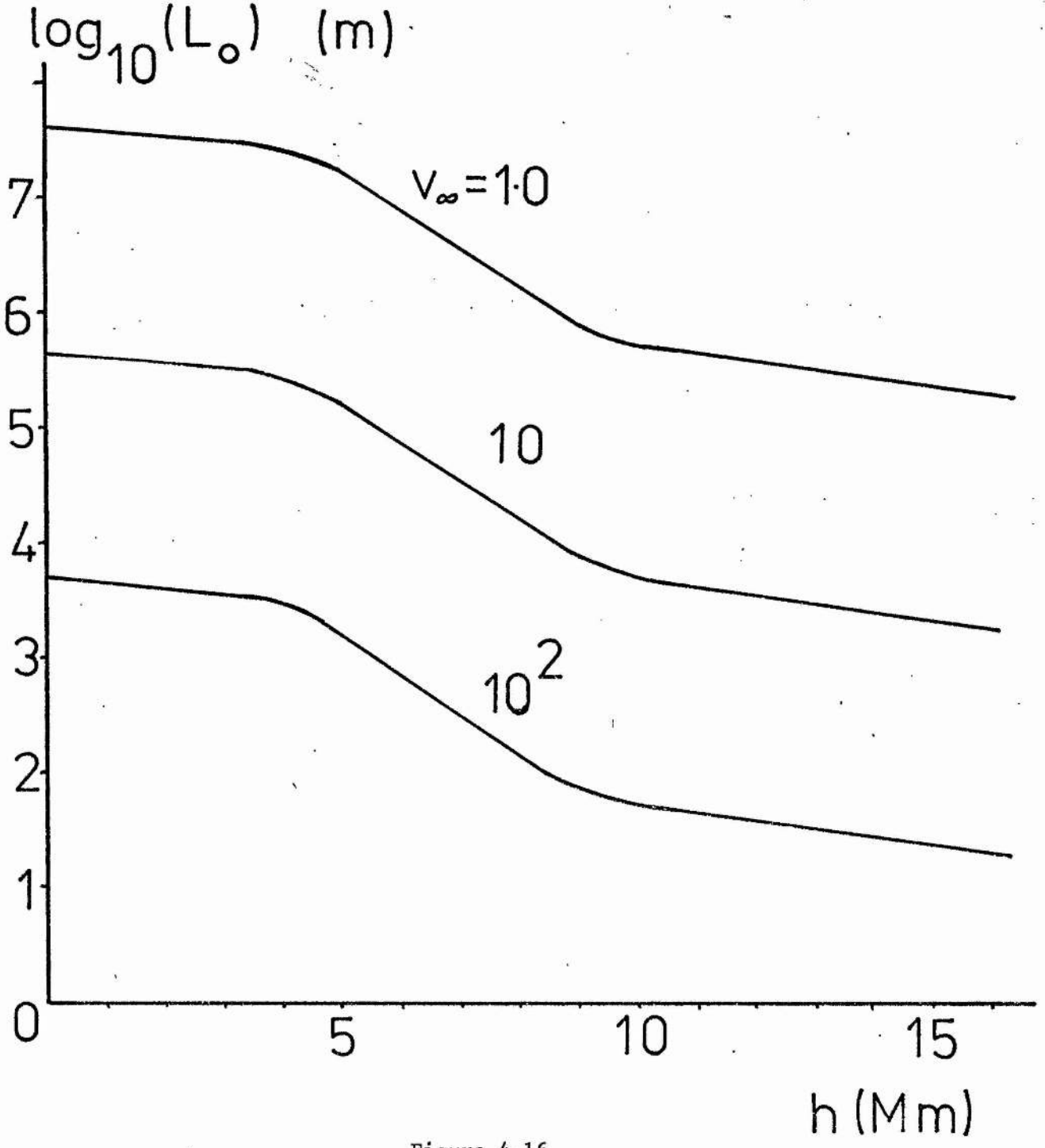

Figure 4.16

Variation of the order of magnitude approximation to the length of the current sheet

$$L_o \left(= \frac{2\eta_o}{v_\infty^2} \left(\frac{2p_\infty}{\rho_\infty T_\infty^3} \right)^{\frac{1}{2}} \right)$$

with height h in the model atmosphere for a classical diffusivity. A turbulent diffusivity, larger by a factor of 100, would increase L_o by the same factor.

methods for obtaining a critical height, namely reaching the region of parameter space where no solution is possible. In fact, had we neglected this possibility and looked only at the solutions of (4.63), the B_∞ variation would have been similar to the order of magnitude solution.

Next we note that the predicted height for the onset of flare activity is rather low in this model (typically upper chromosphere heights for $v_\infty \gtrsim 10^2$ m s^{-1}). Only for very small inflow velocities can equilibrium solutions exist well into the transition region.

As discussed in Section 4.3.3, there is evidence that the solar atmosphere is in a turbulent state with the diffusivity enhanced by a factor of at least 100. One effect of this is to increase the length scales ℓ_o and L_o by this same factor (see equation (4.32) and (4.34)) over the values shown in Figures (4.15) and (4.16). Also, increasing the resistivity will act so as to increase the critical height in the emerging flux model. We plot (in Figure 4.18) the critical height predicted by the model with the resistivity enhanced by a factor of 100. The effect of this is to allow equilibrium to persist into the middle of the transition region for significantly higher values of the inflow velocity than were allowed in the non-turbulent model.

In both these cases, however, the effect is the same. As the current sheet rises through the atmosphere, a point is reached where no equilibrium is possible (h_{crit}). The emerging flux model suggests that the sheet now heats up seeking a new equilibrium configuration. In so doing however a threshold value of the current density j_{crit}, beyond which turbulent behaviour ensues, is exceeded. This is regarded as the onset of the impulsive phase of the solar flare, as described in Section 4.2. As stated above, h_{crit} in our model arises through moving from the "solution" region of parameter space (Figure 4.8) to the "no solution" region. From the profiles shown in Figures (4.11-4.13) we note that as the critical

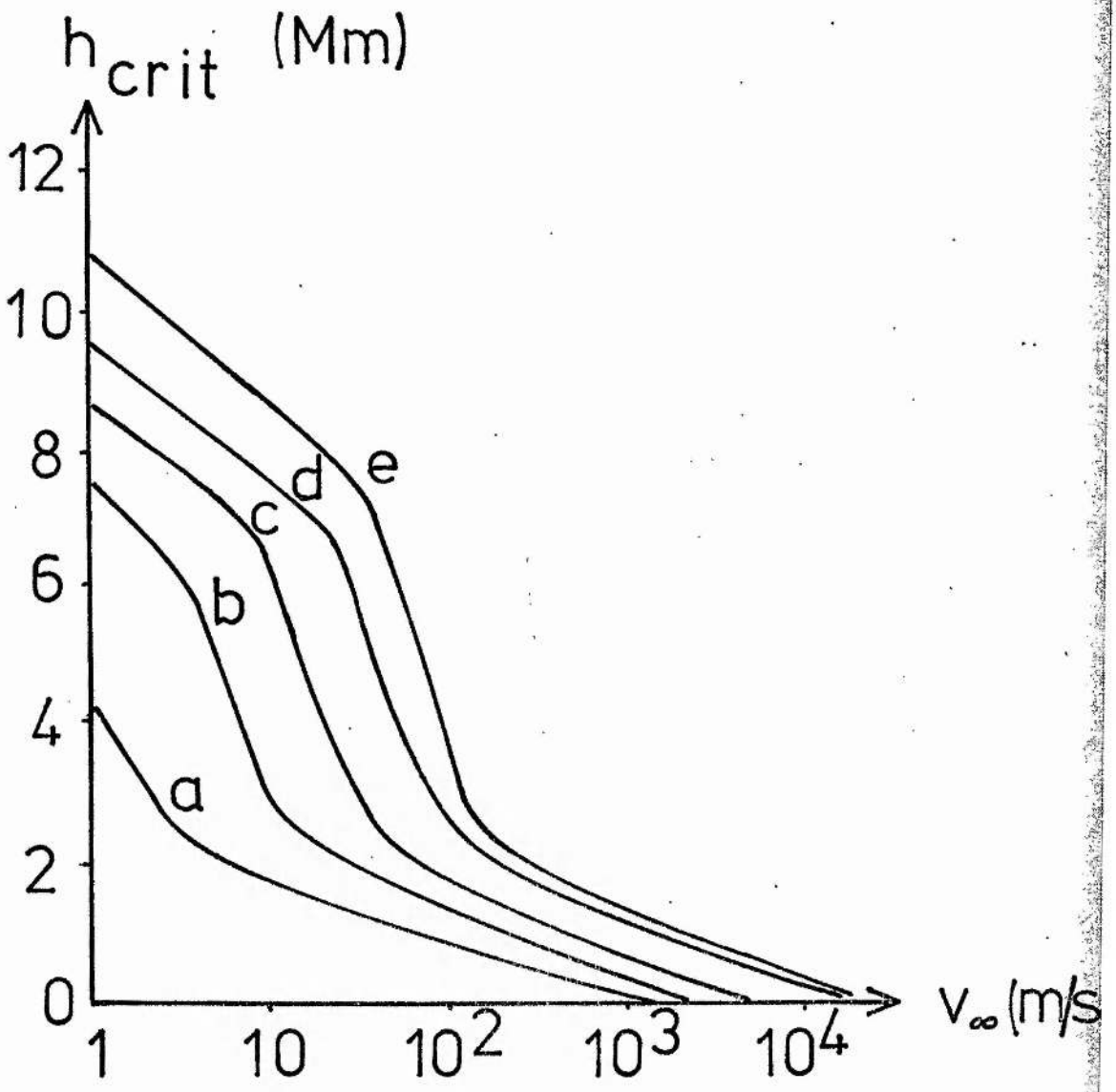

Figure 4.17

The variation of the critical height for the onset of non-equilibrium with v_∞ for several values of B_∞ (tesla) assuming a classical diffusivity: (a) $B_\infty = 10^{-1}$, (b) $B_\infty = 10^{-1.5}$, (c) $B_\infty = 10^{-2}$, (d) $B_\infty = 10^{-2.5}$, (e) $B_\infty = 10^{-3}$.

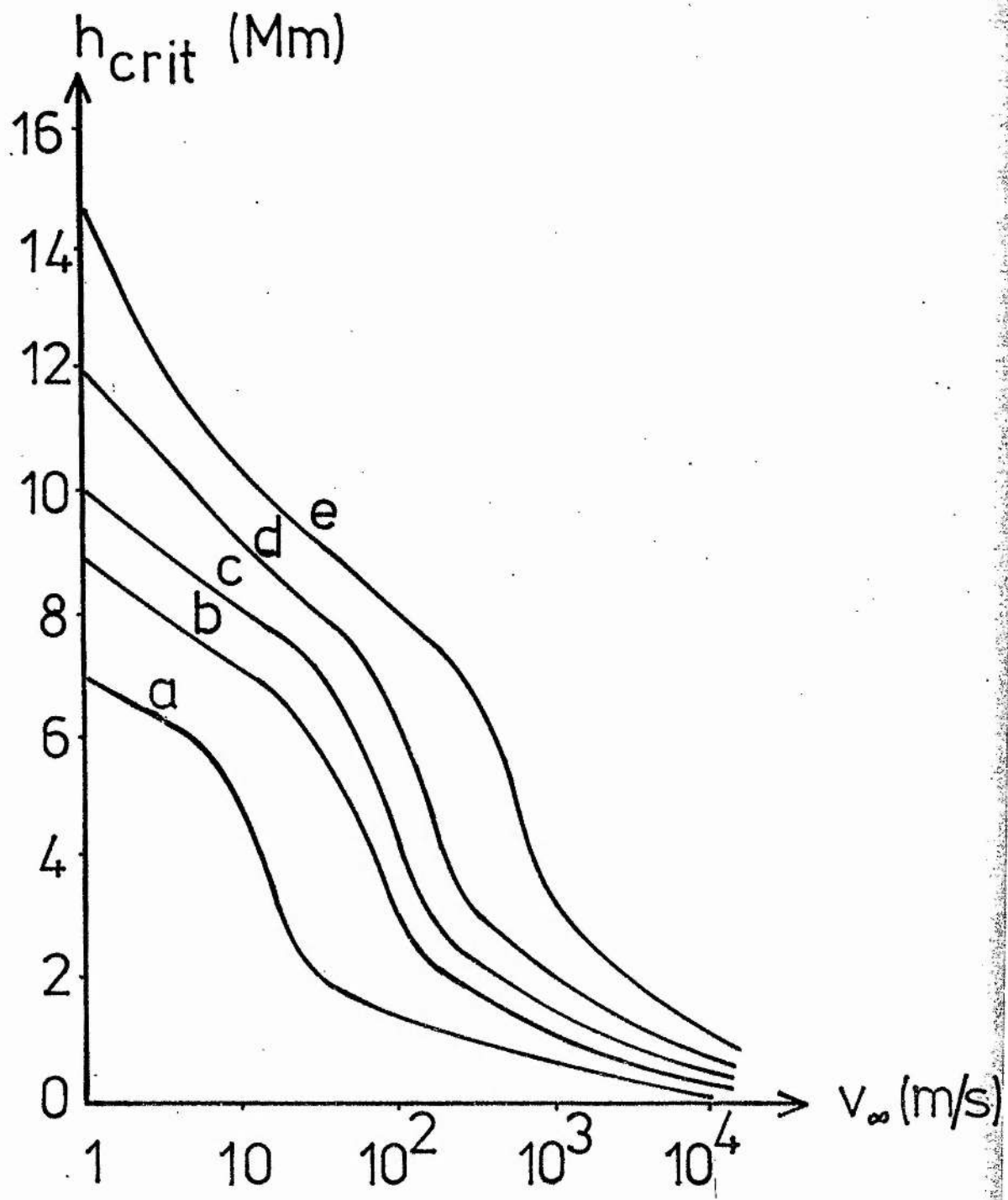

Figure 4.18

The variation of the critical height with v_∞ and B_∞ for a turbulent diffusivity ($\eta_o \times 100$). The value of B_∞ (tesla) considered are (a) 10^{-1}, (b) $10^{-1.5}$, (c) 10^{-2}, (d) $10^{-2.5}$, (e) 10^{-3}.

values are approached the gradients become very steep locally.

This suggests that the threshold for the Buneman instability, j_{crit} is attained locally within the sheet (when $d\bar{B}/d\bar{x}$ is large) rather than right through it. It will also occur just before h_{crit} is attained in our model, rather than just after as previously suggested.

Finally we note from Figures 4.10 and 4.16 that for both very small β and very small inflow velocities (e.g. $\beta \lesssim 10^{-4}$ and $v_\infty \lesssim 1$) the theory must be invalid since the predicted sheet length L is in excess of the upper realistic values of 10^7 or 10^8 m.

4.5 Discussion

In the above we have considered a one-dimensional equilibrium model for a reconnecting current sheet in the solar atmosphere. We have used the full energy equation save for the thermal conduction term, the neglect of which has many simplifying features. The region of validity of our solutions with this assumption is discussed in Section 4.3. For the sake of generality our results are given in terms of dimensionless parameters, two of which are of particular interest. We find that if either the external plasma beta (β) or the ratio of radiation to convection (r) fall below minimum values then no steady solution is possible. An interesting feature of our equations is the ability to determine the central values of temperature and density, without solving the full system of equations. In order to find the length (L) and width (ℓ) of the sheet we need to solve the full system of equations numerically, and thus obtain the appropriate spatial profiles. As the critical values of β and r are approached these profiles develop steep gradients over a relatively small length scale. As a result of this the critical current density for the onset of turbulence is exceeded. Also we must beware that thermal conduction may become important in this region as a result of the small length scales. We would thus wish to know how steep the gradients (or how

small the local length scales) would require to be to make conduction dominant before the turbulent threshold j_{crit} is exceeded. In fact we note that both the Joule heating term (which results from the current density) and the thermal conduction term are inversely proportional to the square of the local length scale. Thus, as this is decreased, the ratio is unchanged and so we expect the threshold current density j_{crit} to be exceeded as predicted above. We note here that the inclusion of thermal conduction in the system of equations would pose extremely serious problems since the simplifying method of solution (as described in Section 4.3.2) would no longer be applicable.

In the last Section of this chapter we have concerned ourselves with the application of the above results to the emerging flux model (as described in Section 4.2). The order of magnitude approach to current sheets, as used by Tur and Priest (1978) has been replaced by the above model. We find that the non-equilibrium feature of allowing only certain values of β and r determines the critical height (h_{crit}) at which a flare is triggered according to the emerging flux model and so alters its dependence on the magnetic field. More important, however, is the fact that such a critical height is still found to exist. We have thus verified the main prediction of the emerging flux model, namely that as a current sheet rises through the solar atmosphere it ultimately reaches a critical height (which varies according to the external conditions), beyond which no equilibrium is possible. The effect of a turbulent resistivity on this critical height is to increase its value from typically the chromosphere to the upper transition region.

Chapter 5: CONCLUSIONS AND SUGGESTIONS FOR FURTHER WORK

We now wish to summarise the results of the previous chapters and suggest possible extensions to this work which may be of value. Firstly, however, we shall turn our attention to the concept of non-equilibrium (a feature common to the results of Chapters 2-4). In each of these chapters we have found that by varying one (or more) of the parameters beyond some critical value, the equilibrium (or, in the case of Chapter 4, the steady state) equations no longer admit a solution satisfying the prescribed boundary conditions. This parametric onset of non-equilibrium should be distinguished from the concept of instability. A necessary condition for the existence of an instability is that some basic state is possible (highly unlikely in nature), about which perturbations from the equilibrium state will grow in time. By contrast, non-equilibrium means that the above basic state is completely absent,(i.e., no solution of the equilibrium equations and boundary conditions exists). The existence of magnetostatic non-equilibrium has been pointed out by Parker (1975 a,b). In the first of these papers he showed that no hydrostatic equilibrium exists for a flux tube anchored at the ends in a stratified atmosphere if the whole tube is twisted by more than a critical amount. In the second of these papers he showed that any temperature variation along the axis of symmetry of an azimuthal field will cause continual convective instability (i.e. no static equilibrium) except for very special cases. It is this fact, he argues, that explains the observed continual activity associated with flux tubes extending through the photosphere.

Recently some useful theorems related to non-equilibrium were quoted by Birn et al (1978). They consider the problem

$$\nabla^2 D + \lambda F(D) = 0 \qquad \ldots (5.1)$$

with

$$D = 0 \quad \text{on the boundary,} \qquad \ldots (5.2)$$

where λ is some non-negative parameter of the problem. It may be shown that

(a) if $\frac{\partial F}{\partial D} \lesssim 0$, then the problem has a unique solution for all λ;

(b) if $F > 0$, $\frac{\partial F}{\partial D} > 0$, $\frac{\partial^2 F}{\partial D^2} > 0$, then there exists a positive number λ_{crit} such that the problem has no solution at all if $\lambda > \lambda_{crit}$, and at least two solutions if $\lambda < \lambda_{crit}$.

As an application of this theorem let us consider the energy equation in the limit of constant pressure. Because of the temperature dependence of the thermal conductivity it is useful to consider the variable $T^{7/2}$. The non dimensional form of the energy equation may be written as

$$\frac{d^2\tau}{dx^2} + L^2\bar{p}\chi\left[(1-\tau)^{2(\alpha-2)/7} - H(1-\tau)^{-2/7}/p\chi\right] = 0 \qquad \ldots (5.3)$$

where $\tau = 1 - \bar{T}^{7/2}$, L is the length scale of the system and $\bar{p}$ is the non dimensional pressure (χ, α and H are as defined previously). If we are interested in the symmetric temperature distribution, such that $\bar{T} = 1$ at the edges, we have the condition

$$\tau = 0 \quad \text{at} \quad x = \pm 1 \quad , \quad \text{say} \quad .$$

Thus our problem is in a form where the theorems of Birn et al are applicable, and our parameter is the length scale L. In particular let us consider the high temperature region where $\alpha = -1$. The second of Birn's theorems shows that, if radiation dominates over heating ($H/p\chi < 1$), then there exists a maximum allowable value of $L = L_{crit}$, beyond which, no thermal equilibrium is possible. For $L < L_{crit}$, multiple solutions are possible.

The above problem is exactly that considered by Hood and Priest (1979) to model the thermal equilibrium of solar coronal loops. Their numerical solutions to the problem show the behaviour predicted by the theorem and give exact values for the critical parameters (something that the above theory is unable to yield). The non-equilibrium of coronal loops

was also suggested by Priest (1978) in a paper which outlined some general physical considerations of loop structure, while Roberts and Frankenthal (1979) considered approximations to the energy equation, for which analytic solutions, exhibiting non-equilibrium, are available.

In the limit of radiation dominating heating the energy equation may be written as

$$\frac{d}{d\bar{x}} \left(\bar{T}^{5/2} \frac{d\bar{T}}{d\bar{x}} \right) = \bar{C}_p^{-2} \bar{T}^{\alpha-2} \qquad \ldots (5.4)$$

where we have non-dimensionalised all the variables against their boundary values, so that our edge condition on $\bar{T}$ is

$$\bar{T} = 1 \quad \text{at} \quad x = \pm \ell \quad , \quad \text{say} \quad .$$

If we approximate (5.4) by an order of magnitude equation, we obtain

$$\bar{T}^{5/2}(1 - \bar{T}) = L T^{\alpha-2} \quad , \qquad \ldots (5.5)$$

where

$$L = \bar{C}_p^{-2} \ell^2 \quad .$$

The solution of (5.5) is shown graphically in Figure 5.1 for three possible values of the parameter L. We note that there arises a critical value of L ($= L_{crit}$) for which only one solution is possible. If $L > L_{crit}$ then no solution is possible (non-equilibrium); while if $L < L_{crit}$, then two solutions occur. We thus see that increasing either the length scale ℓ or the pressure $\bar{p}$ beyond some critical values will preclude the possibility of an equilibrium solution.

Having shown that the energy equation admits the possibility of non-equilibrium, let us now turn our attention to the magnetostatic equations. Following Low (1975), for a two-dimensional system independent of z, say, with gravity in the direction of the negative y-axis, the magnetostatic equations may be written in the form

$$\nabla^2 A + \frac{\partial}{\partial A} \left(\mu p(A) e^{-y/\Lambda} + \frac{1}{2} B_z^2(A) \right) = 0 \qquad \ldots (5.6)$$

where p is the gas pressure, Λ is the temperature scale height ($= RT/g$) and

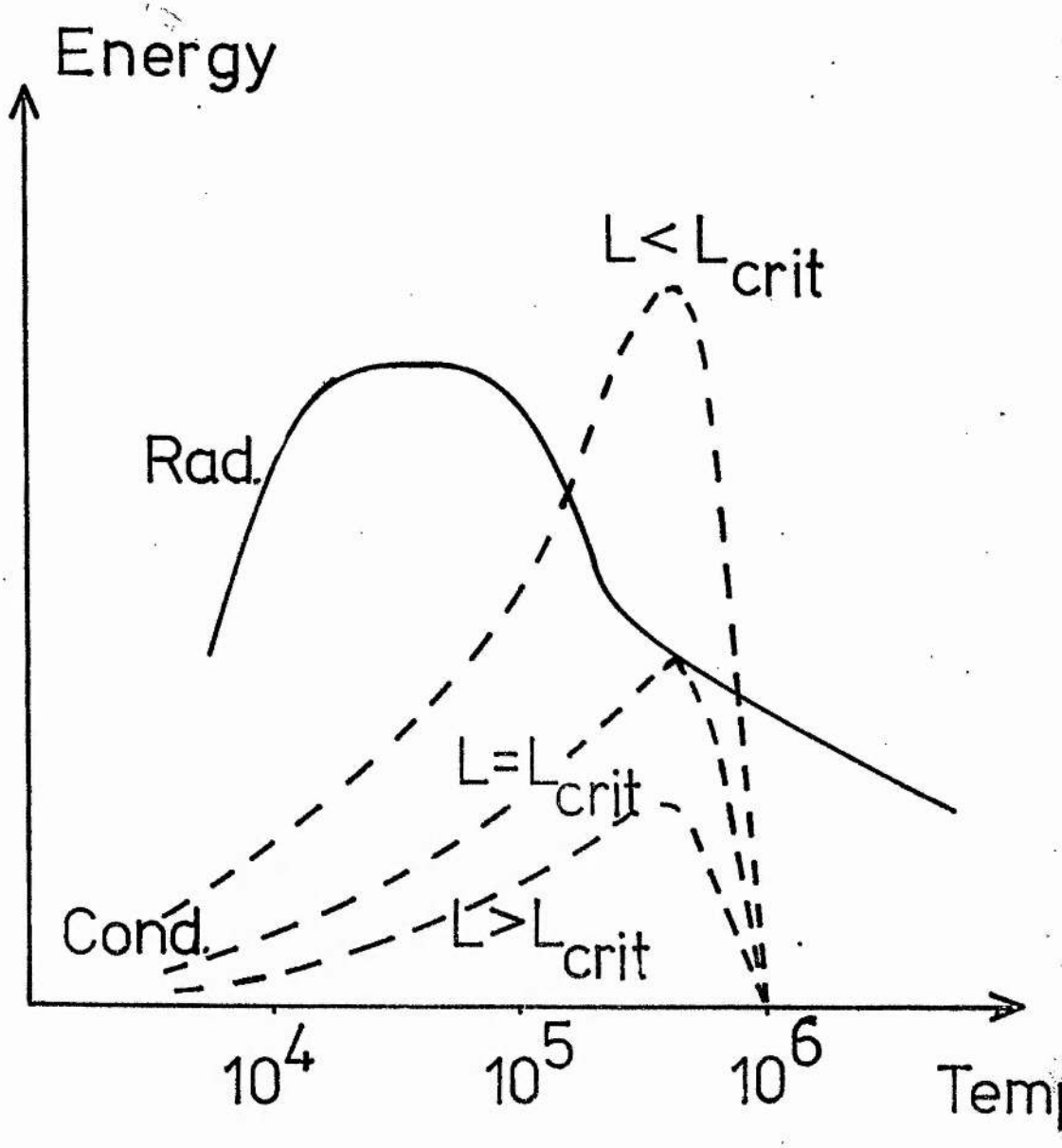

Figure 5.1

Graphical representation of the solution to the order of magnitude approximation to the energy equation (5.5). Solutions exist where the radiation and conduction curves intersect. Two solutions exist for small enough L, and a critical value is reached (L_{crit}) when only one solution is possible. For $L > L_{crit}$ no solution is possible.

A is the z-component of the magnetic vector potential defined such that

$$\underline{B} = \left(\frac{\partial A}{\partial y} , - \frac{\partial A}{\partial x} , B_z(A) \right) \quad .$$

We note here that with gravity present the y dependence of the pressure rules out the application of Birn's theorems. In spite of the fact that the theorems are not applicable to a prominence model with gravity present it will be remembered that magnetostatic non-equilibrium was shown by a different method in Chapter 2. In the special case of the force-free field approximation, the gas pressure is absent and we see from (5.6) that the form and strength of the magnetic field component B_z will determine whether non-equilibrium is present or not.

From the above we note that the feature of non-equilibrium is possible in both the magnetostatic and energy equations; a fact which proved to be extremely important in the prominence model of Chapter 2. In that Chapter a one dimensional static equilibrium model was presented for quiescent solar prominences. Our object was to couple realistically the constraints of magnetostatic and thermal equilibrium subject to symmetry conditions at the centre of the prominence, while demanding that the pressure and density attained coronal values at a distance of one scale height from the centre. Two parameters were present in the problem, namely the coronal plasma β (which can be considered as a measure of the strength of the horizontal magnetic field permeating the prominence at any given height), and the shear angle Φ which the magnetic fieldlines make with the prominence normal. Simple analytic considerations were used to obtain the basic features of the model before resorting to a numerical solution of the full equations to obtain the spatial variation of the physical parameters. It was found that if either of the parameters β and Φ exceeded certain critical values, then no equilibrium solution was possible. (In the cases where some heating mechanism was present, a minimum allowable value for β was also found). Because of the measure of uncertainty over the accuracy

of the standard forms for the terms in the energy equation, several modified models were considered. In each of these models the general feature of non-equilibrium for large β and Φ was still present.

Two possible physical interpretations of the maximum β were presented. Firstly, if we consider the coronal gas pressure as constant, then the maximum β is equivalent to a minimum allowable magnetic field strength. If the field strength is less than this minimum then the prominence plasma cannot be supported and will sag down, taking the magnetic field with it. This, as was suggested, was a possible explanation for the "feet" observed in some prominences. Secondly, if the horizontal magnetic field strength is held constant, then the maximum β is equivalent to a maximum external pressure. Since pressure decreases with height we have the prediction of a minimum height of formation for prominences and, since active region magnetic fields are much larger than those in the vicinity of quiescent prominences we expect the former to exist at much lower heights than quiescent prominences.

A useful extension of this model would be to consider more realistic boundary conditions. In particular it would be of interest to have a model which matches on to the coronal magnetic field at the boundary as well as coronal temperature and density. Another improvement would be a model which couples the magnetostatic equations with the full radiative transfer equations.

In our model, no attempt has been made to consider the question of stability. As we saw in Chapter 2, several authors have considered the stability of prominences, but as yet no account has been taken of the effect of the shear angle Φ. Such an analysis would be of interest, especially in view of the results of Tandberg-Hanssen and Anzer (1970) which showed that the majority of prominences have large shear angles, Φ. Following Cowling (1976), one might expect a prominence to be unstable if

Φ is small, since the structure is likely to be Rayleigh-Taylor unstable. We know, however, that the Rayleigh-Taylor mechanism may be stabilised by a transverse field. Although this assumes that the fieldlines are not fixed at the ends (free to move with the plasma), Cowling believes that this type of instability will be present in some form unless the field is sheared in some way to stabilise it.

In Chapter 3 we have considered one possible candidate for a trigger mechanism for solar flares. We considered the possibility that the predominantly force-free magnetic field of the solar atmosphere may have two configurations available to it, for the same photospheric boundary conditions. In particular we are interested in the possibility of these boundary conditions evolving passively until an alternative, lower energy, state is possible. If this were the case we would expect the magnetic field to change rapidly into this configuration, thus providing the trigger mechanism for the solar flare event. Since a two-ribbon flare is much longer than it is high or wide we consider a two dimensional model independent of the longitudinal coordinate. Two types of boundary conditions were considered and we labelled these Problems I and II respectively. In Problem I the normal photospheric field was specified as well as the longitudinal component of the magnetic field (B_z) at the photosphere. For this problem the theorems of Birn et al (1978) are immediately applicable and several solutions with non-equilibrium features were found. In fact, for one particular case the parametric equation governing non-equilibrium was identical to that obtained in our study of prominences (Chapter 2). In Problem II the photospheric shear was prescribed in addition to the normal field component. We consider the latter case to be more relevant to the sun, since it is photospheric motions that cause the field to evolve.

To make analytic progress we considered first the simple case of

linear force-free fields, but found no possibility of an eruptive instability. Next we made the simplifying assumption of cylindrical symmetry. For Problem I a previous solution due to Low (1977) was easily generated, as were several other fields with similar properties. For Problem II we obtained two fields, satisfying the same photospheric boundary conditions of prescribed normal field and shear. As the shear increases, the energy of the first field ultimately exceeds that of the second (which contains a magnetic island where the fieldlines do not connect to the photosphere), and therefore the first field may become unstable and erupt towards the second. Since it has proved difficult to obtain numerical solutions to the force-free field equations we feel that the above analytic result, which gives an example of a feature that may well exist for more general force-free fields, should act as a stimulus to seeking the general conditions under which force-free fields become unstable.

A third analytic approach was to employ the method of separation of variables. This led to the solution discussed in detail by Birn et al (1978), as well as the well-known linear and potential force-free fields. It also produced a wider class of fields where the potential satisfies

$$\nabla^2 A + \lambda^2 (1 + 1/k)(Ak)^{(1+2/k)} = 0 \quad .$$

For the particular case of $k = -\frac{1}{2}$ a useful analytic solution was obtained. The solutions have similar properties to the field of Birn et al. In terms of Problem I, we found a maximum allowable $\lambda = \lambda_{max}$ for a solution to exist, with two possible solutions occurring when $\lambda < \lambda_{max}$. (Note that λ is a measure of the strength of B_z). However, for Problem II there is a unique solution for a given photospheric shear, with no untoward behaviour as λ approaches λ_{max}.

In Chapter 4 an alternative trigger mechanism, in the form of the emerging flux model (Heyvaerts et al, 1977; Tur and Priest, 1978), was considered. To apply this model one requires an understanding of the

behaviour of a reconnecting current sheet in the solar atmosphere. A simple one-dimensional model for this behaviour is presented. The results are given in terms of non-dimensional parameters describing the external region surrounding the current sheet in order to make these results applicable for a wide range of external conditions. We found that no steady equilibrium was possible if either the external plasma β or the ratio of radiation to convection (r) fell below certain independent minimum values. Our equations also have the property that we may evaluate the central temperature and density of the current sheet, for any given external conditions, without solving the full system of equations. The full numerical solution of this system yields the spatial profiles of the physical variables and thus marks a significant improvement on the order of magnitude approximation to current sheets. Application of these general results to the emerging flux model gives results similar to those obtained by Tur and Priest (1978). As the current sheet rises through the solar atmosphere it eventually reaches a point where no equilibrium is possible and then heats up seeking a new, turbulent, equilibrium. This critical height represents the point at which the flare event starts.

Our results show that as the onset of non-equilibrium is approached the spatial profiles steepen dramatically in a small region. It may be that thermal conduction (which we have neglected in our analysis) becomes important in this regime and, as such, an improvement on the present model would be the inclusion of a conduction term in the energy equation. In so doing, however, we would lose the ability to predict the central temperatures and densities with ease. This fact, coupled with the increase in the order of the system of equations would greatly increase the difficulty in obtaining a numerical solution to the eigenvalue problem. If we also recall that in formulating the one-dimensional problem we had to approximate the longitudinal velocity component we must begin to assess the

benefits of such an improved model. We suggest that the effort involved in extending this simplified approach might better be spent in tackling the numerical solution of the two-dimensional system of partial differential equations.

We have presented two possible models for a trigger mechanism for solar flares. Both models appear plausible in view of the fact that commonly observed flare precursors are photospheric shear and the emergence of new magnetic flux through the photosphere. There is, of course, no reason to suppose that there will be a unique trigger mechanism for solar flares and, until observations indicate otherwise, every theoretical possibility must be investigated fully.

REFERENCES

Alfvén, H. and Carlqvist, P.: 1967, Solar Phys., 1, 220.

Anzer, U.: 1969, Solar Phys., 8, 37.

Barbosa, D.D.: 1978, Solar Phys., 56, 55.

Barnes, C.W. and Sturrock, P.A.: 1972, Astrophys. J., 174, 659.

Benz, A. and Gold, T.: 1976, Astron. and Astrophys., 55, 229.

Bernstein, I.B., Frieman, E.K., Kruskal, M.D. and Kulsrud, R.M.: 1958, Proc. Roy. Soc. A244, 17.

Bhatnagar, P.L., Krook, M. and Menzel, D.H.: 1951, Dynamics of Ionised Media, Conference report, University College London.

Birn, J., Goldstein, H. and Schindler, K.: 1978, Solar Phys. 57, 81.

Boyce, W.E. and Di Prima, R.C.: 1969, Elementary Differential Equations and boundary value Problems, Wiley, New York.

Boyd, T.J.M. and Sanderson, J.J.: 1969, Plasma Dynamics, Barnes and Noble, New York.

Braginskii, S.I.: 1958, J.E.T.P. (Soviet Physics), 6, 358.

Brown, A.: 1958, Astrophys. J., 128, 646.

Brown, J.C.: 1975, I.A.U. Symp. No. 68, 245.

Bruzek, A. and Kuperus, M.: 1972, Solar Phys., 24, 3.

Buneman, O.: 1959, Phys. Rev., 115, 503.

Campbell, G.A. and Foster, R.M.: 1948, Fourier Integrals for practical applications, Van Nostrand, New York.

Chiu, Y.T. and Hilton, H.H.: 1977, Astrophys. J., 212, 873.

Cowling, T.G.: 1957, Magnetohydrodynamics, Interscience, New York.

Cowling, T.G.: 1976, Magnetohydrodynamics (2nd Ed.), Adam Hilger.

Cox, D.P. and Tucker, W.H.: 1969, Astrophys. J., 157, 1157.

d'Azambuja, L. and d'Azambuja, M.: 1948, Ann. Obs. Paris-Meudon, 6, 7.

de Feiter, L.D.: 1966, Rech. Astron. Obs. Utrecht, 18, 2.

de Jager, C.: 1959, Handbuch der Physik, 52, 80.

Doherty, L.R. and Menzel, D.H.: 1965, Astrophys. J., 141, 251.

Dungey, J.W.: 1953, Mon. Not. Roy. Ast. Soc., 113, 180.

Dunn, R.: 1960, Ph.D Thesis, Harvard University.

Engvold, O.: 1971, Physics of Solar Prominences, Coll. Anacapri German Solar Obs.

Harvey, J.W.: 1969, Ph.D. Thesis, University of Colorado.

Harvey, J.W.: 1974, in "Flare-related magnetic field dynamics", Y. Nakagawa and D.M. Rust (eds), NCAR, Boulder, Colorado.

Heasley, J.N. and Mihalas, D.: 1976, Astrophys. J., 205, 273.

Heyvaerts, J. and Kuperus M.: 1978, Astron. Astrophys., 64, 219.

Heyvaerts, J., Priest, E.R. and Rust, D.M.: 1977, Astrophys. J., 199, 237.

Heyvaerts, J. and Priest, E.R.: 1976, Solar Phys., 47, 223.

Heyvaerts, J.: 1979, in preparation.

Hildner, E.: 1971, Ph.D. Thesis, University of Colorado.

Hildner, E.: 1974, Solar Phys., 35, 123.

Hirayama, T.: 1963, Publ. Astr. Soc. Japan, 15, 122.

Hirayama, T.: 1964, Publ. Astr. Soc. Japan, 16, 105.

Hirayama, T.: 1971, Solar Phys., 17, 50.

Hirayama, T.: and Endler: 1975, Paper presented at AAS Meeting, Boulder, Colorado.

Hood, A.W. and Priest, E.R.: 1979, Astron. and Astrophys., in press.

Hudson, J.: 1973, in Symp. on High Energy Phenomena on the Sun, NASA GSFC, p.207.

Ivanov-Kholodny, G.S.: 1959, Sov. Astron., 3, 578.

Jefferies, J.T. and Orrall, F.Q.: 1963, Astrophys. J., 137, 1232.

Jockers, K.: 1978, Solar Phys., 56, 37.

Kiepenheur, K.O.: 1953, in "The Sun", G. Kuiper (ed), Chicago Univ. Press.

Kippenhahn, R. and Schlüter, A.: 1957, Z. Astrophys., 43, 36.

Knudsen, J. and Katz, D.: 1958, Fluid Dynamics and Heat Transfer, McGraw Hill, New York.

Kuperus, M. and Tandberg-Hanssen, E.: 1967, Solar Phys., 2, 39.

Kurochka, L.: 1970, Astron. Zh., 47, 111.

Lerche, I. and Low, B.C.: 1977, Solar Phys., 2, 39.

Levine, R.H. and Nakagawa, Y.: 1974, Astrophys. J., 190, 703.

Low, B.C.: 1975, Astrophys. J., 197 251.

Low, B.C.: 1977, Astrophys. J., 212, 234.

Low, B.C. and Nakagawa, Y.: 1975, Astrophys. J., 199, 237.

Malville, J. McKim: 1976, Solar Phys., 50, 79.

Martin, S.: 1973, Solar Phys. 31, 3.

Martres, M.J., Michard, R., Soru-Iscovici, I. and Tsap, T.: 1968, I.A.U. Symp. No. 35, 318.

Mihalas, D., Heasley, J.N. and Auer, L.H.: 1975, NCAR Technical Note, STR-104, Boulder, Colorado.

Nakagawa, Y. and Malville, J.M.: 1969, Solar Phys., 9, 102.

Newkirk, G.: 1969, Ann. Rev. Astron. Astrophys., 5, 213.

Orrall, F.Q. and Zirker, J.B.: 1961, Astrophys. J., 134, 72.

Parker, E.N.: 1975a, Astrophys. J., 201, 494.

Parker, E.N.: 1975b, Astrophys. J., 201, 502.

Petschek, H.E.: 1964, A.A.S.-N.A.S.A. Symp. on Physics of Solar Flares, W.N. Hess (Ed), NASA Sp. 50, p425.

Piddington, J.H.: 1973, Solar Phys., 31, 229.

Piddington, J.H.: 1974, Solar Phys., 38, 465.

Poland, A. and Anzer, U.: 1971, Solar Phys., 19, 401.

Pottasch, S.R.: 1965, Bull. Astr. Inst. Netherlands, 18, 7.

Priest, E.R.: 1976, "Physics of Solar Planetary Environment", D.J. Williams (Ed), American Geophysical Union, Vol. I, p144.

Priest, E.R.: 1978, Solar Phys., 58, 57.

Raadu, M.A.: 1972, Solar Phys., 22, 445.

Raju, P.K.: 1968, Mon. Not. Roy. Astr. Soc., 138, 479.

Raymond, J.: 1978, Private Communication to Rosner et al (1978).

Roberts, B.R. and Frankenthal, S.: 1979, Solar Phys., Submitted.

Rosner, R., Tucker, W.H. and Vaiana, G.S.: 1978, Astrophys. J., 220, 643.

Rust, D.M.: 1966, Ph.D. Thesis, University of Colorado.

Rust, D.M.: 1968, I. of U. Symp. No. 35, 77.

Rust, D.M.: 1972, Solar Phys., 25, 141.

Rust, D.M.: 1973, Solar Phys., 33, 205.

Rust, D.M.: 1976, Phil. Trans. Roy. Soc. A, 281, 427.

Severny, A.B.: 1958, Izv. Krym. Astroliz. Obs, 20, 22.

Smith, E.A.: 1976, Ph.D. Thesis, University of St. Andrews.

Smith, H.J. and Smith, E. v.P. 1963, Solar Flares, MacMillan, New York.

Smith, D.F. and Priest, E.R.: 1972, Astrophys. J., 176, 487.

Sobolev, V.V.: 1963, A Treatise on Radiative Transfer, Van Nostrand.

Soward, A.M. and Priest, E.R.: 1976, Phil. Trans. Roy. Soc. London.

Spicer, D.: 1976, N.R.L. Report 8036.

Spitzer, L. Jr.: 1962, Physics of fully ionised gases, 2nd Edn. Interscience, New York.

Sturrock, P.A.: 1972, Solar Phys., 23, 438.

Sturrock, P.A. and Woodbury, E.T.: 1967, p168 in P.A. Sturrock (Ed), Rendiconti della Scuola Internazionale de Fisica, "Enrico Fermi", 39 Corso, New York - London.

Svestka, Z.: 1963, Bull. Astron. Inst. Czech, 14, 234.

Svestka, Z.: 1965, Adv. Astron. Astrophys, 3, 119.

Svestka, Z.: 1965, Space Sci. Rev., 5, 388.

Svestka, Z.: 1976, Solar Flares, D. Reidel.

Syrovatsky, S.I.: 1976, Letters Sov. Astron., 2, 1.

Tanaka, K. and Nakagawa, Y.: 1973, Solar Phys., 33, 187.

Tandberg-Hanssen, E.: 1974, Solar Prominences, D. Reidel.

Tandberg-Hanssen, E. and Anzer, U.: 1970, Solar Phys., 45, 351.

Tranter, C.J.: 1968, Bessel Functions with some physical applications, English Universities Press, London.

Tur, T.J. and Priest, E.R.: 1978, Solar Phys., 58, 181.

Vasyliunas, V.M.: 1975, Rev. Geophys. and Space Phys., 73, 303.

Waldmeir, M.: 1970, Solar Phys., 15, 167.

Weyman, R.: 1960, Astrophys. J., 132, 380.

Yoshimura, H., Tanaka, K., Schimizu, M. and Hiei, E.: 1971, Publ. Astron. Soc. Japan, 23, 443.

Zirin, H.: 1974, Vistas in Astron., 16, 1.

Zirin, H.: 1966, The Solar Atmosphere, Blaisdell, Toronto.

Zirin, H. and Tanaka, K.: 1973, Solar Phys., 32, 173.